Controls on strain localisation in the Middle to Late Jurassic North Sea rift system

Caroline E. Gill MSci. M.A. Hons (Cantab)

April 2005

Declaration

The results of this thesis have not been submitted for the examination of any other degree or qualification. The observations and conclusions presented in this volume are the result of my own studies except where cited or acknowledged otherwise.

Caroline E. Gill

Edinburgh 2005

Abstract

Extensional fault propagation and linkage play an important role in the structural and sedimentological development of rift basins. In this study, use of 85,000km² 3D seismic data provides a new and unique opportunity to evaluate and quantify the processes of fault growth within an evolving rift system. The study uses a comprehensive dataset from the East Shetland Basin and North Viking Graben, northern North Sea to document the evidence for, and effects of fault growth during the Mid to Late Jurassic (Bajocian to Ryazanian) rift episode. Integration of excellent biostratigraphic control with these seismic data enables enhanced temporal control than that which can be achieved in the field. The data allows the development of a new 4-dimensional holistic model in which strain localisation can be shown to be the dominant control on the spatial and temporal evolution of structure in an evolving rift province.

The significance of my approach is the integration of seismic stratigraphic analysis combined with facies analysis and biostratigraphy in the East Shetland Basin to demonstrate that during the Mid to Late Jurassic rift episode the locus of extension migrated from west to east towards the Viking Graben. Systematic documentation of the variation in age of syn-rift deposits across the basin shows that motion on faults ended progressively throughout the Kimmeridgian and Portlandian with the latest motion occurring on the Visund-Gullfaks-Alwyn fault array during the Volgian. The effect of strain localisation towards the basin centre with time caused passive rotation of earlier (more westerly) structures (e.g. Snorre) and their hangingwall depocentres.

This is the first study to challenge the traditional view that the Mid to Late Jurassic structures in the East Shetland Basin were active synchronously throughout the rift episode. Detailed interpretation of the syn-rift architecture associated with four major faults situated on a 100km long, east-west transect across the basin allows the development of a detailed model in which the timing of activity on a suite of faults can be accurately quantified. Initially, during the Upper Bajocian, extension was characterised by a large number of small faults of both dip directions which grew by radial tip propagation and subsequent segment linkage. Strain was initially focussed onto a small number of throughgoing fault arrays at the expense of less optimally positioned structures. The focussing of strain onto these structures resulted in an increased slip rate and upward bowing of the footwalls, leading to the development of release faults formed as a result of differential vertical displacements along the length of the fault. These small (less than 10km long) structures form perpendicular to the main fault and show maximum displacement of c. 300m at their proximal end decreasing away from the main fault.

As the rift episode progressed, strain was gradually localised towards the rift axis. It culminated in the Ryazanian with localisation of strain onto the rift axis. At this time activity was primarily confined to a single thoroughgoing fault, the Visund-Gullfaks Fault, defining the western edge of the North Viking Graben. As such the Visund-Gullfaks Fault developed to be the largest fault in the basin both in terms of length (125km) and maximum accumulated displacement (>5km) as a result of the basinward (eastward) migration of the locus of extension.

Acknowledgements

This project was conceived by John Underhill, Patience Cowie and Aileen Mcleod. John has put together the huge 3D seismic and well database over his many years in Edinburgh. His contribution in terms of inspiration, ideas and encouragement over the past three years cannot be underestimated. Patience's input into the project has often been timely and her numerical modelling has greatly enhanced the science. I am greatly indebted to the wider staff team in the department for excellent supervision and support throughout the course of my PhD.

As a member of the postgraduate population I have received scientific and technical advice and overwhelming support from a large number of my fellow students. In particular, Alex Whittaker and Richard Martin, with whom I shared both a flat and a keen interest in Geology, and Nick Banbury, who has always been a fellow soya user.

The submission of this thesis will no doubt be a relief to everyone in parental roles who have provided financial, personal and linguistic support throughout my eight years as a student. To the other Dr. Gill, who got there first, thanks for the support and medical advice.

Finally immeasurable thanks to Gwilym Lynn. Only he can understand how much he has contributed to this thesis; field assistance, technical advice, geological discussion and his huge impact on my everyday life.

Project Funding and Data Release

This study was funded by a Natural Environment Research Council (NERC) Industrial Case Studentship, NER/S/A/2001/06169, with industrial partners Amerada Hess Ltd. Additional funding was attained through an ExxonMobil Research Scholarship, a Shell International postgraduate bursary (2001-2004) and the Johnstone and Florence Stoney Studentship from the British Association of Women Graduates (2004-2005). All are gratefully acknowledged for their support.

The subsurface dataset used in this study was released by Amerada Hess, ExxonMobil, Statoil, Shell Expro, ConocoPhillips, TotalFinaElf, Norske Shell and Norske Chevron and the data is presented in this thesis with their permission. Well data was obtained from the Norweigen Petroleum Directorate and the Department of Trade and Industry in addition to the companies mentioned above. The assistance of those who facilitated data release and transfer is gratefully acknowledged in particular Mark Atree, Iain Batholomew, Paul Brockbank, Lisa Chapman, Philip Cox, Simon Davey, Glenda Green, Mark Hempton, Jamie Middleton, James Roberts, John Smallwood, Bernie Vining and Alistair Welbon.

Computing support in Edinburgh was provided by James Jarvis and Chris Place.

Field studies in Greece were undertaken with the permission of the Institute of Geology and Mineral Exploration and Elena Kotronia is acknowledged for her help in securing fieldwork permits and the permission to remove samples from Greece.

Finally, Eleri Lynn is acknowledged for translation of French language literature.

Abbreviations and Terminology

The following abbreviations and terminology are used in this thesis

BCU	Base Cretaceous Unconformity
c.	*Circa*
ESBBF	East Shetland Basin Bounding Fault
FSDC	Fault scarp degradation complex
FWF	Footwall Fault
Kyr	Thousands of years
Ma	Millions of years ago
Myr	Millions of years
Ms	Milliseconds
TWT	Two way time
VFWF	Visund Footwall Fault
VG	Visund-Gullfaks
VGF	Visund-Gullfaks Fault
MNE	Murchison Northeast
MSW	Murchison Southwest

Antithetic Fault	A fault, usually of one set, which in vertical section shows a sense of slip opposite to that of the major fault from which it originates
Synthetic Fault	A fault whose sense of displacement is the same as that of the main zone of faulting when seen in vertical section

‘Heather on Rannoch’

CONTENTS

LIST OF FIGURES

2. BACKGROUND TO RESEARCH

1. Introduction

1.1 Rationale

Our understanding of fault development in rift provinces has advanced rapidly in the past two decades. Use of field data, neotectonic studies, analogue modelling and, latterly, 3D seismic reflection data and numerical modelling have provided the opportunity to investigate the evolution of crustal structure in extensional settings. Recent results suggest that extensional fault growth and linkage plays an important role in the development and evolution of rift systems (Dawers and Underhill, 2000; McLeod et al, 2000, Cowie et al., 2000). Despite the important insights that these studies have provided for our understanding of the main controls of structural styles, and hence, consequent effects on the temporal and spatial evolution of basin physiography, stratigraphic geometries and sediment dispersal in rift basins, surprisingly little evidence has been provided by subsurface examples. The advent and release of well-calibrated 3D seismic datasets from extensional provinces provides an opportunity to develop and extend models of rift basin development and evolution.

The development of normal fault arrays in rift provinces has been a focus of structural research since the mid 1980's. Throughout that decade there was considerable debate about whether the major faults that accommodate crustal extension were essentially planar structures throughout the seismogenic layer or whether they form linked networks of listric faults within the upper crust (Roberts and Yielding, 1994). Earthquake data indicate that active, large normal faults are essentially planar normal faults throughout the seismogenic layer with dips in the range 30˚ to 60˚ (e.g. Stein and Barrientos, 1985; Jackson, 1987; Jackson et al., 1988; Jackson and White, 1987). Conceptually, the easiest way to accommodate linkage of fault strain in an evolving basin is to transfer slip on individual fault surfaces downwards onto a detachment horizon (Gibbs, 1983, 1984). However, this model is not consistent with observations (Rippon 1985; Watterson, 1986; Barnett et al.,1987) and as a result strain is interpreted to be accommodated by a three-dimensional linkage/overlap of fault deformation volumes. This work led to the development of models in which individual faults initially grew in relative isolation but subsequently linked to form a larger, fault surface or fault network. The understanding that individual normal faults grow by radial tip propagation and subsequent segment linkage emerged in the early 1990's (e.g. Cartwright et al., 1996) and is now widely accepted. However, the basin-wide structural controls on this system are not well documented and are now under investigation in the Northern North Sea.

Research to date has concentrated on isolated fault strands and not on the holistic evolution of a rift province as a coherent unit. This study will therefore consider the generic problem of how strain is localised in an evolving rift province using data from the Northern North Sea Mid to Late Jurassic rift province.

A distinctive and repeated feature of actively extending regions is the presence of long, sub-parallel normal fault arrays distributed over large areas in excess of thousands of kilometres wide. This can be observed in ancient examples, such as the Northern North Sea (McLeod et al., 2000) and also in regions undergoing extension at the present time for example the East African Rift (McClay and Khalil, 1998) and the Aegean Sea (Goldworthy and Jackson, 2001).

The scale and scaling relationships of a suite of normal faults in an extensional basin has been intricately linked to the thickness of the seismogenic layer (Jackson, 1987). Deeper earthquakes, in areas with thicker seismogenic layer, occur on longer faults and shallower earthquakes, in areas with less seismogenic crust, occur on smaller faults. For example in the East African Rift, Malawi, earthquakes occur to a depth of 30-40km on faults in excess of 100km long (Jackson and Blenkinsop, 1997).

Recent results from field and model data suggest that as strain increases in a rift province, an initial fault population of large numbers of small displacement normal faults will evolve into a small number of long, throughgoing, large displacement faults (Cowie, 1998). Data from field areas suggest that in addition to the dominance of larger structures over time the locus of extension migrates towards the centre of the rift province during the rift episode. This is thought to be an important process in the development and evolution of rift provinces. Examples of this phenomenon can be seen in the Gulf of Corinth, Greece (Dart et al, 1994, Goldsworthy and Jackson, 2001) and Gulf of Suez, Egypt (Gupta et al, 1999, Jackson et al, 2002). However, field examples of exhumed continental rift basins such as these often offer very limited exposure and as a result detailed regional reconstruction and quantification of the syn-rift episode is generally not possible. In the past subsurface studies have been limited by the spatial extent of 3D seismic data, poor data quality and wide line spacing. The closely spaced nature of the available subsurface data in the Northern North Sea will allow the interpretation of a suite of normal faults in order to examine the role of strain localisation in rift provinces.

In this study use is made of comprehensive, densely spaced 3D seismic data over the East Shetland Basin, densely spaced exploration wellbores and most importantly well constrained

biostratigraphic data to present the detailed syn-rift interpretation and associated structural interpretation of an area which underwent 15% extension in the Late Jurassic.

The rationale behind this study was to integrate 3-D seismic data sets from the Northern North Sea with theoretical models for the evolution of normal faulting in rift systems and field data on rates of uplift in actively extending basins. Although limited by resolution, the use of subsurface data provides coverage over a much larger geographical area than is possible using other data sources. The three dimensional nature of the data also removes some of the uncertainty present in the subsurface when undertaking field studies. In addition the higher resolution biostratigraphic control in the North Sea results in the potential for much better timing controls than can be achieved in the field. This integrated approach has not been previously attempted and allows greater understanding on the controls on rift basin architecture, in particular demonstrating which faults were active at what stage of the rift event.

Work on this theory was initiated in the late 1990's when McLeod (2000) examined the control of fault array evolution and sediment dispersal using the Statfjord Fault in the East Shetland Basin, Northern North Sea. This work suggested that the migration of the locus of extension towards the centre of the Northern North Sea Rift Basin was an unproven but very likely possibility. In addition McLeod (2000) recognised the importance of footwall degradation. Her work showed that poorly documented cross fault elements existed in the footwall to the Brent Fault, the genesis of which were unexplained.

This thesis attempts to address these issues and take further the work instigated in the late 1990's. The overall aim of the thesis is the development of a holistic model in which the development of the Mid to Late Jurassic Northern North Sea rift province is presented as a fully integrated model. The thesis will first examine the role of the migration of the locus of extension during the Mid to Late Jurassic Northern North Sea rift episode. This will be achieved by documentation of systematic variability in the age of the syn-rift deposits associated with a suite of normal faults across the basin. Throughout the thesis the variation in syn-rift thickness and geometry will be used to determine a record of the fault evolution and as a proxy for variations in slip generated subsidence. The thesis will further document the nature, role and underlying causes of footwall degradation in the East Shetland Basin.

The study area of this thesis is located to the north of McLeod (2000). This provides the opportunity to examine a suite of normal faults in a continuous transect across the East Shetland Basin. The increased availability of data allows examination of both the across-srrike and along-strike localisation of strain and allows the footwall and hangingwall

deformation associated with the suite of normal faults to be compared and contrasted for faults of different displacement and location.

1.2 The thesis

The main objective of this study is to document the evidence for, and controls on, the structural evolution of an extensional basin. The primary aim is to test and develop ideas of fault growth and development in extensional settings using a unique dataset from the Northern North Sea. Specifically three issues will be addressed:

- **To determine the role of strain localisation during the progressive extension of rift basins using examples from the East Shetland Basin and Viking Graben.**
- **To determine the character of footwall deformation during an extensional episode and how the styles and magnitudes of faulting are affected by position in the rift province.**
- **Application of these models of the development of rift basins to field and less well documented subsurface examples.**

1.3 Structure of Thesis

This thesis documents the rationale, investigative procedures, applications and conclusions of the study to other rift basins in six, self-contained chapters. In chapter 2 the background to the research is considered through examination of the structural evolution of rift basins, the controls on sedimentation within the basin and the resultant development of accommodation space and syn-rift architecture. A greater understanding of field basins is then developed through examination of two field examples; the Gulf of Corinth in Greece and the Gulf of Suez in Egypt. The chapter concludes with a declaration of the specific aims of this research.

Chapter 3 outlines the methodology adopted in the research for this thesis and the data available for incorporation into the study. It also outlines the stratigraphy of the Northern North Sea which forms the basis for detailed interpretation in the following chapters.

Chapters 4 and 5 present the results of the subsurface study as applied to two specific themes in the structural development of the Northern North Sea. Chapter 4 documents the evidence for the migration of the locus of extension towards the North Viking Graben throughout the Mid to Late Jurassic rift episode. Chapter 5 documents the role and differing styles of footwall deformation in the Mid to Late Jurassic rift province examining the role of footwall-parallel deformation, footwall-perpendicular deformation and the degradation of footwall scarps.

Chapter 6 introduces a holistic model for the development of the Northern North Sea Mid to Late Jurassic rift province and places this in a global perspective through examination of contrasting fault styles in the North Sea and their shared characteristics with other major world rift provinces. It then examines the success of different approaches to modelling the development of rift systems before considering the implications of the model for petroleum prospectivity. Finally, the chapter summarises the key conclusions of the study and discusses the broader implications of strain localisation for the development of rift provinces.

2. Background to Research

2.1 Introduction

Continental break-up usually begins with rifting, often at a triple junction, (Burke and Dewey, 1973) it is initially intra-cratonic and becomes progressively more inter-cratonic as oceanic crust generation proceeds in the axial rift zone. As stretching continues, each half of the rift evolves into a passive continental margin. Our understanding of the structure, evolution and sedimentation history of continental rift provinces has advanced greatly in the past fifteen to twenty years. The increasing availability of seismic reflection data, the undertaking of deep seismic refraction profiling and an increased understanding of the physical processes that are likely to operate in the lower crust and upper mantle have all contributed to the development of our understanding of the processes by which rift basins are formed and subsequently evolve (Roberts and Yielding, 1994).

This chapter will provide a review of the structures associated with rift provinces and of currently accepted views on the methods by which these structures are formed. Firstly, the overall structure and development of rift systems will be considered before examination of the growth and linkage of individual normal faults and the interaction between faults in an evolving rift province. The resulting sedimentary architecture will then be examined.

Secondly, the chapter will focus on well-exposed examples of exhumed continental rift basins in order to examine their contribution to our understanding of the development of such systems. Two primary examples are given, the Gulf of Corinth in Greece and the Gulf of Suez in Egypt. The geological setting of these rifts will be introduced before consideration of the role of strain localisation in the evolution of the rift systems. Primary field observations will be presented for the Gulf of Corinth.

Finally, having reviewed the literature, the chapter will explore the two overall aims of this thesis: To document the evidence for strain localisation in rift provinces and to examine the role of footwall deformation and degradation at various locations within an evolving rift province.

2.2 The structural evolution of rift systems

2.2.1 Structure and development of rift basins

Continental rift systems are the linear, crustal, expression of tensional forces affecting the lithosphere (Sellwood and Netherwood, 1984). They are defined as zones beneath which the entire lithosphere has ruptured during extension (Burke, 1977) and are commonly associated with basic volcanism, high heat flow, seismicity and anomalous crust and mantle indicating that rifts are not confined to crustal levels but are closely linked to dynamic processes in the upper mantle (Ramberg and Morgan, 1984). Continental rift basins are widespread and occur in a variety of tectonic settings and range up to 2,600Ma in age (Ramberg et al., 1984).

Rift basins are the precursors to complete rupturing of continental lithospheric plates and the development of an oceanic spreading centre. For example, the Gulf of Suez represents the failed north-west arm of the Red Sea rift system, the southern part of which has continued to extend to produce an active spreading centre. In addition, the North Sea, East African rift and Baikal rift are examples of failed rift systems in which extension has not progressed to the axial formation of new oceanic crust. In contrast to these areas with axially concentrated deformation, extension in some areas is characterised by distributed extension, (e.g. Basin and Range Province, USA), and does not appear to have ever been tending towards continental break up.

Traditionally, continental rift systems have been modelled in terms of simple lithospheric stretching (McKenzie, 1978; Jarvis and McKenzie, 1980). McKenzie (1978) was the first to describe quantitatively the implications of extension of the continental lithosphere (Roberts and Yielding, 1994). He proposed a simple model in which the continental lithosphere is uniformly and rapidly stretched. The amount of vertical thinning accommodated by the stretching in comparison to the unstretched lithosphere is called the stretching factor, β. In his model, McKenzie proposed that the initial and rapid stretching thins the continental lithosphere causing instantaneous passive upwelling of hot asthenosphere below the stretched lithosphere. Subsidence occurs initially by block faulting, the faults propagating downwards as curved, normal faults bounding rotated fault blocks. Later, the lithosphere thickens by heat conduction to the surface and further, slower, regional subsidence occurs that is not associated with faulting (Sellwood and Netherwood, 1984).

The brittle response of the upper crust to extension has been modelled using both listric and planar fault geometries. Listric fault models use a linked fault model in which the fault blocks ride on a physical detachment surface, for example Gibbs (1983 & 1984). However,

listric faults are difficult to model quantitatively as there is considerable disagreement on how their hangingwalls deform internally (Barr, 1987). In addition they are inconsistent with results of earthquake induced co-seismic slip on faults (Jackson et al., 1988) and are largely incompatible with depth-converted seismic sections. As a result, deformation using planar normal faults has been modelled using the domino fault block model (Ransome et al., 1910; Morton and Black, 1975; Davidson, 1989) which was developed by Barr (1987) in conjunction with the McKenzie model (1978). The domino model uses a number of assumptions to make structural and stratigraphic predictions about an evolving half graben. These assumptions are that the lithosphere is in thermal equilibrium prior to extension, that stretching is instantaneous (McKenzie, 1978), that Airy isostatic laws are observed, that an extending half graben is kept full to sea level with sediment and that the fault blocks are rigid and and all move simultaneously. The resulting model shows how the shape of the dominos is defined by the initial fault spacing, fault plane dip and stretching factor, β. It shows how footwall and hangingwall cut-offs move vertically during the formation of a basin and predicts where footwalls will become emergent and provide a sediment source by erosion. For example, closely spaced fault blocks never become emergent whereas widely spaced blocks will become emergent and will be eroded by shallow water and sub-aerial processes (Barr, 1987).

This simplified model breaks down at the basin margins where the geometric simplification cannot represent the complex flexural-isostatic responses to extension (Roberts and Yielding, 1991). Application of flexural isostacy to the model allows consistent treatment of basin subsidence histories and its associated margins and shows marginal uplift throughout the rift basin as observed on the basin margins of the North Sea and Mid Norway (Roberts and Yielding, 1991).

The surface expression of a continental rift system is commonly as a linear, normal fault-bounded depression, typically a few tens of kilometres wide and several tens to a few hundreds of kilometres long. Rift systems are characterised by a central depression or rift valley, under which thinned crust and lithosphere is usually present. The rift system usually shows along-strike segmentation on a few tens to few hundreds of kilometres scale (Scholz and Contreas, 1998).

Most major intra-continental extensional systems are asymmetric in both plan view and cross section, (e.g. the East African Rift and Oslo Graben; Colletta et al., 1988). Evidence for asymmetry is derived from a number of sources for example gravity field gradients, relative rift shoulder elevations, sediment isopach maps and seismic reflection profiles (Bosworth,

1985). The preferred development of half-graben basins can be explained with a simple model in which the rift initiates with a series of conjugate normal faults, but as the faults propagate downwards they intersect at depth, locking one of the faults. The other fault continues to grow and becomes the basin bounding fault (Scholz and Contreas, 1998). Alternatively, a continental rift may be inherently asymmetric as a result of the initial asymmetry corresponding to the first formed boundary fault (Meinesz, 1950).

2.2.2 The growth and linkage of individual fault segments

The evolution and linkage of along strike fault segments to form continuous, basin-bounding normal faults is recognised as the primary control on the size and shape of sedimentary basins in extensional settings (Anders and Schlische, 1994; Gawthorpe et al., 1994). The process of fault nucleation, growth by radial tip propagation and subsequent segment linkage is a process that has become gradually better understood over the past decade. Since the early 1990's, the process of fault growth has been generally understood to be bilateral tip propagation resulting in a fault segment with maximum displacement at its centre decreasing to zero at the faults tips. This characteristic bell shaped normal distribution profile (figure 2.1) in which displacement on a normal fault is at a maximum at the centre of the fault, was applied by Schlische (1991) to models of depocentre development. Further work into fault growth mechanisms subsequently showed that radial tip propagation was of secondary importance and the dominant mechanism of fault growth was by segment linkage (Trudgill and Cartwright, 1994; Childs et al., 1995). The segmented nature of faults is now understood to be a fundamental characteristic of natural fault arrays (Mansfield and Cartwright, 2001). The contrast between these two types of fault growth is shown in figure 2.2. A fault growing by radial tip propagation alone would follow a linear growth path throughout its evolution. In comparison, a fault growing by segment linkage increases in overall length through cycles of propagation, interaction and linkage of segments. A fault growing by segment linkage shows a step-like growth path (Cartwright et al., 1995). The bell-shaped profile applied to isolated fault segments was then understood to be applicable to linked fault arrays (Davies et al., 2000, Dawers and Anders, 1995). In this model, the overall displacement-length scaling of a linked fault array is the same after linkage as that of the isolated segments prior to linkage. This work found that a particular structure may experience periods of enhanced displacement accumulation with little length change prior to a linkage event but subsequent to a linkage event fault length is increased and the scaling relationship is restored.

The relationship between the length of a fault and the maximum displacement that the fault can accumulate is the subject of prolonged research (Schlische et al., 1996 and references therein). It has long been accepted that many fault populations follow a power-law distribution of fault sizes and considerable research has focussed on which power-law distribution best describes a global population of faults. Schlische et al. (1996) used field observations to show the relationship between the maximum length of a fault and the displacement that can be accommodated on that fault. The work showed maximum displacement on a given fault scales linearly with fault length. The published global population of faults gave the relationship $D=0.03L^{1.06}$ where D is maximum displacement and L is the length of the fault (figure 2.3).

The relationship between normal faults and their immediate topography (bathymetry) plays an important role in the reconstruction of fault evolution. Intrabasin highs form where fault linkage has occurred and where displacement has been accommodated on several anastamosing splays distributed across a fault zone (Anders and Schlische, 1994). For example, this seen in Greece where overlapping bell-shaped scarps dominate the topography around the Gulf of Corinth (figure 2.4). In addition, modern earthquakes studies, for example, Stein and Barrientos (1985), have shown that displacement on normal fault arrays is taken up by a combination of footwall uplift and hangingwall subsidence. Maximum slip occurs near the centre of the fault plane and the magnitude of slip decreases away from the fault in three dimensions: Along the strike of the fault maximum displacement is seen at the centre of the fault and dies away towards the fault tip. Across the strike of the fault displacement is at a maximum at the fault plane and dies away from the fault in elliptical contours (figure 2.5).

2.2.3 Rift province evolution – existing ideas

The evolution of actively extending rift provinces has been extensively studied in a number of ‘classical’ locations. For example, the Basin and Range Province, USA, the Gulf of Corinth, Greece and the Gulf of Suez, Egypt. These studies have highlighted the main controls on structural styles.

In addition to field based studies, the structural evolution of rift basins has been extensively modelled (e.g. Cowie et al., 2000). Initially, models concentrated on the evolution of single fault strands. More recently, work has become focussed into models which describe the

evolution of a population of faults constituting an evolving rift basin. This can be described in four stages (Cowie et al., 2000; figure 2.6):

1. Rift initiation: The stage in which faults nucleate and grow by radial tip propagation in relative isolation. Fault segments are short, and each has a small isolated depocentre associated with it.
2. Mid rift initiation: During this stage fault nucleation continues and there begins to be interaction between segments. The previously isolated depocentres enlarge by coalescence with neighbouring depocentres.
3. Late rift initiation: This stage forms the dominant period in which segment interaction and linkage occurs. There is a marked decrease in the nucleation rate of new faults and an overall decrease in the number of active faults. Depocentres undergo major growth through linkage.
4. Rift initiation-Rift climax transition: This stage culminates in the full linkage of fault segments to produce single through-going fault strands each with a single isolated depocentre. The number of total number faults stabilises as the number of active faults continues to decrease.

The model gives rise to a prediction of the total number of faults and total number of active faults at different times in the evolution of the rift basin. Initially, the model shows a gradual increase in the number of active faults. After 2 Myr, the number of active faults remains constant while the total number of faults continues to increase. This is a reflection of some faults being inactive or linking with adjacent faults to become a single-throughgoing fault. The number of active faults in the rift system is predicted to decline from 3.5 Myr onwards. This is due to a decline in the rate of fault nucleation and the increased dominance of fault linkage to produce larger faults. In addition, the model also predicts the point where fault linkage across the entire model is first complete (Cowie et al., 2000; figure 2.7).

Fault linkage in a system such as that described above has been attributed to a mechanism termed “stress feedback” which leads to enhanced growth of optimally positioned faults and cessation of activity on other less optimally positioned structures (Gupta et al., 1998). This occurs as a result of differences in the spatial distribution of strain around propagating normal faults which has been shown to lead to areas of increased and decreased stress compared to a non-extending area (figure 2.8). Segment growth and subsequent linkage occurs in areas where stress is enhanced as a result of movement on neighbouring structures.

However, recent research using earthquakes of magnitude greater than 7.0 has shown that only 61% of subsequent earthquakes that occurred near the 7.0 magnitude events are associated with shear stress increases. Approximately 39% are associated with shear stress decreases (Parsons, 2002). This work shows that 8% of earthquakes in the Harvard centroid moment sensor catalogue can be shown to be triggered earthquakes, as a result of calculated shear stress increases following an earlier event. Earthquakes associated with calculated shear stress increases occur at higher rates than the background seismicity up to 240km away from the main shock centroid (Parsons, 2002).

2.3 The controls on sedimentation in rift basins

The development of rift basins is not limited to tectonic processes but also involves surface processes that liberate sediment through erosion of fault-generated topography and redistribute this to depositional sinks (Gupta and Cowie, 2000). The stratigraphy in a sedimentary basin is the long-term response to prolonged subsidence (Allen and Allen, 1990). The processes by which sedimentation in rift basins occurs have been widely discussed in literature over the past fifteen years and the processes examined in a wide range of rift basins. The principal controls on sediment stratigraphy in extensional settings have been identified to be eustatic sea level, tectonic subsidence or uplift, sediment supply, climate zone and the physiography of the basin (Gawthorpe et al., 1994).

The sedimentary fill associated with a rift province can be considered on two scales; the large scale features traceable along the entire length of a rift and the smaller scale features associated with individual tilted fault blocks or half graben (Allen and Allen, 1990). The initial deposits in a rift system are typically non-marine, fluvial, lacrustine and aeolian deposits which often have a volcaniclastic character. As the rift episode progresses fault controlled subsidence shapes the basin, marine conditions dominate and first shallow and later deep marine sedimentation prevails. For example, in the Viking Graben, fluviatile deposits of the Ness Formation pass laterally up into the shallow marine deposits of the Tarbert Formation which in turn pass up into the deeper marine shales of the Heather and Kimmeridge Clay Formations.

The spatial and temporal evolution of depositional systems in active fault bound basins is significantly influenced by tectonics (Prosser, 1993). Fault movement controls the potential for erosion and the rate of sediment flux in a fault-bounded basin. Gawthorpe and Leeder

(2000) state that rift basin architecture is a function of the 3-D evolution of the basin through fault propagation and linkage, the evolution of sediment pathways and drainage catchments and the effects of changing climate and relative sea level. They state that gaps in our knowledge of rift basin sedimentary evolution are due to sediment, fault and landscape evolution, dating limitations and to the lack of fully integrated stratigraphic and structural controls. A number of factors will be considered here: the specific architecture demonstrated by syn-rift sedimentation, the controls on the development of accommodation space into which sediment can be deposited and the controls on sediment supply to rift basins.

2.3.1 Syn-rift architecture

The evolution and development of normal faults control the creation of accommodation space and consequent syn-rift architecture in a rift basin (figure 2.9). Sequence stratigraphy has become a widely accepted technique for analyzing the dynamics of sedimentary basin fill. Fault movement in an evolving basin controls the potential for erosion, the rate of sediment flux and the accommodation space available for deposition (Gawthorpe et al., 1997).

The evolution of normal fault bounded rift systems is recorded in their syn-rift stratigraphy and in the geomorphology and internal sediment geometries of the bounding footwall and hangingwall sections. The relationship between an evolving fault population and syn-rift sedimentation during the earliest stages of rifting has been shown to be an important factor in the reconstruction of rifting histories.

Where a normal fault is blind, for example at the tips of a young, propagating fault, syn-rift stratigraphy thins onto the overlying growth fold and thickens into hangingwall synclines, (figure 2.10; Gawthorpe et al., 1997). Once the fault has broken the surface, syn-rift stratigraphy thickens, diverges and is rotated into active faults resulting in the deposition of a wedge of material thickening towards the fault. The wedge of sediment can often be imaged using three-dimensional seismic reflection data. On such data, the sediment wedge associated with the rift episode can be divided into four discrete packages based upon characteristic basin infill stratigraphies: Rift initiation is characterised by perfect wedge-shaped reflector packages which may show minor onlap onto the hangingwall. The rift climax is recorded as a chaotic zone close to the footwall scarp in which aggradation and downlap can often be seen. In contrast to syn-rift deposits, post-rift stratigraphy forms a unit of continuous depositional thickness where it is draped over inactive faults, although

differential compaction over the fault may result in the introduction of thickness contrasts. During the immediate post-rift, parallel reflectors tend to be discontinuous but become continuous into the late post-rift (figure 2.11; Prosser, 1993). For example, the early syn-rift Tarbert Formation of the Northern North Sea is of very variable thicknesses with the thickness contrasts defining a number of 1-5km wide depocentres bounded by active normal faults. They can be used in the reconstruction of the active fault and slip magnitude at the time of deposition (Davies et al., 2000). Similar relationships have been examined by Corfield and Sharp (2000) who discuss the importance of lateral and vertical fault propagation in sediment geometries in active rift settings. They used an example from the Halten Terrace, Mid Norway, to demonstrate how fault tip folding above a blind normal fault affects sediment dispersal as the basin evolves.

The evolution of two overlapping fault segments has been considered by Anders and Schlische (1994). As displacement accumulates, the two fault segments grow towards one another by radial tip propagation. Initially, each fault is associated with a discrete sedimentary basin. Shortly after linkage of the fault segments the composite hangingwall basin consists of two synclinal sub-basins separated by an intra-basin high. As the displacement deficit is overcome, subsidence is accumulated at the position of the intra-basin high resulting in a single hangingwall depocentre along the entire length of the linked fault array (figure 2.12).

In addition to the sedimentary architecture expected within an evolving half graben, work has also focussed on the type of depositional system to dominate at different stages of the basin evolution. These divisions are used as a basis to define the transition from rift initiation to rift climax. Rift initiation is dominated by coarse grained fluvial or shallow marine deposits which are overlain by finer grained lacrustine or deep marine sediments of the rift climax (figure 2.13). Post-rift deposits initially record an increase in sedimentation rates and grain size before gradual degradation of the source area leads to fining up sequences and infilling of the basin (Prosser, 1993).

In summary, the large scale growth and segmentation of normal fault zones controls accommodation, sediment supply and basin physiography in actively extending regions. The sediment supply is also influenced by pre-rift drainage networks and variations in the bedrock lithology (Gawthorpe et al., 1994).

2.3.2 Controls on sediment supply to rift basins

The controls on sediment supply to rift basins is controlled by a number of influencing factors whose controls change on a variety of timescales. These include the local bedrock lithology, climate, sediment transport mechanism and direction and catchment size. Sediment supply to rift basins may be hangingwall derived, footwall derived, axially derived (parallel to fault plane), transfer zone or relay ramp derived or may be sourced from an extra-basinal source. Footwall drainage basins tend to be small, steep and with short length in contrast to larger, gentler dipping hangingwall derived drainage basins (figure 2.9; Gawthorpe et al., 1994). Extra-basinal sources form an important component of the volume of sediment deposited in rift basins as the distribution of slip results in a volume deficiency to source all sediment internally within in rift basin (Contreras et al., 1997). However, this sediment source is typically only important in the early stages of rift basin development.

Gawthorpe et al. (1994) present a model to describe sediment dispersal and deposition in a subaerial rift basin. They describe characteristic sequence geometries in different structural settings within the rift basin with reference to segments of a major normal fault system. The large-scale segmentation of normal fault zones are shown to control accommodation space, sediment supply and basin physiography.

2.3.3 Development of accommodation space

Accommodation space is defined as the space available in which deposition of sedimentary material can occur. The development of accommodation space in an extensional basin is a function of relative sea level change which itself is a function of changes in eustatic sea level and tectonic uplift and/or subsidence (Gawthorpe et al., 1994). Eustatic sea level fluctuations are well documented as having occurred at varying magnitudes and on a variety of timescales (Haq et al., 1988). Present day estimates of eustatic sea level change for the British Isles are 1.0mm/yr (Woodworth et al., 1999). The dominant signal for the Pleistocene is a period of 100 Kyr and an amplitude of 50m. However, eustatic variation as determined from the stratigraphic record shows a dominance of longer duration cycles (0.5 – 2 Myr) of lower amplitudes (10 – 20m) (Allen and Allen, 2005 and references therein).

Changes in eustatic sea level arise from either changes in the volume of ocean basins or changes in the volume of water within those basins. Continental and mountain glaciation is

the most efficient and rapid means of storing and releasing ocean water. Continental glaciations are capable of driving high amplitude (10 – 100m) and high frequency (1 – 100 Kyr) eustatic changes (www[1]).

Therefore, a considerable variation may be present in the rates of eustatic sea level change. Allen and Allen (2005) consider that for a glacio-eustatic sea level cycle of wavelength 100 Kyr with an amplitude of 50m (i.e. Pleistocene parameters) the tectonic subsidence rate is required to be greater than 3.14mm/yr in order for subsidence to outpace the effects of eustatic sea level change. However, when the wavelength and amplitude of the glacio-eustatic cycle are 1 Myr and 10m respectively, as determined from the stratigraphic record, this critical rate can be as low as 0.06mm/yr.

Changes in tectonic subsidence rates are an integral part of an actively extending basin. An example of varying rates of tectonic subsidence is seen in the Cretaceous to Recent history of the Gualala Basin on the Californian margin (Loomis and Ingle, 1994). During the Late Cretaceous (80 Ma) the Gualala basin underwent slow rates of tectonic subsidence (0.3mm/yr). In contrast during the late Palaeocene (57 Ma) tectonic subsidence in the basin increased to 1.4mm/yr. In the overlying Neogene Point Arena Basin extremely high rates of tectonic subsidence (10.6mm/yr) are recorded from the Oligocene (24 Ma).

Since even relatively slow rates of tectonic subsidence in extensional basins (0.3mm/yr) are often greater than the critical rates discussed above, then the magnitude and rate of change of eustatic sea level is small compared to that of tectonic subsidence (Allen and Allen, 2005). As such, tectonic processes are considered to be the principal control on the development of accommodation space in an evolving rift system. Subsurface evidence for such a dominance of tectonics over eustatic sea level variations was shown by Underhill (1991) in the Late Jurassic of the Inner Moray Firth.

2.4 Use of field studies to further understanding of extensional basins

Field studies in actively extending basins have a number of advantages over subsurface studies of ancient extensional basins. Active faulting provides an indication of the concentration of seismic activity and since most large earthquakes occur on major slip surfaces they can give an indication of the large scale motions in the area (figure 2.14). In

addition, seismogenic events provide slip vectors and fault orientations and allow determination of the interaction of normal faults. These factors are difficult to deduce from ancient systems.

The excellent three-dimensional exposure in both the Gulf of Corinth and the Gulf of Suez provide ideal locations in which present-day fault and sediment geometries can be studied in the field. The incision of both areas by large river valleys also provides cross-sectional geometries of eroding tilted fault blocks on a much finer scale than can be achieved using subsurface data.

However, despite these advantages the primary limitation of the use of extensional field basins in a study of rift basin evolution remains that the rocks exposed in the field do not give a fully three-dimensional, time-calibrated picture and so conclusions are limited both spatially and temporally.

2.5 Gulf of Corinth, Greece

2.5.1 Introduction and rationale

It has proved notoriously difficult to determine fault kinematics from seismic studies alone. Several efforts have been made in the North Sea, which attempted to place its three rift arms into a single stress regime (for example Roberts et al., 1990 and Bartholomew et al., 1993). In that basin, it only became clear that local stress regimes controlled the fault kinematics of each rift arm once a comprehensive and robust biostratigraphic framework (i.e. Partington et al., 1993a) was in place (Davies et al., 2001). Furthermore, in the absence of clear cross cutting relationships and a very good stratigraphic control, such as those that depict the Basin-and-Range extensional province of the Western USA (Proffert, 1987), the timing of individual fault activity relative to its neighbours remains impossible to access. Only with good 3 dimensional field exposures and excellent biostratigraphic control can insights normally be gained into fault growth, linkage, kinematics and timing (as has been demonstrated in the Gulf of Suez; e.g. Young et al., 2001; Jackson et al., 1988; Jackson et al., 2002).

The Gulf of Corinth in central Greece is the most rapidly extending of a number of extensional basins in the Aegean region (Taymaz et al., 1991). It is approximately 120km

long and 30km wide and trends WNW-ESE. The topography and bathymetry of the southern margin combine to give 3km of relief. In addition there is 1km of syn-rift sediment imaged on seismic reflection profiles in the present day Gulf of Corinth (Brooks and Ferentinous, 1984; Higgs, 1988).

The Gulf of Corinth was selected as a possible field analogue with which to compare the North Sea results with because it provided a unique opportunity to:

(i) assess the role of fault kinematics within a well-calibrated, accessible and well-exposed region of active extension. Importantly, whilst the use of GPS studies permits us to have an accurate handle on the overall slip vectors for the area characterised by normal faulting, field measurements of the faults themselves allows a comparison between actual slip kinematics and the regional trend and

(ii) to examine the field evidence that has been used to document a progressive northward movement in the locus of extension (Jackson & Goldsworthy, 2001).

The results of the field studies undertaken as part of this project provide a basis through which to compare and contrast field-based kinematic and fault-timing studies with those obtained solely through subsurface analysis in the North Sea.

2.5.2 Geological Setting

The neotectonic setting of the Aegean makes it distinctive as one of the most seismically active and rapidly deforming regions of the world. The kinematics of the area are controlled by three principal factors: the westward motion of Turkey with respect to Europe, the continental collision between northwest Greece – Albania and the Apulian-Adriatic platform in the west and the presence of the Hellenic subduction zone in the south (Taymaz et al., 1991). Turkey is moving west at 32mm/yr (Jackson and McKenzie, 1988) via right lateral accommodation on the North and East Anatolian Faults. This westward expulsion of Turkey is accommodated by shortening in the Hellenic Trench as the Southern Aegean overrides Mediterranean seafloor. Fault plane solutions suggest that the lateral movement of the Turkish Microplate from the collision zone between Arabia and Eurasia may help avoid crustal thickening. The interaction between these three tectonic elements results in rapid extension in the north and eastern Aegean (McKenzie, 1978) quantified for the Aegean as a

whole as 50mm/yr for the past 5 Ma (Jackson and McKenzie, 1988). Global Positioning System (GPS) data from central Greece also show a similar pattern of crustal deformation and reveals that strain rates are highest within the Gulf of Corinth and lower elsewhere (figure 2.15, Clarke et al., 1998). In addition, measurement of strain made over a few years are compatible with 100 year measurements and provide a good constraint on long-term strain in central Greece (Clarke et al., 1998).

The Gulf of Corinth is an ensialic marginal basin which developed due to north-south directed rollback-related extension in the forearc area behind an active subduction zone located along the outer Hellenic arc (figure 2.16). The age of initiation of subduction is not known but the present subduction regime has probably existed for at least 5 – 15 Myr (Le Pichon and Angelier, 1979, 1981). Two lines of evidence support this age for onset of subduction: Using the location of volcanics of known age to the position of the slab tip and assuming constant rate of subduction an age of 13 My is proposed (Kissel and Laj, 1988). Alternatively, considering rotations of the Africa - Eurasia and the Hellenic arc - Eurasia boundaries, a reconstruction of the tectonic regime gives an age of 12-13 My (Le Pichon and Angelier, 1979, 1981).

The onset of rifting in the Gulf of Corinth occurred during the latest Miocene to earliest Pliocene (Kelletat et al., 1976). Present day extension in the back arc to the Hellenic trough is 10-20mm/yr (Billiris et al., 1991) and is characterised by zones of high extension separating more slowly deforming blocks (Jackson and McKenzie, 1988).

North-south extension in the Gulf of Corinth is expressed as a series of predominantly right stepping, north-dipping normal faults. In places these are submerged (e.g. the Gulf of Corinth Master Fault located offshore in the present day Gulf of Corinth). A number of south-dipping antithetic faults characterise the northern flank. The inherent asymmetry of the rift is evidenced in the topography, bathymetry and differential uplift of the area (Jackson et al., 1982, Roberts and Jackson, 1991). The overall effect is to produce an asymmetric half graben with larger faults and thicker syn-rift deposits located on the southern margin of the Gulf, on the northern edge of the Peloponnese peninsula (figure 2.17; McNeill and Collier, 2004). The current fault systems have been active for at least the last one million years (Dart et al., 1994; Armijo et al., 1996; Goldsworthy and Jackson, 2001). The position of active faulting appears to have stepped northward over time (e.g. Dart et al., 1995; Goldsworthy and Jackson, 2001) leaving inactive faults abandoned and rotated in the footwall to younger faults and earlier sedimentary depocentres uplifted and eroded (figures 2.17 and 2.18). Although some workers believe that normal faults dip shallowly northward (Sorel, 2000), the

majority of published material interprets the normal faults as steeply-dipping planar structures (e.g. Goldsworthy and Jackson, 2000).

The present-day, large, active faults are defined as those that with dimensions comparable or greater than the thickness of the seismogenic upper crust (e.g. Shimazaki, 1986; Scholz, 1990). These typically dip at around 45˚, reach typical maximum lengths of 15-25 km, extend to depths of 10-15km and move in earthquakes with magnitudes (Ms) > 6.0 (Goldsworthy and Jackson, 2000). The ratio of footwall uplift to hangingwall subsidence on these faults is typically in the ratio 10-20% both for coseismic and longer term motions (Jackson and McKenzie, 1983; Stein and Barrientos, 1985; Armijo et al., 1996).

2.5.3 The migration of the locus of extension in the Gulf of Corinth, Greece

Examination of the migration of activity into the hangingwall of active normal faults has been shown via examination of the geomorphological features that result from fault migration which can often be represented in surface slopes and drainage patterns (Goldsworthy and Jackson 2001). These features control how the migration of the locus of extension is preserved in the structure and sediments of the geological record (Paton, 1992; Dart et al.,1995).

Migration of activity on the temporal and spatial timescales seen in the Gulf of Corinth (10-20km and less than 1 million years) is much easier to study on structures that have been active in the late Quaternary where earthquake seismology, surface faulting and relative vertical motions can contribute to a greater understanding of fault movements than in older, inactive systems.

The area to the south of the Gulf of Corinth comprises a sub-parallel array of normal faults, each 25-30km long with accumulated slips of up to 3km (figure 2.17). Earthquake focal mechanisms suggest that slip orientation is north-south (Roberts, 1996). The main depocentres in the area have moved in response to the complex movement histories along intra-basinal and basin-bounding faults. The basin has narrowed over time as fault controlled subsidence has migrated north. As a result segmented, linked normal faults have been progressively abandoned and passively rotated in the footwalls of younger faults and thick Pliocene lacrustine sequences and Quaternary terrestrial sediments have been rapidly uplifted above sea level in the footwalls to active normal faults (Gawthorpe et al., 1994). Sedimentation in the present day Gulf of Corinth is dominated by fine grained turbidites and settling out of fine grained material from suspension. Coarse grained sedimentation is

restricted to a fringe of deltas which lie along the southern coastal plain of the Gulf. The deltas are under a strong structural control from the faults which control the surrounding topography. Growing tectonic topography during the Plio-Pleistocene provided the bathymetric differentiation required for the formation of Gilbert-type deltas at the mouths of incised valleys (McMurray and Gawthorpe, 2000). Today, these form part of a stacked array of delta topsets with a staircase morphology in which successively younger deltas offlap each other and step downwards towards the modern coastal plain. Delta topsets are found at between 3 and 1700m elevation above the Gulf of Corinth and have been incised by the rivers that once fed them as a result of footwall uplift (figures 2.19 and 2.20). The southern coast of the modern Gulf of Corinth is being actively uplifted as a result of movement on the present-day active fault. When combined with eustatic sea-level change this uplift results in the long-term destruction of accommodation space, with short-term intervals of accommodation creation associated with rapid post-glacial eustatic sea-level rise (McMurray and Gawthorpe, 2000).The southern coastline of the Gulf of Corinth comprises coast-parallel Pleistocene age terraces which are younger at successively lower levels (figure 2.21). This basinward shifting and stratigraphically falling character of the deposits reflects forced regression during long-term relative sea-level fall (McMurray and Gawthorpe, 2000).

An alternative explanation for the geometries of normal faults in the Gulf of Corinth, Greece, in which a migration of the locus of extension towards the rift axis is still seen, is of an active, shallow, low-angle (c. 20˚) north-dipping normal fault, present underneath the Gulf of Corinth rift (Sorel, 2000; figure 2.22). This major detachment fault was active at the surface during the earliest stage of rifting. Then, steeper faults formed successively northward, as southern parts of the detachment became inactive and stranded the southern parts of its hangingwall. Sorel, (2000) interprets the formation of successively more northwards faults as a result of uplift and backtilting of the southern part of a detachment fault.

2.6 Gulf of Suez, Egypt

2.6.1 Introduction and Definitions

The Gulf of Suez rift province stretches from 30˚N to 27˚N and forms the northwest-southeast trending extension to the Red Sea rift. It separates the massifs of the Sinai Peninsula, a microplate, from those of those forming the backbone of the Eastern Desert in

mainland Africa (figure 2.23). The centre of the Gulf is occupied by water and the edges are characterised by elongate ridges of varying age and lithology. The Gulf of Suez rift system is contemporaneous with the Red Sea rift, and forms a failed arm, in which mature continental drift and the associated production of oceanic crust was never achieved. The Gulf of Suez appears to be largely inactive at the present day. However, left-lateral strike-slip movement still occurs on the Dead Sea Transform Fault onto which strain appears to have been transferred.

The Gulf of Suez has attracted interest from geologists for the past 100 years. Some of the earliest accounts of the gulf were given by Ball (1916) and Barron (1917). The first description of the structure was attempted by Busk in 1929 and described the overall rift valley structure and typical fault patterns. Increased interest in the Gulf of Suez rift province occurred in 1938 when a change in Egyptian law regarding petroleum concessions and the discovery of oil at Ras Gharib provided the impetus for widespread interest in the structure (Robson, 1971). Since then a large number of workers have studied the rift from both academia and industry and an overall understanding of the stratigraphy, structure and evolution has resulted from a wide range of research areas.

2.6.2 Geological History

The present day configuration of the Gulf of Suez rift system formed in the Oligo-Miocene (Robson, 1971; Garfunkel and Bartov, 1977; Moustafa, 1993; Patton et al., 1994) as a result of the separation of the Arabian and Africa sub-plates (Patton et al., 1994). The evolution of the rift can be considered in three stages: The rift initiation stage, a period of active rifting and finally rift abandonment. These relate to a three part subsidence history (Patton et al., 1994). The initiation of rifting in the Gulf of Suez is indicated by the presence of red beds in the Late Oligocene- Early Miocene aged Abu Zenima Formation (figure 2.24). Initiation of rifting was accompanied by widespread, but volumetrically minor, basaltic volcanism (Jackson et al., 1988). Subsidence in the rift initiation phase was gentle. In contrast the period of active rifting that followed in the Burdigalian saw a pronounced increase in subsidence rates and led to the development of deep marine conditions throughout the gulf recorded by the deposition of the marls and sands of the lower Rudeis Formation. During this period deepening and widening of the rift occurred, and the asymmetry and major transfer zones in the rift were established. Finally, during the Langhian and early part of the Serravalian rift abandonment saw a return to gentle subsidence rates and records a period of quiescence and the onset of abandonment of the Gulf of Suez as an area of active extension.

During this time the basin began to fill as subsidence waned and the gulf became more restricted. Final abandonment occurred in the Pliocene when the Dead Sea transcurrent fault separated the Gulf of Suez rift from the Red Sea, which has continued opening since then by sea floor spreading (Cochran, 1983). The separation was achieved by decoupling as a result of 105km of left-lateral shear along the Aqaba transform zone thought to have accumulated since the late Cretaceous (Quennell, 1958) or Miocene (Bartov et al., 1980). A 40km offset in the Plio-Pleistocene may have provided the final decoupling (Garfunkel, 1981). To the north, propagation of the Gulf of Suez Rift System is thought to have been precluded by the presence of stronger Mediterranean oceanic lithosphere situated just north of the present day northward termination of the Gulf. The presence of this stronger material is postulated to have both precluded northward propagation of the Gulf of Suez rift and led to a transfer of activity onto the Aqaba Fault Zone (Steckler and Ten Brink, 1986). Following cessation of activity in the Pliocene the Gulf of Suez rift system has continued to subside leading to the accumulation of up to 1500m of sediment. During the Serravalian and Messinian the gulf became restricted and a thick sequence of evaporites were deposited. Later in the Pliocene and Holocene, renewed subsidence of the central and offshore Gulf of Suez (Moretti and Colletta, 1987) and Red Sea rift system has led to connection to the Indian Ocean in the Pliocene and the introduction of Indo-Pacific faunas.

The total amount of extension in the Gulf of Suez rift system has been estimated to vary from 16km (β=1.33) in the northern part of the rift, to about 30km (β=1.51) in the southern part (Patton and Nelson, 1988).

The rift system is up to 400km long and up to 80km wide and consists of individual half graben basins bounded by major normal faults that define larger tilted fault blocks up to 20km wide. Fault-controlled depocentres are filled with Neogene sedimentary deposits. The structure of the rift is dominated by the normal faults and their associated tilted blocks which trend northwest-southeast. The pattern demonstrated by the fault blocks on the eastern side of the rift has been described by Robson (1971). A synthetic, crescentic fault forms the south-western border of each block and dies out northwards in a series of splay faults. Parallel synthetics and antithetic faults occur within the block and occasionally unite as a double hinge fault forming a small horst or graben. All blocks are bounded by the synthetic marginal fault (figure 2.25).

The amount of tilt on the fault blocks varies along the rift axis from less than 10˚ around Melaha to over 20˚ near the July and Ramadam oil fields (Angelier, 1985). The normal faults adjacent to the tilted fault blocks have often been tilted and cut by younger and steeper

faults. Angelier corrects for these later events to obtain an average initial fault dip of 55-70˚ in Miocene and Eocene terranes. This is consistent with geological mapping in a different area of the Gulf where Chenet and Letouzey (1983) obtained similar dip values. The dip values are in the range typical for dip-slip normal faults.

In addition to the dominant normal faults, the Gulf of Suez rift is bisected by north to south and north-north-east to south-south-west trending transverse faults which are parallel to the nearby Aqaba transform (Moustafa, 2002). The transverse faults are inherited passive discontinuities and show strike-slip displacement, acting as transfer faults or relays between major normal faults (figure 2.26). The transverse faults have a limited capacity to take up extension and only affect a small number of fault blocks. They are never found to propagate through the rift as large transform faults (Colletta et al., 1988). The two sets of faults were simultaneously active during Oligo-Miocene rifting resulting in a zigzag pattern and rhombohedral shaped fault blocks (Colletta et al., 1988).

The normal faults and their adjacent fault blocks change polarity along the axis of the rift, dividing the rift into three longitudinal dip provinces defining three geographically successive half grabens (Moustafa, 1976). The faults are planar and dip predominantly to the east in the northern and southern sections of the rift, and to the west in the central part of the rift (Jackson et al., 1988; Patton et al., 1994). The dip provinces are separated by transfer or twist zones which stretch transversely across the rift. In the northern transfer zone the transition from easterly to westerly dip is accompanied by a graben type 'twist zone' which has an absence of transverse faulting. In the southern transfer zone the transition back to easterly dipping normal faults is accompanied by more complex structure involving a major transverse fault and horst type 'twist zone' (Colletta et al., 1988).

During the early Miocene, the gulf was a complex of small troughs, reefs, islands and channels the form of which were controlled by uplift and subsidence of the tilted fault blocks. The block crests were often sub-aerially exposed and consequently eroded and were often colonised by capping or fringing reefs (Angelier, 1985). Thick deposits of clastic sediments dominated by sands and conglomerates with occasional marls, shales and reefal limestones were deposited in the troughs between adjacent fault blocks. These can be divided into three main groups separated by a series of evaporitic saliferous and gypseous deposits; pre-evaporitic (Early Miocene), evaporitic (Middle to Late Miocene) and post-evaporitic (Plio-Quarternary; Angelier, 1985). Extension was accompanied by widespread subsidence and the onset of marine sedimentation occurred in the early Miocene and

comprises some clastic material but mostly evaporates and marls. The sedimentary fill locally reaches 6km.

The Gulf of Suez is an ideal natural laboratory in which to examine the evolution of a rift province as the combination of regional uplift, lack of fault reactivation and post-rift fluvial incision provide excellent quasi-3D exposure (Jackson et al., 2002).

2.6.3 Migration of the locus of extension in the Gulf of Suez

Recent results from a wide variety of studies have highlighted the role of strain localisation during the development of the Gulf of Suez rift system.

Integrated tectono-stratigraphic analysis carried out by Jackson et al., (2002) has documented the evidence for the migration of fault activity in the East Tanka fault zone of the Gulf of Suez rift system. The East Tanka fault zone is situated in the Hammam Faraun fault block in the Central Gulf of Suez rift (figure 2.26). It is comprised two 1-1.5km long northwest trending, southeast dipping fault segments which have been hard linked by a smaller structure. Jackson et al. (2002) show that initial growth on the faults was by linkage of early isolated fault segments but that after linkage migration of activity to the zone of linkage resulted in modification to drainage systems in the footwall to the linked fault.

Detailed mapping of the geometry of fault zones, associated folds and syn-rift stratigraphy carried out by Gawthorpe et al. (2003) on the Hammam Faraun fault block documented the role of strain localisation in the evolution of the fault block. This work showed that initial fault activity was distributed across the fault block on fault segments which either grew by linkage or died during a rift initiation phase that lasted 6-8My. Following the rift initiation phase displacement is shown to have become localised onto greater than 25km long border fault zones bounding the fault block at the expenses of the early faults present within the block. From the border faults the locus of extension then continued to migrate towards the western edge of the fault block and post-Middle Miocene displacement has been exclusively focussed on the western margin of the Hammam Faraun fault block.

Fault segment linkage, migration of the locus of fault activity and displacement localisation were important processes controlling the late Oligocene to Recent evolution of part of the Gulf of Suez rift system (Gawthorpe et al., 2003).

2.7 Aims of Research

To date, relatively few studies have integrated structural observations with detailed analysis of syn-rift stratigraphy in order to constrain the temporal evolution of rift provinces and the associated development of faults and other structural elements within a particular extensional province. Recent results from ancient rift systems (e.g. Contreras et al., 2000; Dawers and Underhill, 2000; Young et al., 2001) have unravelled the detailed temporal development of fault growth histories but have in general been confined to a single fault trace and have not investigated the fault population as a whole. Recent results from active rift systems (e.g. Leeder et al., 1991; Goldsworthy and Jackson 2000) have shown the transfer of activity between major fault zones. As a result the detailed temporal evolution of individual faults and fault populations from ancient examples is poorly constrained and can only be further investigated by detailed examination of the syn-rift stratigraphy associated with a large, fully developed rift province.

This study uses densely spaced 3D seismic data from the East Shetland Basin Northern North Sea to document the detailed syn-rift evolution of the basin during the Mid to Late Jurassic rift episode. In particular, two key aims are to be addressed: The first will document the evidence for strain localisation in an evolving rift system. Data will be presented from the Northern North Sea Mid to Late Jurassic rift system where the locus of extension migrated towards the rift during the rift episode. The second principal aim is to document the different styles of footwall deformation present in different locations within the Northern North Sea rift province. Data will be presented from the footwalls of major faults in the rift system in order to compare and contrast the differing types and styles of footwall deformation at different locations in the rift province.

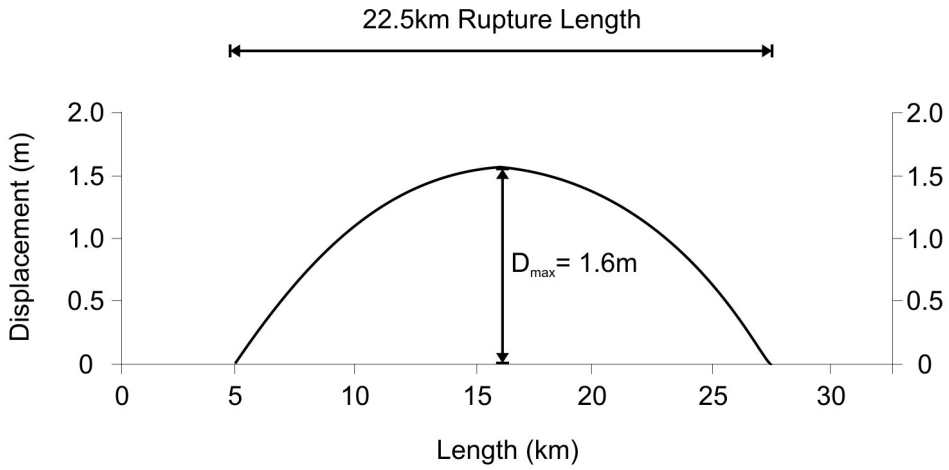

Figure 2.1A:
Bell shaped displacement-length profile for the 1983 Borah Peak Earthquake, USA.
After Underhill, 2002.

Figure 2.1B
Photograph of a surface break associated with the 1983 Borah Peak earthquake
From : http://www.idahogeology.org/Services/GeologicHazards/Earthquakes/nisnpics.html

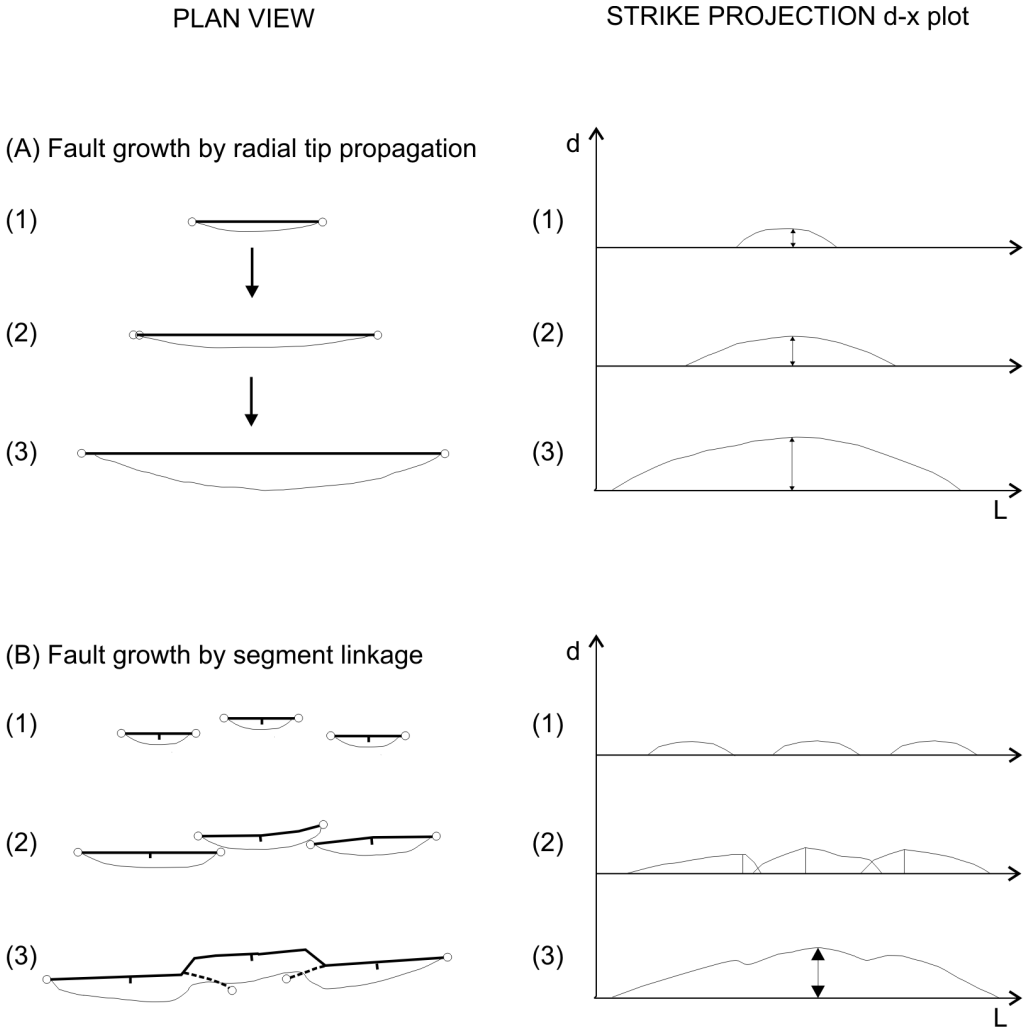

Figure 2.2
A comparison of two models of fault growth (A) radial tip propagation and (B) segment linkage. Three stages of growth are compared for both models in plan view and on a displacement-length profile.
After Cartwright et al., 1996.

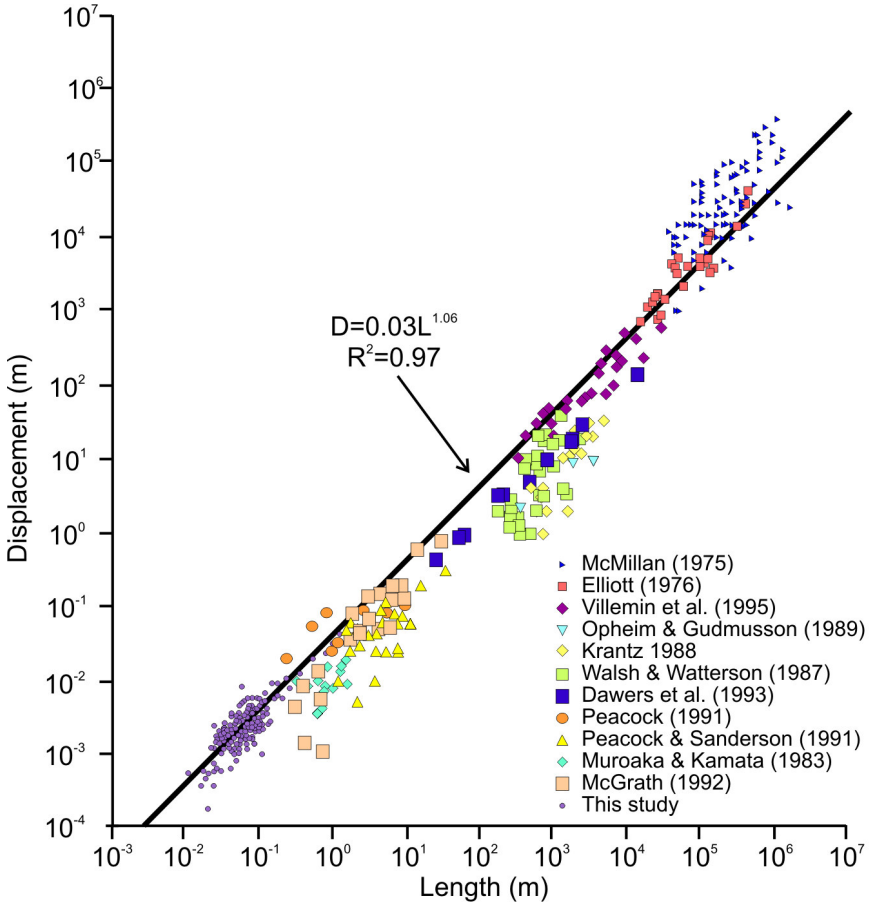

Figure 2.3
Log-log plot of displacement vs. Length for various published fault populations
Best fit curve for all data is shown as a heavy solid line.
From Schlische et al, 1996.

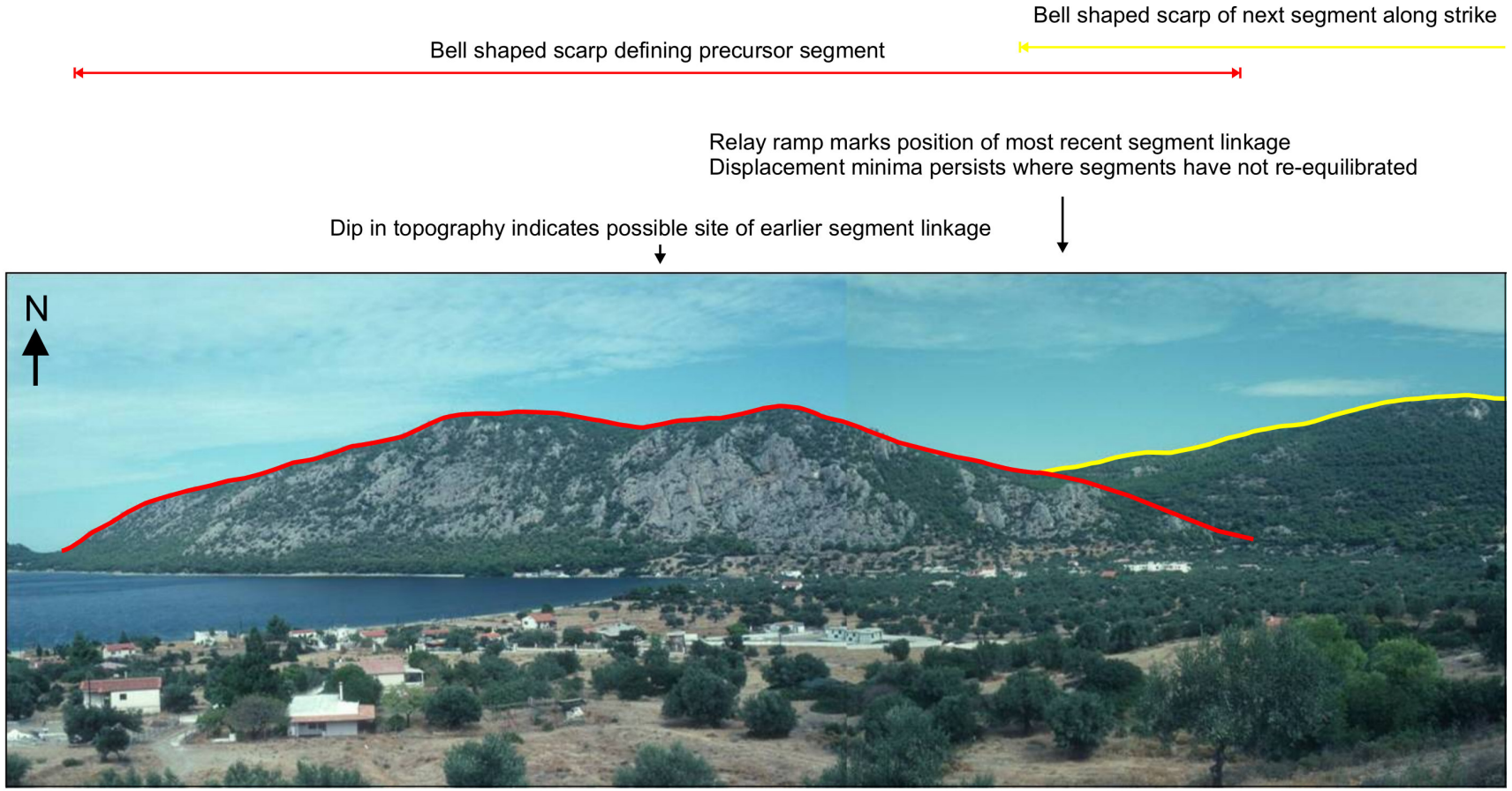

Figure 2.4
View North across Alkyonides Gulf showing two active normal fault footwall scarps with vaying elevation along strike and position of segment linkage. Lagoon in Alkyonides Gulf is located in hangingwall depocentre of westerly segment.

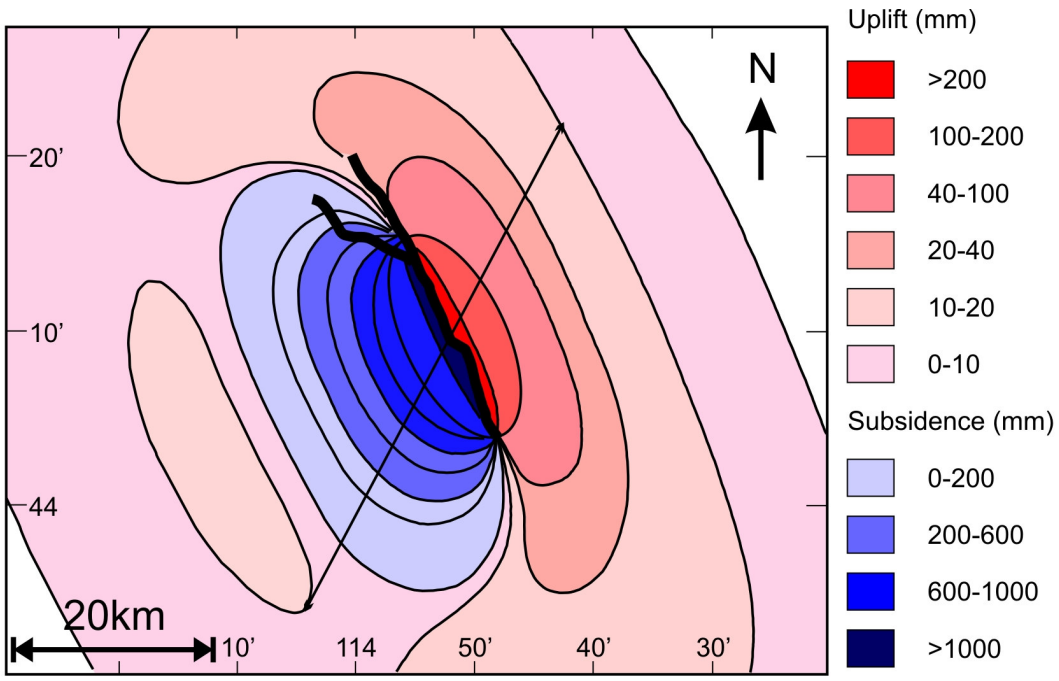

Figure 2.5a
Schematic map of Borah Peak Earthquake site showing surface rupture (bold) and contours of elevation change predicted by a coseismic model.
Straight line shows position of figure 2.5b.
After Stein and Barrientos, 1985.

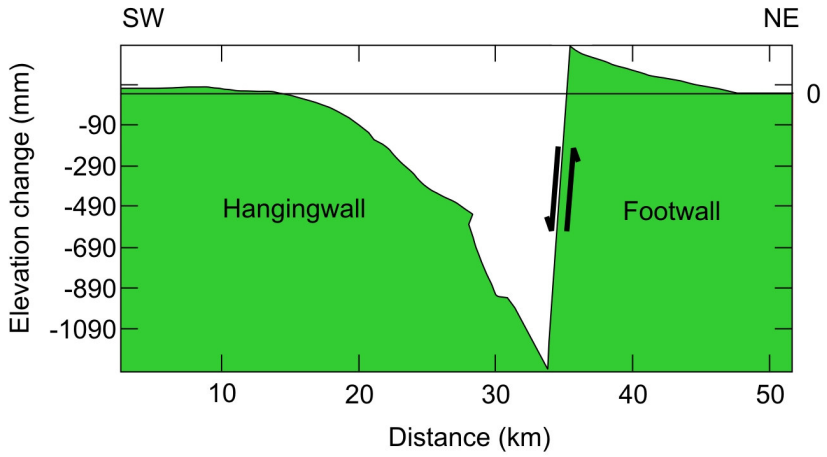

Figure 2.5b
Profile of co-seismic elevation change predicted normal to the fault. For location see figure 2.5a.
After Stein and Barrientos, 1985.

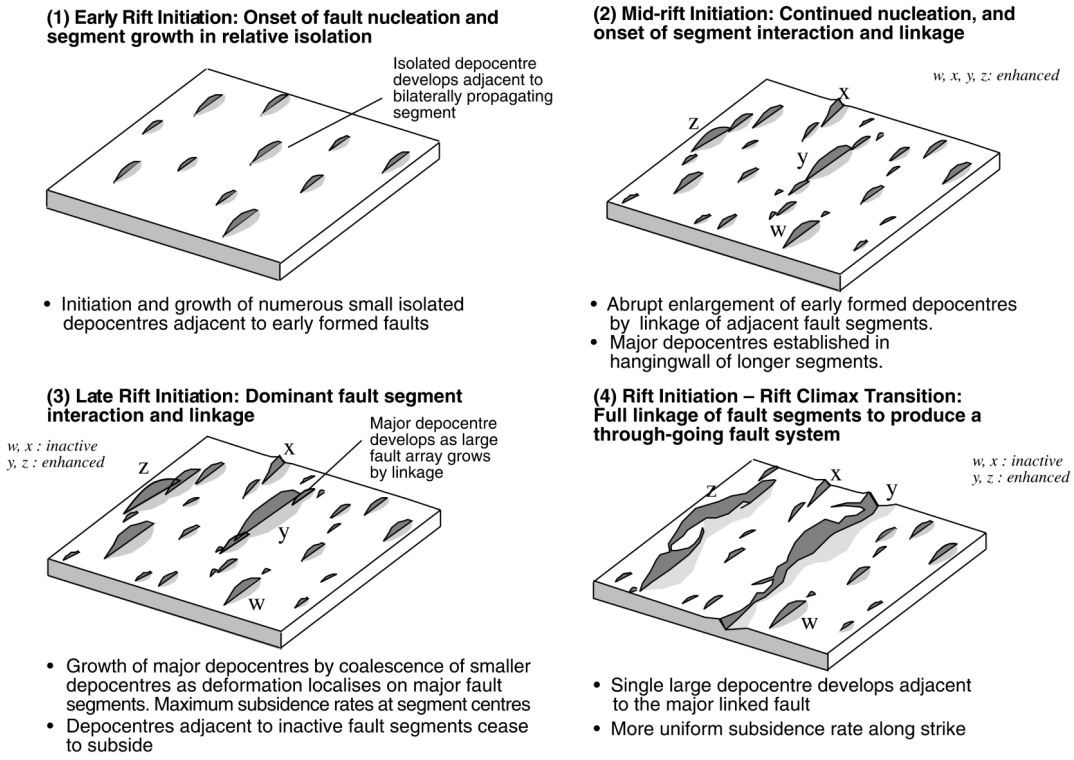

Figure 2.6
Tectono-stratigraphic model for syn-rift depocentre evolution in response to fault array development that is derived from the results of a numerical simulation.
From Cowie et al., 2000.

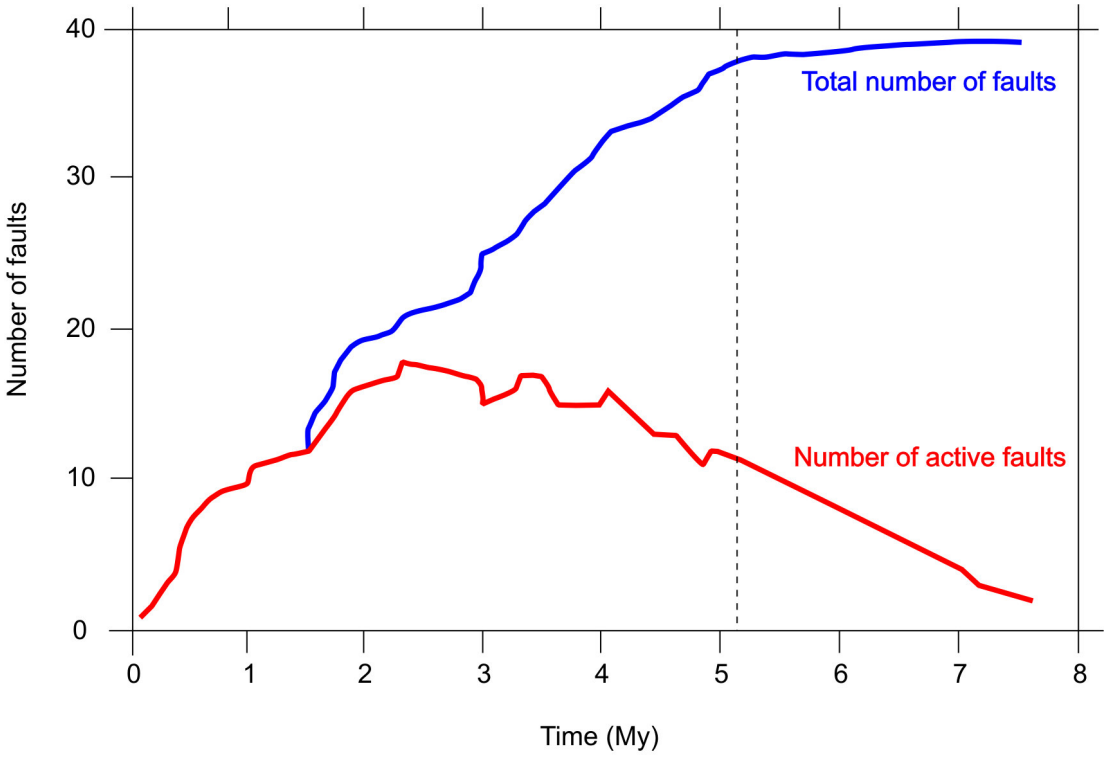

Figure 2.7
Total number of faults and number of active faults as a function of time for a model. Vertical dashed line indicated the point where fault linkage across the entire model is first complete.
Modified from Cowie et al., 2000.

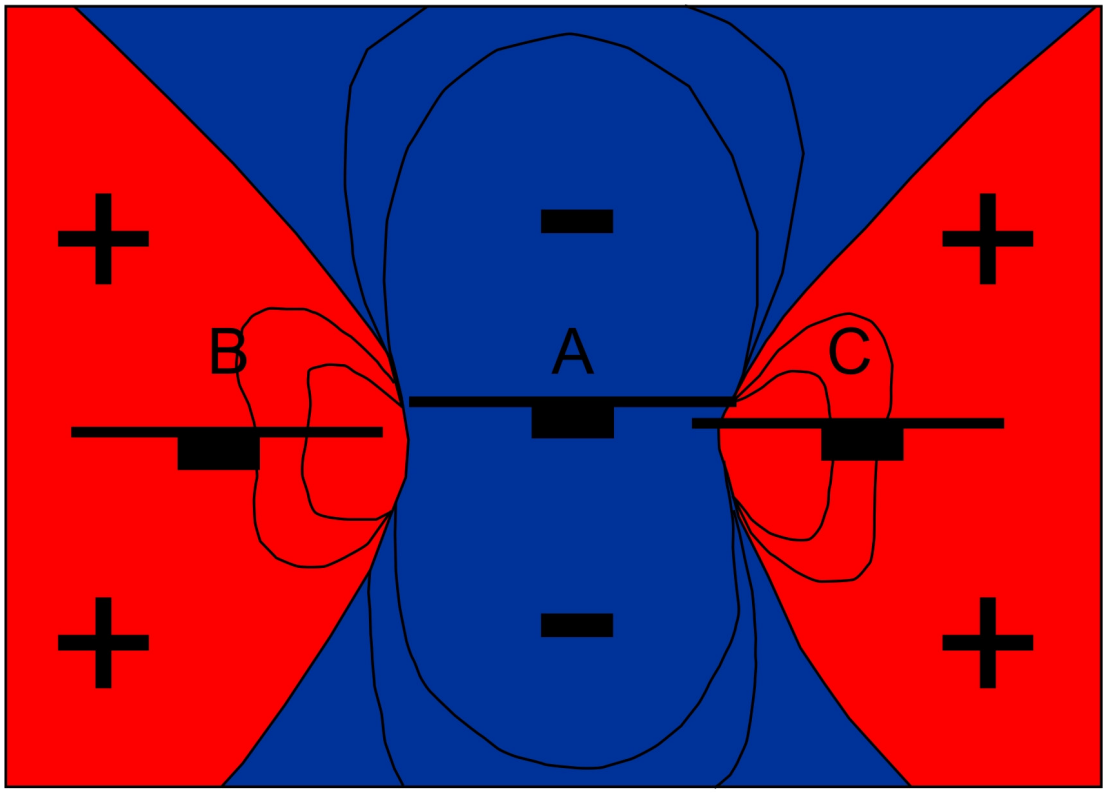

Figure 2.8
Coulomb stress changes due to slip on a 60 degree dipping normal fault (A) which enhances (red) or relaxes (blue) stress on nearby normal faults (B and C).
Modified from Hodgkinson et al., 1996.

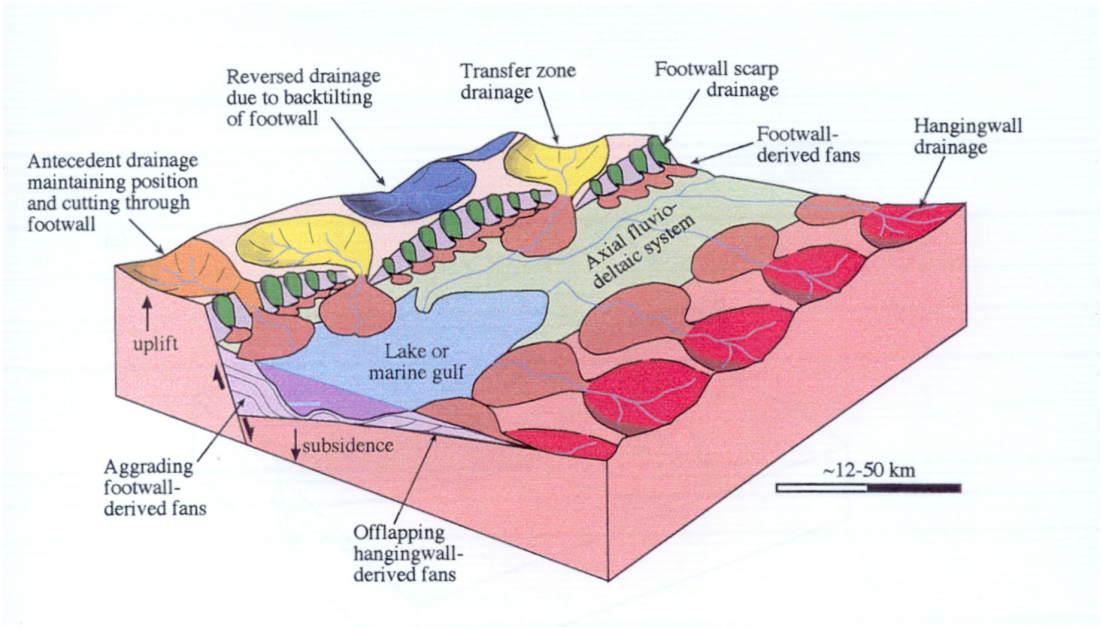

Figure 2.9
Block diagram showing relationship between drainage, deposition and fault segmentation in a half-graben consisting of three normal fault segments. Vertical scale greatly exaggerated. Length of individual fault segments is 12-50km.
After Gawthorpe et al., 1994

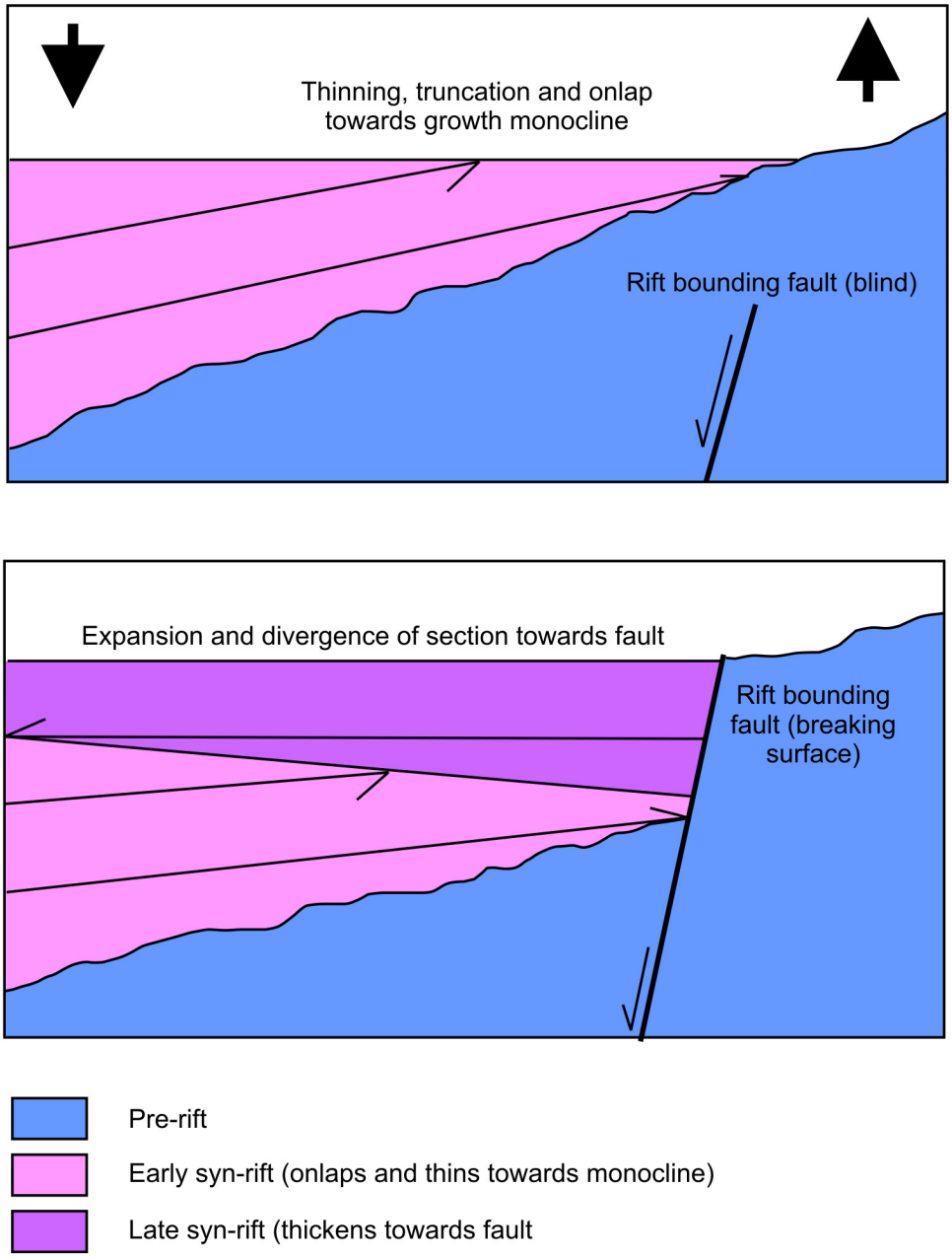

Figure 2.10
Schematic diagram of the evolution of a monocline from above a buried, active normal fault to the eventual breaching of the monocline. This process results in an early syn-rift sequence that onlaps and thins towards the monocline overlain by a later syn-rift sequence that thickens towards the emergent normal fault.
After Gawthorpe et al., 1994

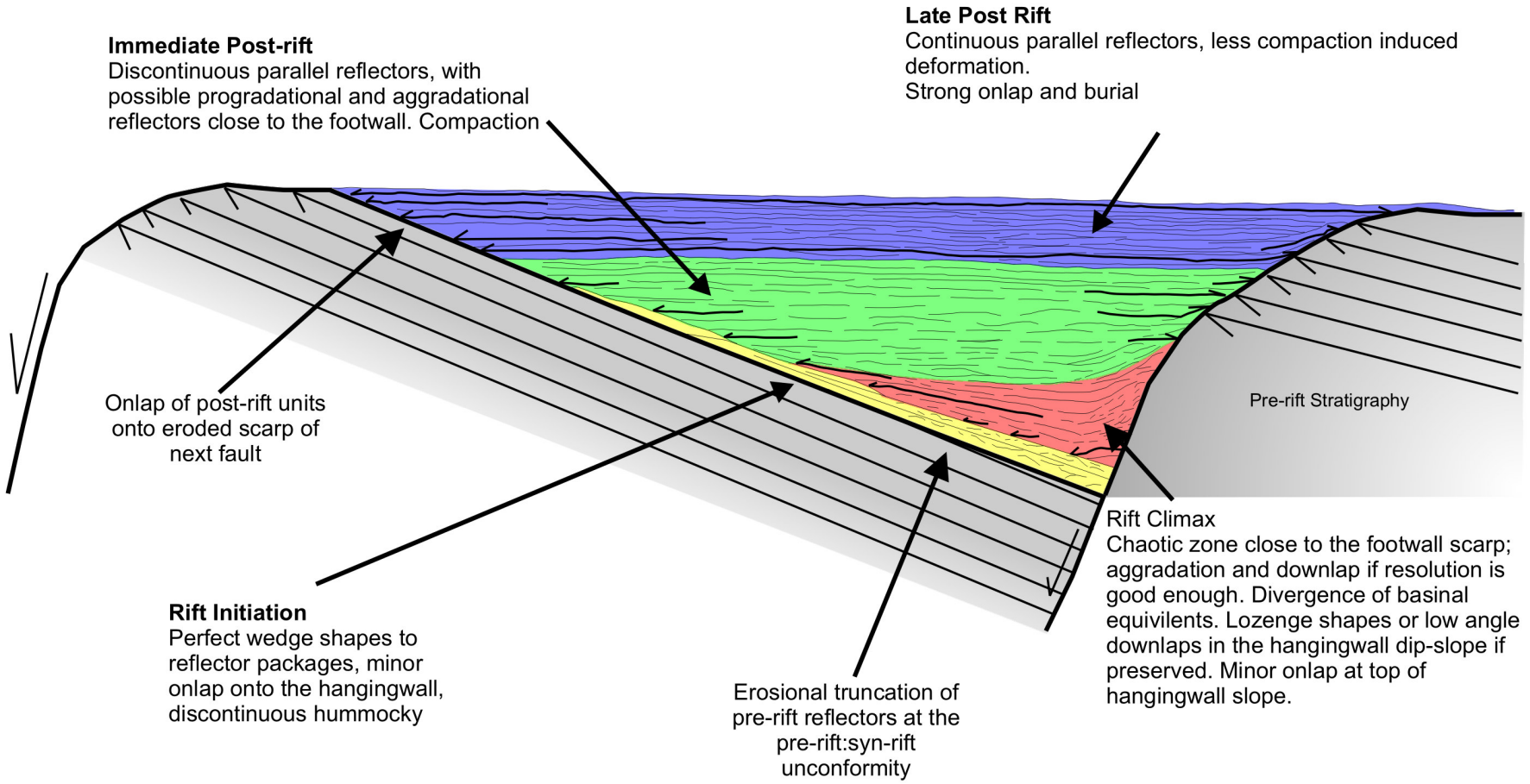

Figure 2.11
Line drawing of an idealised seismic section through an ideal basin, where each tectonic systems tract can be identified. The characteristic seismic expression of each stage is summarised in the captions.
After Prosser, 1993.

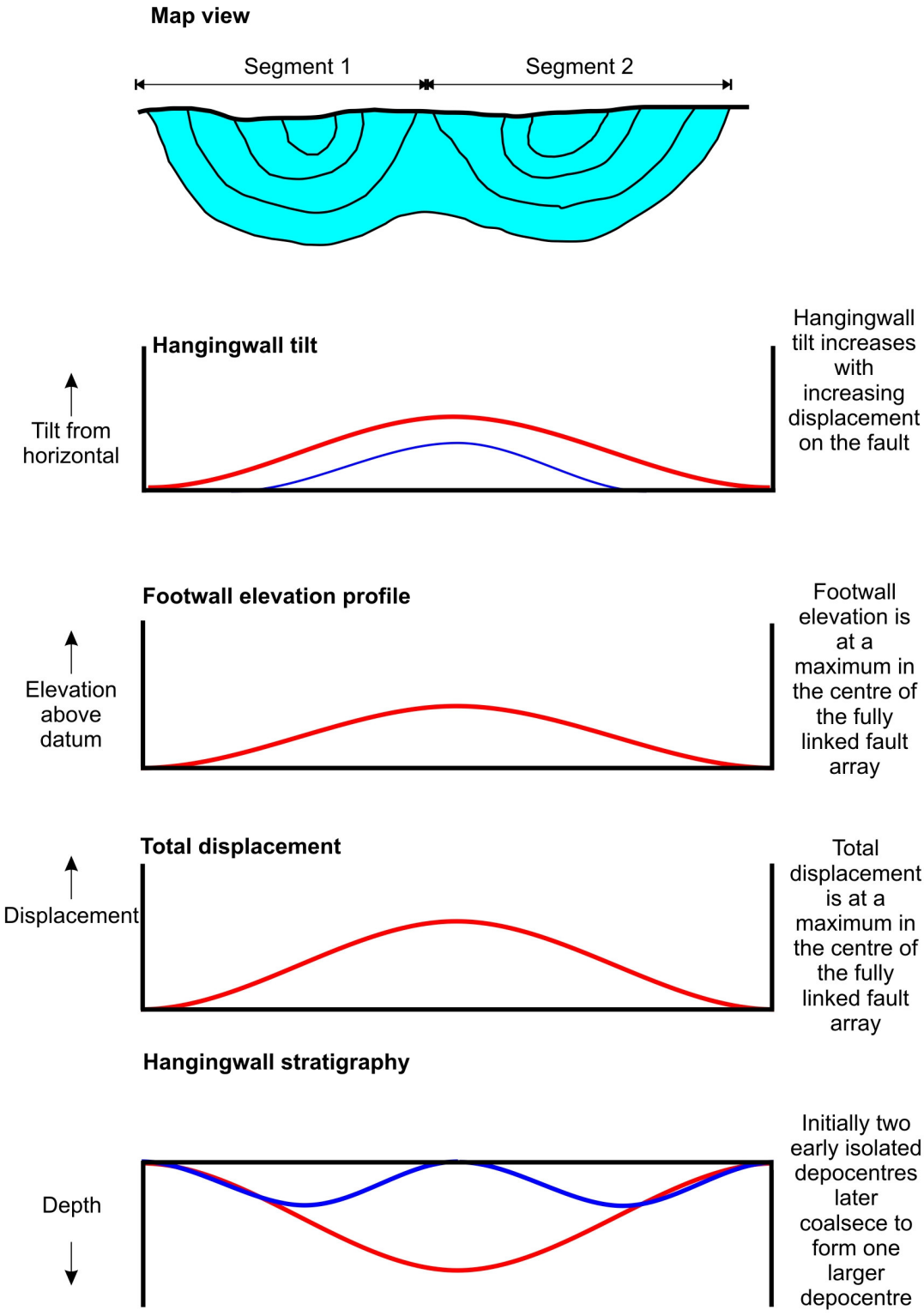

Figure 2.12
Features associated with two overlapping normal fault segments.
Red lines indicate younger features, blue lines indicate older features.
Coloured areas show hanging wall accomodation space.
After Anders and Schlische, 1994

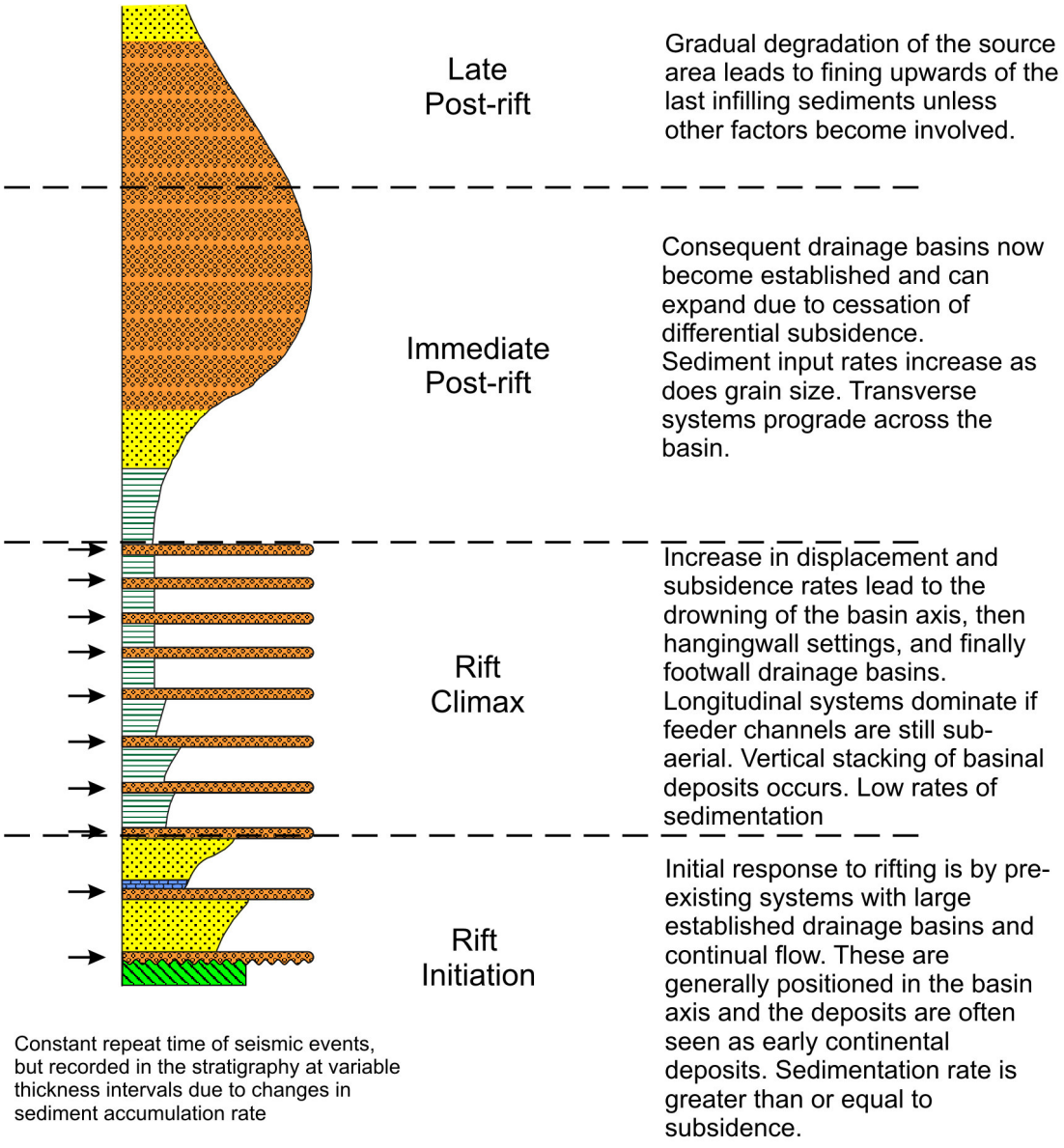

Figure 2.13
A schematic log of the vertical syn-rift stratigraphy through a rift basin centre
After Prosser, 1993.

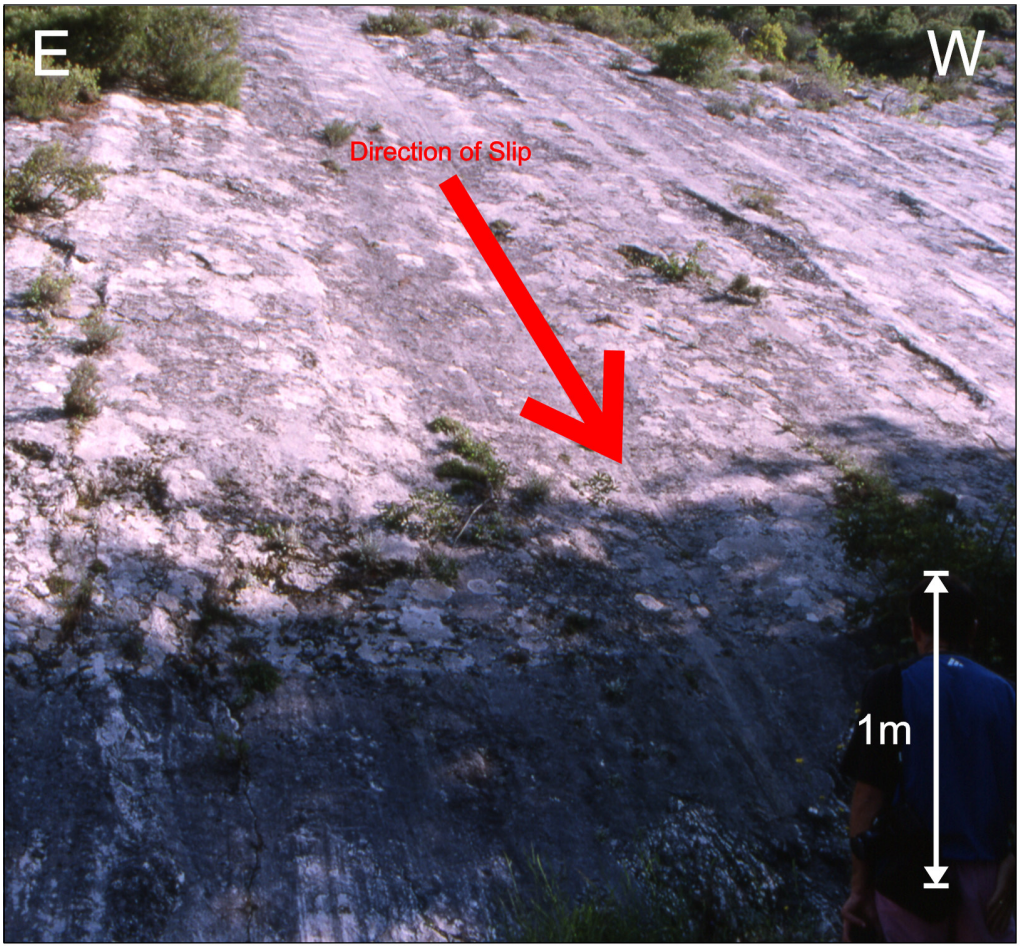

Figure 2.14
Field Photograph of exposed active fault plane of Helike Fault in Gulf of Corinth, Greece
Fault plane shows striations and corrugations indicating direction of slip. Soil horizons indicate magnitude of slip event.

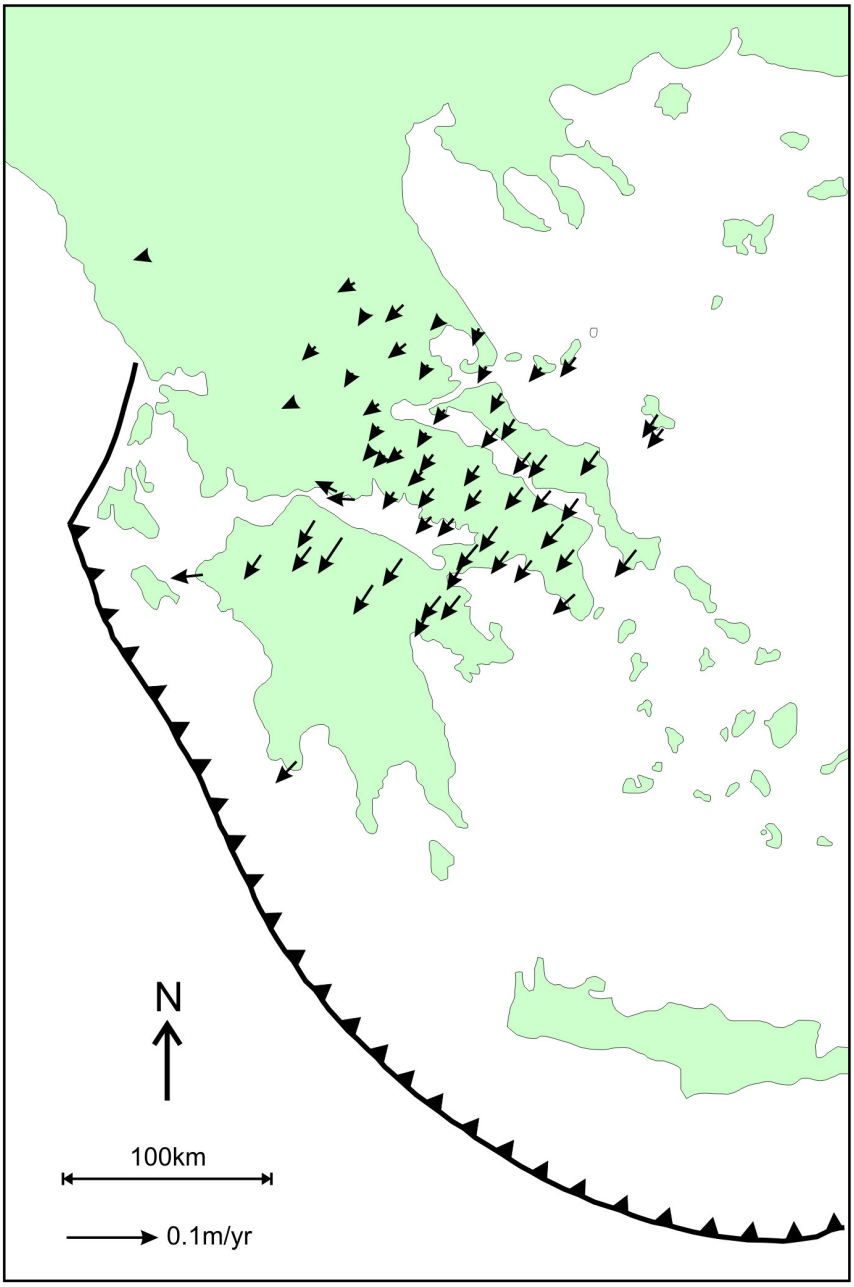

Figure 2.15
Interseismic velocities of CGN sites averaged over the interval 1989-1997, after effects of the Egion earthquake and whole network translations have been eliminated.
After Clarke et al., 1997.

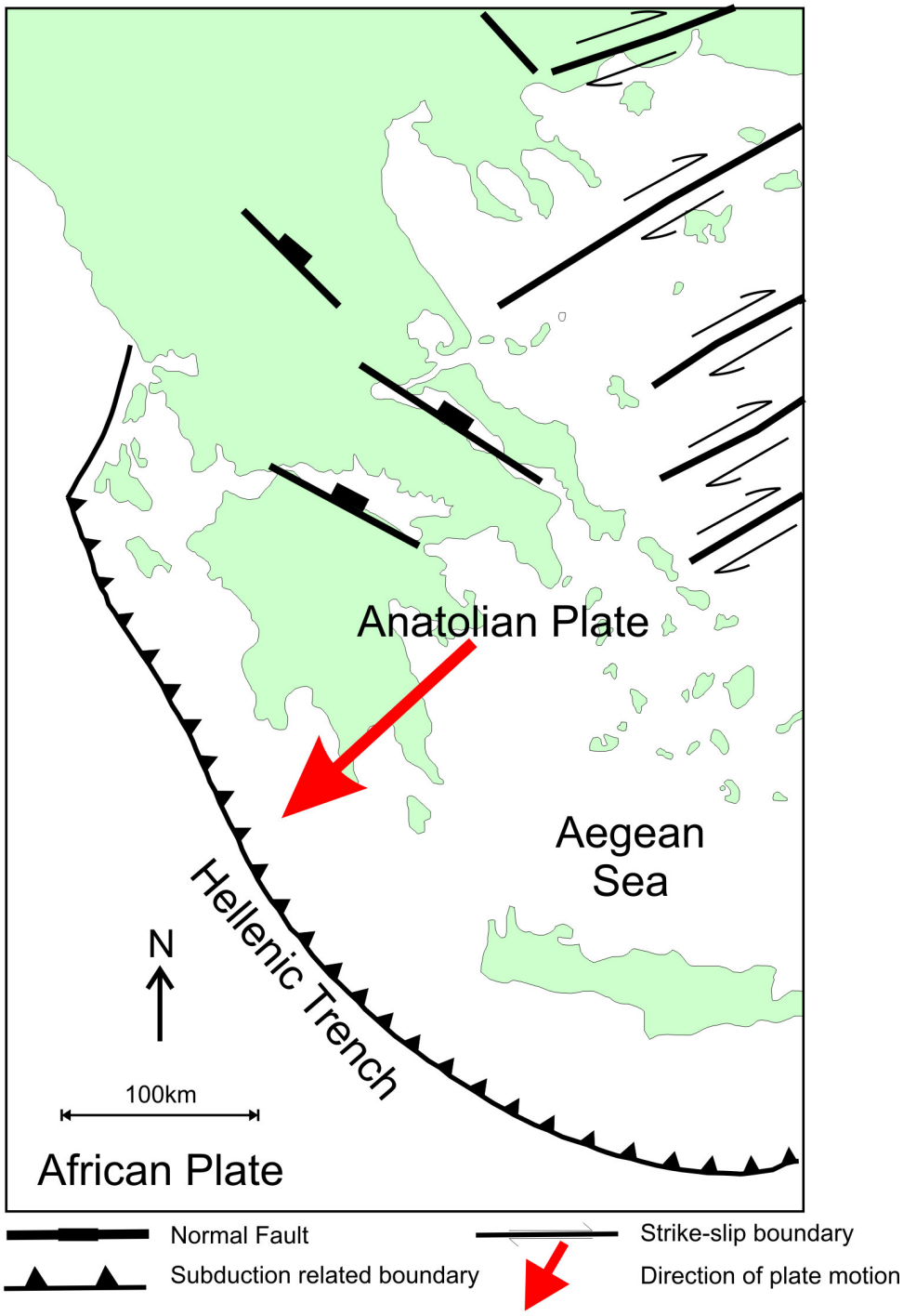

Figure 2.16
Principal tectonic elements of the Aegean Region

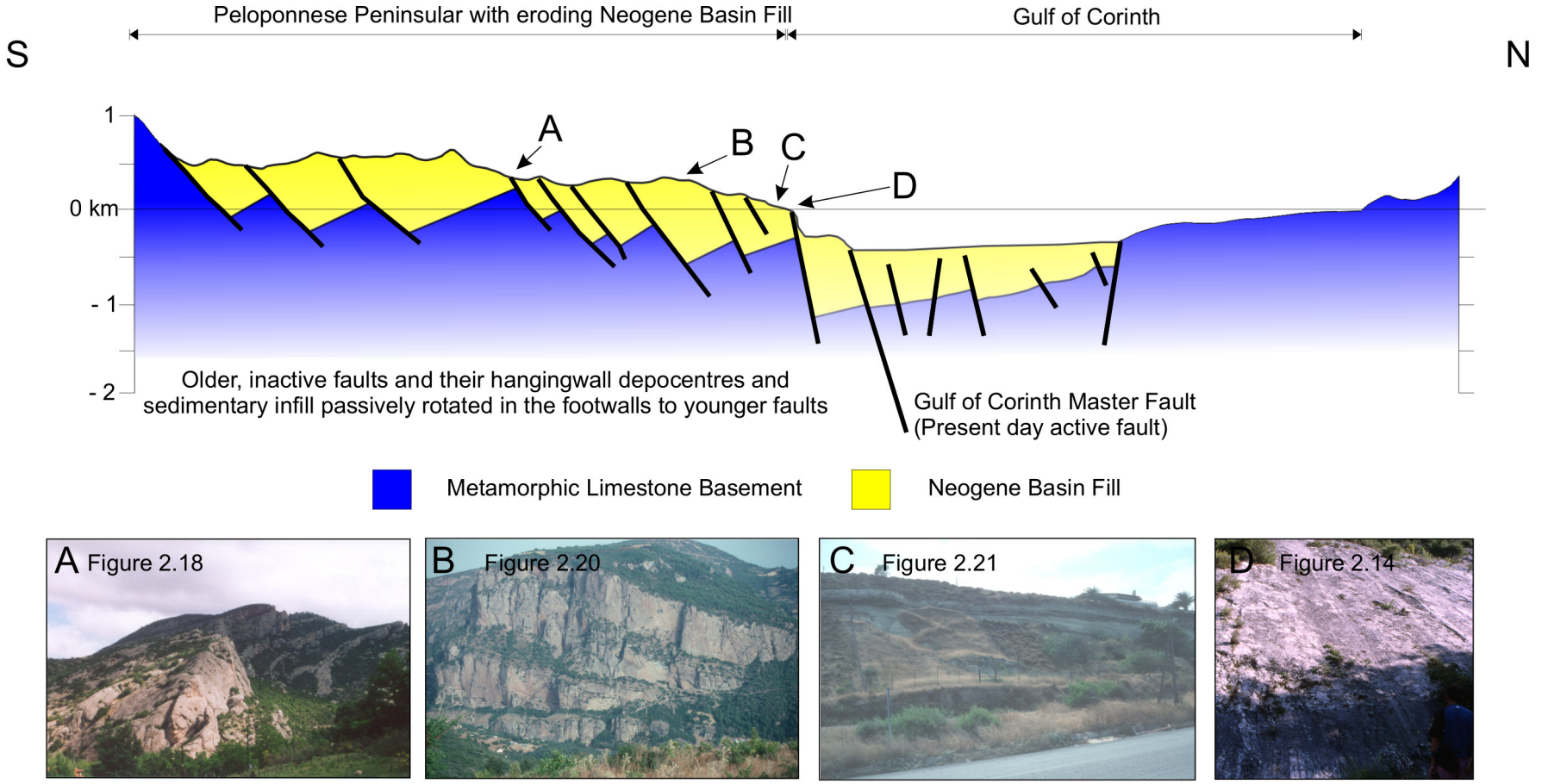

Figure 2.17
Schematic Cross Section across the Gulf of Corinth and Peloponnese Peninsular.
Adapted from Leeder and Jackson, 1993 and Doutsos et al, 1988.

Figure 2.18
Field photograph showing back-tilted sediments in the footwall to a younger fault to the north

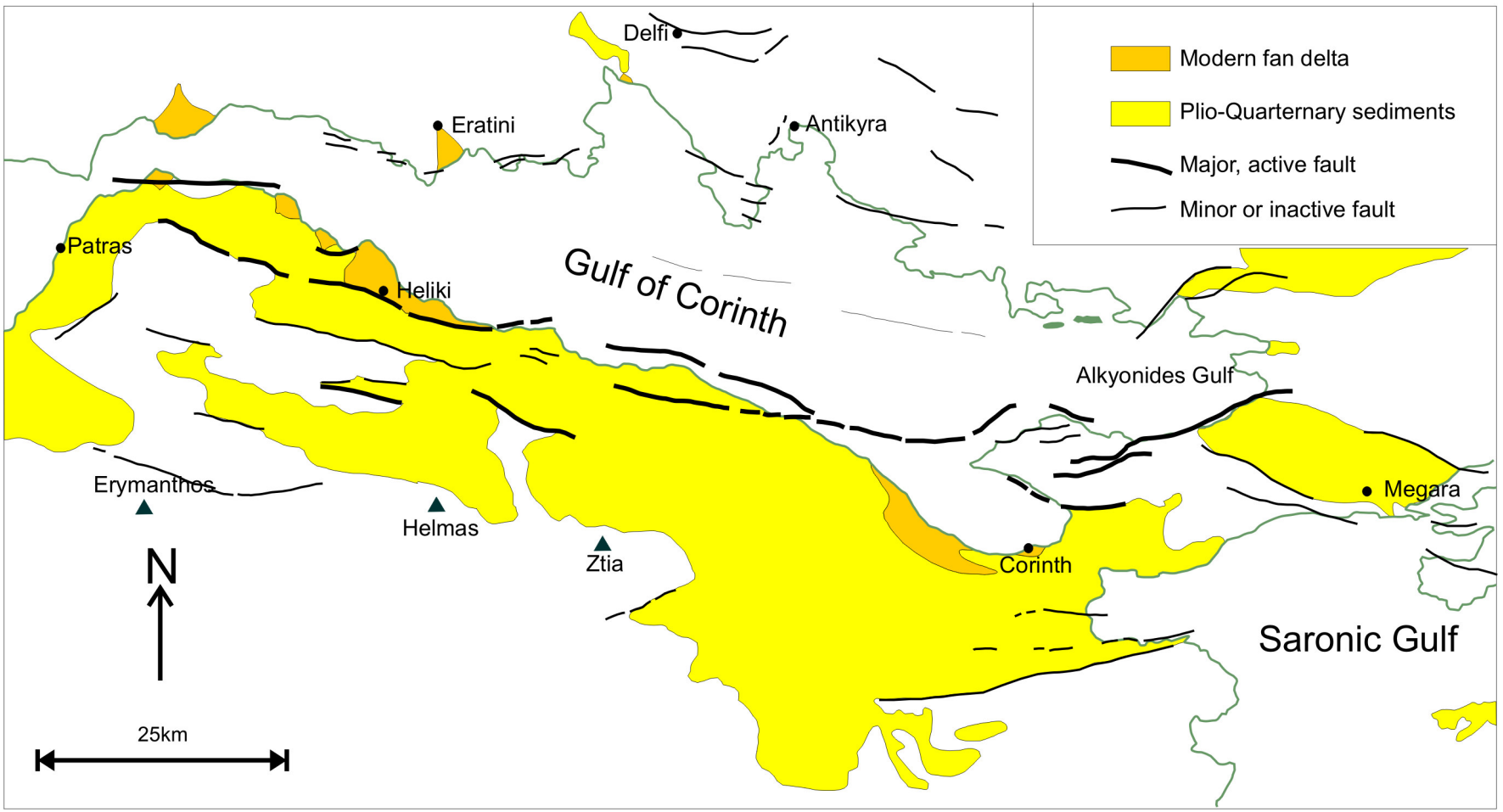

Figure 2.19
Schematic map showing major faults and Plio-Quarternary sediment fill in the Gulf of Corinth, Greece.
After Armijo et al, 1996.

Figure 2.20
Field photograph of cliff section through the Keranitis Fan Delta. The Plio-Pleistocene deposits have been uplifted to 600m above present day sea level.
Migration of normal fault activity has resulted in the uplift and passive rotation of these deposits in the footwalls to younger faults located to the north.

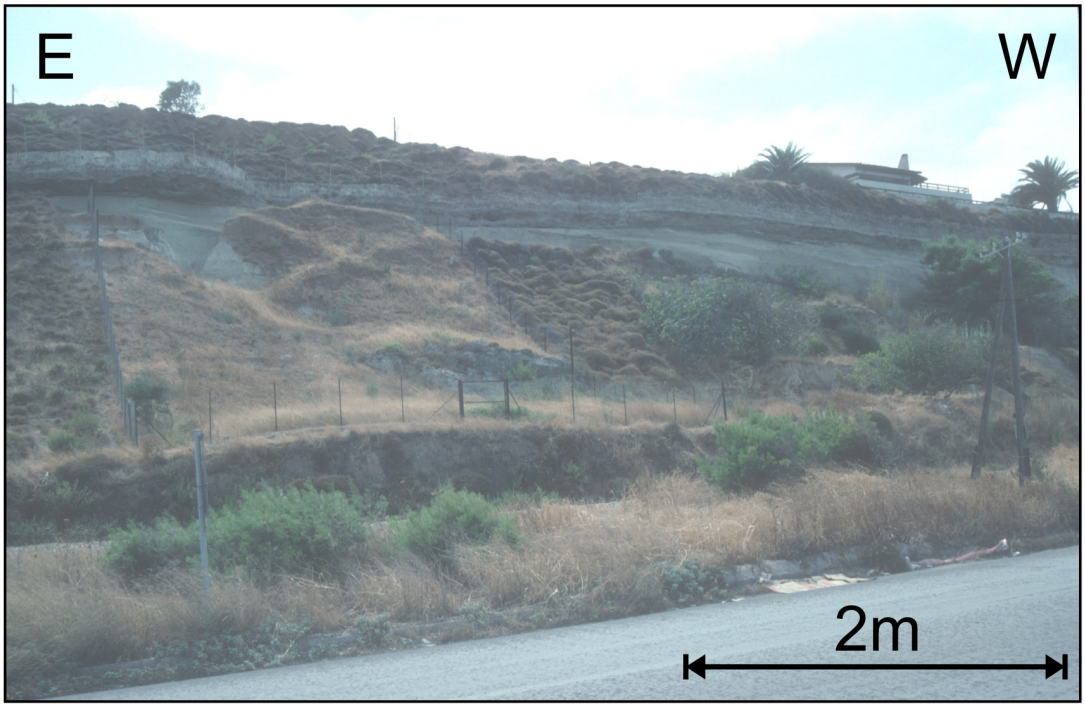

Figure 2.21
Field photograph showing Quaternary terraces uplifted to approximately 10m above present day sea-level.

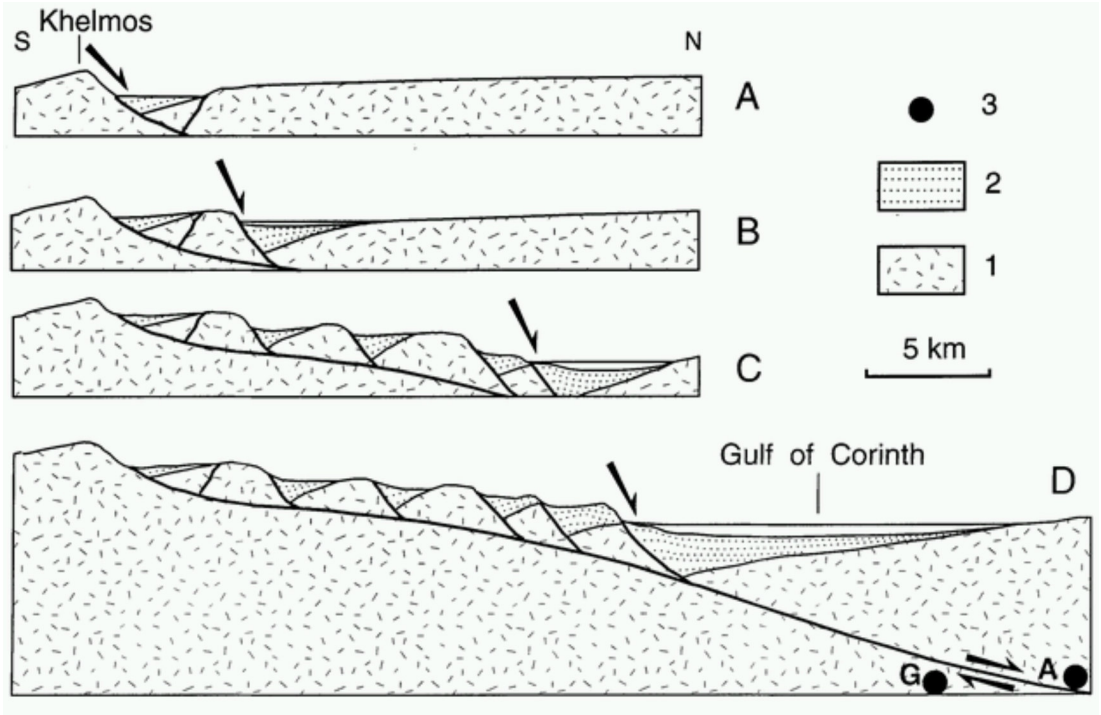

Figure 2.22
Four step sections in development of Corinth-Patras rift
A: Early rift, along active Khelmos fault.
B: During activity of Stolos fault.
C: When Akrata fault was active (300–400 ka).
D: Present state, showing proposed connection of Khelmos detachment with low-angle seismic fault beneath gulf.
1: Alpine basement.
2: Syn-rift sediments.
3: Microearthquakes, recorded along a north-south section located 15 km west of our geological section (from Rietbrock et al., 1996).
4: Centroid location of Galaxidi (G) and Aigion (A) earthquakes projected on section.

From Sorel, 2000.

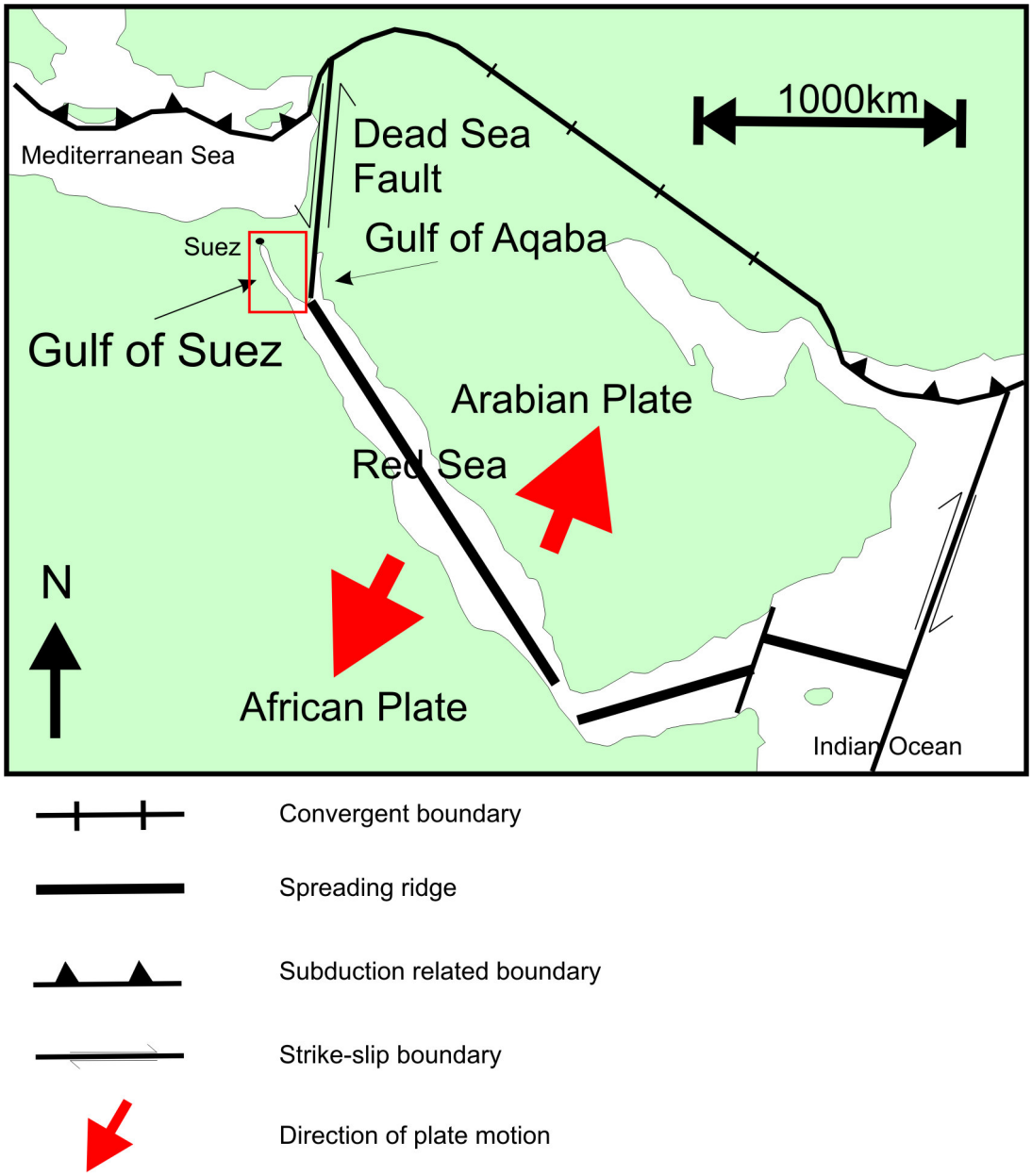

Figure 2.23
Principal tectonic elements of the Red Sea Region
Red box shows location of figure 2.26
After Moustafa, 2002.

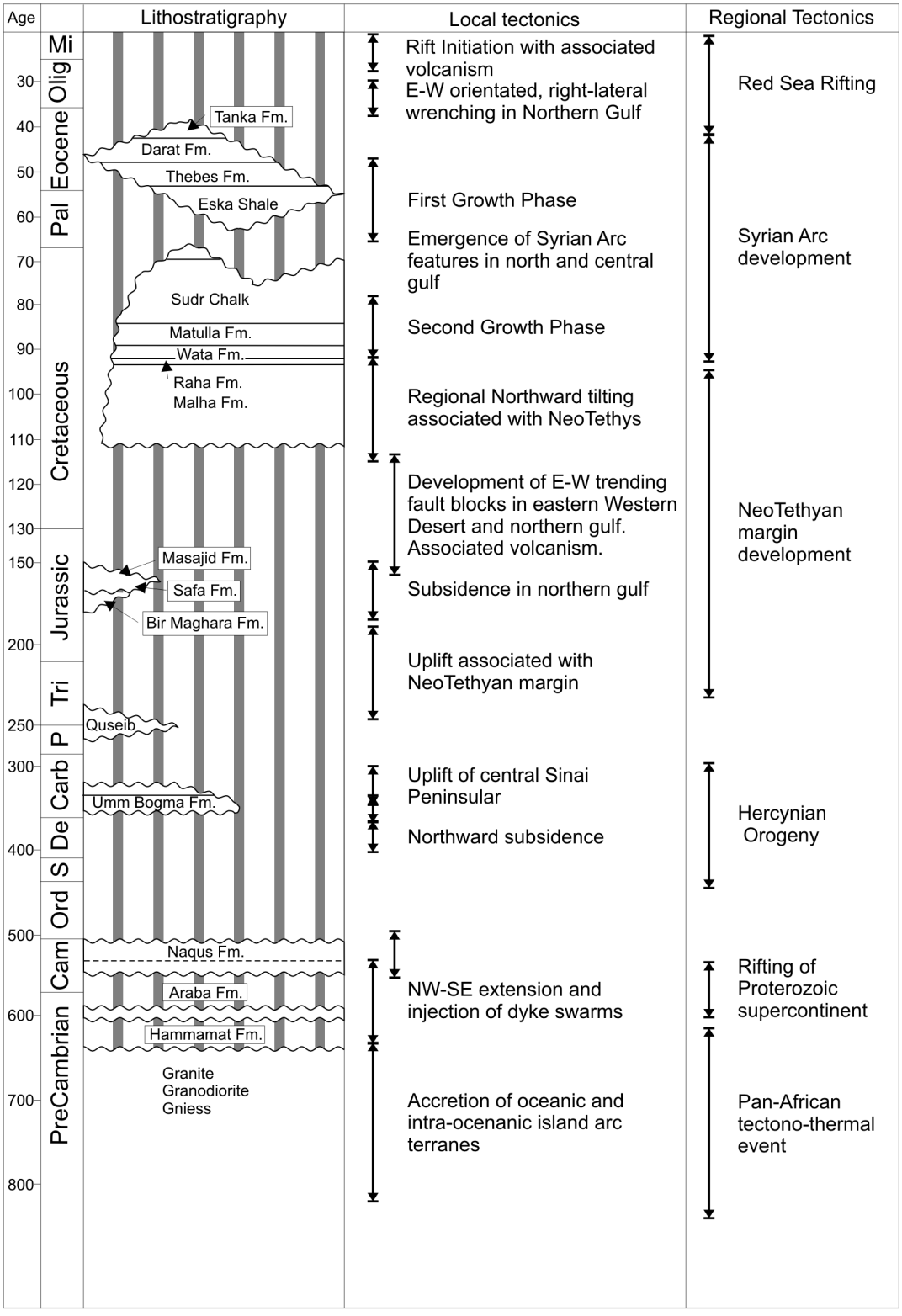

Figure 2.24
Generalised stratigraphy of the Gulf of Suez
Modified from Patton et al, 1994.

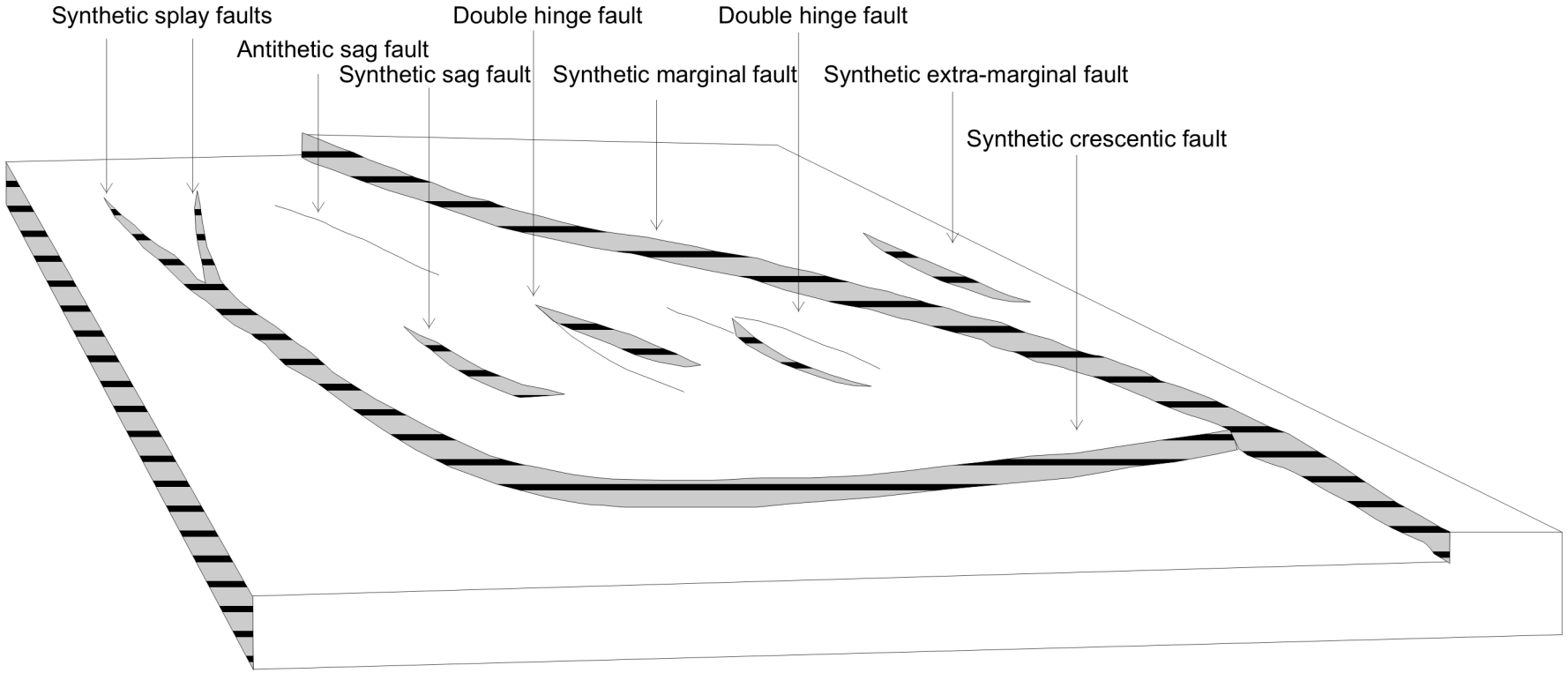

Figure 2.25
Perspective block diagram showing characteristic fault pattern associated with a single synthetic marginal fault in the Gulf of Suez Rift
After Robson, 1971.

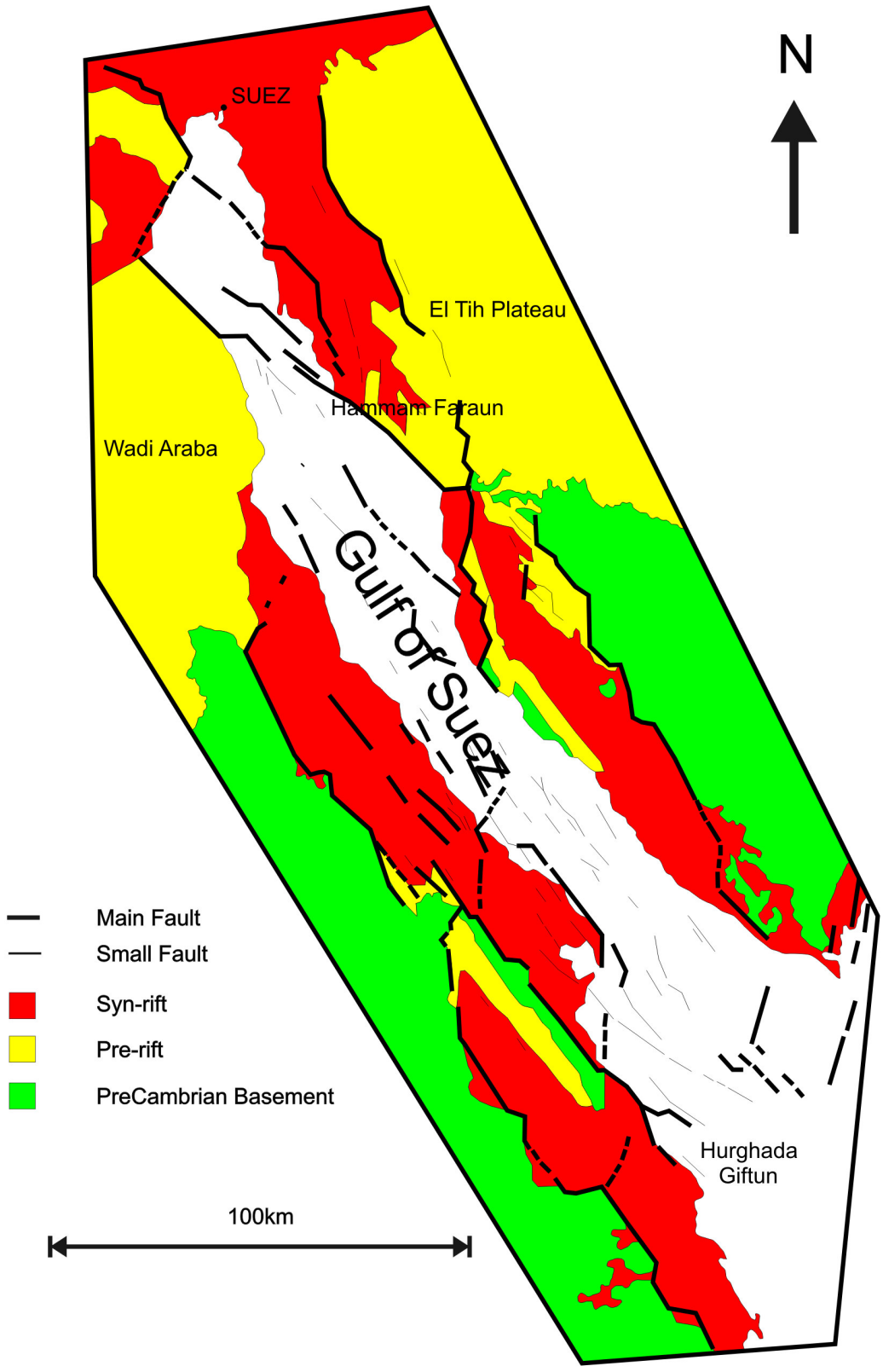

Figure 2.26
Schematic structural map of the Gulf of Suez Rift showing Pre-rift, Syn-rift and Basement stratigraphy
For location see figure 2.23
After Colletta et al, 1988

3. Dataset and Methods

3.1 Introduction and definitions

The principal dataset interpreted in this study adopts a two-fold approach: Interpretation of 2D and 3D seismic data provides regional horizons from which the evolution of the rift basin can be quantified. This is calibrated with exploration, appraisal and development well data. The two fold approach is necessary to obtain a regional, well calibrated dataset.

This chapter will consider the different datasets in turn before examining how the differing data sources have been integrated and synthesised. The chapter will then consider the resolution of the different data types and the resulting time to depth relationships. It will then examine the methods by with the sedimentary sequence is sub-divided and categorised before finally placing the data in its stratigraphic context and examining the sequence stratigraphy of the study area in detail. A detailed understanding of the stratigraphy in the study area is critical to the development of a detailed structural model for the development of the Northern North Sea Mid to Late Jurassic rift province.

3.2 2D and 3D seismic database

The study area is defined by the areal extent of fifty-five 3D migrated seismic reflection surveys (figure 3.1). These cover the majority of the northern part of the East Shetland Basin extending from the East Shetland Platform in the west through the North Viking Graben to the Horda Platform in the east (0˚ to 3˚E), and from the Magnus Basin in the north to the Beryl Embayment in the south (62˚N to 60˚N). The area incorporates in excess of 30 hydrocarbon fields which have been in production since the early 1960's and have oil accumulations in pre-rift sediments back tilted in the footwalls to Late Jurassic normal faults. The total area of 3D seismic data coverage is in excess of 190 thousand square kilometres.

In addition to the 3D seismic database a series of long, regional 2D seismic lines (figure 3.1) with numerous well ties were incorporated within the study area. These provided a tie across areas with sparse or no 3D seismic coverage and in addition provide more extensive regional lines for correlation.

Data on the individual seismic reflection surveys incorporated into this study are presented in appendix 1.

Data quality is variable throughout the study area and is influenced by a number of factors: The seismic data itself is of varying vintages and has been processed using various generations of procedures. The quality of the seismic correlates in a positive manner with age. The position of the data within the rift province also exerts a control over data quality. In the North Viking Graben the syn-rift strata are typically 5000 ms TWT deep and are typically poorly imaged (figure 3.2). In addition, on an individual fault-by-fault basis, data quality in the hangingwall to faults tends to be poorer than in the corresponding footwall, this is again largely due to the deep burial of hangingwall sediments in comparison to the uplifted footwall. In addition, the areas targeted in data acquisition tend to be the footwalls and thus data is processed to preferentially enhance quality in these areas.

Seismic data were analysed using Geoquest's seismic interpretation software Geoframe 3.7.1 (IESX) running on a Sun Microsystems Ultra 60. This software was available in-house at the University of Edinburgh. The software is supported by a telephone helpdesk and hardware and data support is available in-house.

3.3 Well database

The seismic data are constrained by over 560 exploration, appraisal and production wells. The area straddles the United Kingdom-Norway international median line (figure 3.1). Well data was obtained via a number of sources. Paper composite, completion and velocity logs were derived from industrial sources and electronic logs were retrieved from the Common Access Database (CDA). Formation tops were manually read from these logs, validated with biostratigraphic reports (where available) and the corresponding times computed from velocity logs. These are presented on enclosure 1.

In addition, some formation tops and corresponding times over the Kvitbjorn area were received from industry.

Core was examined at the Department of Trade and Industry Core Store in Edinburgh and at ConocoPhillips Core Store in Bergen.

3.4 Integration of well and seismic data

Seismic interpretation was based on seismic-to-well ties and the subsequent lateral extrapolation and correlation of key surfaces. Well ties to key stratigraphic horizons were

read from paper and digital composite logs based on the log character and the classification supplied on the logs in terms of group, formation and member status. This depth information was transformed to two way travel time (TWTT) using calibrated velocity logs and checkshot surveys where available. The data are summarised on enclosure 1. A time shift between well logs and seismic data was encountered in a number of wells and this was corrected for by application of a bulk time shift via comparison with the seabed, top Balder Formation and the Base Cretaceous Unconformity, all are regionally well-identified reflectors which form distinctive signatures on seismic reflection data. The construction of synthetic seismograms was considered to be unnecessary and of inferior quality to use of raw seismic and well data. The large number of different seismic surveys with differing vintages and polarities and varying processing and subsequent merging histories results in it not being possible to reliably tie synthetic seismograms to the seismic reflection data. As a result use of calibrated checkshot surveys and well ties gave a more accurate well to seismic tie.

A database of times and depths to nine regional horizons was constructed (see enclosure 1). Well locations were manually entered into the seismic database using 7 digit latitude and longitude data obtained from the Department of Trade and Industry (UK) and the Norwegian Petroleum Directorate. Formation tops times were then manually interpreted at the position of each individual well to correspond to an individual reflector. Well correlation panels were then constructed. These included in excess of 200 seismic traverse pathways through a number of wells both within a given fault block (pre-rift reflectors) or regionally across the East Shetland Basin (post-rift reflectors). Figure 3.3A and B show examples of the seismic traverse pathways for both a pre-rift correlation and post-rift correlation.

3.5 Resolution

Resolution is the ability to discern that more than one feature is contributing to an observed effect (Sheriff, 1985). The resolution of a structure obtainable with seismic reflection profiling is controlled by the wavelength of the source signal. Seismic reflection surveys are usually designed to provide a specified depth of penetration and a particular degree of resolution of the subsurface geology in both vertical and horizontal dimensions. This section will consider three aspects of resolution; vertical, horizontal and that of throw on normal faults.

Vertical resolution is the minimum distance between two interfaces needed to give rise to two distinct reflections on a seismic reflection profile. It is controlled by the wavelength of

the source signal and a shorter wavelength gives rise to a higher frequency and therefore greater vertical resolution. Resolution declines with depth as the seismic velocity increases. This decrease is amplified by the preferential absorption of higher frequencies as seismic energy travels further into the crust and the signal to noise ratio gets worse. In addition, filters applied at the processing stage commonly remove the highest frequency components of the waveform.

Vertical resolution is also affected by closely spaced, parallel beds where the seismic energy is limited by the frequency of the source signal due to interference effects. The best seismic resolution expected is between one quarter and one eighth of a wavelength under best noise-free conditions (Sheriff, 1985) and is 25-50m for data incorporated into this study.

The vertical resolution of an individual reflector on seismic reflection data is also affected by tuning. Two reflected wavelets of opposite polarity will be separated in time so long as the time thickness between them is greater than half the wavelength of the seismic wavelet. So, the top and base of an individual unit can be resolved if the thickness of the unit is greater than half the seismic wavelet. If the unit is thinner than half the seismic wavelength then the two opposite polarity reflections begin to constructively interfere to form a single reflector with anomalously high amplitude. This thickness is known as the tuning thickness (figure 3.3; Badley, 1985). This tuning effect is most marked if the reflection coefficients at the top and base of a unit have opposite signs. Tuning may result in a modification of amplitudes on seismic reflection data and care has been taken in this study to identify where such effects may be important. In addition, tuning may show features that appear to be onlap which are in fact two reflectors coming close together but not stratigraphic onlap. These are generally associated with amplitude anomalies.

Horizontal resolution is determined by the radius of the Fresnel Zone and the detector spacing. The Fresnel Zone is defined as the area where the seismic wavefront hits on a particular reflector and over which coherent, in-phase arrivals are returned. The radius of the Fresnel Zone determines the lateral resolution of seismic reflection data (figure 3.4). The detector spacing also exerts a control of the horizontal resolution of seismic reflection data. Figure 3.4 shows that for a flat-lying, horizontal reflector, the horizontal resolution is equal to half the detector spacing. For migrated 3D seismic data the horizontal resolution is a function of trace spacing, length of the migration operator, time/depth of an individual reflector and the bandwidth of the data. The data incorporated into this study area is at line spacing 12.5-25m.

The resolution of fault displacement is limited by the wavelength of the seismic wavelet and as with vertical resolution a fault with throw less than one eighth to one quarter of the seismic wavelet would be difficult to resolve on seismic reflection data. The faults in this study can be resolved to approximately 10ms TWT throw. This limitation of data resolution results in the loss of small displacement normal faults and the low displacement tips to larger structures. Previous scaling studies (for example Badley et al., 1990 and Pickering et al., 1997) have applied corrections which are outside the scope of this study.

3.6 Depth conversion

Seismic reflection data are presented in time throughout this study. Depth conversion via an accurate technique, such as the layer-cake method, for an area of 190 thousand square kilometres is beyond the scope of this project. Individual depth conversions have been carried out in the proximity of wells where an accurate depth measurement is necessary for interpretation and analysis. Depth conversation in the Northern North Sea is not an important issue when considering the regional structure of the basin. This is in stark contrast with other areas, for example the Southern North Sea, where the presence of large differences in velocity, such as the presence of salt, require accurate depth conversion. For example the overburden in the Northern North Sea (Base Cretaceous Unconformity to seabed) has a mean velocity of 1.062 and a standard deviation of 0.043. This uniformity of overburden is also shown in a graph comparing time and depth to Base Cretaceous Unconformity which shows a uniform increase in time with depth (figure 3.6). In addition, consideration of time data from the Northern North Sea allows future interpreters raw data to which velocity functions can be applied without consideration of pre-existing prejudices.

3.7 Seismic Interpretation - Methodology

One of the most important factors in understanding the development of extensional basins is identification of the start and end of the rifting episode. This is usually achieved by identification and dating of the syn-rift deposits associated with a specific rifting event. In extensional basins with a half graben geometry, it is assumed that since the overall rift is asymmetric then the syn-rift deposits will be divergent in form. The transition from an underlying parallel stratal geometry to an overlying divergent geometry is traditionally taken as the boundary between pre-rift and syn-rift deposits and the upper transition from divergent

geometries to parallel infill is taken as the transition from syn-rift to post-rift deposits. The end of the rift period is generally difficult to establish but can generally be identified as the marker horizon that forms the base of the first sequence to pass across the upper tip of the fault block undisturbed (Cartwright, 1991). This method requires detailed examination of the stratigraphy in both the footwall and hangingwall of an extensional fault in order to identify the earliest and latest times that stratigraphic expansion into the fault occurred.

Bertram and Milton (1989) stated that determination of the structural evolution of a basin could not be reconstructed from sedimentary thickness alone without data on paleobathymetry. They defined two classes of geological horizon: Profiles, time lines bounding depositional units, and traces which form at known water depth and contain implicit paleobathymetric information. The history of a basin can only be determined uniquely if the sediments contain enough traces. Their work used seismic traces to reconstruct the Triassic to Recent subsidence history of the Central and Northern North Sea. The limitations of the reconstruction of basin history from sedimentary history alone has largely been overcome by the large number of tools available to the geologist studying the development of the Mid to Late Jurassic Northern North Sea rift province. Integration of detailed biostratigraphic, paleoenvironmental and paleobathymetric data from well logs with detailed interpretation of seismic reflection data largely removes these limitations.

The methodology described above has also been critically appraised in a number of papers. Cartwright (1991) used the Coffee Soil Fault in the Central Graben as an example of how stratigraphic onlap onto a remnant fault scarp during a post-rift interval can be mistaken for syn-rift deposition leading to an error in the timing of the end of rifting. This results from a fault which has an under-filled hangingwall depocentre at the time of termination of rifting. The problem can be overcome by detailed interpretation of the internal morphology of the syn-rift stratigraphy, a process which is becoming more accurate with the development of seismic reflection data quality.

In addition, Cartwright, (1991) states that in rift basins which are prone to sediment starvation the earliest time that stratigraphic expansion into a normal fault is observed may lag significantly behind the onset of fault controlled subsidence. This is not considered to be a problem in the northern part of the North Sea Basin where a complete stratigraphic succession is recorded in wells penetrating hangingwall depocentres, for example 34/8-7 in the hangingwall to the Visund Fault (figure 3.7).

Recent work in the Faroe-Shetland Channel has highlighted the need for a seismic interpreter to understand the limitations and artefacts that form an inherent part of seismic reflection

data (Bulat, 2005). The work shows that commercial seismic data can be successfully used for purposes other than which they were originally designed and that knowledge of the acquisition and processing parameters may help an interpreter understand any variation in observed image quality. In particular, the work highlights the need for care when interpreting data at a depth at which the survey was not targeted. As previously discussed, this is a problem in the North Viking Graben where a combination of great depth and the graben not having been the target area result in it not being possible to interpret syn-rift reflectors in the hangingwall to the Visund-Gullfaks Fault.

In this thesis, nine regionally identifiable horizons have been interpreted. The resulting two-way time maps are shown in appendix 5. Throughout the thesis throw is used as a proxy for fault displacement. Throw is measured in time as vertical offset at Top Statfjord Formation level across the fault plane (figure 3.8).

3.8 Stratigraphic Context

3.8.1 Regional setting

The Jurassic sediments of the North Sea were deposited in an intraplate setting south of the weakly linked Laurentian, Greenland and Fennoscandian Shield areas and north of the Tethyan Ocean which was experiencing active extension (Ziegler, 1982, 1990). The steady rise in sea level which commenced in the Late Triassic established marine conditions throughout the Northern North Sea in the Early Jurassic. In the Early Jurassic, deposition was predominantly controlled by erosion of the surrounding shield areas, with either permanent or transient land areas providing sediment to an epeiric sea, comprises an array of shallow marine shelves separated by deeper troughs (Ziegler 1982, 1990). However, following thermal doming in the Middle Jurassic (Underhill and Partington, 1993, 1994), erosion removed much of the presumed Lower Jurassic marine cover enabling deltaic systems to build outwards from the volcanically updomed area, depositing the sandstones which comprise the Brent Group. As the dome lost support, a trilete rift system developed in the later Jurassic comprising the Viking and Central Grabens and the Moray Firth. The dominant depositional regime returned to marine as shales accumulated in the basin centres while local marine sands formed on the basin flanks and around intra-basinal highs.

3.8.2 Biostratigraphy and sequence stratigraphy

The Middle and Upper Jurassic of the North Sea (Late Oxfordian to Late Ryazanian) is subdivided into eleven genetic stratigraphic sequences using biostratigraphically constrained maximum flooding surfaces (MFS), (Partington et al., 1993). A genetic stratigraphic sequence is a package of sediment recording a significant episode of basin margin outbuilding and basin filling, followed by periods of widespread basin margin flooding (Galloway, 1989). A MFS is a key marine condensed horizon identified using sedimentological, lithostratigraphic, biostratigraphic and seismostratigraphic data. MFS are the most prominent throughgoing reflectors in the basin fill and generally show downlap or marine onlap on seismic reflection data. The MFS represent basin-wide isochronous events across northwest Europe and can be recognised in exploration wells and at outcrop from Greenland to the Wessex Basin (Partington et al., 1993). The MFS have been biostratigraphically calibrated to provide a consistent stratigraphic framework. Each MFS has been named by reference to the standard ammonite biozonation scheme for the Jurassic (Woolam and Riding, 1983). Key MFS are named by Partington et al., (1993; figure 3.9).

The stratigraphy in the following section is identified according to a British Stratigraphic Framework and is correlated with Norwegian stratigraphic nomenclature. The age of the Mesozoic stages included in the discussion below are standardised to the International Commission on Stratigraphy Geological Timescale 2005 (figure 3.10).

A stratigraphic outline for the East Shetland Basin is shown in figure 3.11.

3.8.3 Pre-rift Stratigarphy

3.8.3.1 Lower Jurassic Stratigraphy

Lower Jurassic rocks conformably overlie Triassic rocks throughout most of the Northern North Sea. Lower Jurassic sedimentation in the Northern North Sea was dominated by the prevalence of widespread open marine conditions which resulted in the deposition of laterally continuous coarse clastic units. The Early Jurassic was a time of relative tectonic quiescence in the Northern North Sea (Badley et al. 1988) and sedimentation is inferred to have occurred in a shallow, well-aerated epicontinetnal basin (Underhill, 1998) which was thermally subsiding following the end of the Permo-Triassic rift episode.

3.8.3.2 The Banks Group

The Banks Group is predominantly arenaceous, representing a fluvial and coastal depositional system (Roe and Steel, 1985). The unit is transitional between the underlying Triassic continental red beds and the overlying marine muds and sands of the Dunlin Group. The Banks Group does not have good biostratigraphic control due to its continental nature. However, lithostratigraphically it comprises a lower, Statfjord Formation and upper, Nansen Formation comprising the Raude, Eriksson and Nansen Members.

The Statfjord Formation (Rhaetian to Sinemurian)

The Statfjord Formation is conformable with and overlies the Upper Triassic Hegre Group throughout the Northern North Sea. It is subdivided into the Raude, Erikson and Nansen Members. At its base the formation comprises grey, green and sometimes red shale interbedded with thin siltstones, sandstones and dolomitic limestones. Above are massive white to grey sandstones interbedded with grey to brown shales. The top part of the formation consists of massive white, fine to coarse grained sandstones interbedded with grey, silty, micaceous, lignitic shales. An upward increase in marine influence is seen throughout the Statfjord Formation and the formation exhibits a transition from semi-arid continental to more humid shallow marine sediments (Doré et al., 1984). In the upper sections of the formation coarse sandstones with pebble beds, cross bedding and channel structures appear to have been deposited in a coastal environment. The topmost units contain marine fossils and glauconite. This is interpreted to be as a result of eustatic sea level rise which introduced widespread marine conditions to the basin during the deposition of the Statfjord Formation.

The base of the formation is defined by an upward change from the predominantly red, shaly Hegre Group to a more arenaceous, varicoloured sequence. The transition is only visible in some well sections.

Sandstones of the Statfjord Formation form important reservoirs in the East Shetland Basin, for example the Alwyn, Brent, Statfjord, Gullfaks and Snorre fields.

The Nansen Formation (*Hettangian – Sinemurian)*

In the East Shetland Basin the Nansen Formation predominantly comprises medium to coarse grained, fairly well sorted, occasionally calcite cemented sandstones with occasional intercalated shales. The sands are cross-bedded in places and contain horizontal and vertical burrows in addition to wave-ripple lamination. The shales yield marine fossils. The unit reaches a depositional thickness of 50m in the East Shetland Basin and oversteps the older members of the Statfjord Formation to the west. The Nansen Formation was deposited in a shallow marine environment in the East Shetland Basin (Deegan and Scull, 1977). The upper boundary of the Nansen Formation is defined by a downward change from mudstones of the Amundsen Formation to sandstones, reflected by a distinct downward decrease in gamma-ray values. The lower boundary is defined by a transition from interbedded sandstone, mudstone and minor coals of the Statfjord Formation to the cleaner sands of the Nansen Formation.

In the Norwegian sector, and formally in the UK sector, (Deegan and Scull, 1977) the Banks Group is known as the Statfjord Formation and comprises the Raude, Eriksson and Nansen members.

The Raude Member (Hettangian to Sinemurian)

The Raude Member is characterised by fine to very coarse grained varicoloured sandstone with interbedded varicoloured siltstones up to 4m thick. It has been interpreted as a braided stream deposit (Deegan and Scull, 1977), a floodplain dominated succession with meander channels (Kirk, 1980; Chauvin and Valachi, 1980) and as a complex system of distal fans and coastal floodplains (Roe and Steel, 1985). It reaches a maximum depositional thickness of 50m in the East Shetland Basin.

The Eiriksson Member (Rhaetian-Hettangian)

The Eiriksson Member is characterised by sandstones interbedded with grey shales. The sandstones are white to pale grey, medium to coarse grained and extensively cross-bedded. The environment of deposition is uncertain and has been interpreted as coastal barrier, mouth bar and swamp (Deegan and Scull, 1977), sinuous stream, braided stream and coastal plain (Kirk, 1980, Chauvin and Valachi, 1980), or coastal floodbasin and lagoonal bay (Roe and

Steel, 1985). It reaches a maximum depositional thickness of 160m in the East Shetland Basin.

3.8.3.3 The Dunlin Group

The Dunlin Group conformably overlies the Statfjord Formation and is separated into four main units; The Amundsen, Burton, Cook and Drake Formations. The four formations are recognised in almost all exploration wells in the basin, but are absent from the crests of some tilted fault blocks where they have been removed by erosion. All four of the formations thicken towards the North Viking Graben where they reach a maximum depositional thickness greater than 250m and thin to zero on the margins of the East Shetland Basin. The group is characterised by dark to black shallow marine shales and white to light grey, fine to medium grained sandstones which are Sinemurian to Toarcian in age. It reaches a drilled thickness of 600m in the Northern North Sea. The lower boundary with the Statfjord Formation and the upper boundary with the Brent Group are both marked by a high gamma-ray peak. The Dunlin Group is recognisable over most of the East Shetland Basin.

The Amundsen Formation (Sinemurian to Pliensbachian)

The Amundsen Formation marks the onset of Dunlin Group deposition. It is marked by a change from the variably cemented sandstones of the Nansen Formation to bioturbated and carbonaceous mudstones and siltstones which are locally carbonaceous and pyritic. The lower units of the Amundsen Formation are characterised by light to dark grey, non calcareous mudstones and siltstones which are in part carbonaceous and pyritic. These units grade up to fine grained sandstones. The sands increase in prominence towards the top of the formation and locally contain kaolinite, glauconite and mica. The unit was deposited on a shallow shelf under marine conditions as sea level continued to rise throughout the Early Jurassic (Deegan and Scull, 1977). The unit reaches a maximum thickness of 109m in block 3/15 in the East Shetland Basin. The formation is present over most of the East Shetland Basin and extends eastwards into the Viking Graben. It ranges in thickness from 0-110m, but is thin or missing over some structural highs.

The base of the formation is marked by the base of the Dunlin Group (above) the top of the unit is marked by the change to the more regular gamma-ray and sonic log of the overlying Burton Formation.

The Burton Formation (Sinemurian - Pliensbachian)

The lower boundary of the Burton Formation is marked by a transition to mudstones. The formation is dominantly dark to reddish grey, soft, non-calcareous claystones and shales with thin sandstone bands. It was deposited in a low-energy setting throughout most of the East Shetland Basin which may have had restricted sedimentation at the time although the unit is present throughout most of the Northern North Sea (Underhill, 1998). It reaches a maximum depositional thickness of 65m thick in the East Shetland Basin.

The upper and lower boundaries of the formation are identified by its distinct internal acoustic character: both the gamma-ray and sonic logs show a smooth, constant character throughout the formation.

The Cook Formation (Pliensbachian to Toarcian)

The Cook Formation is a laterally persistent, fine to coarse grained sand-prone unit which sits between the mud-prone Burton and Drake Formations. The sands are white to greyish brown, sub-angular to sub-rounded and well sorted with silica cement. Occasional mica, glauconite, carbonaceous material and carbonate cement is also present. The formation was probably deposited in an offshore setting and is up to 70m thick in the East Shetland Basin (Johnson et al., 1993). The formation is distinguished from the units above and below by a decrease in gamma-ray and increase in velocity on the acoustic logs. It is found throughout the East Shetland Basin where it locally forms a reservoir interval.

The Drake Formation (Toarcian - Bajocian)

The Drake Formation comprises carbonaceous, very fine siltstones and shales. In addition towards the top, the formation commonly comprises beds of oolitic sideritic ironstones with occasional belemnites. The formation is commonly up to 60m thick in the North Viking Graben but thins over intrabasin highs. The top of the Drake Formation is commonly marked by an erosion surface (sequence boundary) often referred to as the Mid Cimmerian Unconformity (Underhill and Partington, 1993, 1994). The dominance of mud in the unit means it is easily recognisable by a distinct gamma log signature because of its high radioactive response. The unit is widely distributed throughout the East Shetland Basin and is interpreted to have been deposited in a prodelta and delta environment (Doré et al., 1984).

3.8.3.4 Middle Jurassic Stratigraphy

The boundary between Lower and Middle Jurassic sediments in the East Shetland Basin is traditionally considered to be a widespread correlative conformity marked by a basinward shift in facies known as the Mid Cimmerian Unconformity (Underhill and Partington, 1993, 1994). Its formation is linked to the inferred presence of a warm, transient and diffuse hotspot of buoyant material present in the North Sea which resulted in doming and subsequent erosion of the Early Jurassic units. The 'North Sea Dome' as it is known, instigated non-marine fluvio-deltaic deposition as recorded in the Middle Jurassic Brent Group. However, in the East Shetland Basin, the Brent Group sits conformably on the underlying Lower Jurassic Dunlin Shales.

3.8.3.5 The Brent Group

The Brent Group is a deltaic sequence which built out northwards from the North Sea Dome and represents a major regressive-transgressive sequence which is postulated to have been deposited between the Late Toarcian and Middle Bathonian (Ryseth, 1989) or post Aalenian (Helland-Hansen et al., 1989). It has five constituent formations, the Broom, Rannoch, Etive, Ness and Tarbert (BRENT) Formations designated by Deegan and Skull (1977). The Brent Group records three distinct phases of sedimentation: The Broom Formation documents a sub littoral sand sheet deposited by an estuarine channel-shoal system, the Rannoch, Etive and Ness Formations record the shoreface and coastal plain progradation of a major delta front and finally, the Tarbert Formation reflects abandonment of the delta and is a transgressive sequence. It forms the principal reservoir in the East Shetland Basin.

Brent Group sediments are present throughout the East Shetland Basin where their thickness ranges from zero over some tilted fault blocks to a maximum of 300m in their hangingwall depocentres. The lateral extent of the Brent Group is defined by the progradational extent of the delta. The northern edge of the Brent delta is located within the study area and has been a subject of disagreement in the literature. The Brent Group shales out to the north (between 61˚30N and 62˚N) where the sand-dominated Rannoch and Etive Formations are not present. In the study area, the Brent Group reaches a maximum of 500m depositional thickness but is in general 100-300m thick.

The base of the group sits on a disconformity with the underlying shales. This is clearly visible on logs. Similarly the sharp upper contact with the overlying mud-dominated Heather

Formation is a prominent log marker. The Brent Group is present throughout the East Shetland Basin.

The Broom Formation (Aalenian)

(Oseberg Formation in Norwegian Waters)

The base of the Broom Formation sits upon the Mid Cimmerian Unconformity.

The formation comprises medium to coarse-grained, poorly sorted, cross stratified marine sandstones interpreted to be local, fault related deposits fed from the East Shetland Platform to the west (Morton, 1985; Richards, 1990). They are commonly carbonate cemented. The sands are locally interbedded with mudstones exhibiting floating, coarse sand grains. Burrowing is common in some horizons and the presence of the bivalve *Arenicola* indicates a shallow marine environment of deposition. The Broom Formation has been interpreted to be tidal-flat sands (Hay, 1978), offshore sheet-sands (Budding and Inglin, 1981) or cliff-base beach deposits (Eynon, 1981). However, the formation shows an overall eastward thinning and an overall eastward trend from shallow to deeper water, suggesting that the Broom Formation was deposited as a fan delta system, like the coeval, but geologically separate Oseberg Formation on the eastern side of the North Viking Graben (Graué et al 1987). The uppermost parts of the formation are transgressive and probably interfinger with the overlying Rannoch and Etive Formations (Steel, 1993). The formation ranges in thickness from a maximum of 50m along the western edge of the basin to zero in the east and north east.

The Rannoch Formation (Aalenian – Bajocian)

The lower part of the Rannoch Formation comprises interbedded shales, siltstones and micaceous, very fine grained sandstones. The basic unit in the Rannoch Formation is a micaceous siltstone dominated unit with thin sharp-based sands at its base and generally coarsens upwards to very fine grained micaceous sandstones (Johnson et al., 1993). The upper part of the formation is dominated by fairly well sorted, micaceous, very fine and fine grained sandstones which display hummocky cross stratification which passes upwards into undulose lamination or symmetrical wave ripples. The Rannoch Formation is interpreted to be the storm wave-influenced middle shoreface facies of the delta front and combined with the overlying Etive Formation represents the main marine coastal, progradational phase of

the Brent Delta (Graue et al., 1987). Deposition in shallow water is indicated by large scale wave generated structures. The high mica content of the Rannoch Formation gives it an anomously high gamma-ray response which distinguishes it from the overlying and underlying units.

The Etive Formation (Bajocian)

The Etive Formation overlies the Rannoch Formation as part of an upward coarsening sequence. The lower part of the unit is composed dominantly of fine grained, moderately well sorted, structureless sandstones which are commonly sharp based. The upper section dominantly comprises fine to medium grained sandstones which exhibit low angle laminated and trough cross bedding with rare erosional contacts (Johnson et al., 1983). The formation documents the formation and migration of a prograding barrier bar-sand complex mixed with barrier beach sands and tidal channel deposits (Graue et al., 1987). The Etive Formation is thought to represent a complex 3D shoreline topography which records the development of a microtidal, wave-dominated barrier island, made up of nearshore bar and trough systems, cut by tidal-inlet channels, which pass up into a foreshore environment (Underhill, 1998).

The Ness Formation (Bajocian)

The Ness Formation is lithologically the most diverse of the Brent Group and consists of interbedded shales, siltstones, coals and sandstone. It is commonly subdivided into three components: a lower and upper unit characterised by deposition on the delta top partitioned by a middle unit, referred to as the Mid Ness Shale, thought to represent a temporary halt in progradation (Engelstad, 1987).

The Lower Member is 60m thick and comprises a wide variety of interbedded lithologies ranging from mudstones to coarse grained sandstones thought to represent a range of facies including multi-storey distributory channel sands, mouth bars, crevasse splays, overbank deposits and interdistributory muds and coal swamp deposits (Budding and Inglin, 1981). Trace fossils including the infaunal deposit feeding *Planolites montanus* are common accompanied by *Diplocraterion* and *Arenicolites* structures (Johnson et al., 1993).

The Mid Ness Shale is a medium to dark grey, lenticular to wavy bedded siltstones with some sharp based possibly wave-ripple, cross-laminated sandstones. It reaches a maximum of 18m thick although is commonly 4.5 – 8m in the East Shetland Basin and acts as a vertical

barrier within the Brent Group. It was deposited isochronously across the basin during a temporary deviation from continental progradation in a wide interdistributory bay. Palyomorphs in the Mid Ness Shale indicate marine and brackish water assemblages (Johnson et al., 1993).

The Upper Member varies in thickness from 10 to 15m reaching a maximum of 41m in the East Shetland Basin. It is characterised by an increase in shallow marine sands interpreted as dominantly upper delta plain deposits and marks the resumption of deltaic processes with an increasing marine influence (Livera, 1989). The top of the unit is commonly eroded but where present the topmost section of the Upper Ness Member has a much lower sand: shale ratio and is dominated by lenticular siltstones with thin sandstones and some coals. The siltstones tend to be bioturbated and contain a marine fauna. The siltstones are thought to result from a fall in the supply of coarse grained sediment possibly due to a rise in base level (Johnson et al., 1993).

The base of the Ness Formation is marked by the first significant shale or coal present in contrast to the underlying sandy Etive Formation. The top of the formation is marked by the transition to the cleaner, more massive sandstones of the Tarbert Formation. This may be a minor disconformity (Doré et al., 1984)

The Ness Formation is a delta-plain time equivalent of the Rannoch/Etive delta front during the period of Brent delta advance and reaches a maximum thickness of 180m in the deep North Viking Graben.

3.8.4 Syn-rift Stratigraphy

The Tarbert Formation (Bajocian – Bathonian)

The Tarbert Formation consists of transgressive sandstones deposited during the retreat of the Brent Delta and is the oldest unit of the syn-rift stratigraphy in the Northern North Sea. It represents the early stages of footwall uplift and hangingwall subsidence. The unit is characterised by fine grained and highly bioturbated sandstones, locally calcite cemented which are interpreted as shelf-ridge deposits. The Tarbert Formation was deposited at the onset of the marine transgression which deposited the overlying argillaceous units. Conditions are therefore interpreted to have been marginal marine.

The base of the unit is an unconformity defined by the transition from the shales and coals of the Ness Formation to the sharp based, coarse to very coarse marine sandstones of the

Tarbert Formation. This is often taken in wells to be the last coal band. The lowest sandstone is interpreted to be a transgressive lag deposit developed above a ravinement surface (Brown et al., 1987). This boundary is dated biostratigraphically to be of latest Bajocian age.

The top of the unit is marked by a maximum flooding surface (MFS) and the transition to the shale dominated Humber Group. Biostratigraphy dates this MFS as Early to Mid Bathonian in age. The top, and in places all, of the unit is eroded over tilted fault blocks.

The Tarbert Formation is a separate stratigraphic unit to the rest of the Brent Group and shows a distinct depositional distribution being limited to downflank areas of the tilted fault blocks (e.g. Ninian Field, Underhill et al., 1997) throughout the western part of the East Shetland Basin.

3.8.4.1 Middle to Upper Jurassic Stratigraphy

The Middle Oxfordian to Early Kimmeridigian in the Northern North Sea saw the onset of a major phase of extension (Ziegler, 1982, 1990; Underhill. 1991; Rattey and Hayward, 1993; Thompson and Underhill, 1993). Extension was accommodated in a trilete rift system (see section 4.2) in which movement on dip-slip faults predominated over strike-slip faults (Davies et al., 2001). East-west direction extension in the North Viking Graben led to deepening and the subsequent deposition of the Humber Group which records drowning and the onset of widespread marine conditions into the basin as the North Sea Dome subsided.

In addition, Mid to Late Jurassic extension of the Northern North Sea Rift Province caused syn-sedimentary footwall uplift. These footwall highs provided a sediment source and were eroded and redeposited downslope from the structural crest of the fault block. Several sandstone units, for example the Munin Sands, were deposited via this process. In contrast to the Middle Jurassic, there is much greater regional continuity of Upper Jurassic Sediments in Northern North Sea. The sediments to be considered range from Bathonian to Ryazanian (Lower Cretaceous) in age and are up to 3000m thick and are dominated by siltstones and shales.

The Upper Jurassic interval is biostratigraphically subdivided using dinoflagellate cysts (Poulsen and Riding, 2003).

3.8.4.2 The Humber Group (Viking Group in Norwegian waters)

(Mid Bathonian to Early Ryazanian)

Lithostratigraphically, the Late Jurassic stratigraphy in the Northern North Sea is dominated by the Humber, or Viking Group. The group is predominantly dark, grey to black marine mudstones, claystones and shales laid down in the subsiding Viking Graben. However, it comprises several diachronous lithostratigraphic formations including sandstone dominated intervals such as the Magnus Sandstone Member and coastal deltaic deposits such as the Sonefjord Formation. The thickness of the group varies considerably since the sediments were deposited on a series of tilted fault blocks produced by predepositional and syndepositional tectonic activity. The measured thickness varies between a few metres and in excess of a kilometre. The formation is principally divided into two mudstone dominated units, the Heather and Kimmeridge Clay Formations. The Humber Group records a syn-rift transgressive succession from the coastal plain deposits of the Middle Jurassic through sand bearing coastal, shelf and deep-water systems to the aerobic and dysaerobic mud-dominated marine facies towards the top of the Late Jurassic (Fraser et al., 2003).

The lower boundary of the Humber Group is marked by the distinct contrast between the Humber Group and the underlying Brent Group. In the northern part of the East Shetland Basin, where the Brent Group is absent, the Humber Group rests unconformably on the Dunlin Group. The upper boundary is a regional unconformity normally overlain by higher velocity and lower radioactivity Cretaceous to Paleocene sediments.

The Heather Formation (Bathonian - Late Oxfordian)

The Heather Formation is dominated by grey, silty mudstones with occasional limestones (Johnson et al., 1993). The lower boundary of the Heather Formation is locally unconformable with the underlying Brent Group. The upper boundary with the Kimmeridge Clay Formation is taken as the first downhole occurrence of the dinocyst *S. crystallinum* (Underhill, 1998). Deposition of the Heather Formation occurred as several major fault blocks began to tilt, creating highs, some of which formed islands close to the North Viking Graben. The Heather Formation was deposited in wedge shaped depocentres adjacent to the tilting fault blocks. The unit therefore exhibits a wide range of depositional thicknesses from a few metres over tilted fault blocks to thousands of metres in the graben depocentres. The unit is a continuation of the transgressive Tarbert Formation below reflecting the full establishment of open marine conditions (Deegan and Scull, 1977). The transgression may

have persisted due to eustatic sea level rise, but may have been maintained by increased subsidence associated with the onset of the Mid to Late Jurassic rift episode.

Both upper and lower boundaries of the Heather Formation are marked by distinct log breaks. Both the lower boundary with the Brent Group and the upper contact with the Kimmeridge Clay Formation have anomously high gamma-ray and low velocity responses. The formation is present throughout the East Shetland Basin north of 58˚N and east of the East Shetland Platform bounding faults.

The Kimmeridge Clay Formation (Draupne Formation in Norwegian Waters)

(Late Oxfordian – Ryazanian)

The type section of the Kimmeridge Clay Formation is found in Kimmeridge Bay in Dorset where it is present as organic rich mudstones of Late Jurassic age (Underhill, 1998). In the Northern North Sea the unit is dominated by dark grey to black, non-calcaerous, organic rich mudstones . A number of reservoir sandstones are additionally present. The mudstones reflect hemipelagic deposition in a marine environment with restricted bottom circulation and resultant frequent anaerobic conditions. In contrast, the sands are thought to have been deposited in submarine-apron fans, basin-floor fans or shallow marine shelves.

The unit shows a high gamma-ray response due to its high organic content. Total organic content in the formation reaches 15% (Stow and Atkin, 1987) although average values are about 5% (Cornford, 1990).

The base of the Kimmeridge Clay Formation is conformable with the top of the underlying Heather Formation; however, the top of the formation is marked basinwide by a widespread discordance. This is marked by a strong, regionally mappable, acoustic impedance contrast on seismic data and is widely referred to as the 'Base Cretaceous Unconformity' (BCU). On the basin margins the BCU represents considerable missing stratigraphy; in contrast there is little or no missing stratigraphy in the deep North Viking Graben (Rattey and Hayward, 1993; Partington et al., 1993).

The boundaries of the formation are marked by distinct log breaks due to the high gamma-ray response and low velocity characteristic of the Kimmeridge Clay Formation.

The Munin and Kimmeridge Clay Sandstone Members

The uplift of tilted fault blocks in the Brent Province promoted resedimentation of erosional products down-flank from the crest of the eroding fault blocks (Underhill, 1998). As a result a number of discrete sandstone bodies were deposited within the mud-prone Kimmeridge Clay Formation (Badley et al., 1988). Several sandstone members are formally recognised within the offshore Kimmeridge Clay Formation. In the East Shetland Basin the unit is formally referred to as the Magnus Sandstone Member although informal names such as the Munin Sands and the Kimmeridge Sandstone Member are designated on exploration well logs.

The Magnus Sandstone Member consists predominantly of sub-arkosic to arkosic, fine to coarse grained, poorly sorted sandstones (De'Ath and Schuyleman, 1981). The Munin Sands are a sand prone unit locally present within the Kimmeridge Clay Formation in the Northern part of the Statfjord area. They are penetrated by wells 33/9-15, 33/9-16 and 33/9-17. The unit comprises medium to coarse, well sorted sands with generally good porosity. They are typically 50-100m thick. The upper and lower boundary of the Munin Sands are designated on the basis of gamma-ray and velocity contrasts with the mud-dominated Kimmeridge Clay Formation within which they are present.

3.8.5 Post-rift Stratigraphy

3.8.5.1 Lower Cretaceous Stratigraphy

Lower Cretaceous strata are present over most of the Northern North Sea but are confined to hangingwall locations. They are dominated by argillaceous lithologies. The Early Cretaceous was essentially a period of transgression with minor regressions (Rawson and Riley, 1982). The anaerobic conditions that dominated in the Northern North Sea during the Late Volgian to Early Ryazanian regression ceased (Hesjedal and Hamar, 1983) and relatively quiet conditions resulted with sedimentation of shales and marls. During the Mid to Late Aptian a regression occurred resulting in a shift from calcareous clay deposition to more organic rich deposits. This event was followed by an Albian regional transgression and the deposition of sandstone sequences (Agat Formation) with an increasing carbonate component. A late Albian-Early Cenomanin regressive event followed leading to erosion and non-deposition of sediments along the flanks of structural highs.

Cromer Knoll Group (Late Ryazanian to Albian)

The Cromer Knoll Group shows considerable thickness variation from a maximum of 600m in the North Viking Graben, thinning onto the basin flanks. The Cromer Knoll Group consists of mainly fine-grained argillaceous marine sediments with a varying component of calcareous material. The group is dominated by calcareous claystones, siltstones and marls with occasional limestone and sandstone layers.

The Cromer Knoll Group comprises four formations: The Barremian age, Mime Formation is dominated by basal limestones, locally interbedded with marls or claystones. The Ăsgard Formation comprises reddish brown to grey, partly silty marls with locally calcareous claystones and bands of white limestone. It ranges in age from Late Ryazanian to Early Aptian and is commonly found to contain mica, glauconite and pyrite (Isaksen and Tonstad, 1989). Above the Ăsgard Formation, the Sola Formation comprises 70m of claystones with thin intercalated limestones and is Early Aptian to Early Albian in age. The Rødby Formation marks the top of the Cromer Knoll Group and is of Albian age. It forms a widespread unit, a few metres thick, characterised by reddish brown to pale green or grey claystone, calcareous claystone and limestone with pyrite and glauconite (Isaksen and Tonstad, 1989).

The lower boundary of the Cromer Knoll Group is usually well defined and is recognised by a distinct decrease in gamma-ray response and increase in velocity on passing up from the more organic rich Kimmeridge Clay Formation below. The upper boundary is marked by the base of the siliciclastic units in the lower section of the Shetland Group. This is characterised by the onset of a decrease in gamma-ray response and coincident increase in velocity.

3.8.5.2 Upper Cretaceous

The Late Cretaceous was a quiet tectonic period during which deposition is dominated by a continuous, argillaceous and calcareous marine sequence, ascribed to the Shetland Group.

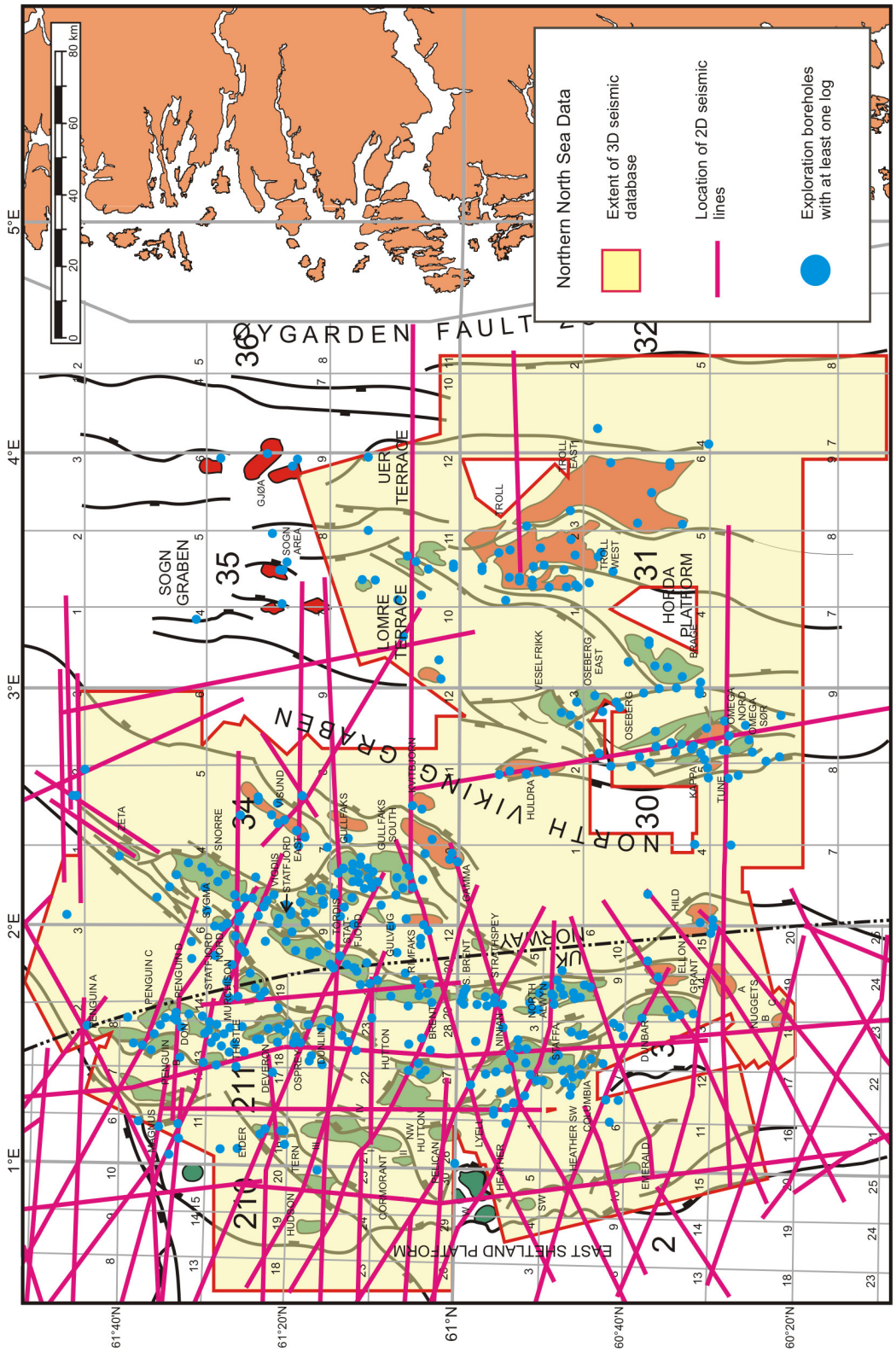

Figure 3.1 Map showing location and extent of data available for incorporation into study

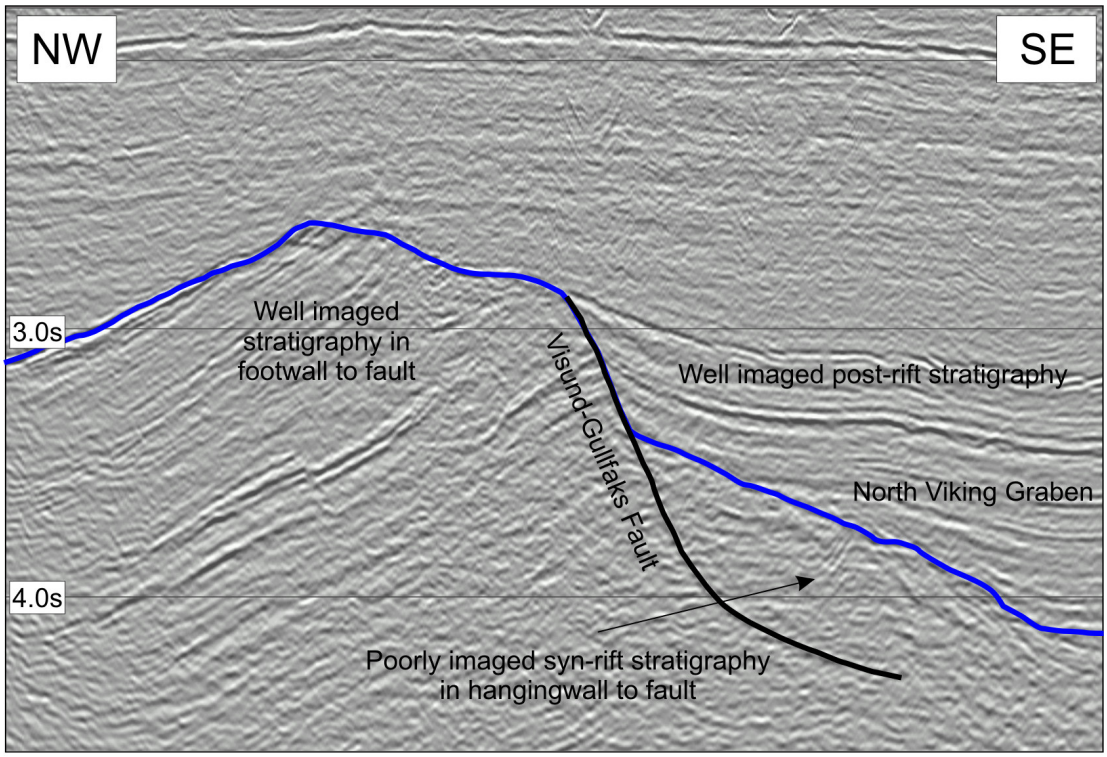

Figure 3.2
Seismic panel showing poor nature of reflectors in the hangingwall to the Visund-Gullfaks Fault
Blue horizon is Base Cretaceous Unconformity
For location see figure 3.12

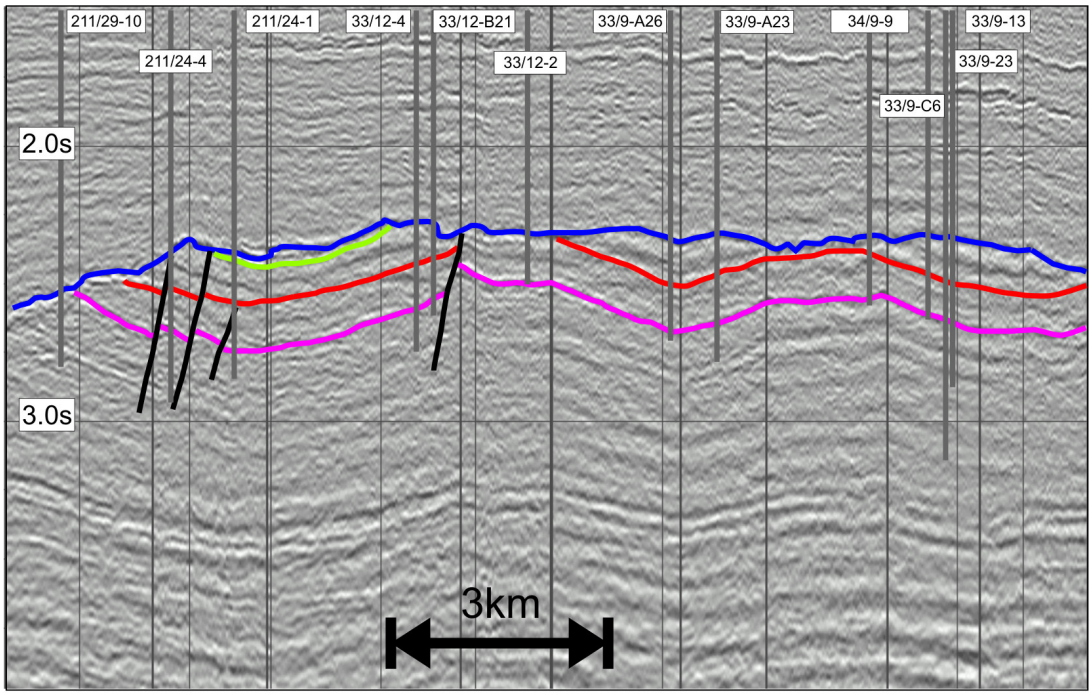

Figure 3.3A
Seismic panel showing an example of a seismic traverse path used in correlation of reflectors between well ties.
Vertical black lines indicate changes to direction of seismic pathway
For location see figure 3.12

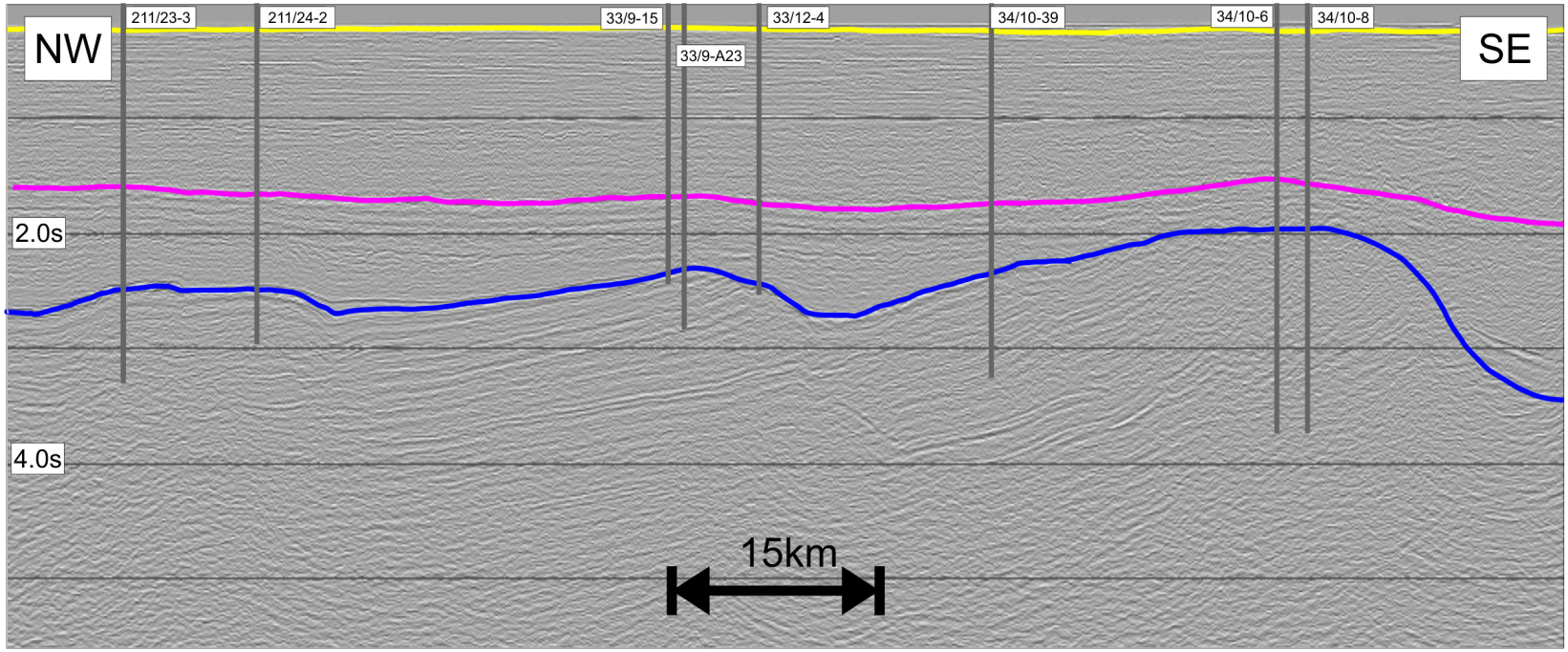

Figure 3.3B
Seismic panel showing regional 2D line and wells used for regional correlation of key reflectors. Three key regional reflectors are shown in the overburden. These were used in well correlation throughout the East Shetland Basin.
Blue reflector is Base Cretaceous Unconformity, pink is Top Balder Formation and yellow is the present day seabed.
For location see figure 3.12

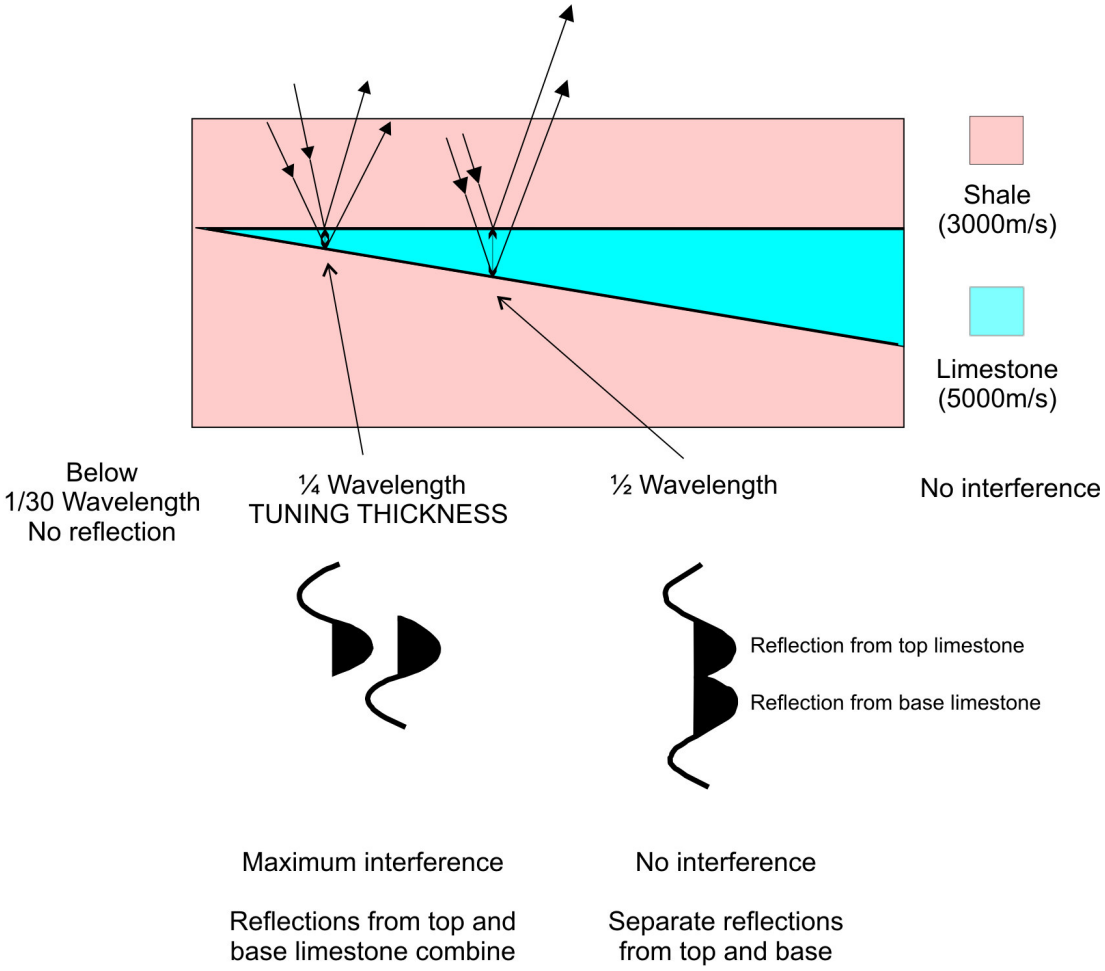

Figure 3.4
Interference effects associated with a high acoustic-impedance wedge encased in a lower acoustic-impedance shale. The limestone must be thicker than half the seismic wavelength for no interference between reflections from its top and base. Maximum interference and amplitude of the resulting reflection occurs at a limestone thickness equivilent to one quarter of the seismic wavelength - the tuning thickness. For limestone thicknesses less than one quarter wavelength, the reflection remains the same shape but decreases in amplitude. Once the limestone is about one-thirtieth wavelength or less, reflections from the top and base effectively cancel out and there is no detectable seismic response.
After Badley, 1985

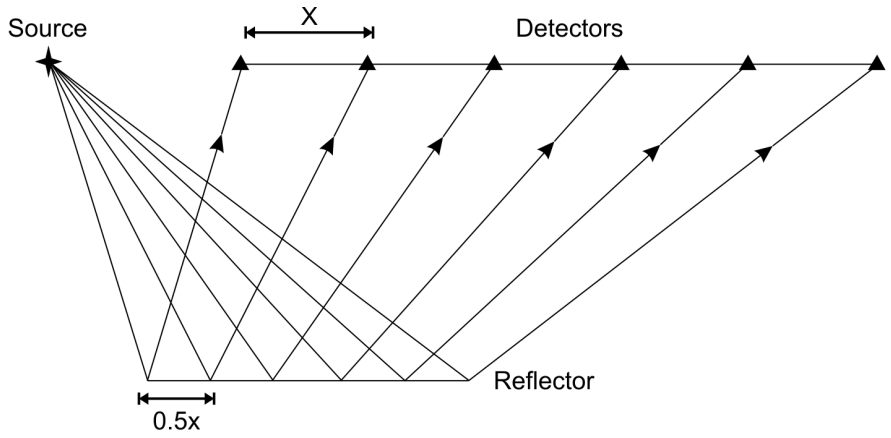

Figure 3.5A
The horizontal resolution of a seismic reflection survey is half the detector spacing
After Kearey and Brooks (1991)

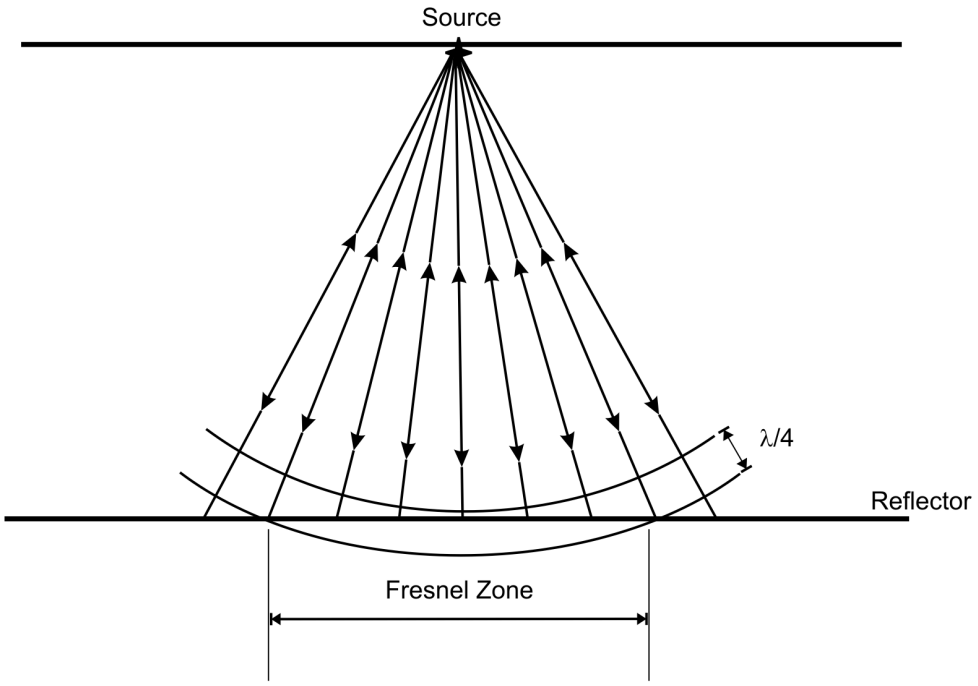

Figure 3.5B
Energy is returned to source from all points on a reflector. The part of the reflector from which energy is returned within half a wavelength of the initial reflected arrival is known as the Fresnel Zone.
After Kearey and Brooks, 1991.

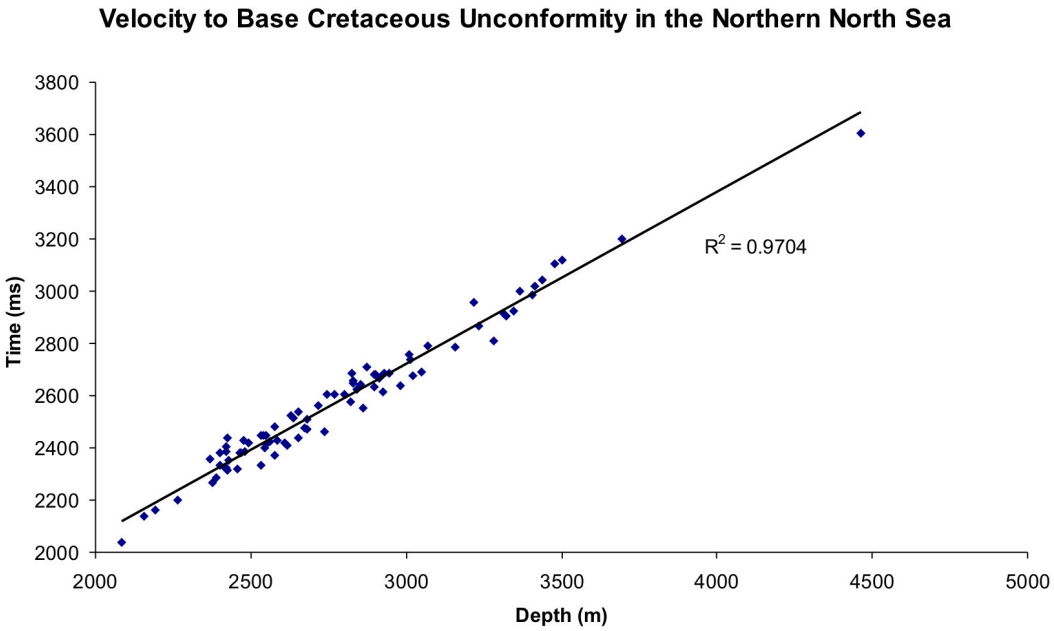

Figure 3.6
Graph showing uniformity of overburden velocity in the Northern North Sea

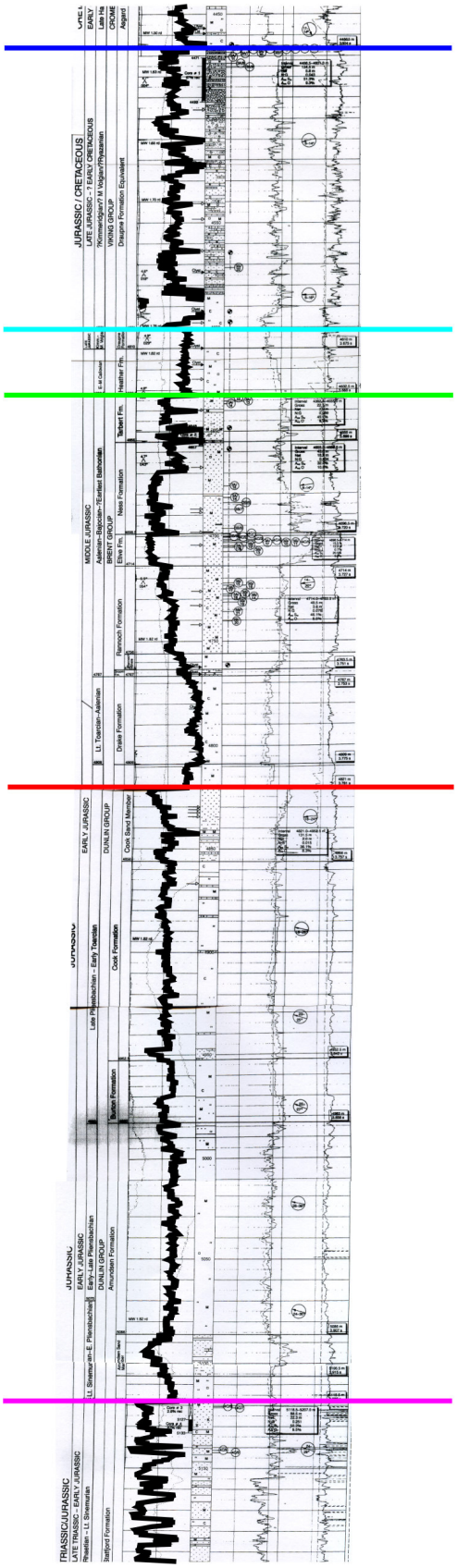

Key to symbols

- Base Cretaceous Unconformtiy
- Top Heather Formation
- Top Brent Group
- Top Dunlin Group
- Top Statfjord Formation

Vertical scale 1cm=50m

Figure 3.7
Extract from composite log for well 34/8-7 showing complete Jurassic Stratigraphy

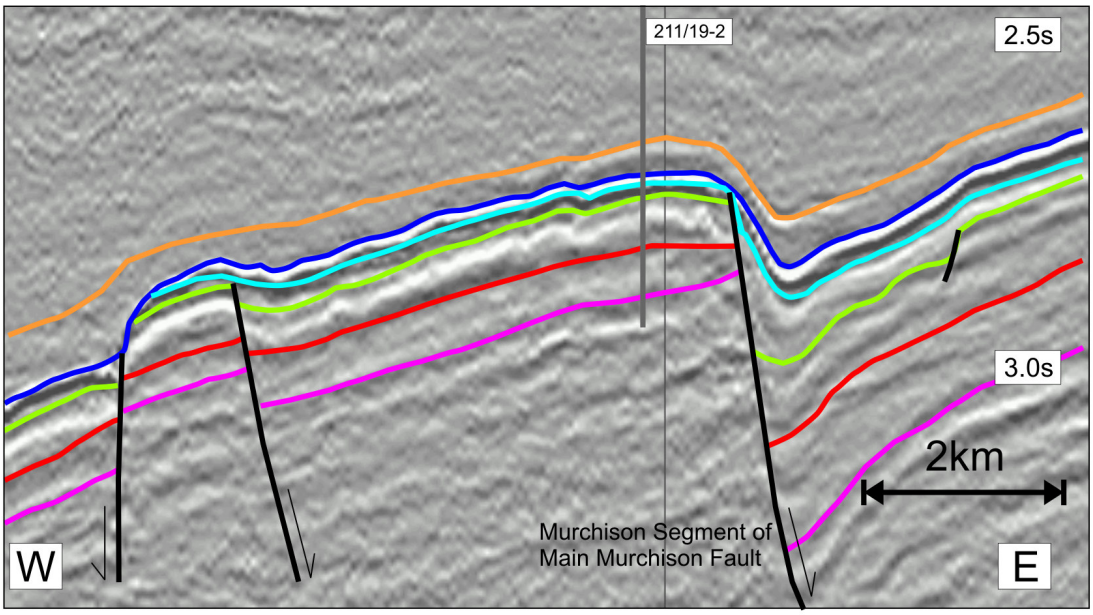

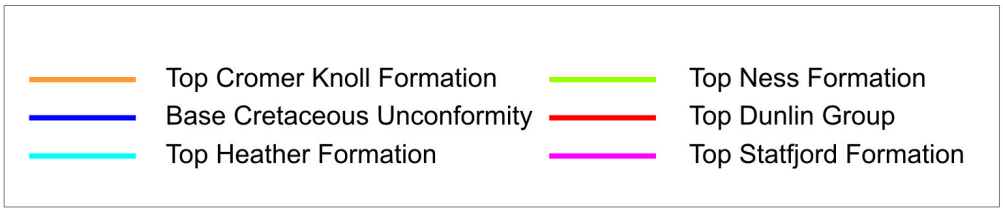

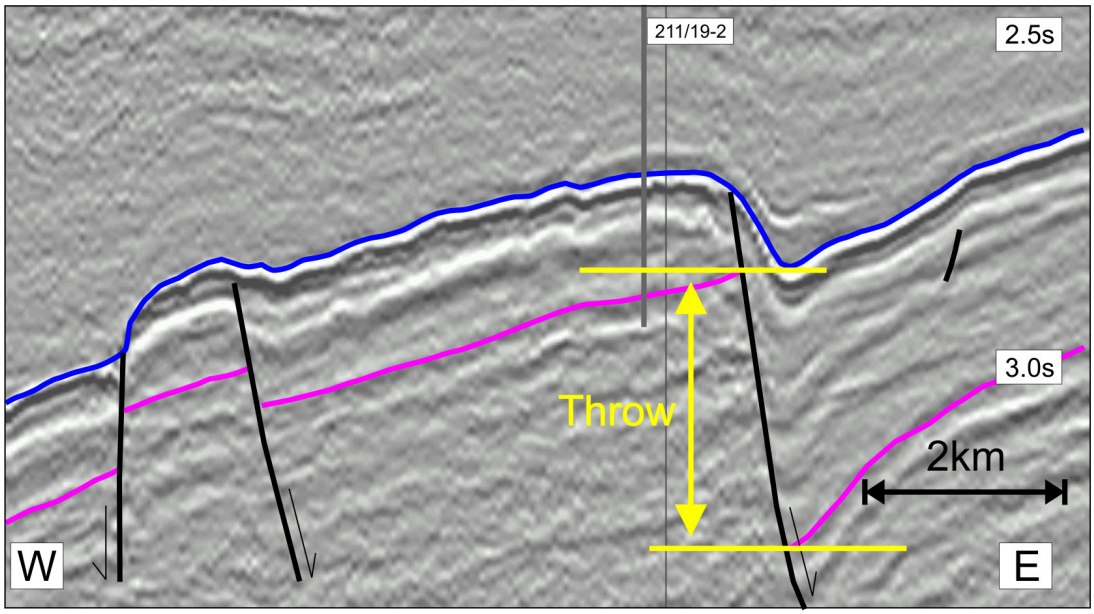

Figure 3.8
Seismic line over the Murchison Fault showing measurement of fault throw at Top Statfjord Formation level
For location see figure 3.12

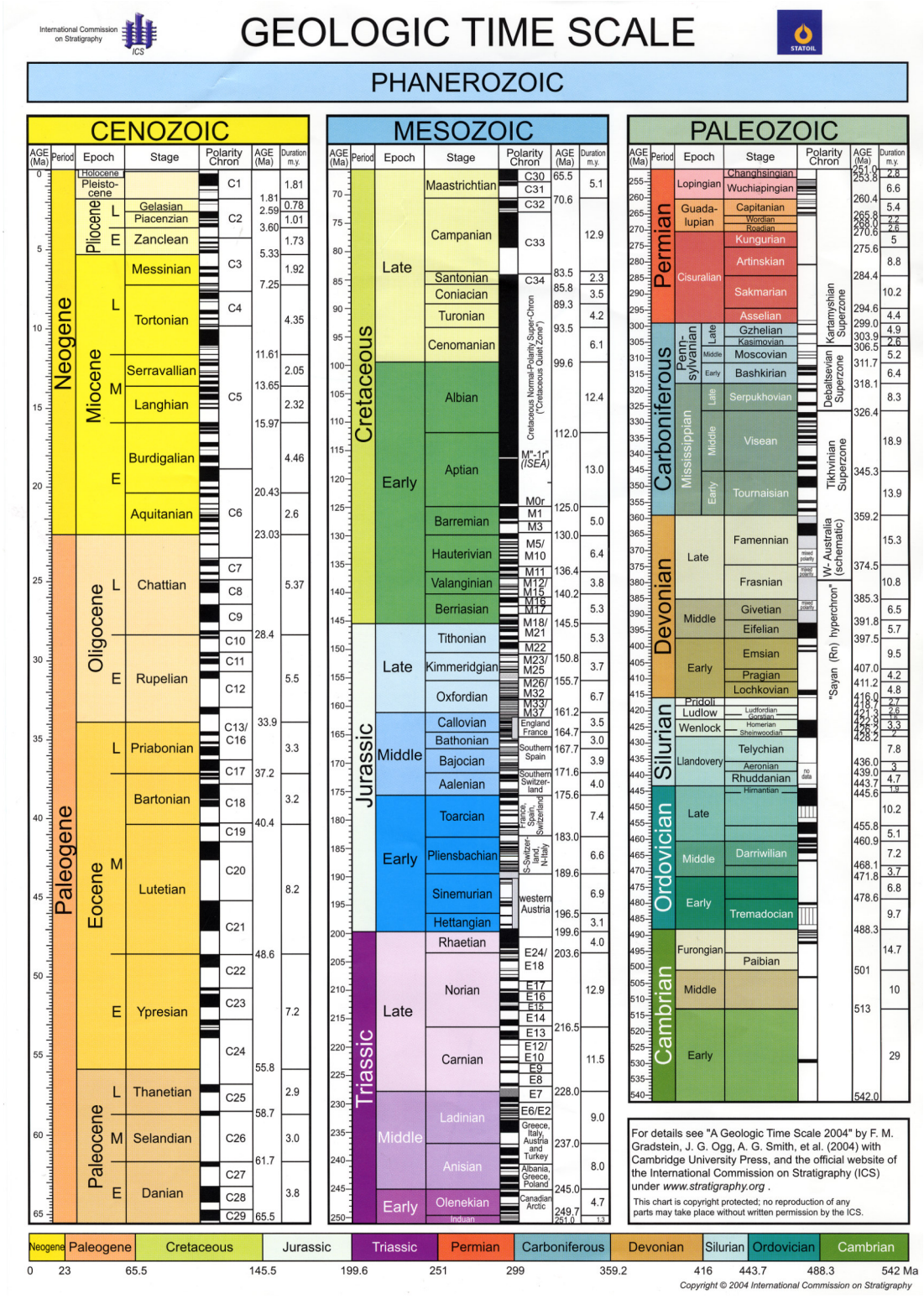

Figure 3.9
New Geological Timescale
From Gradstein et al., 2004

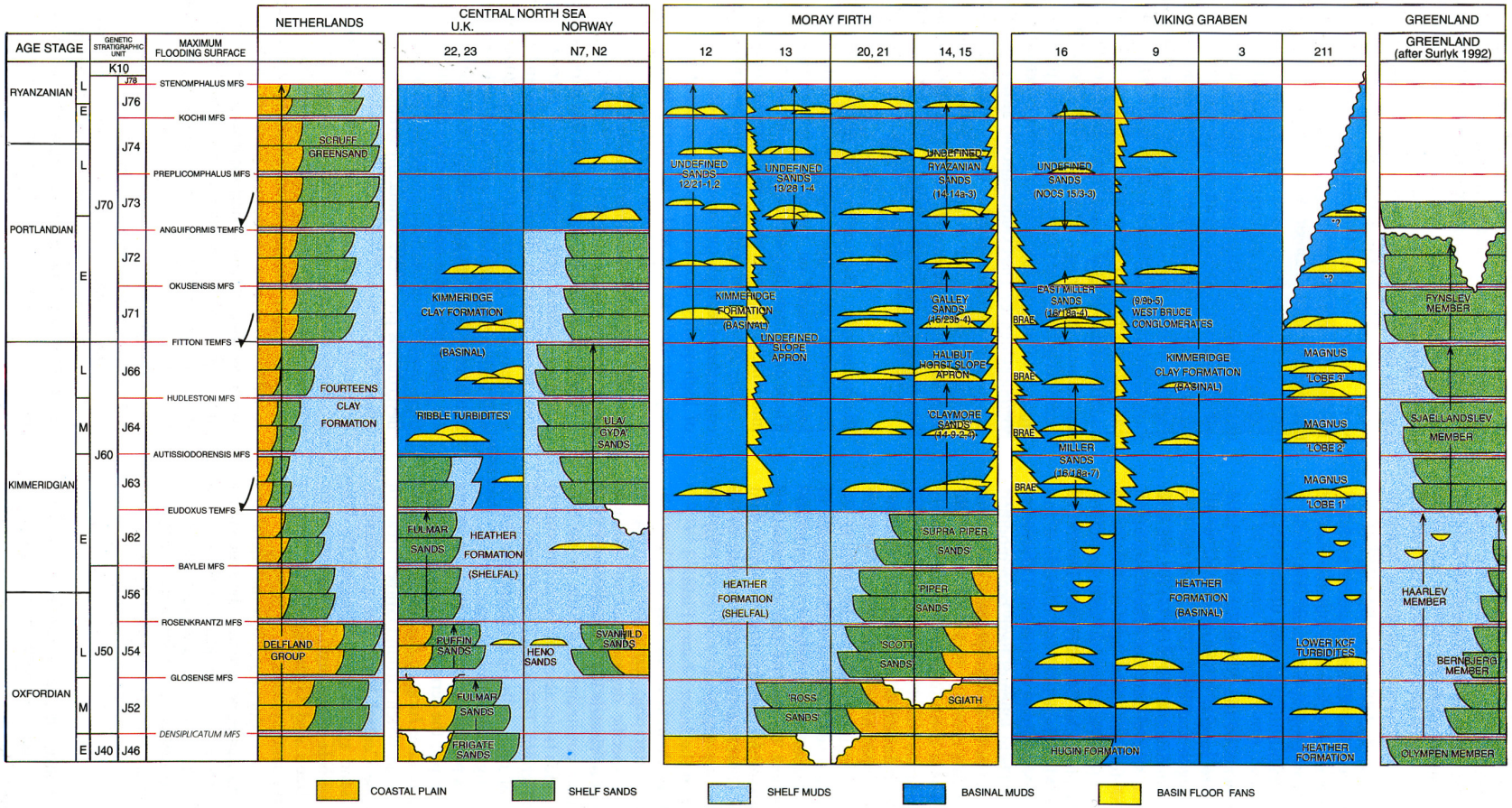

Figure 3.10
North Sea Late Jurassic Genetic Sequence Stratigraphy
From Partington et al., 1993

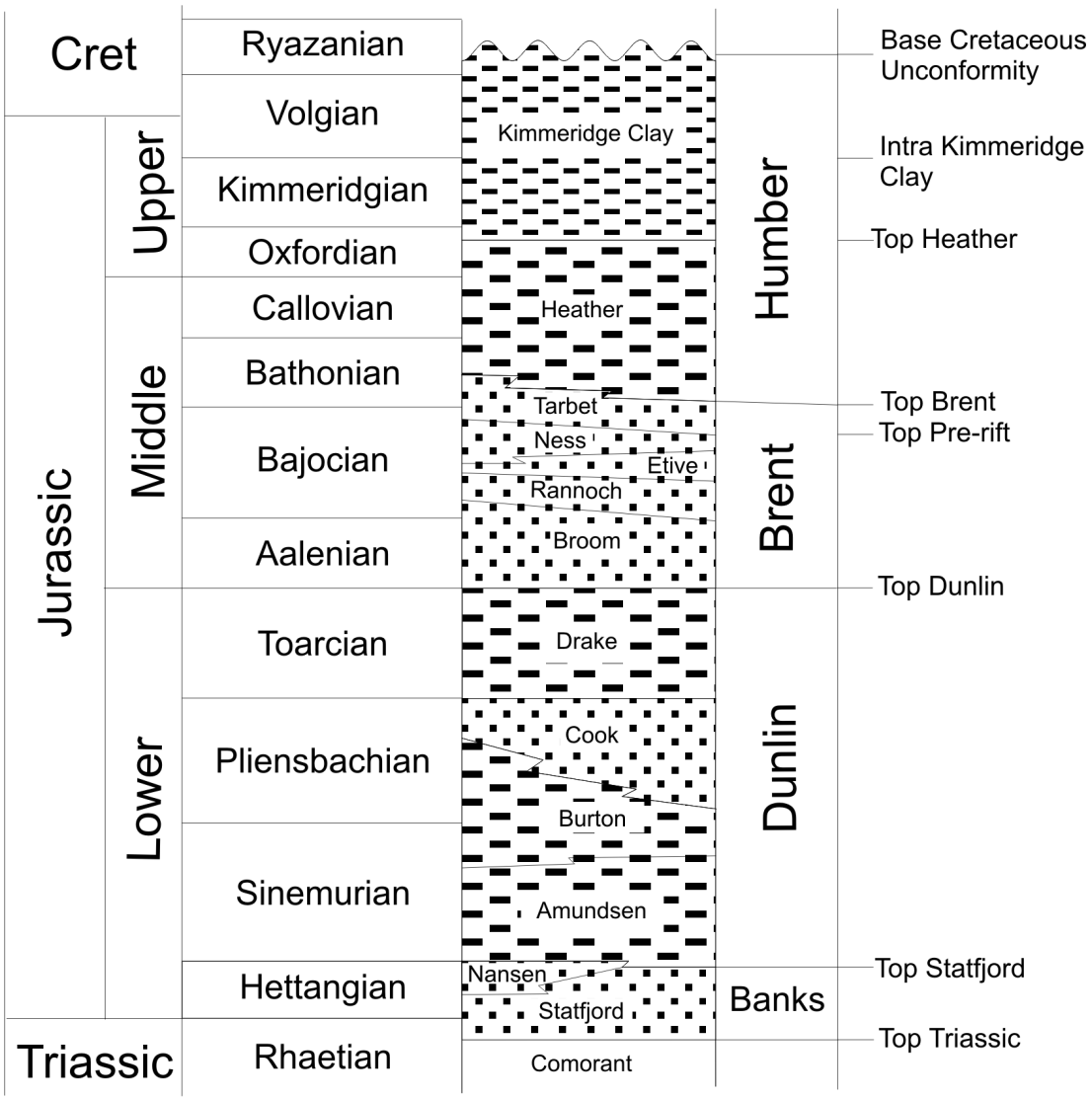

Figure 3.11
Jurassic stratigraphic outline in the East Shetland Basin

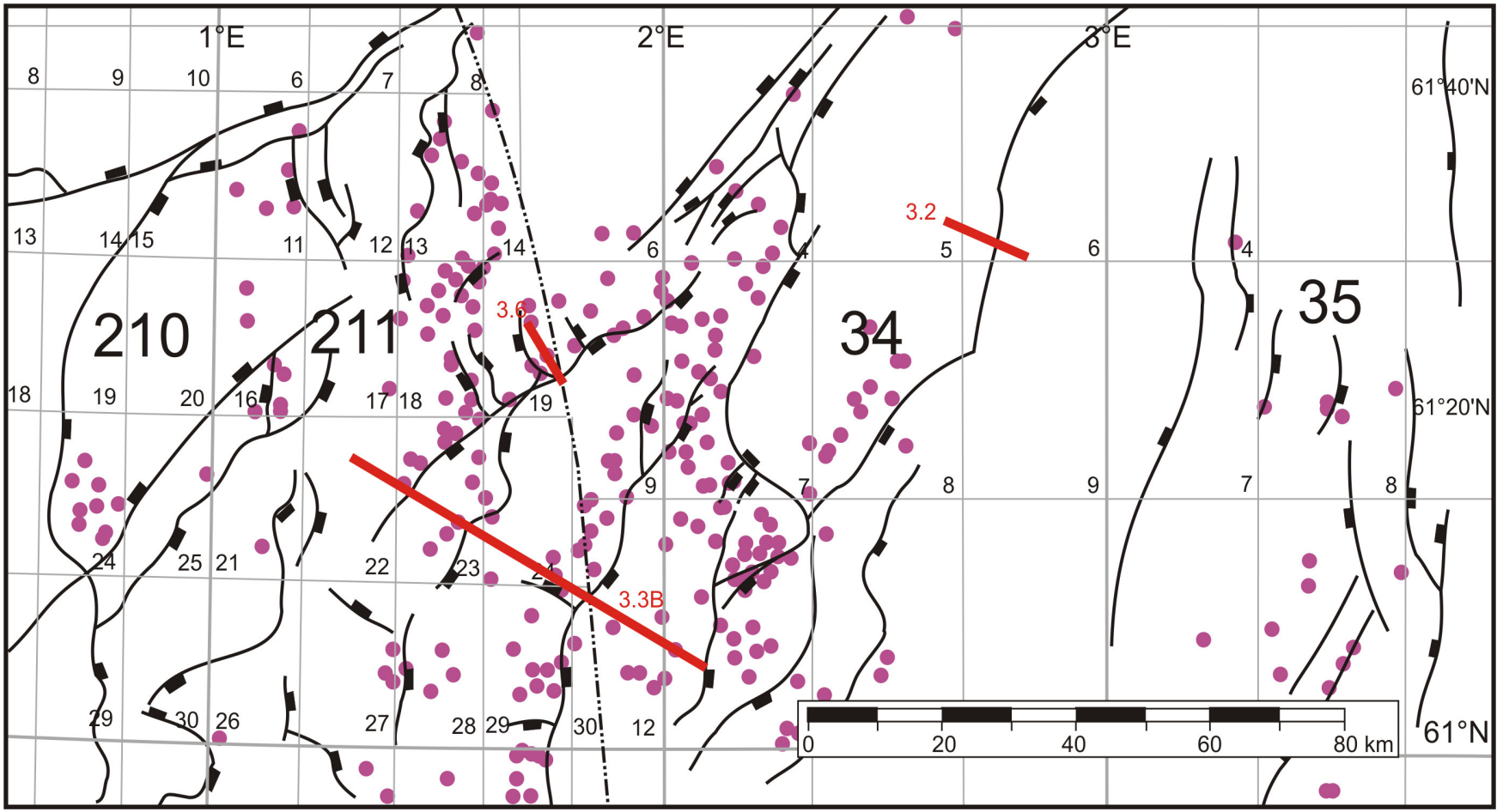

Figure 3.12
Map showing major faults and location of seismic lines presented in chapter 3
Purple circles show positions of exploration, development and appraisal wells with logs available for incorporation into this study

4. Applications to subsurface data 1 - Migration of the locus of extension in the Mid to Late Jurassic Northern North Sea Rift Basin

4.1 Introduction and Definitions

The North Sea is an important extensional basin which forms an integral part of the Northwest European Continental Shelf and is one of the most prolific hydrocarbon provinces in the world. As one might expect after more than thirty years of exploration high quality seismic, gravity, magnetic and borehole data exists from the subsurface. Having such a wealth of available data, the North Sea is an ideal laboratory for the study of extensional provinces. In this thesis the structures and processes resulting from the Mid to Late Jurassic rift episode are studied in detail. The Northern North Sea is an ideal extensional basin for this study for the following reasons:

1. Although an earlier rift event occurred in the Triassic, there is little evidence for reactivation of extensional structures (Faerseth, 1996; Faerseth and Ravnas, 1998).

2. The basin was marine, resulting in dating with relative ease and a limited amount of footwall erosion.

3. The post-Jurassic history of the North Sea is dominated by subsidence and relative stability and hence the Mid to Late Jurassic structures have generally not been modified by further tectonic episodes.

This chapter provides a record of the integration and interpretation of the subsurface data and uses it to develop a new, unified model for the structural development of the Northern North Sea Basin during Mid to Late Jurassic rifting.

The chapter will concentrate first on the regional setting and structural history of the Northern North Sea. It will then consider the evidence that shows how the migration of the locus of extension played an important role in the development of the rift province through examination of a suite of normal faults across the basin. These are the Hudson Fault in the west through the Murchison, Statfjord and Snorre faults to the Visund-Gullfaks fault in the east on the western edge of the Viking Graben (figure 4.1). The North Sea rift is arguably

one of the most studied in the world yet despite this no agreement has been reached on the kinematics of Middle and Late Jurassic rifting (Davis et al., 2001). The scale and resolution of the three-dimensional seismic data make it impossible for primary fault kinematic indicators such as slickensides to be identified. In this study reference is made to recent research and the kinematics of faulting in the Northern North Sea are considered to be pure dip-slip during the Late Jurassic rift episode (Davies et al., 2001; see section 4.2 below). The focus of this chapter is on the detailed stratigraphic history of each individual structure in the rift province. As a result, a detailed, regional fault map is not presented and the role of fault kinematics will not be considered further in this thesis.

In this chapter a detailed movement history is presented for each fault in turn before a regional synthesis is proposed.

4.2 Regional Setting and Structural History

Our understanding of the North Sea area is derived from two main sources: the surface and subsurface geology of the surrounding land areas and the subsurface geology of the North Sea itself. Since the Permo-Carboniferous Variscan Orogeny, the British Isles have lain in an intraplate setting and have only been affected by far-field stresses (e.g. diffuse extension and structural inversion caused by compressional reactivation of former normal faults) generated by active plate margin forces and by deformation caused by thermal effects (e.g. generation and decay of mantle plume heads). The structural history of the Northern North Sea has been varied and complex since the Permian when it first lay in an intraplate setting. This history is reflected in the complex tectonic framework underlying the present day North Sea Basin (figure 4.2). Early Permian subsidence led to the development of two east-west trending sedimentary depocentres, the Northern and Southern Permian Basins (figure 4.3) into which deposits of the Rotliegend and Zechstein Groups were subsequently deposited (Glennie 1998, Ziegler 1990). Basin formation was locally accompanied by Lower Permian age rift-related intrusion and volcanic products particularly in the eastern part of the basin. Extensional activity continued into the Triassic with the development of half graben depocentres in areas such as the Irish Sea, Wessex Basin and parts of Norway where the basins formed along lines of inherited basin weakness. During the later part of the Triassic the region underwent more uniform basement subsidence as rifting gave way to thermal relaxation. Triassic rifting was characterised by the development of north-south trending faults that formed easterly or westerly tilted half-grabens (Zanella and Coward, 2003).

Permo-Triassic extension is defined by a broad basin from the Unst Basin in the west to the Øygarden Fault Zone in the east (Roberts et al., 1995; Faerseth, 1996). The Permo-Triassic rift system in the Northern North Sea is asymmetric; maximum stretching occurred on the Horda Platform (40%) in contrast to a lower mean extension in the west of the basin (<30%). Although the occurrence and trend of the Permo-Triassic fault system in the North Sea are often thought to be a major contributory factor in subsequent fault activity, recent seismic interpretation in the Northern North Sea has suggested that earlier events are largely independent of Mid to Late Jurassic extension (figure 4.4). In particular, recent studies on the eastern flank of the North Viking Graben (Horda Platform) have shown that Mid to Late Jurassic extension is accommodated independently of earlier structures (Faerseth, 1996; Faerseth and Ravnas, 1998). For example, many Late Jurassic faults cross-cut earlier Triassic structures and the variation in β factors for the two rift events are uncorrelated over most of the area (Odinsen et al., 2000). Consequently, as a result of contrasting basin architectures, there is little evidence that the trilete rift system that has dominated the late Jurassic to recent history of the North Sea can be attributed to reactivation of Permo-Triassic structures (Tomasso et al., In Press). Post-rift subsidence allowed flooding of the Permo-Triassic basin and the increasing dominance of marine conditions by the Early Jurassic. The development of widespread marine conditions, preserved in the Southern North Sea but absent from parts of the Central and Northern North Seas, is recorded by uniform deposition of coarse clastic units deposited in a shallow, well aerated epicontinental basin experiencing broad patterns of subsidence following Permo-Triassic rifting.

Permo-Triassic post-rift thermal subsidence continued until the Toarcian when the North Sea underwent a phase of uplift attributed to the presence of a warm, diffuse and transient plume of mantle material causing doming of the surface (Underhill and Partington, 1993). The transient nature of this uplift means it is attributed to the upward transport of a plume head or blob rather than the initiation of a permanent upward hot jet. There is no recorded volcanic trail. The development of the North Sea Dome caused widespread concentric depositional shallowing and erosion marked by the onset of non-marine deposition (figure 4.5). Erosion of the domed area led to the production, dispersal and progradation of significant volumes of fluvio-deltaic sequences, the most significant of which led to the development of the Brent Group delta in the Northern North Sea (figure 4.6), (Helland-Hansen et al., 1992). The dome was large enough to restrict faunal exchange although probably never reached greater than two kilometres in vertical elevation (Underhill and Partington, 1993 and 1994). It had a low

lying nature but highly irregular relief and as a result allowed accumulation of paralic sediments.

The collapse of the thermal dome helped initiate Mid to Late Jurassic to Earliest Cretaceous extensional tectonics in the Northern North Sea (Glennie and Underhill, 1998). Mid to Late Jurassic extension reached a maximum of 30% at the rift axis (North Viking Graben) with a mean extension across the basin of 15% (Roberts et al., 1993). The associated deformation led to the development of a trilete rift system consisting of the Viking Graben, Moray Firth and Central Graben (figure 4.7), all of which are linear structures characterised by fault block rotations and the formation of major structural traps (Yielding, 1990; Yielding et al., 1992). Research in the past has tried to place the Middle and Upper Jurassic extensional faults within one simple overall stress regime. This results in it being necessary to invoke considerable amounts of strike- and oblique-slip deformation on faults within the rift arm not optimally orientated for dip-slip motion (Davies et al., 2001). Such a model was advocated by various workers in the 1990's, for example Bartholomew et al., (1993) discuss reactivation of strike-slip basement lineaments in the Mesozoic history of the Northern North Sea and conclude that 'the total amount of movement on basement lineaments is probably very limited'. However, recent research has highlighted a sequential faulting history in which the development of the trilete rift system was dominated by dip-slip extension with a negligible content of strike-slip faulting (figure 4.8; Davies et al., 2001). The dominance of dip-slip movement during Late Jurassic extension in the Northern North Sea is shown by integration of structural styles and subsidence analysis derived from well-constrained two- and three-dimensional seismic and well interpretation. This work challenges the uncertainty surrounding the kinematics of faulting in the North Sea during the Jurassic rift episode discussed above and uses data from all three rift arms in order to present a unified model in which the development of the Northern North Sea rift is dominated by dip-slip movement on east and west dipping normal faults.

The predominantly east-west directed extensional stresses which developed in the Northern North Sea during this time (Davies et al., 2001) led to accelerated subsidence of the area and the development of major faults which dissected and tilted earlier stratigraphy. The fault system developed as a result of the growth, propagation and linkage of planar normal faults throughout the rift interval (Underhill, 1998; Dawers and Underhill, 2000; McLeod et al 2000 and 2002; Young et al., 2001; Fraser et al 2003). Each fault block was characterised by pronounced footwall uplift and associated hangingwall subsidence. Footwall uplift in some

of the larger fault blocks associated with larger extensional faults exposed the pre-rift sediments to erosion, in some places removing material down to Triassic levels and developing associated fault scarp degradation complexes (Underhill et al., 1997; McLeod and Underhill, 1999).

Structural inheritance has proved to be an important consideration in the development and evolution of structural styles in many hydrocarbon provinces (Glennie and Underhill, 1998). The varied and complex history of the Northern North Sea results in later structural events having the potential to exploit pre-existing structures and reactivate weaknesses in the underlying crust. The kinematics of faulting in the Mid to Late Jurassic North Sea rift province has long been a subject of controversy (Davies et al., 2001). In order to understand the role of inherited basement structure in the Northern North Sea it is necessary to visualise the deep crustal structure underlying the Mid to Late Jurassic rift province. This is achieved using deep seismic, gravity and magnetic data.

A Bouguer gravity field over the Northern North Sea shows linear anomalies over the Viking Graben. This is an effect caused by the elevation of the Moho and denser upper mantle underneath the rifted crust. The Bouguer gravity field can be separated long wavelength regional and shorter wavelength residual fields (figure 4.9). The regional gravity field provides a good indicator of the Moho structure whereas the residual field illustrates the rift fabric (Zanella et al., 2003). The regional field shows no evidence for regional discontinuities in a preferred orientation which could have been reactivated during the Mid to Late Jurassic rift episode.

The Northern North Sea basin has an overall graben-like morphology centred about a low: the North Viking Graben. The Viking Graben forms the most northern simplest arm of the failed trilete rift system which was formed during Mid to Late Jurassic to earliest Cretaceous extensional tectonics. The graben trends north-south and is arranged into five discrete structural elements arranged in a left stepping, en-echelon pattern. Each element has a half graben geometry, bounded on one side by a major normal fault (Zanella and Coward, 2003). The Viking Graben was created as the extensional fault blocks experienced post rift thermal subsidence (figure 4.10). The North Viking Graben is 20-35km in width and at its centre is approximately 7km deeper than the adjacent platform areas. The graben is in general asymmetric, especially in its central and southern parts. For example, the western margin of the North Viking Graben is bounded by a major easterly dipping set of faults against which

in excess of 3000m of Upper Jurassic syn-tectonic sediments have been deposited. In contrast, the eastern margin of the graben is defined by smaller, westerly dipping faults with maximum throws of 100-500m that are interpreted as antithetic faults (Zanella and Coward, 2003).

The East Shetland Basin is located on the western edge of the North Viking Graben and comprises a series of north-north-east to north-east striking, westerly tilted fault blocks which are typically 10-20km wide. The faults have dips of 40-45˚ and the pre-rift stratigraphy in the uplifted footwalls are tilted to 3-9˚. Each fault block in the East Shetland Basin is characterised by pronounced footwall uplift and hangingwall subsidence.

During the Mid to Late Jurassic rift epiosde, erosion and deposition occurred in the subsiding East Shetland Basin and included syn-sedimentary footwall degradation of the uplifted fault crests (Underhill et al., 1997, McLeod and Underhill, 1999). The area continued to experience thermally-driven subsidence throughout the Cretaceous and Cenozoic and is still an active sedimentary basin (Underhill, 2003).

4.3 The Hudson Field

4.3.1 Location

The Hudson field, bounded by the westerly-dipping Hudson Fault, lies 65km northeast of the Shetland Islands on the western edge of the East Shetland Basin in the Hudson-Otter half graben in United Kingdom block 210/24 (figure 4.11). The basic structure of the area is a simple tilted fault block from which oil is produced from the Brent Group. However, the Hudson Field is a rollover on the hangingwall of the main East Shetland Basin Bounding Fault at its western (distal) end. The field bounding faults are antithetics to both the main basin bounding fault and other major faults in the East Shetland Basin (figure 4.12). Furthermore, the Hudson-Otter half graben is located at an embayment of the East Shetland Basin into the neighbouring East Shetland Platform where the platform is bounded by two intersecting faults. These structures trend south-south-east to north-north-west and north-north-east to south-south-west and it is their movement that has controlled the development of the Hudson-Otter half graben (figure 4.12). In addition, the Greater Hudson Area is bounded to the east by the Tern-Eider Ridge, a northeast-southwest orientated horst structure formed during Permo-Triassic rifting. The Greater Hudson area sits upon a major Triassic half-graben located to the west of the Tern-Eider Ridge (Banbury and Underhill, 2002).

4.3.2 Structure of the Greater Hudson Area

Detailed interpretation of the syn-rift stratigraphy associated with the faults in the Greater Hudson area reveal two discrete structural themes; the first associated with the suite of antithetic faults which have controlled the development of the Hudson Field through time and the second associated with the major basin-bounding faults defining the edge of the East Shetland Basin to the east. These will be considered in turn.

The structural development of the Hudson Field is in the context of the Hudson-Otter Half Graben. This is a small basin delineated to the west by the East Shetland Basin Bounding Fault and to the east by the Tern-Eider Ridge (figure 4.12). The development of the Hudson Field is primarily controlled by antithetic faults which dip to the west and back-tilt pre-rift stratigraphy towards the North Viking Graben. This is the reverse of most other faults in the East Shetland Basin which dip to the east and back-tilt pre-rift stratigraphy away from the North Viking Graben, for example the Murchison, Statfjord and Visund-Gullfaks Faults (see sections 4.4, 4.5, and 4.6).

The antithetic faults controlling the development of the Hudson Field have formed as a result of rollover of the hangingwall into the easterly dipping East Shetland Basin Bounding Fault (ESBBF). The ESBBF is a regionally important structure extending over 300km in length and separating the relatively undeformed high area of the East Shetland Platform from the intensely deformed East Shetland Basin. In the Greater Hudson Area the fault is defined by two westerly dipping, normal displacement, segments. The northerly segment trends north-north-east to south-south-west and the southerly segment trends south-south-east to north-north-west. The segments intersect in a position adjacent to the Hudson Field and define the western limit of the Hudson-Otter half graben.

4.3.3 Timing of Activity in the Greater Hudson Area

The antithetic faults controlling the development of the Greater Hudson Area can be dated by examination of the geometries of well-dated stratigraphy present in their hangingwall depocentres. The sediments of the Brent Group show thickening into antithetic faults in the Greater Hudson Area. These units are therefore syn-rift deposits associated with the antithetic faults controlling the Greater Hudson area. The Top Brent Group reflector is cut by

the Hudson Fault and the Top Heather Formation reflector is draped across the fault. This is likely to be the result of uplift and erosion of the footwall of the Hudson Fault during the latest part of Brent Group deposition and the earliest part of Heather Formation deposition. The upper part of the Heather Formation and the Kimmeridge Clay Formations drape over the antithetic faults as post-rift horizons. The Hudson structure was therefore formed during deposition of the Brent Group and lower Heather Formation during the Middle Jurassic. The antithetic faults controlling the development of the Greater Hudson Area were therefore active very early in the rift episode and ceased to become active during deposition of the Heather Formation (167-155Ma).

The main East Shetland Basin Bounding Faults reveal a different activity history. Fault activity on the East Shetland Basin Bounding Fault was initiated in the later part of the Triassic (Zanella and Coward, 2003) during regional extension. Deposition of the Dunlin Group and Brent Group show expansion into the northeast - southwest trending section of the ESBBF in the Greater Hudson Area. The upper part of the Brent Group shows expansion of stratigraphy into both segments of the ESBBF in the Greater Hudson Area (figure 4.12). During the early Jurassic (202-169Ma) extension was therefore concentrated on the northeast -southwest trending part of the East Shetland Basin Bounding Fault (ESBBF) to the northwest of the Hudson area and there was no recorded activity on the northwest-southeast trending section to the west and southwest of Hudson. In the later part of the Jurassic extension was accommodated on both strands of the ESBBF in the Greater Hudson area.

During the Middle Jurassic, the Greater Hudson Area underwent further east-west orientated extension which was accommodated principally on pre-existing structures such as the ESBBF. Accommodation of extension on the two strands of the ESBBF led to the passive westerly rotation of the Hudson Field into the active fault.

Examination of the post-Jurassic stratigraphy associated with the ESBBF shows a wedge of Early Cretaceous age material deposited against both segments of the fault (figure 4.14). Activity on the East Shetland Basin Bounding Fault therefore continued into at least the Lower Cretaceous.

Evaluation of a transect across the East Shetland Basin, such as is undertaken in this thesis, would examine structures relating to the Tern-Eider Ridge after consideration of the Greater Hudson Area. However, in this study these structures are not examined in detail. The

reservoirs and their related structures in both the Tern and Eider hydrocarbon fields are Triassic in age and therefore do not relate to the Mid to Late Jurassic rift episode. Seismic data quality is poor in some Jurassic sections. In addition, there is a lack of Mid to Late Jurassic biostratigraphic and well control in the hangingwall depocentres to these structures. Furthermore, work by Banbury and Underhill (2002) showed that the structural setting in the Tern-Eider area of the Northern North Sea was fundamentally different in the Triassic to that in the Jurassic and that although some reactivation of Triassic structures occurred in the Jurassic, overall the Triassic and Jurassic structural trends are largely unrelated. As a result this study will not focus on the Tern-Eider area and will concentrate on four Jurassic structures, the Murchison, Statfjord, Snorre and Visund-Gullfaks faults situated to the east of the Tern-Eider ridge. These will be examined in order from west to east.

4.4 The Murchison Fault

4.4.1 Location and structure

The Murchison Fault is a northeast-southwest trending, east dipping structure over 40km in length (figure 4.1). It bounds the Dunlin, Thistle, Murchison and Statfjord-Nord hydrocarbon fields and the Sygma hydrocarbon discovery. It comprises a number of palaeosegments representing short, precursor fault segments which grew by radial tip propagation and subsequently linked to form the single structure observed today. Displacement minima on a displacement-length profile indicate linkage points which never fully equilibrated as a single structure (figure 4.15). This study is concerned with the northern part of the fault bounding the Murchison and Statfjord Nord hydrocarbon fields. The study section comprises two principal paleosegments, the Murchison Fault segment to the south with a length of 15km and maximum displacement 450ms (c. 710m) and the Statfjord Nord Segment to the north with a length of 11km in the study area and a maximum displacement of 380ms (c. 600m). These are hard-linked by a structure that has previously been referred to as the Jog Fault (Young et al., 2001).

4.4.2 Definition of syn-rift units

Detailed interpretation of the syn-rift units associated with the Murchison Fault can be used to reconstruct a history of activity for the structure. The syn-rift stratigraphy associated with

the Murchison Fault is subdivided into two discrete packages: syn-rift unit 1 and syn-rift unit 2. Syn-rift unit 1 comprises the Tarbert and Heather Formations. It is marked at its base by the Top Ness Formation or Top Pre-rift reflector and at its top by Top Heather Formation. Syn-rift unit 2 comprises the Kimmeridge Clay Formation (Draupne Formation in Norwegian Waters). It is defined at its base by the Top Heather Formation and at its top by the Base Cretaceous Unconformity.

4.4.3 Syn-rift Unit 1 – Top Ness (169Ma) to Top Heather (155Ma)

Tarbert and Heather Formations

Syn-rift unit 1 shows marked across-strike thickening in both the hangingwall of the easterly dipping Murchison fault segment and the hangingwall of the Statfjord Nord segment. (figure 4.17A). The unit reaches a maximum thickness of 150ms at the fault in comparison with 80ms 100m away from the fault. Thickening of the unit is seen to occur in semicircular depocentres of approximately 8km in along-strike diameter (northeast-southwest). These occur at intervals of approximately 10km along the fault trace and are not associated with any brittle deformational structures (figure 4.18). Syn-rift unit 1 shows no thickening into the Jog Fault. Syn-rift unit 1 shows no marked across strike thickening in the footwall to the Murchison fault and is present as a uniform thickness unit of approximately 30ms which is deposited throughout the footwall.

4.4.4 Syn-rift Unit 2 – Top Heather (155Ma) to Base Cretaceous Unconformity (140Ma)

Kimmeridge Clay Formation

Syn-rift unit 1 shows no variation in depositional thickness across the Murchison fault and is present as a uniform drape of approximately 25ms thickness in the hangingwall depocentres associated with both segments of the fault (figure 4.18). The unit shows onlap onto the Murchison Fault along the entire length of the structure (figure 4.16).

4.4.5 Evolution of the Murchison Fault

The evolution of the Murchison Fault will be considered for the two units associated with the syn-rift units 1 and 2 defined above for the two discrete segments that comprise the fault in the study area (the Murchison and Statfjord Nord Segments).

Observed thickening into both the Murchison and Statfjord Nord segments of syn-rift unit 1 indicate that the hangingwall of the fault was actively subsiding during deposition of this unit creating accommodation space for a wedge of sediment to be deposited against the fault. In comparison, the drape of syn-rift unit 2 over both segments of the Murchison Fault indicate that the fault was not active during deposition of the Kimmeridge Clay Formation. Therefore, cessation of activity on the Murchison Fault can be shown to have occurred at or shortly before the deposition of Top Heather Formation (155Ma). Traditionally, the syn-rift deposits associated with the Murchison fault are taken to be those sediments between the Top Ness to Base Cretaceous horizons (169-140Ma). Detailed stratigraphic interpretation has shown that the true syn-rift deposits are restricted to the interval between Top Ness Formation and Top Heather Formation.

In addition, the small semicircular depocentres seen in syn-rift unit 1 in the immediate hangingwall to the Murchison Fault can be interpreted to represent isolated depocentres each present as an early (Tarbert/Lower Heather age) point of high subsidence rate in the immediate hangingwalls to short unlinked fault segments. As these segments grew by radial tip propagation, their associated depocentres coalesced and formed a single throughgoing depocentre along the entire length of each of the major segments of the Murchison Fault.

The Jog Fault has been interpreted to be the result of late linkage of the Murchison segment with the Statfjord Nord segment reported to have occurred during the last seven million years of the Northern North Sea Mid to Late Jurassic rift episode during the deposition of the Kimmeridge Clay Formation (147 – 140Ma), (Young et al., 2001). The Jog Fault appears to have not fully equilibrated after linkage occurred as evidenced by its saw-toothed displacement-length profile and as maximum slip is not observed at the position of hard linkage (figure 4.15). Hard linkage of the Murchison and Statfjord Nord segments occurred late in the evolutionary history of the Murchison Fault, but this fault was not active throughout the Mid to Late Jurassic rift episode and as a result the Jog Fault formed relatively early in the rift episode as a whole. Hard linkage must have occurred at or near Top Heather (155Ma) before total cessation of activity on the Murchison Fault occurred.

4.5 The Statfjord and Snorre Faults

The Statfjord and Snorre faults are separate and individual faults that are the along-strike lateral equivalents of each other. Both faults are single throughgoing fault strands striking northeast-southwest with an easterly dip. The northern tip of the Statfjord Fault overlaps with and is in the immediate footwall to the Southern part of the Snorre Fault (figure 4.1).

4.5.1 Structure of the Statfjord Fault

The Alwyn-Brent-Statfjord Fault is a 62km single throughgoing fault strand with a planar easterly dip and maximum displacement in excess of 2km (McLeod et al., 2000). The fault strikes north-north-east to south-south-west in the north and north-south in the south. It bounds the North Alwyn, Strathspey, Brent, Statfjord and Statfjord East hydrocarbon fields. The fault comprises a number of discrete segments; the Strathspey, Brent and Statfjord Segments (McLeod et al., 2000). In the north, the fault splits into two strands, the Statfjord West and Statfjord East segments (McLeod et al., 2000). This interpretation will focus on the northern 62km part of the Statfjord Fault comprising the Strathspey, Brent and Statfjord Segments with a total accumulated displacement of 1.7km.

4.5.2 Structure of the Snorre Fault

The Snorre Fault is a 70km long single throughgoing fault strand with a planar easterly dip and maximum displacement 1500m. The fault bounds the Snorre, Tordis and Vigdis hydrocarbon fields (figure 4.1). It is orientated north-north-east to south-south-west and bounds uplifted, tilted fault blocks on the shoulder of the North Viking Graben. The present day fault comprises a single throughgoing fault strand with planar character, although abandoned splays indicate an origin from precursor segments. The upper part of the fault has been removed by erosion of the uplifted footwall and as a result the maximum extent of the fault plane is never observed (figure 4.19).

4.5.3 Definition of syn-rift units

Detailed interpretation of the syn-rift units associated with the Statfjord and Snorre Faults can be used to reconstruct a history of activity for the structures. The syn-rift stratigraphy associated with the Statfjord and Snorre Faults is subdivided into three discrete packages: syn-rift unit 1 and syn-rift units 2a and 2b. Syn-rift unit 1 is as defined above for the Murchison Fault. It comprises the Tarbert and Heather Formations. It is marked at its base by the Top Ness Formation or Top Pre-rift reflector and at its top by the Top Heather Formation. Syn-rift unit 2 comprises the Kimmeridge Clay Formation (Draupne Formation in Norwegian Waters). It is further subdivided into an upper and lower section. The lower part (syn-rift unit 2a) is defined at its base by the Top Heather Formation reflector and at its top by an intra-Kimmeridge Clay Formation reflector dated to be top Kimmerigian in age (151Ma). The upper part (syn-rift unit 2b) is defined at its base by the top Kimmeridgian reflector and at its top by the Base Cretaceous Unconformity.

4.5.4 Syn-rift Unit 1 – Top Ness (169Ma) to Top Heather (155Ma)

Tarbert and Heather Formations

Syn-rift unit 1 is as defined above (section 4.4.2). The package shows expansion into the Snorre and Statfjord Faults along their entire lengths (figures 4.17, 4.20 and 4.21). Thickening of syn-rift package 1 occurs in discrete semicircular lobes with diameters of 6-9km and is present along the entire length of the present day fault trace. The maximum thickness of the semicircular features ranges from 250ms on the Statfjord Fault to 500ms on the Snorre Fault. The unit reaches a minimum thickness of c.150ms at the intersections of adjacent thick packages.

4.5.5 Syn-rift Unit 2a – Top Heather Formation (155Ma) to Top Kimmeridgian (151Ma)

Lower Kimmeridge Clay Formation

Syn-rift unit 2a shows marked thickening into both the Snorre and Statfjord Faults. It is present as a 15-25ms thick unit away from the faults and reaches a maximum depositional thickness of 300ms at the Snorre Fault. The unit has a uniform morphology along the strike

of both faults where it is present as a wedge of material, thickening from the hangingwall into the fault, reaching a maximum depositional thickness at the fault plane itself (figure 4.22). The unit shows continuous thickness of deposition over the semicircular features observed in syn-rift unit 1. The unit not present on the footwall crest of either fault where it may have been removed by uplift and subsequent erosion of the footwall crest.

4.5.6 Syn-rift Unit 2b –Top Kimmeridgian (151Ma) to Base Cretaceous Unconformity (140Ma)

Upper Kimmeridge Clay Formation

Syn-rift unit 2b is defined at base by an Intra Kimmeridge Clay horizon which is top Kimmeridgian in age and at top by the Base Cretaceous Unconformity (figure 4.23). The unit shows a uniform thickness of c.100ms deposited in the hangingwall to both the Statfjord and Snorre Faults along the entire length of the present day fault trace. The top Kimmeridgian horizon is subparallel with the Base Cretaceous Unconformity throughout the hangingwall depocentre and where present in the footwall to the Statfjord and Snorre Faults (figures 4.20 and 4.21).

4.5.7 Evolution of the Statfjord and Snorre Faults

The Statfjord and Snorre Faults, as the Murchison Fault, principally grew by the process of radial tip propagation and subsequent segment linkage as evidenced by the abandoned fault tips seen in the footwall and hangingwall to the present day main fault (McLeod et al., 2000). The semicircular packages present in syn-rift unit 1 indicate the positions of early isolated depocentres in the hangingwalls to the faults along their length which are adjacent to the locations of early (Tarbert and Heather in age) isolated fault strands. These early segments can also been seen on a displacement length profile of the Statfjord Fault (figure 4.24) where they are separated by local displacement minima.

The generation of 500ms of accommodation space in 14Ma indicated an average slip rate of c. 57m/Ma for the duration of deposition of syn-rift unit 1. This is calculated as an average for each local precursor fault segment on the Snorre Fault.

The strike-parallel continuous wedge of material seen in syn-rift units 2a and 2b indicates that by the end of Heather deposition these early isolated depocentres had coalesced as a result of segment linkage and that the fault was acting as a continuous coherent fault strand. The early isolated depocentres appear to have persisted until 155 Ma (Top Heather) as indicated by the thin (150ms) deposits of Tarbert and Heather Formations in between early depocentres. The wedge of material seen in syn-rift unit 2a thickening into the fault indicates that the hangingwall of the Statfjord and Snorre Faults were actively subsiding between Top Heather and Top Kimmerigian (155 Ma – 151 Ma) creating accommodation space for a wedge of material to be deposited against the fault plane.

The generation of 300ms of accommodation space on the Snorre Fault in 4Ma indicated an average slip rate of c.118m/Ma. This is in greatly increased from the 57m/Ma inferred from syn-rift unit 1.

The uniform thickness of syn-rift unit 2b over the Statfjord and Snorre Faults indicates that the unit was deposited during a time when there was no movement on the fault. Cessation of activity on the Statfjord and Snorre Faults must have occurred by Top Kimmeridgian (151Ma) in order for a uniform thickness of syn-rift unit 2b to be deposited onto a dormant and no longer subsiding hangingwall. The Statfjord and Snorre Faults were therefore active between 169Ma (Top Ness) and 151Ma (Top Kimmeridgian) inclusive.

Application of displacement-length scalings such as those proposed by Schlische et al., (1996) indicate that the Statfjord Fault is has not accumulated as much displacement as would be expected for a fault of its length and that displacement variations along the length of the normal fault system that developed whilst the fault was in a prelinkage, multi-segment state have not been lost and show only a small degree of equilibration (McLeod et al., 2000). This is taken to reflect the immaturity of the fault system and that it became inactive whilst in the process of linkage and never had the opportunity to accumulate vertical displacement in proportion to its along strike length. This is consistent with the observations that the Statfjord Fault became inactive before the end of the Mid to Late Jurassic rift episode.

The hangingwall to the Statfjord Fault contains numerous faults including an array of antithetic faults situated 3.5km east of and striking parallel to the main fault, with westerly dips and lengths of up to 5km (figure 4.25). McLeod et al (2000) mapped the distribution and characteristics of the hangingwall fault population associated with the Statfjord Fault.

The antithetic array ceased to become active 11-12My after initiation of the rift episode. This can be observed by examination of the syn-rift stratigraphy associated with the antithetic faults (figure 4.26). A similar array of faults is seen in the hangingwall to the Snorre Fault. The faults strike sub-parallel to the main Snorre Fault and dip both antithetic and synthetic to the main Snorre Fault. This population of faults offset pre-rift and lower syn-rift reflectors only (figure 4.27) and indicate cessation of activity on the faults prior to Top Heather Formation (155Ma), 12My into the rift episode.

In addition to interpretation of the syn-rift geometries associated with each fault, it is also possible to examine the position of maximum displacement on each fault and correlate this to the position of maximum elevation. On the Statfjord Fault the position of maximum displacement corresponds to the position of maximum elevation of the uplifted footwall. On the Snorre Fault the position of maximum displacement corresponds to the position of maximum footwall erosion and to the maximum thickness of syn-rift stratigraphy but it is not located at the present day structural high on the fault scarp (figure 4.28). The present day structural high on the Snorre Fault is located to the south of the paleo-crest of the Snorre Fault in the area where the Snorre and Visund-Gullfaks Faults are closest. The uplift of the present day structural high clearly happened late in the rift episode and it is attributed to differential uplift along the footwall of the VG fault to the east. The hangingwall depocentre of the Snorre fault was passively uplifted in the latest part of the rift episode.

4.6 The Visund-Gullfaks Fault

4.6.1 Location and Structure

The Visund-Gullfaks (VG) Fault is the most grabenward fault on the edge of the East Shetland Basin in the Northern North Sea. It bounds the Visund, Gullfaks, Gullfaks South and Alwyn hydrocarbon fields. It is a single throughgoing fault strand which extends from 61˚N in the south to 61˚80'N in the north, a distance in excess of 150km (figure 4.1). The fault block is approximately 25-28km in width and contains pre-rift stratigraphy that has been back tilted to an average of 9-10˚ (Faerseth et al., 1995). It has a total accumulated displacement in excess of 5km. In terms of length, displacement and the footwall dip of pre-rift sediments, it can be defined as the largest fault in the East Shetland Basin. As a direct result of the large accumulated slip, the syn-rift sediments in the hangingwall to the VG fault are at average depths in excess of five seconds. This results in very poor seismic resolution

and it not being possible to carry out detailed mapping of the syn-rift sediments. However, slip magnitude can be estimated from the few exploration wells (for example, 34/5-7) that penetrate the VG hangingwall. The hangingwall to the VG fault contains more than 1000m of Kimmeridge Clay Formation stratigraphy which is present in a wedge shaped geometry increasing into the VG Fault (Faerseth et al., 1995). In addition, the presence of the Kvitbjorn hydrocarbon field on a terrace in the southern part of the hangingwall to the VG fault provides additional well and seismic calibration.

The Visund-Gullfaks fault block has a rounded profile which flattens to the south. The footwall to the VG fault shows considerable degradation (figure 4.29). An estimated 60km³ of material is shown to have been removed from the uplifted footwall during and after the Mid to Late Jurassic Rift episode. This will be considered further in chapter 5.

4.6.2 Evolution of the Visund-Gullfaks Fault

The structural interpretation of the Visund-Gullfaks Fault can be derived from a number of lines of evidence. The fault is 150km long and has accumulated in excess of 5km displacement (Faerseth et al., 1995) in the study area. This is the maximum slip observed on any one fault in the East Shetland Basin. *The fault must therefore have been active over a longer period of time than other faults, or moved at a greater slip rate than other faults, or both*. Using fault displacement-length scaling relationships propsed by Schlische et al., (1996) a fault of 150km length would be expected to accumulate a maximum displacement of c.5km, similar to that observed on the VG fault. This observation suggests that the fault is fully equilibrated and a characteristic bell shaped (figure 2.1) displacement-length profile would be predicted. The equilibrated nature of the fault suggests that it was active for longer than the Murchison, Statfjord and Snorre Faults and therefore active later in the rift episode.

Detailed interpretation of the VG footwall adjacent to the Snorre Fault shows that the syn-rift sediments associated with the subsiding hangingwall to the Snorre Fault are uplifted and eroded in the crest to the VG footwall (figure 4.30). This indicates that either the VG fault was active later than the Snorre Fault, inferred to be activity into the Volgian after cessation of activity on the Snorre and Statfjord Faults at the end Kimmeridgian, or the VG Fault was active with increasing slip rate towards the end of the rift episode. A similar relationship was examined by McLeod (2000) associated with the Statfjord Fault. The hangingwall to the Statfjord Fault was an area of net deposition from the onset of extension in the Latest

Bajocian until the Kimmeridgian and sediments of the Tarbert, Heather and Lower Kimmeridge Clay Formation were deposited in it. However, in the Kimmeridgian the area became uplifted and subsequently erosion of the syn-rift stratigraphy occurred. The transition from a dominantly depositional regime to that of an erosional regime may be the result of either decreased rates of activity on the Statfjord Fault in the Volgian and Ryazanian or uplift of the VG footwall to the east or both.

Interpretation of exploration wells in the hangingwall to the VG Fault show (for example 34/8-7 (figure 4.31)) a considerable thickness of syn-rift units 1, 2a and 2b indicating that there was active hangingwall subsidence and net generation of accommodation space during all three syn-rift intervals on the fault.

The tilt of the pre-rift sediments in the footwall to the VG Fault also provide further evidence for the magnitude of movement on the fault. The present day average dip at pre-rift level is 9˚ (Faerseth et al., 1995). The average dip of the faults blocks in the East Shetland Basin and Tampen Spur Province is 6˚ (Yielding, 1990). The VG fault block possesses the steepest dip of all fault blocks in the Northern North Sea Rift Province indicating a greater magnitude of slip on the block bounding fault (the VG fault). Faerseth et al. (1995) have reconstructed the history of tilting of the VG fault block using depth converted seismic sections. They show that during the earliest part of the Mid to Late Jurassic rift episode (Bathonian), tilt on the VG fault block was probably less than 1˚. By the end of deposition of the Heather Formation (Mid Oxfordian) the tilt on the block had reached a minimum of 2˚. The major period of tilting of the pre-rift stratigraphy occurred during deposition of the Kimmeridge Clay Formation. Between the Mid Oxfordian and late Volgian to Ryazanian the block was back tilted to 10-10.5˚. Increased rates of slip on the block bounding faults are inferred to be responsible for this increase in tilt. Since the end of the rift episode the VG block has been rotated back 1-1.5˚ as a result of post-rift thermal subsidence.

The VG Fault can be shown to be the largest fault in the East Shetland Basin in terms of length, tilt and total displacement. Comparison of structures in the East Shetland Basin with their equivalent structures on the Norwegian side of the Northern North Sea, in the Horda Platform reveals a similar trend. Strain is more distributed on the eastern side of the North Viking Graben although the most proximal fault array, (the Oseberg-Huldra array), bounding the graben to the east has an accumulated displacement at top middle Jurassic level of 4-5km (Fareseth and Ravnas, 1998). This is in excess of any other individual structure on the

eastern side of the Northern North Sea. The faults in the East Shetland Basin increase in length and displacement towards the North Viking Graben. Given that rifting initiated synchronously throughout the Northern North Sea during the latest Bajocian (Ravnas et al., 1997; Davies et al., 2000), the variability in the size of the faults must result from either the faults with greater displacement being active at higher slip rates throughout the rift episode or the larger faults being active for longer. The data presented above on cessation of activity on the more distal faults above supports a non-synchronous termination of faults and is presented as an integrated structural history in section 4.7 below.

4.7 Tectono-stratigraphic evolution of the East Shetland Basin and North Viking Graben

The tectono-stratigraphic evolution of the East Shetland Basin can be considered in five discrete stages (after Cowie et al., 2000).

4.7.1 Upper Bajocian (169Ma – 167Ma)

The onset of extension in the Northern North Sea is characterised by the nucleation and initiation of activity on large numbers of isolated fault segments which grow by radial tip propagation. The segments are short and have small displacements. Isolated depocentres develop next to these bilaterally propagating segments such as those recorded by syn-rift unit 1 associated with the Murchison, Statfjord and Snorre Faults. The Northern North Sea rift province at this time was characterised by large numbers of short, low displacement, distributed normal faults which did not interact with each other. During this stage the deposition of the Tarbert Formation occurred in shallow, local depocentres associated with the short, isolated fault segments.

4.7.2 Bathonian (167Ma - 164Ma)

This is a composite stage in the development of the Northern North Sea rift province when continued nucleation occurred alongside the onset of segment interaction and linkage. Where linkage occurs between adjacent along strike fault segments the associated depocentres coalesce and form large depocentres which are initially underfilled. This stage in the development of the Northern North Sea rift province is recorded by the deposition of the

lower part of the Heather Formation which is predominantly present in discrete depocentres associated with medium length normal faults.

4.7.3 Callovian – Lower Oxfordian (164Ma - 155Ma)

This stage comprises the dominant stage of fault segment interaction and subsequent linkage. There is a marked decrease in the nucleation rate of new faults. During this time in the Northern North Sea, the upper part of the Heather Formation was deposited. Fault segment hard linkage, such as that shown to occur across the Jog Fault linking the Murchison and Statfjord Nord segments of the Murchison Fault, results in the formation of large coalesced depocentres which extend along the entire length of the now throughgoing normal faults. At this stage, fault linkage results in many faults having newly-formed underfilled hangingwall depocentres. During this stage in the development of the basin the previously distributed strain begins to focus towards the centre of the rift province, that is through the East Shetland Basin towards the Viking Graben. This process is recorded in the syn-rift sediments and fault morphology by the cessation of activity on the Murchison Fault.

Situated on the edge of the rift province, the Murchison Fault had only just fully linked via the Jog Fault and established a full thoroughgoing fault strand before it became inactive at c.155Ma. The Murchison Fault was then abandoned, alongside other faults, for example, the Ninian Fault to the south, on the edge of the rift province as strain localisation began to enhance slip rates on more proximal fault arrays closer to the rift axis.

4.7.4 Kimmeridgian (155Ma - 148Ma)

Full linkage of fault segments in the active portion of the Northern North Sea rift basin occurs during this stage to produce single throughgoing fault systems such as the Strathspey-Brent-Statfjord Fault system and the Visund-Gullfaks Fault system. Each of these large fault systems has a single isolated hangingwall depocentre associated with it: these are the result of coalescence of remnant depocentres that formed associated with the earlier, shorter precursor fault segments. The linkage to form long throughgoing fault systems results in more uniform subsidence along strike as shown by the deposition of a wedge of Lower Kimmeridge Clay Formation of uniform thickness along strike deposited in the immediate hangingwall to both the Statfjord and Snorre Faults. However, by 148Ma strain localisation into the North Viking Graben has resulted in cessation of activity on the Statfjord and Snorre Faults. These structures are abandoned and following linkage, never acquire enough slip to

become a fully equilibrated fault system. This disequilibrium is reflected in the displacement length profile of the Statfjord fault, which preserves segment linkage points as displacement lows and is also evidence in the underfilled hangingwall depocentre associated with the Statfjord Fault (McLeod et al., 2000).

4.7.5 Volgian - Ryazanian (148Ma - 140Ma)

The climax of the rift is reached in the Volgian which is dominated by full focussing of strain onto a single throughgoing normal fault, the Visund-Gullfaks Fault. All other faults in the basin have become inactive and some, for example the Snorre and Statfjord Faults, are passively uplifted, rotated and eroded in the footwall to larger, more proximal structures such as the Visund-Gullfaks Fault. The rate of slip on this graben-bounding fault reaches its maximum in the rift climax stage.

The syn-rift deposits associated with the distal suite of faults, for example Murchison, Statfjord and Snorre, show a uniform thickness drape of sediment over both uplifted footwalls and hangingwall depocentres indicating inactivity for the duration of this period. In contrast, the thick package of Upper Kimmeridge Clay Formation deposited in the hangingwall to the Visund-Gullfaks fault reflects its continued activity into the Volgian and Ryazanian.

4.7.6 Post Ryazanian (<140Ma)

The Ryazanian period records the transition from syn-rift to post-rift conditions in the Northern North Sea. During this time, the deposition of the Lower Cretaceous Cromer Knoll Group and Upper Cretaceous Chalk Group occurred. The Cromer Knoll group onlaps the Late Jurassic structures and is preferentially deposited in topographic lows associated with hangingwall depocentres. The chalk is more found more extensively across the basin. The Northern North Sea Mid to Late Jurassic rift basin was generally underfilled during the rift episode and as a result post-rift sediments exploited syn-rift accommodation space in addition to that created by post-rift thermal subsidence.

4.8 Discussion

The development of the Mid to Late Jurassic Northern North Sea rift province was dominated by the migration of the locus of extension towards the rift axis, the North Viking Graben, over time as strain was progressively localised in the East Shetland Basin. Detailed examination of the syn-rift sediments associated with this rift episode for a suite of normal faults across the basin reveals the evolving nature of the rift basin from when it was characterised by a large number of small displacement, distributed normal faults to when it was dominated by a single throughgoing linked fault array situated on the edge of the North Viking Graben. This interpretation is shown from both examination of the seismic stratigraphy and exploration well composite logs (figure 4.32). This interpretation is in stark contrast to earlier ideas which suggest all faults were active until the end of the rift episode (Ryazanian) when rifting ceased synchronously across the whole of the graben (Badley et al., 1988).

The primary implication of the strain localisation model for the development of the East Shetland Basin is that the age of the top syn-rift deposit *cannot* be taken to be synchronous across the entire Northern North Sea Basin. Traditionally, top syn-rift is taken to be the Base Cretaceous Unconformity (BCU), however the systematic cessation of activity on faults across the basin shown in this study results in the BCU only representing top syn-rift for the most axial fault, the Visund-Gullfaks Fault. Instead, BCU in the hangingwall to faults on the edge of the rift province, for example the Murchison Fault, occurs as a post-rift horizon and top syn-rift horizon is a marker at or near Top Heather Formation (155Ma).

The overall thickness of syn-rift units associated with individual faults in the East Shetland Basin also provides an indication of activity levels on different faults as the rift episode progressed. The thickness of syn-rift unit 1 (Top Ness to Top Heather – 169Ma – 155Ma) is much greater in the hangingwall to the Statfjord Fault (max 250ms) than in the hangingwall to the more distal Murchison Fault (max 150ms). Assuming both hangingwall depocentres were under the same sedimentation regime (i.e. access to sediment volume, type and grain size were identical) then the net generation rate of accommodation space must have been greater on the Statfjord Fault than on the Murchison Fault indicating a greater rate of subsidence and greater slip rate. The isolated fault strands comprising each fault were similar lengths (c. 60km) at this time and therefore the process of strain localisation towards the rift axis must have been initiated very early in the rift episode. As a result, increased slip rates on

more proximal fault precursor segments occurred at the expense of more distal segments such as those precursors to the Murchison Fault.

The displacement-length profiles of a suite of faults across the East Shetland Basin also reveal an early termination history for those faults further away from the North Viking Graben. For example the Murchison Fault is in excess of 25km long (Young et al., 2001). According to Schilsche et al. (1996) the displacement-length relationships of a global population of faults can be described by $D= 0.03L^{1.06}$. It is possible to use this line as a reference from which to compare with faults in the Northern North Sea. The Murchison Fault would be expected to accumulate a maximum displacement of c. 1.4km. The maximum observed displacement on this fault is c. 710m (Young et al., 2001). A similar relationship is observed in both the Ninian and Hutton Faults, the along strike lateral equivalents to the Murchison fault located to the south. The Ninian fault is 80km long and has a maximum accumulated displacement of approximately 2km, significantly less than the 3.1km predicted by Schlische et al (1996). The Hutton Fault has a maximum displacement of 300m. The low total accumulated displacement observed on these faults is a result of late linkage of precursor segments to form a single throughgoing fault which ceased to be active shortly after linkage and as a result never accumulated maximum displacement.

The examination of displacement-length profiles for three faults across the strike of the East Shetland Basin show that faults located further away from the rift axis show saw-tooth profiles some of which show areas of zero displacement midway along the fault. They do not show the characteristic 'bell-shaped' profile associated with normal faults with maximum displacement in the centre of the fault decreasing to zero at the fault tips (figure 4.33A). This is a reflection of the early cessation of activity on these faults as strain was localised away from them onto the Visund-Gullfaks Fault, which bounded the evolving North Viking Graben.

4.9 Conclusions

Each individual fault system in the East Shetland Basin has a history characterised by growth and linkage of fault segments, to produce a single throughgoing fault which was active from the initiation of rifting in the basin until a time defined by the position of the fault with respect to the rift axis, the North Viking Graben.

The rift episode was initially characterised by a large number of discrete, distributed, short, low displacement normal faults. These grew by radial tip propagation and subsequent segment linkage to from large (up to 150km long) throughgoing fault arrays with displacements up to 5km. In addition to the controls on along strike fault growth and segment linkage the East Shetland Basin was also subjected to a process in which strain was localised across the basin onto the rift axis (figure 4.33B). This resulted in a sequential cessation of activity from west to east across the basin. Inactive faults were left with underfilled hangingwall depocentres as post-rift sediments of uniform thickness were draped over the inactive structures. Some abandoned faults are shown to be uplifted in the footwalls to faults located nearer the rift axis (e.g. Snorre in the footwall to Visund-Gullfaks). A five stage evolution is presented for the development of the East Shetland Basin during the Mid to Late Jurassic rift episode in which the growth, linkage and strain localisation history is documented through detailed interpretation of the pre, syn and post-rift sediment morphology.

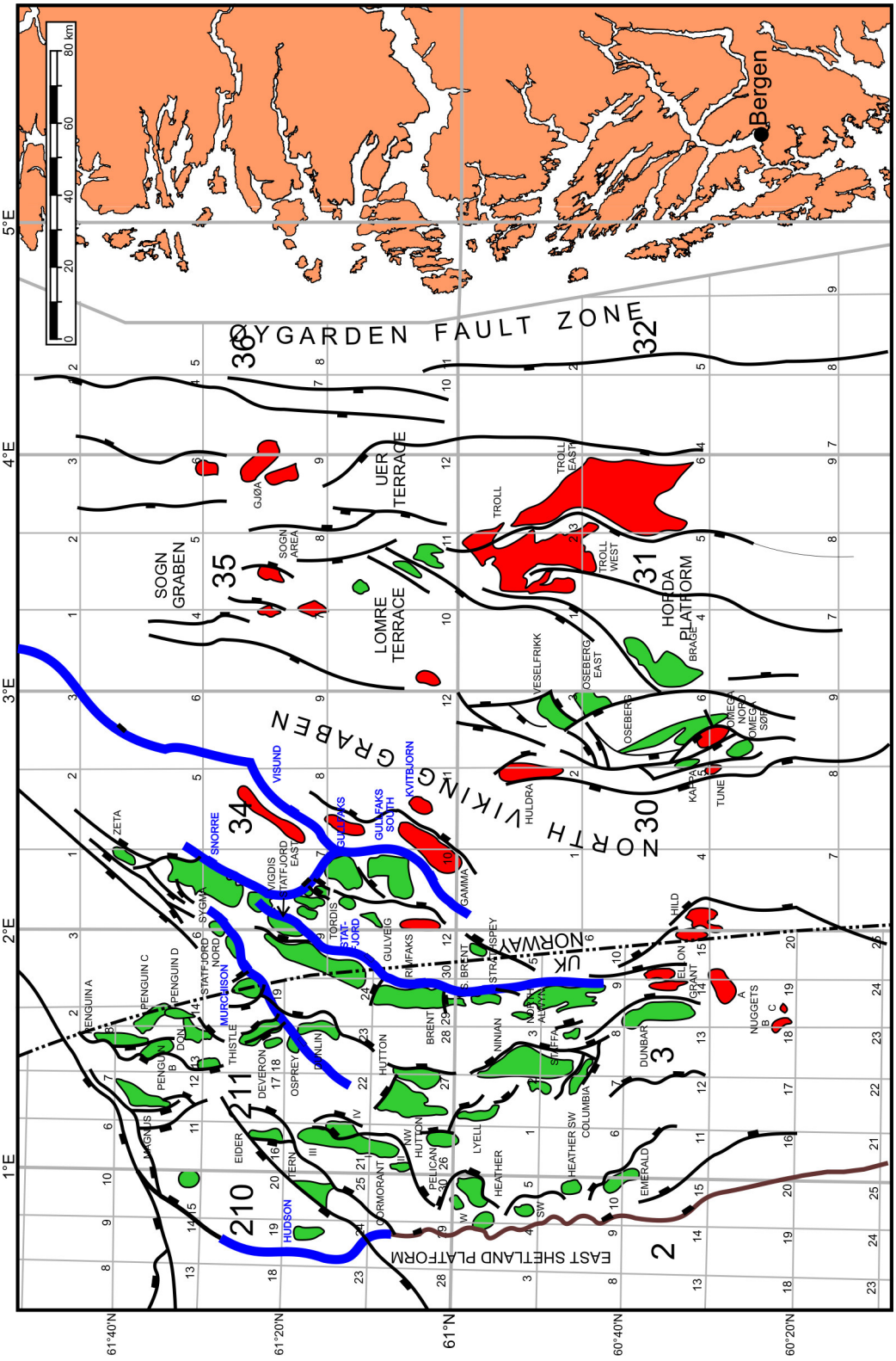

Figure 4.1 Map showing position of faults incorporated into study.

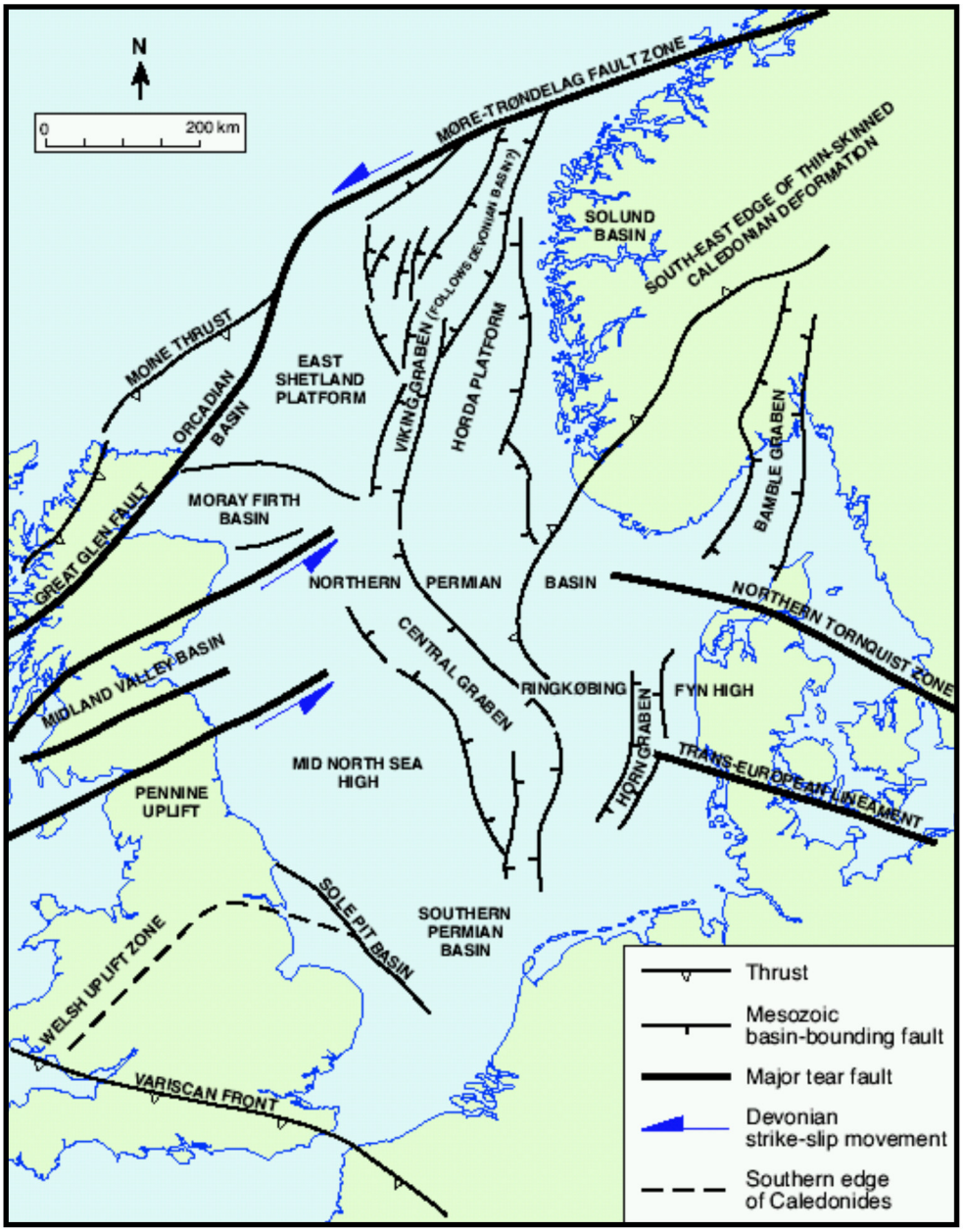

Figure 4.2
Generalised tectonic framework of Northwest Europe
Sinistral strike-slip movements along the Great Glen-Møre-Trøndelag fault zone and the Midland Valley fault system during the Devonian may have produced pull-apart basin, which were subsequently reactivated during Mesozoic extension to form the Viking Graben
From Zanella and Coward, 2003

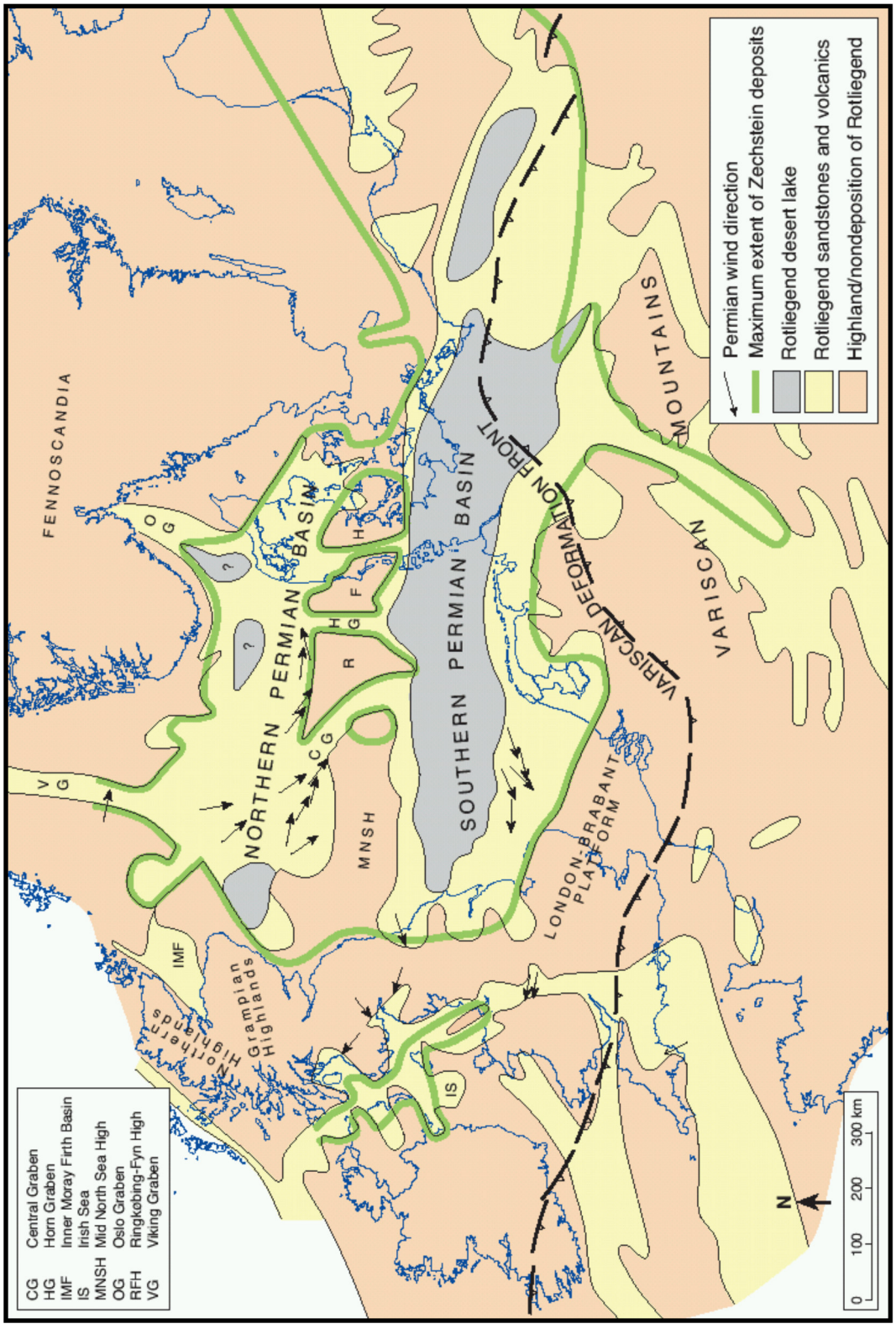

Figure 4.3 Sketch map of Permian Sedimentary Basins in Northwest Europe From Glennie et al., 2003

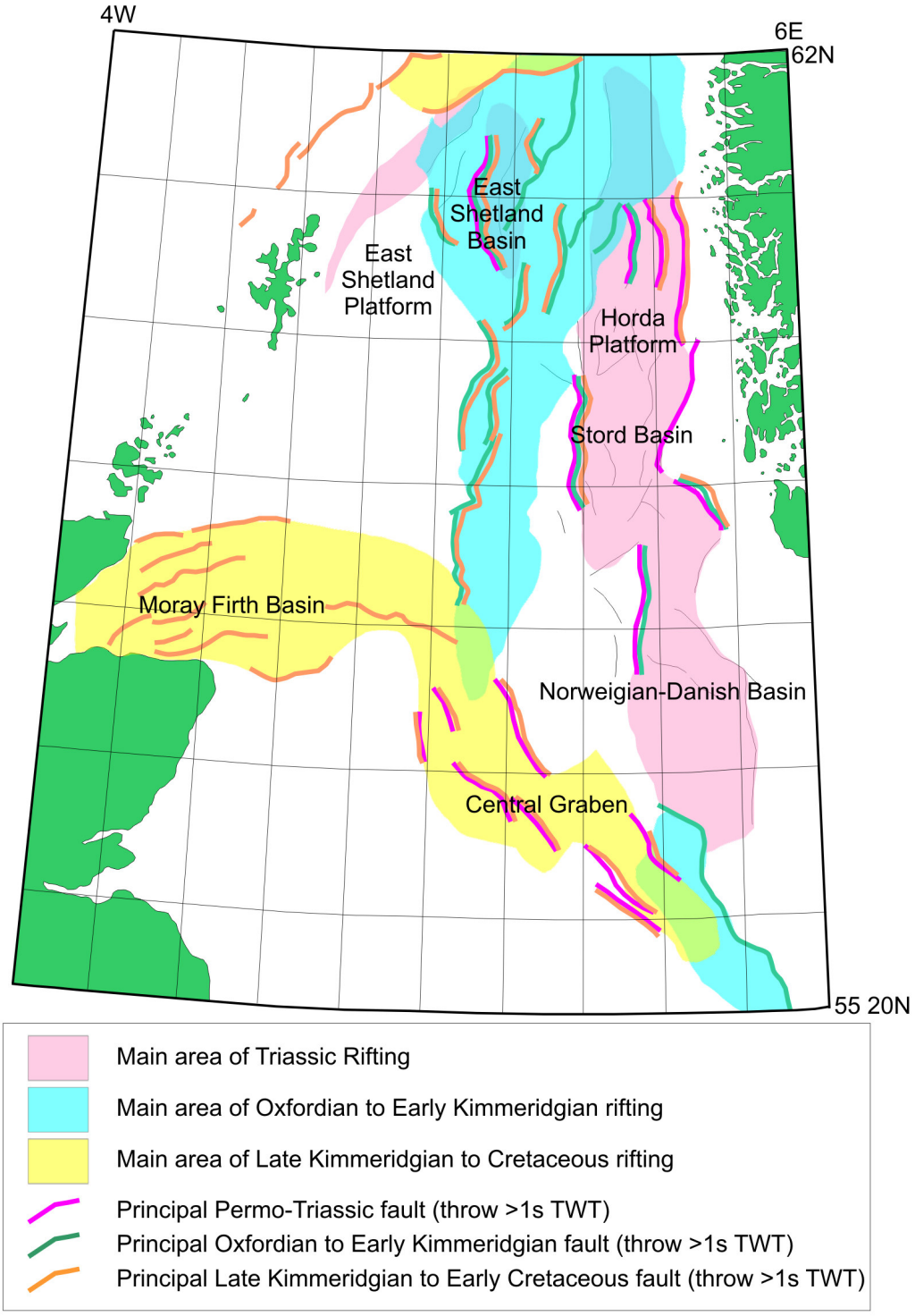

Figure 4.4
Triassic to Early Cretaceous rifting pattern in the North Sea
Triassic extension is characterised in the Northern North Sea by wide, north-south orientated, tilted fault blocks.
Oxfordian to early Kimmeridgian structures are mainly located in the Northern North Sea and form large, north to north-easterly trending, tilted fault blocks. Most faults of Triassic origin show reactivation although the Jurassic throw is smaller.
During the Late Kimmeridgian to early Cretaceous, changes in extensional direction resulted in the creation of north-westerly dipping normal faults, mainly in the Central North Sea and Moray Firth. From Zanella and Coward, 2003.

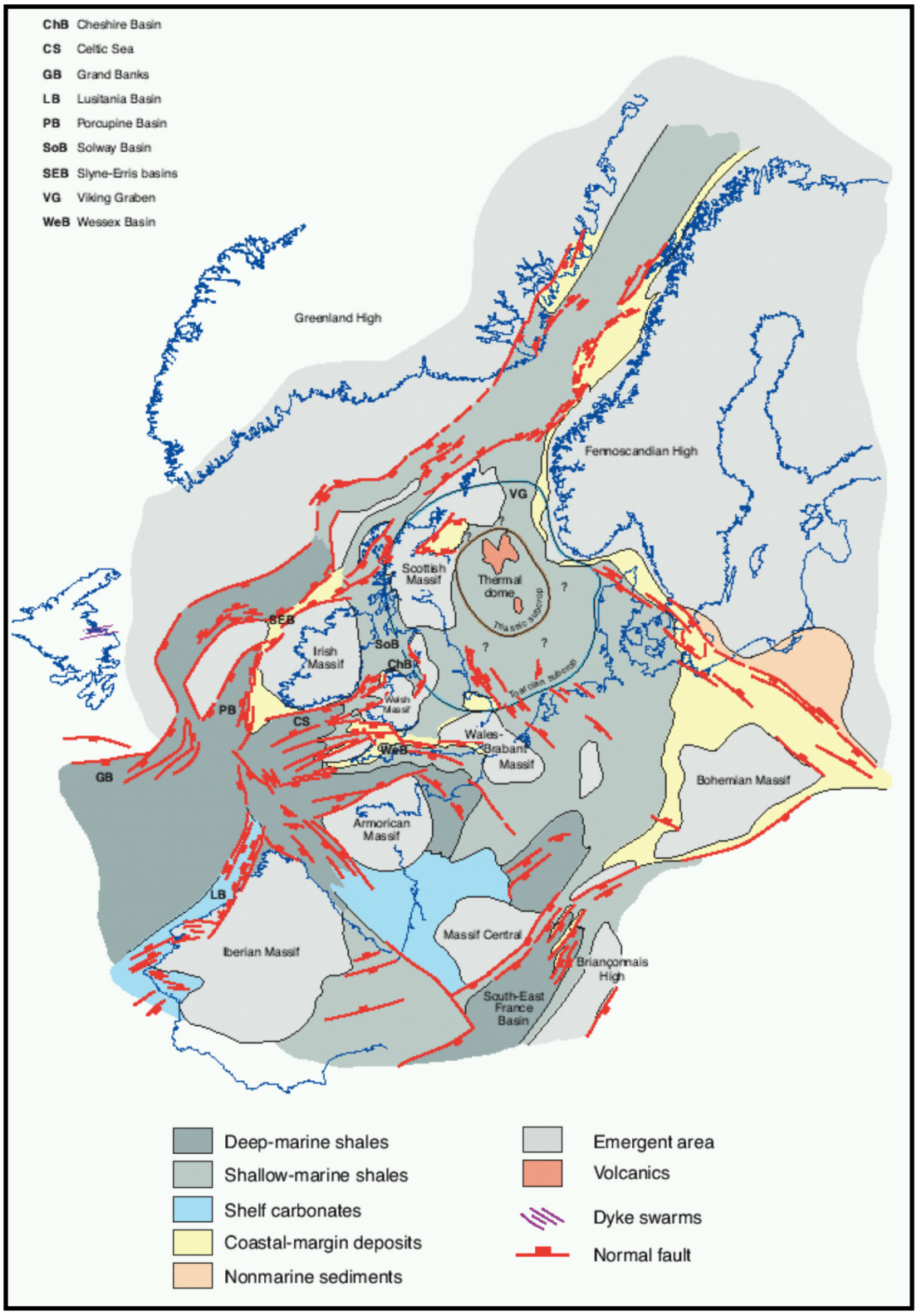

Figure 4.5
Palinspastic map for the Early Jurassic showing the distribution of active structures and sediment facies.
Map also shows location of the Mid-Jurassic thermal dome in the North Sea.
From Coward et al., 2003

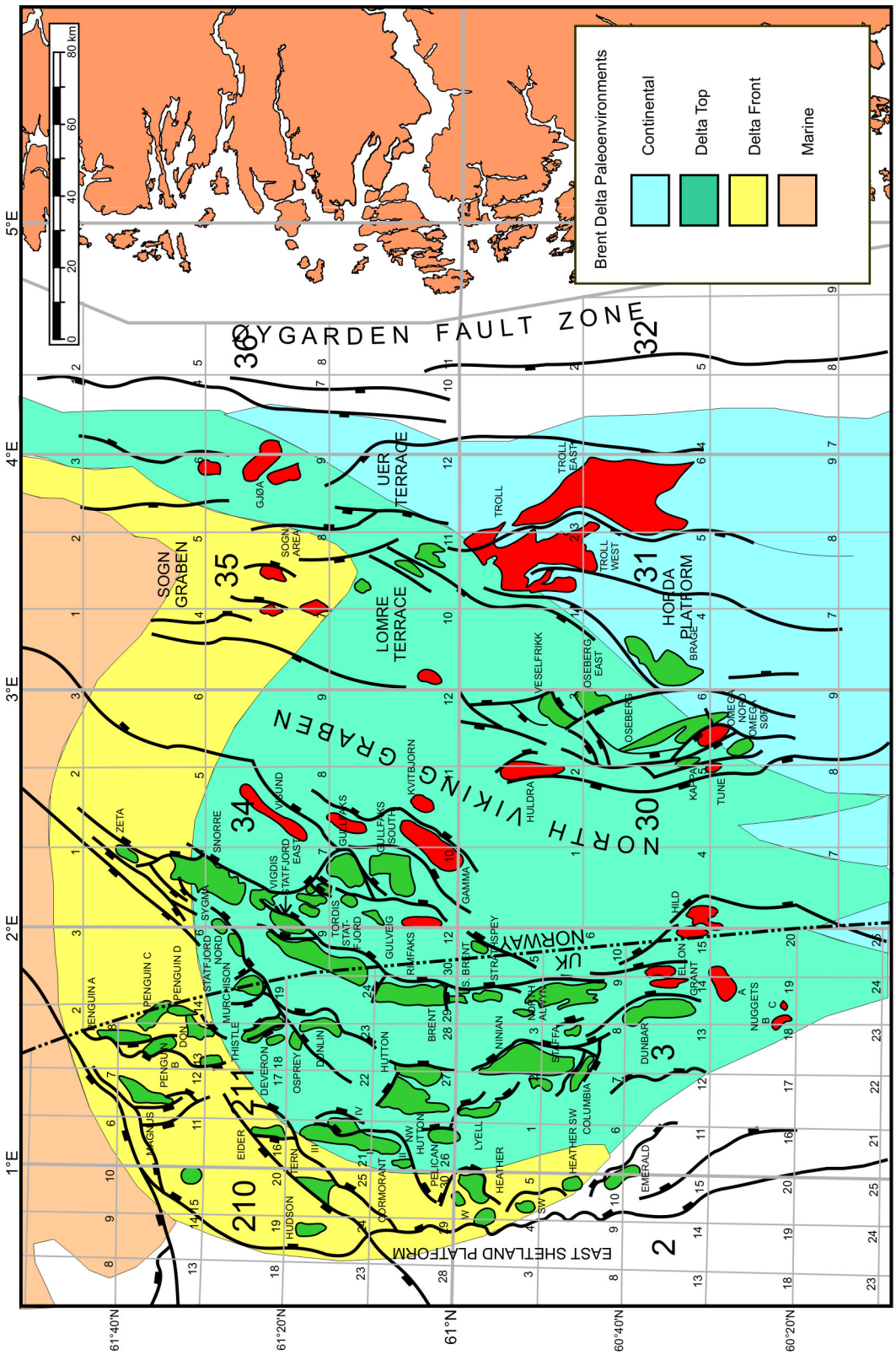

Figure 4.6 Map showing location and extent of the Brent Delta

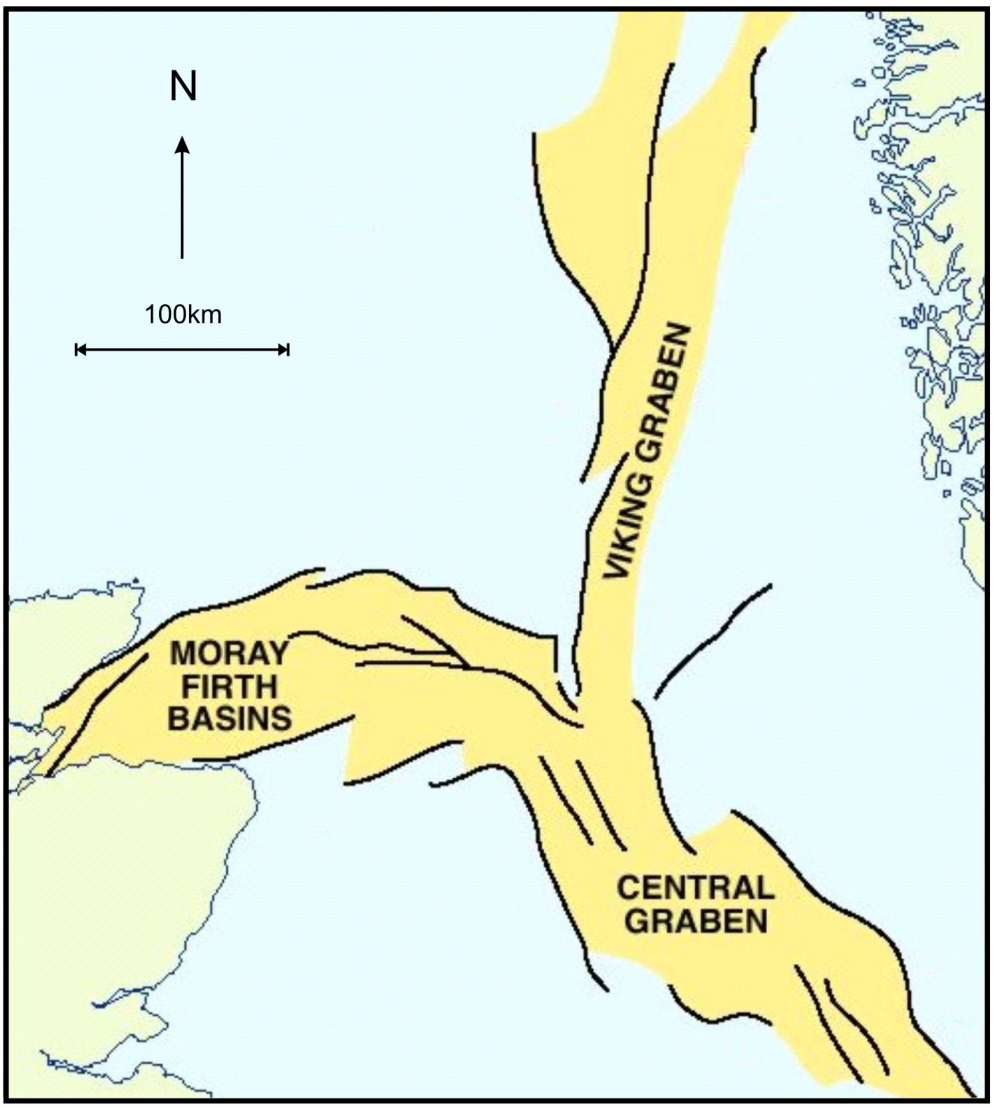

Figure 4.7
Sketch map showing location and nature of Mid to Late Jurassic trilete rift system in the North Sea
After Zanella and Coward, 2003

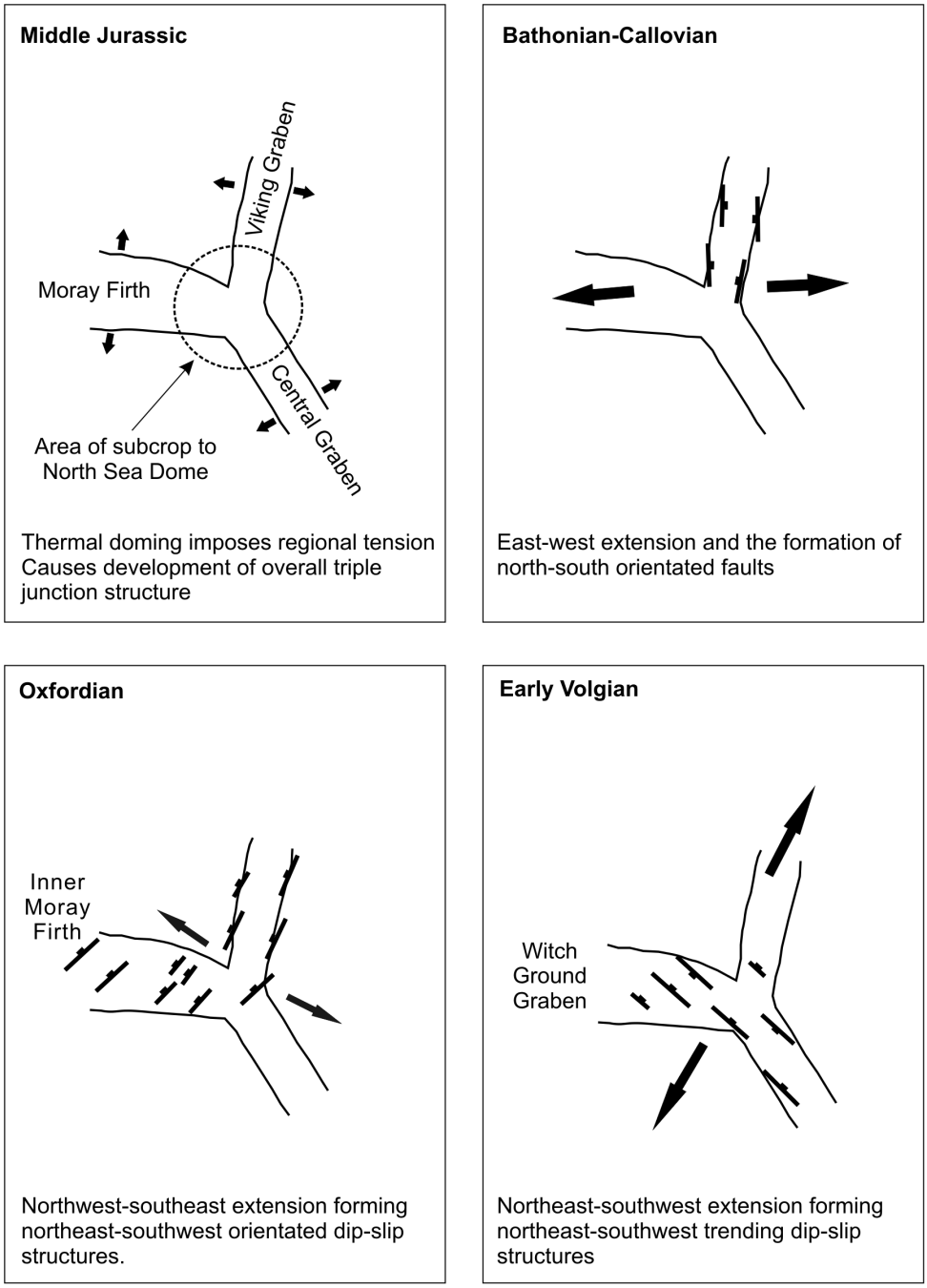

Figure 4.8
Cartoon showing that after Middle Jurassic doming the three resultant rift zones were exploited as zones of weakness during Middle-Late Jurassic rifting. Active faulting during this rift phase varied through time in both orientation and location depending on the prevailing far-field least principal stresses
After Davies et al., 2001

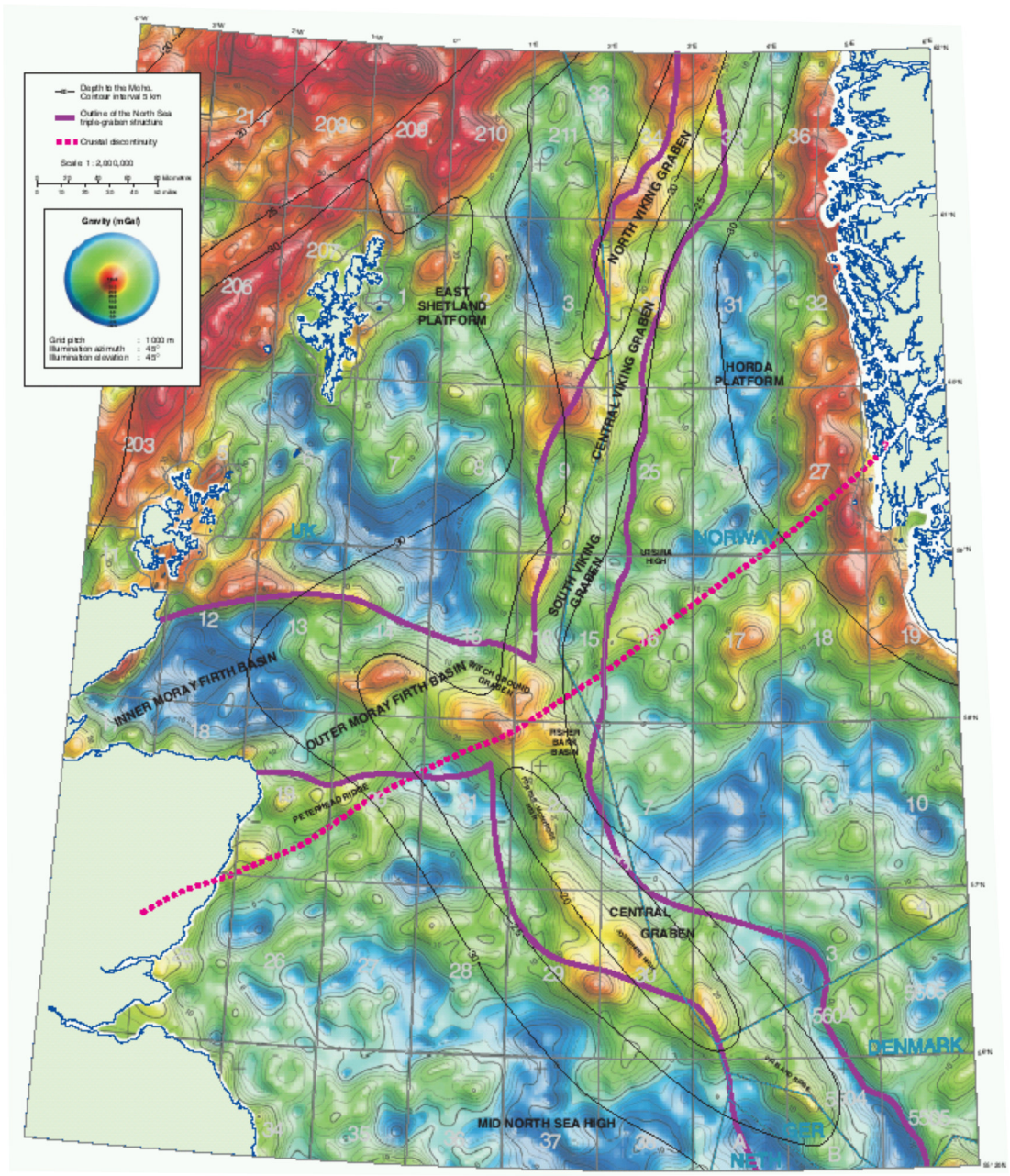

Figure 4.9A
Bouguer gravity anomaly and depth to the Moho based upon free-air gravity data derived from DT Sanwell's Geosat and ERS-1 satellite altimeter profiles (Sandwell, 1990). The bouger correction is derived from the ETOP5 database supplied by the US department of Commerce's National Oceanic and Atmospheric Administration (NOAA). Contours are depth to the Moho based upon seismic data, mainly after Ziegler (1990).
The graben areas are characterised by linear positive anomalies, an effect caused by the elevation of the Moho and denser upper mantly beneath the rifts.
From Zanella et al., 2003

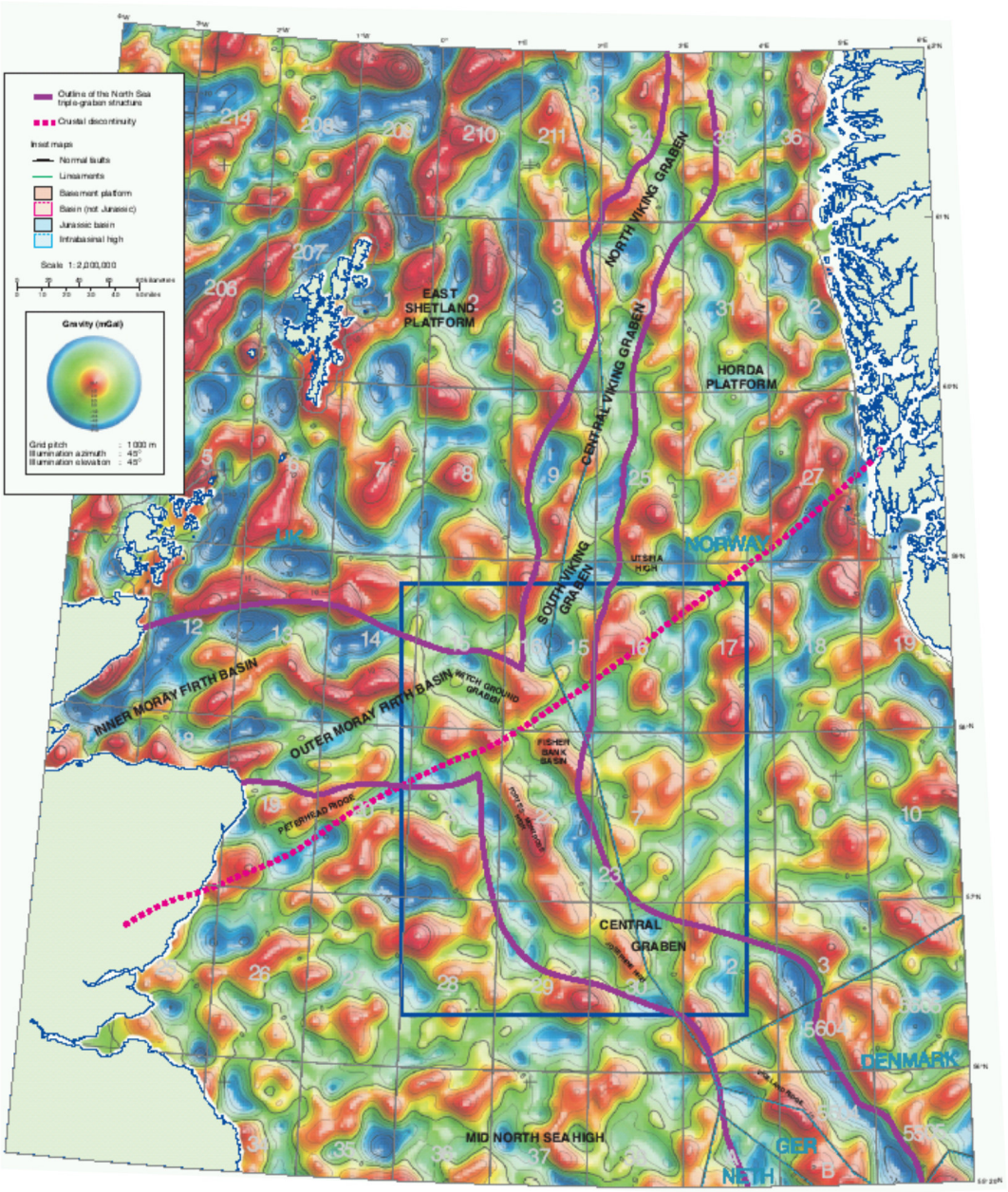

Figure 4.9B
Residual Bouguer anomaly gravity map produced by removing the long wavelength 'regional' component from the Bouguer gravity anomaly map in figure 4.x leaving the shorter wavelength 'residual' anomalies that relate to shallower features, including the rift fabric. From Zanella et al., 2003

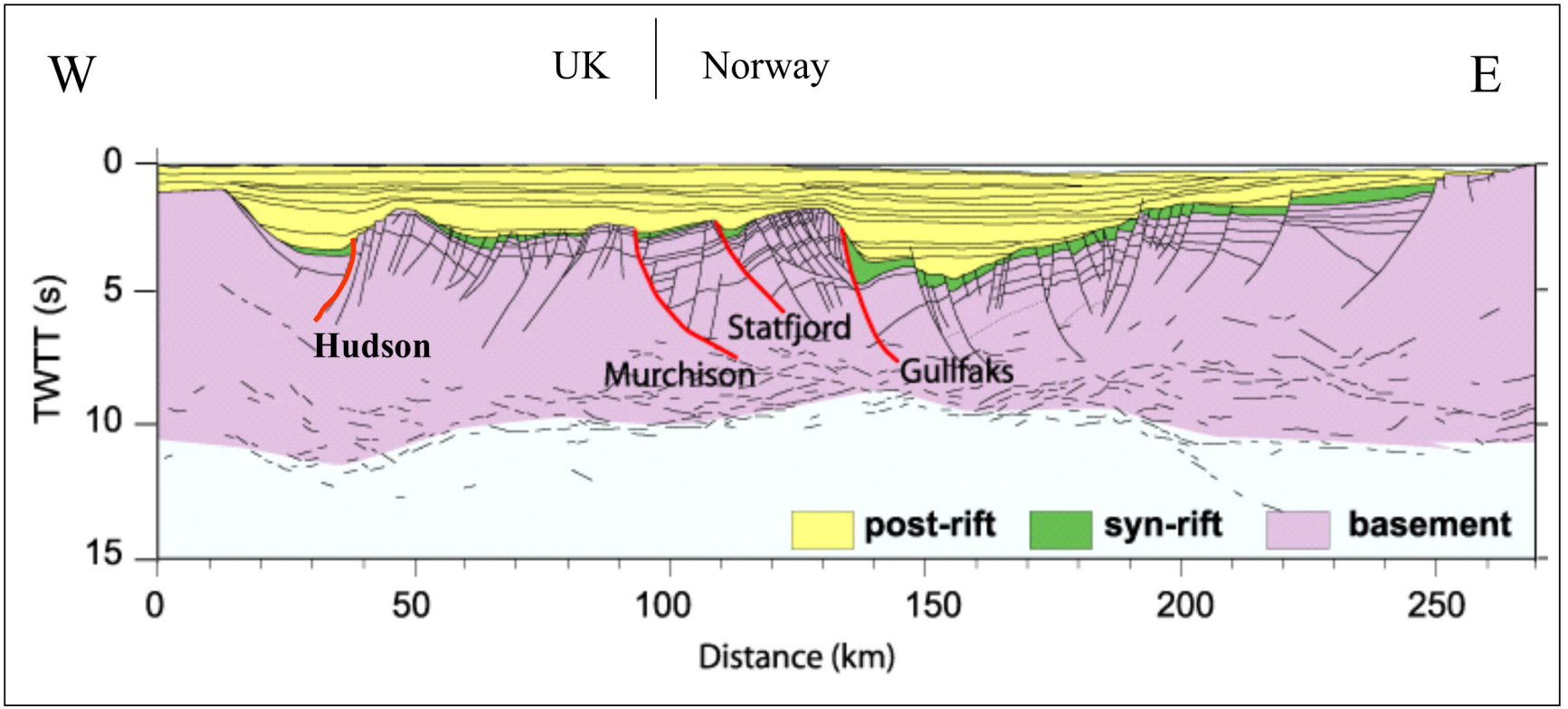

Figure 4.10
Regional Seismic line across the Northern North Sea showing major structures and pre, syn and post rift units.
For location see figure 4.34
After Christiansson et al., 2000

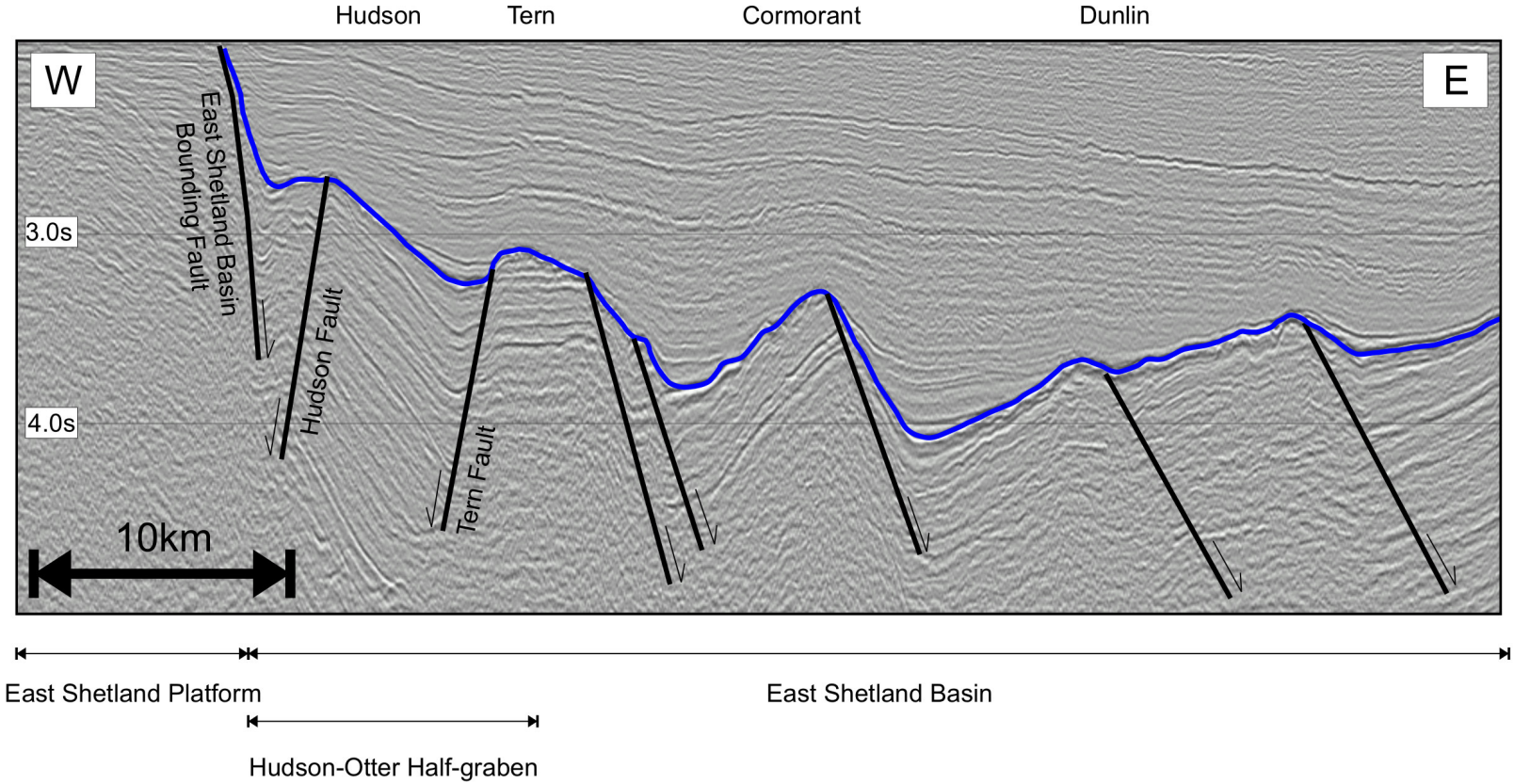

Figure 4.11
Regional seismic line across the East Shetland Basin
Blue interpreted horizon is Base Cretaceous Unconformity, major hydrocarbon fields labelled at top of seismic line.
The Hudson Field is an antithetic to both the main East Shetland Basin Bounding Fault and most other major faults in the East Shetland Basin
For location see figure 4.34

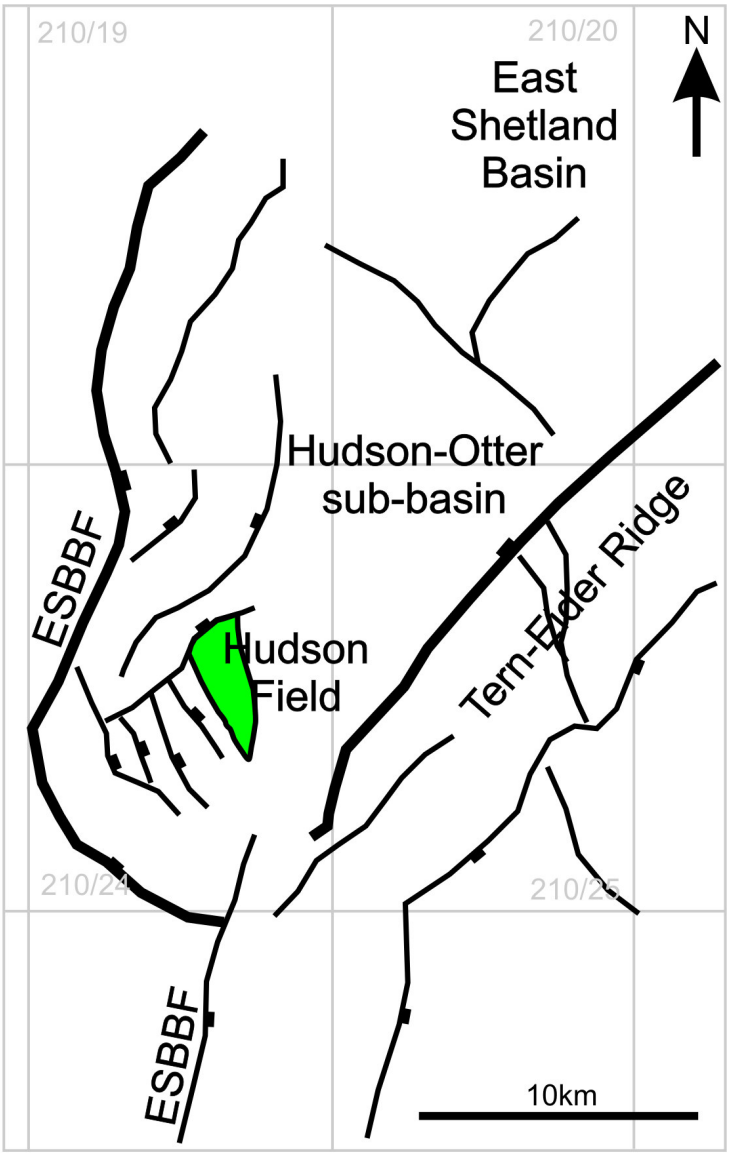

Figure 4.12
Location map of the Greater Hudson area
Major faults shown in black with ticks on downthrown side
Hudson field shown in green

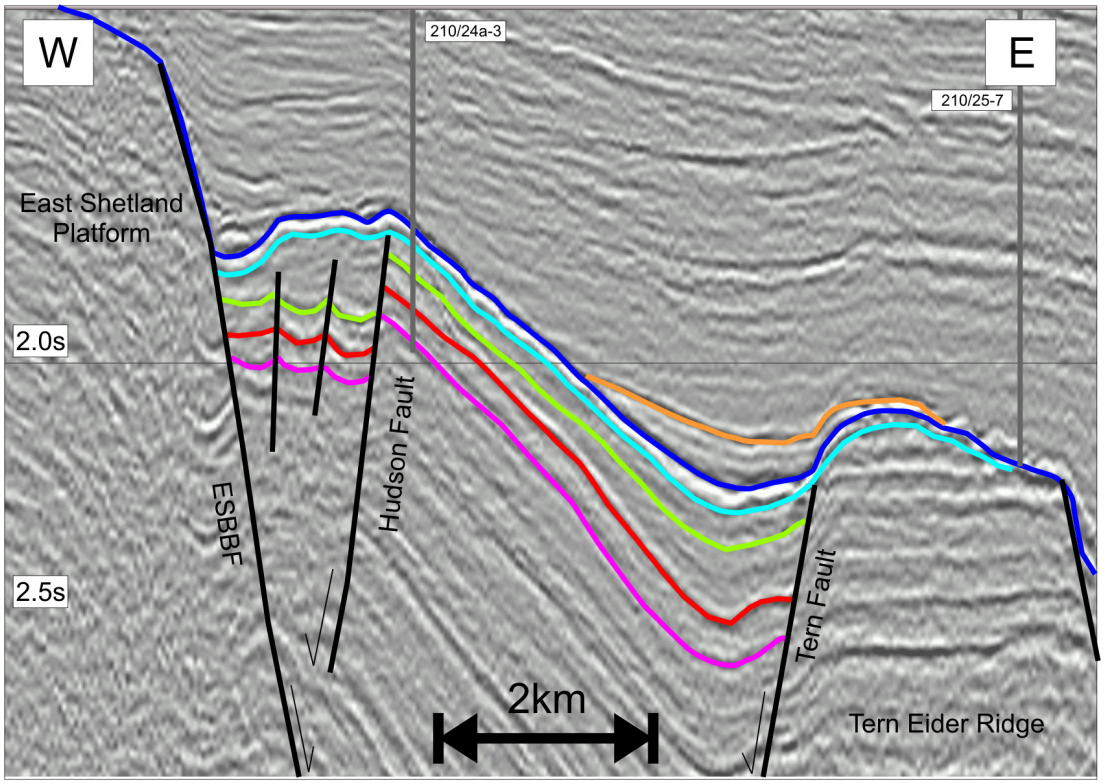

Figure 4.13
Seismic panel over the Hudson Fault
For location see figure 4.34

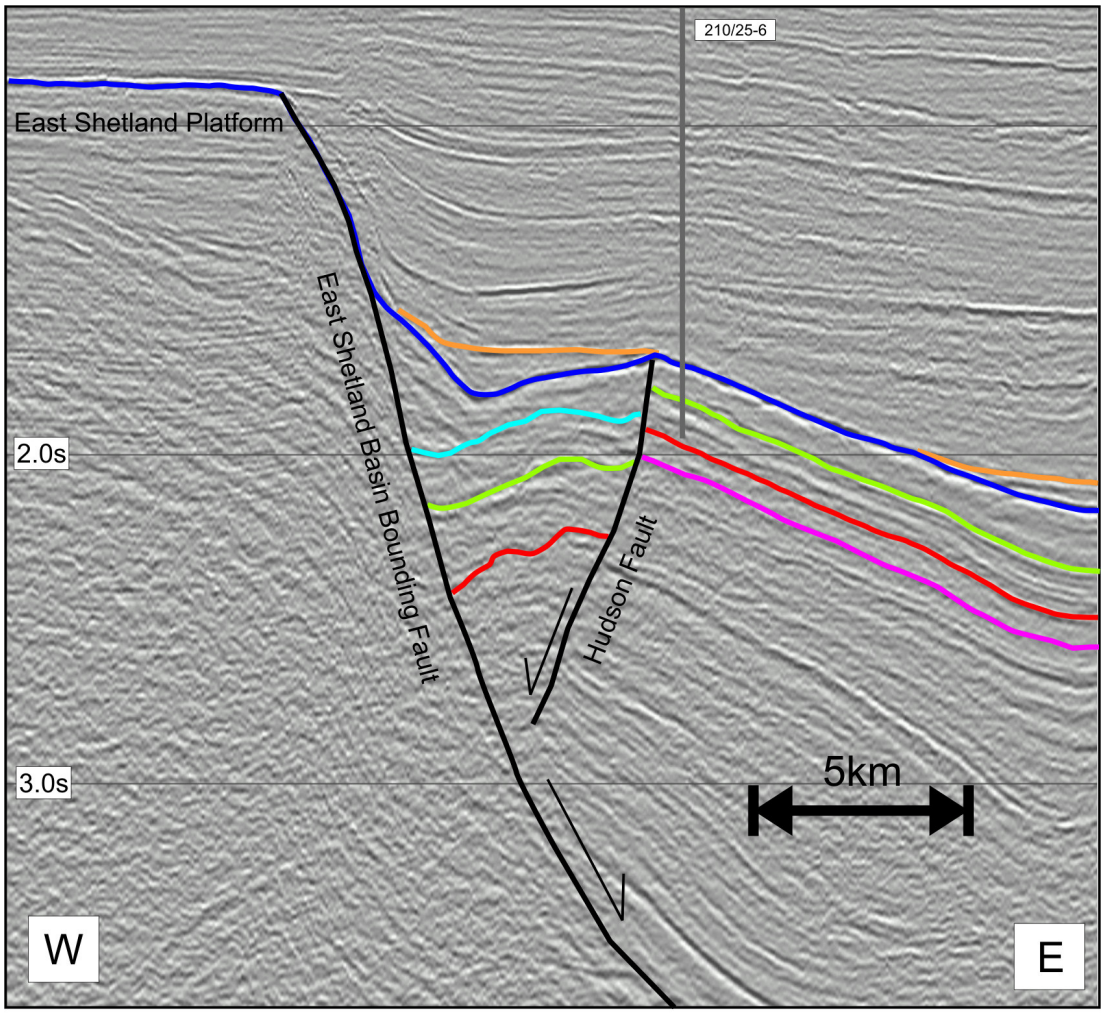

Top Cromer Knoll Formation
Base Cretaceous Unconformity
Top Heather Formation
Top Ness Formation
Top Dunlin Group
Top Statfjord Formation

Figure 4.14A
Seismic line across the northern segment of the East Shetland Basin Bounding Fault
For location see figure 4.34

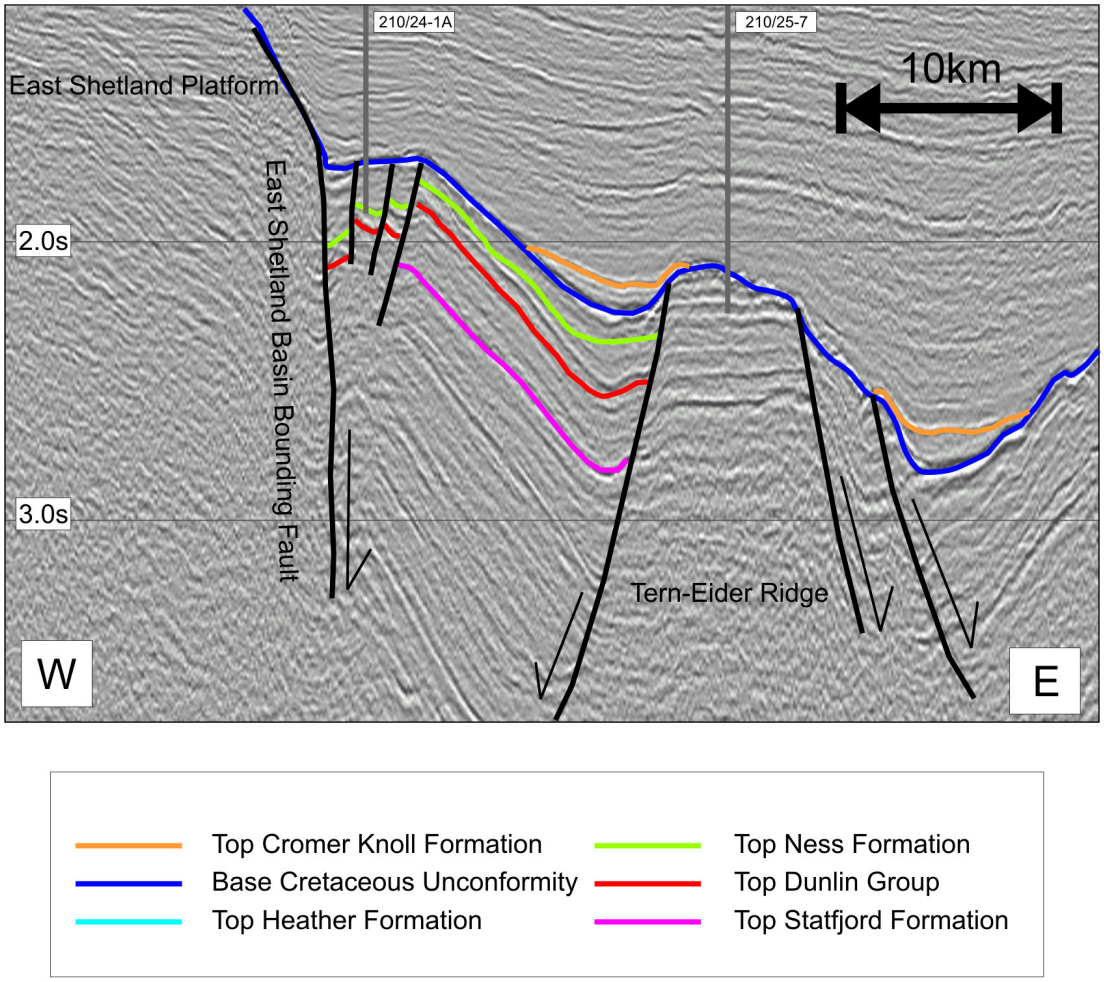

Figure 4.14B
Seismic line across the southern segment of the East Shetland Basin Bounding Fault
For location see figure 4.34

Figure 4.15
Displacement-length profile for Murchison Fault. Dotted lines show positions of former segment boundaries. Constructed from footwall and hangingwall cutoffs at Top Statfjord (intra-prerift) level. Grey profile shows abandoned tip in hangingwall to main fault. Southern tip of fault outside study area

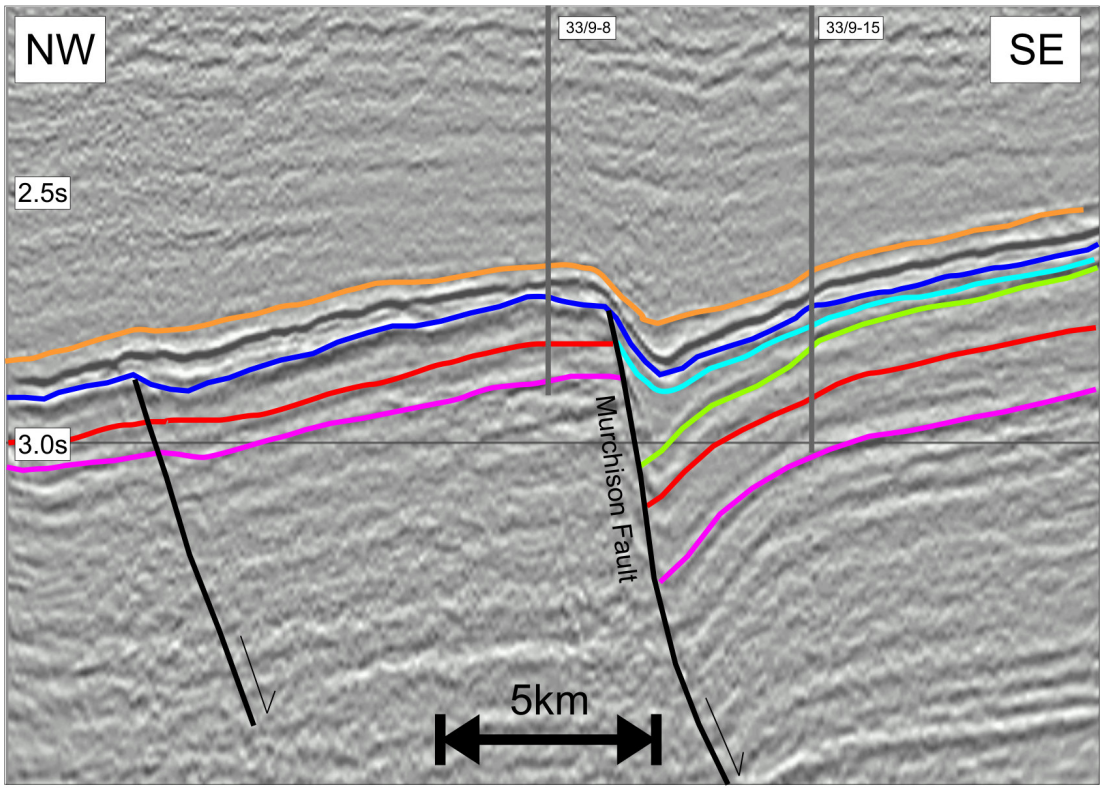

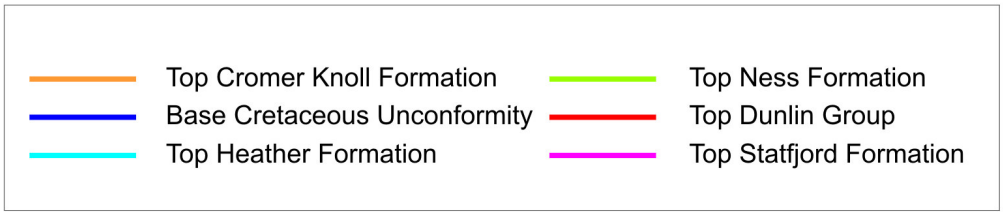

Figure 4.16
Seismic panel over the Murchison fault
Note thickening of syn-rift unit 1 (Top Ness Formation to Top Heather Formation) into the easterly dipping Murchison Fault and uniform thickness of syn-rift unit 2 (Top Heather Formation to Base Cretaceous Unconformity).
For location see figure 4.34

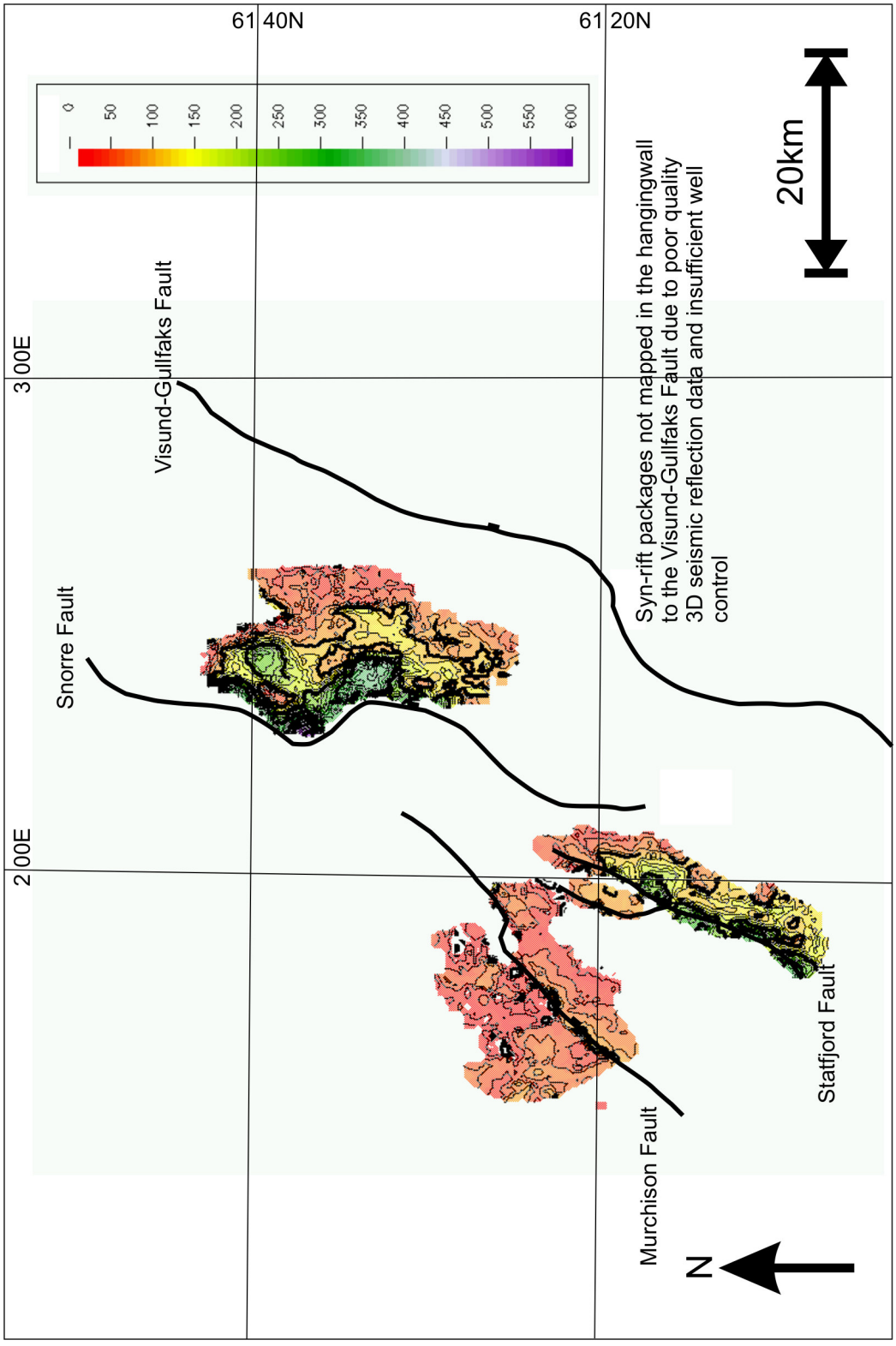

Figure 4.17A Two way time map of syn-rift unit 1 (Top Ness Formation to Top Heather Formation)

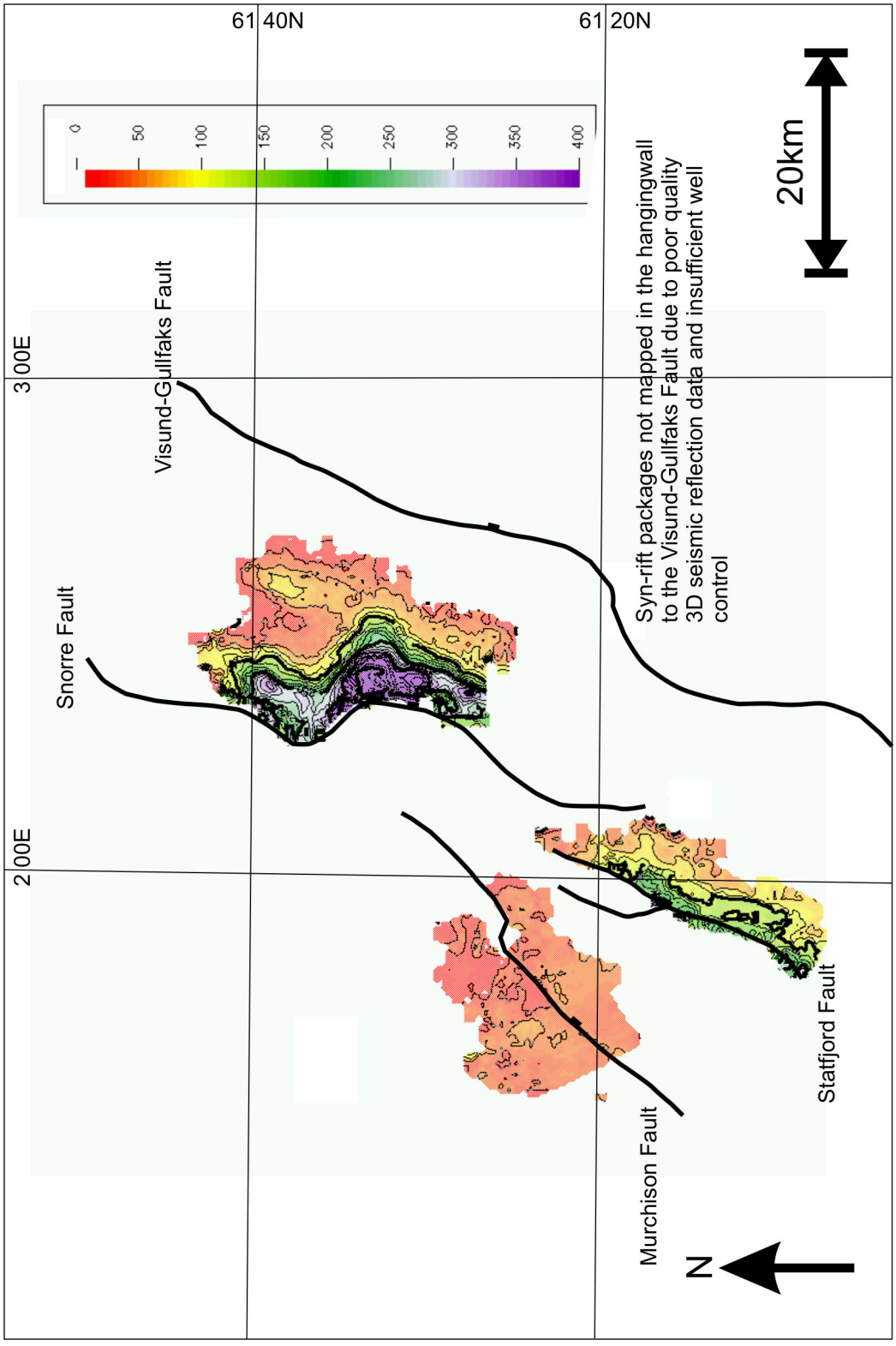

Figure 4.17B Two way time map of syn-rift unit 2 (Top Heather Formation to Base Cretaceous Unconformity)

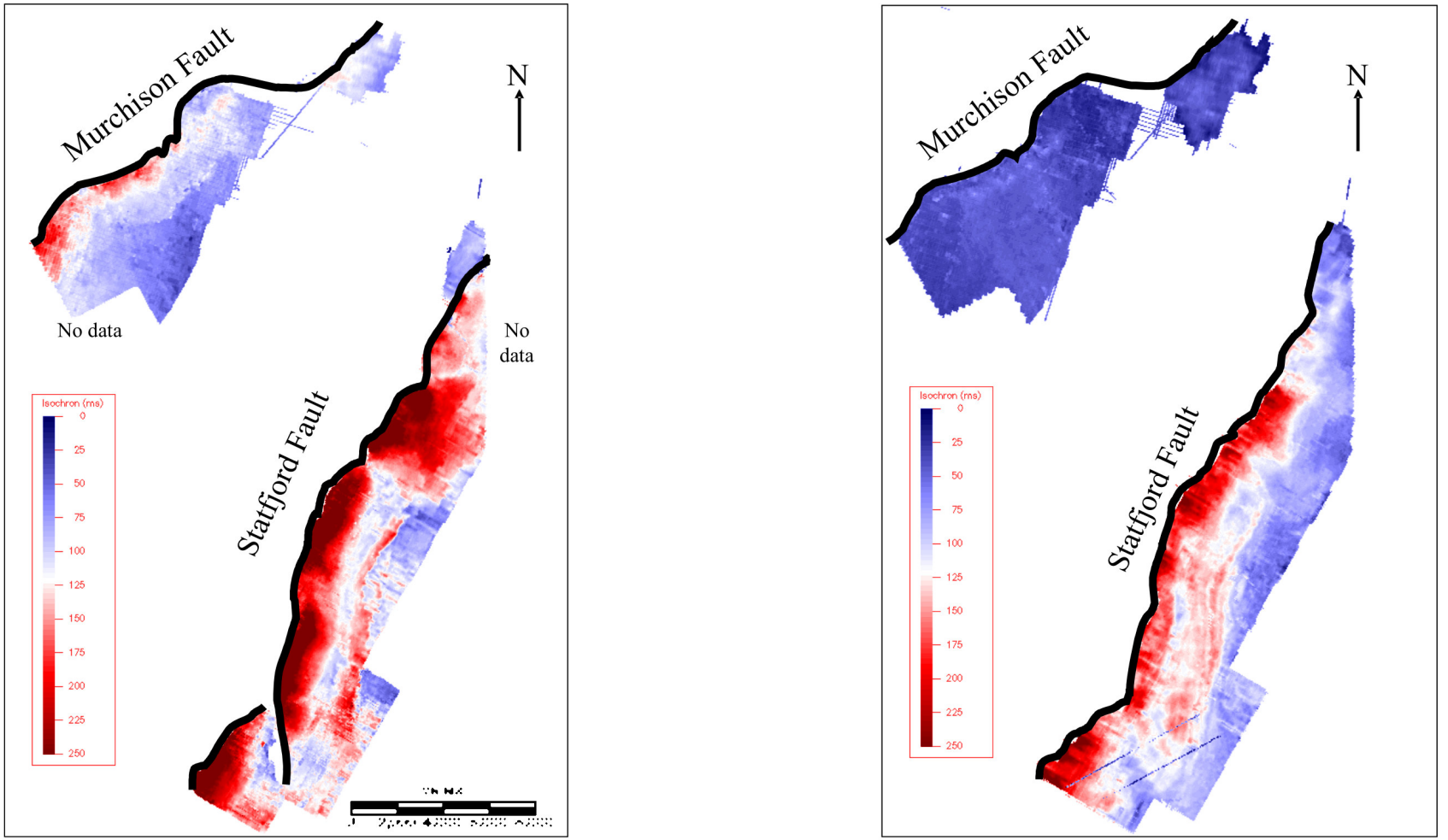

Figure 4.18
Two way time map of syn-rift unit 1 (left) and syn-rift unit 2 (right) over the Murchison and Statfjord Faults.
Note early isolated depoentres ajacent to both faults during deposition of syn-rift unit 1

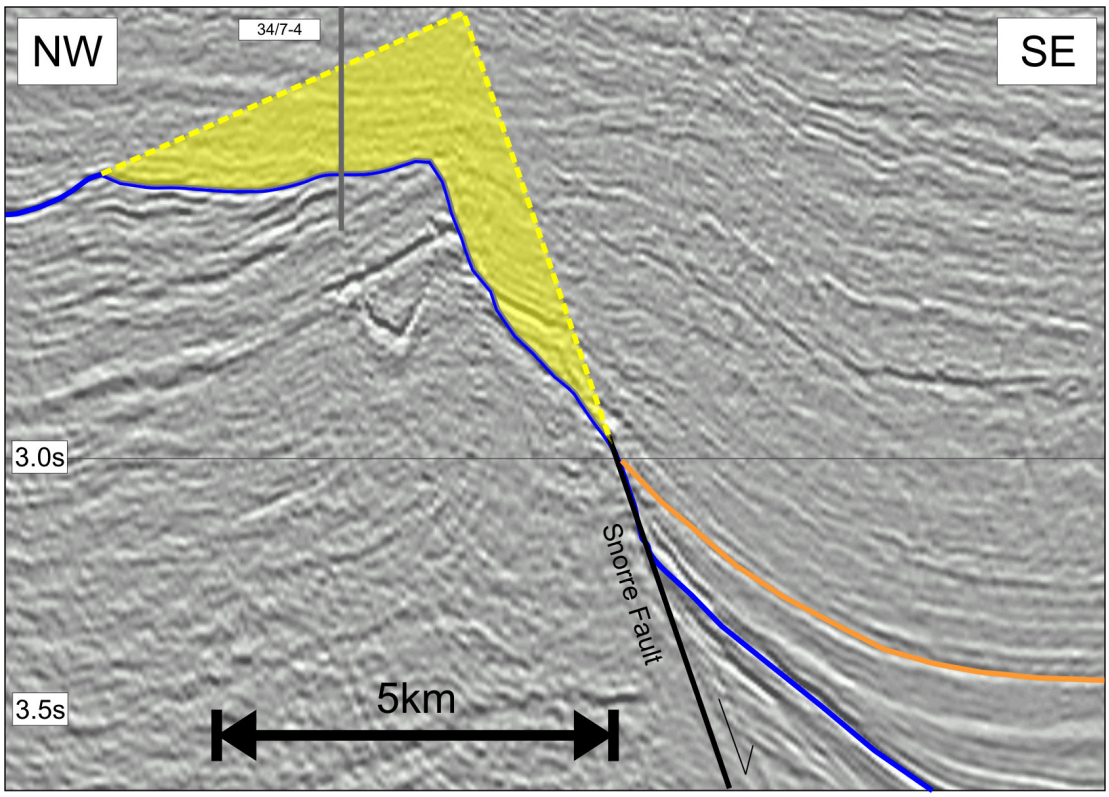

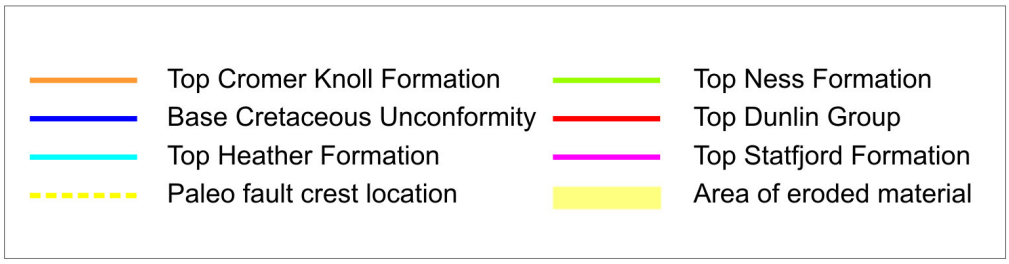

Figure 4.19
Seismic panel showing eroded footwall crest of the Snorre Fault
For location see figure 4.34

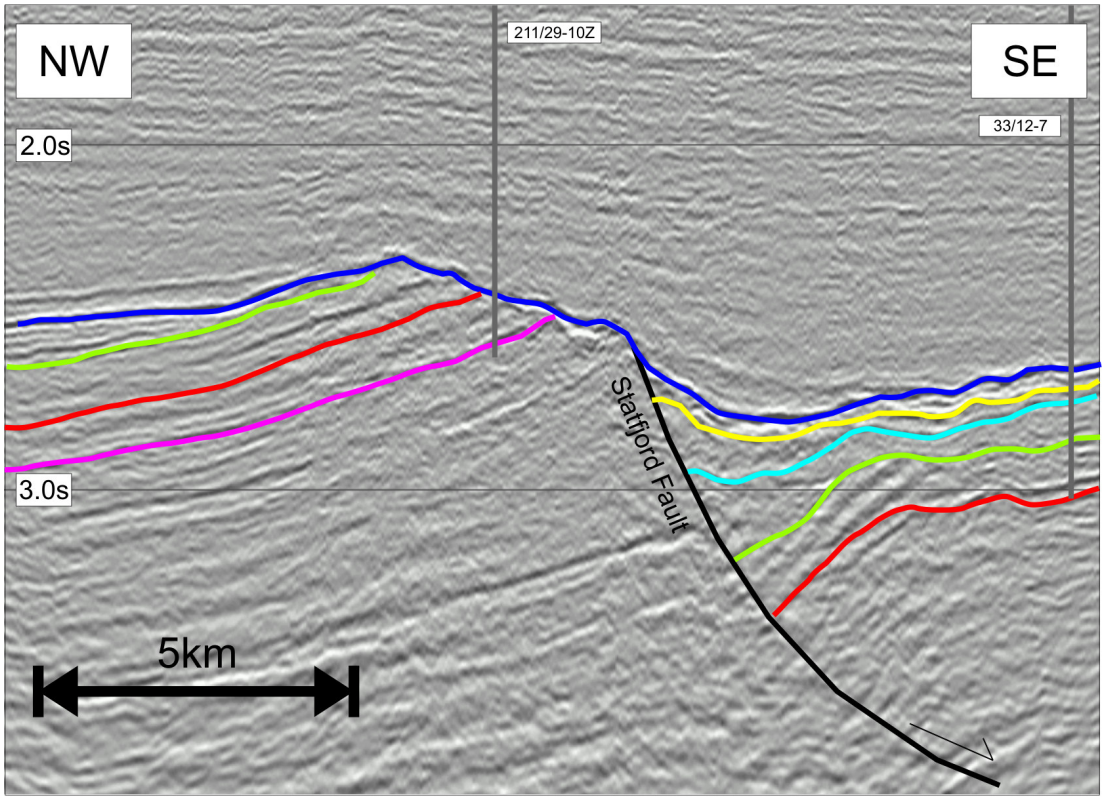

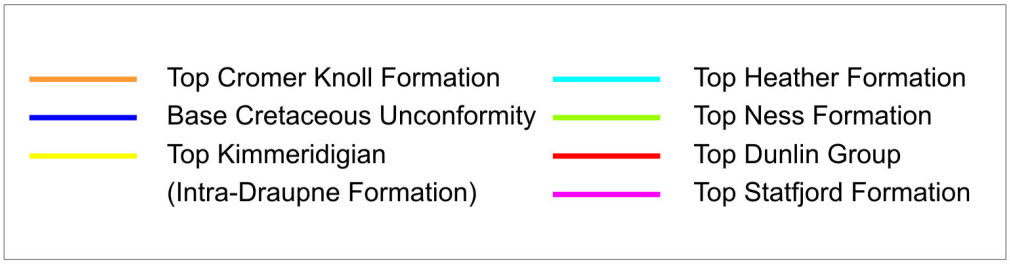

Figure 4.20
Seismic panel showing syn-rift stratigraphy associated with the Statfjord Fault
Note thickening of both syn-rift unit 1 (Top Ness Formation to Top Heather Formation) and syn-rift package 2a (Top Heather Formation to Top Kimmeridgian horizon) into the easterly dipping Statfjord Fault. Syn-rift unit 2b (Top Kimmeridgian to Base Cretaceous Unconformity shows a uniform thickness throughout the hangingwall depocentre to the Statfjord Fault.
For location see figure 4.34

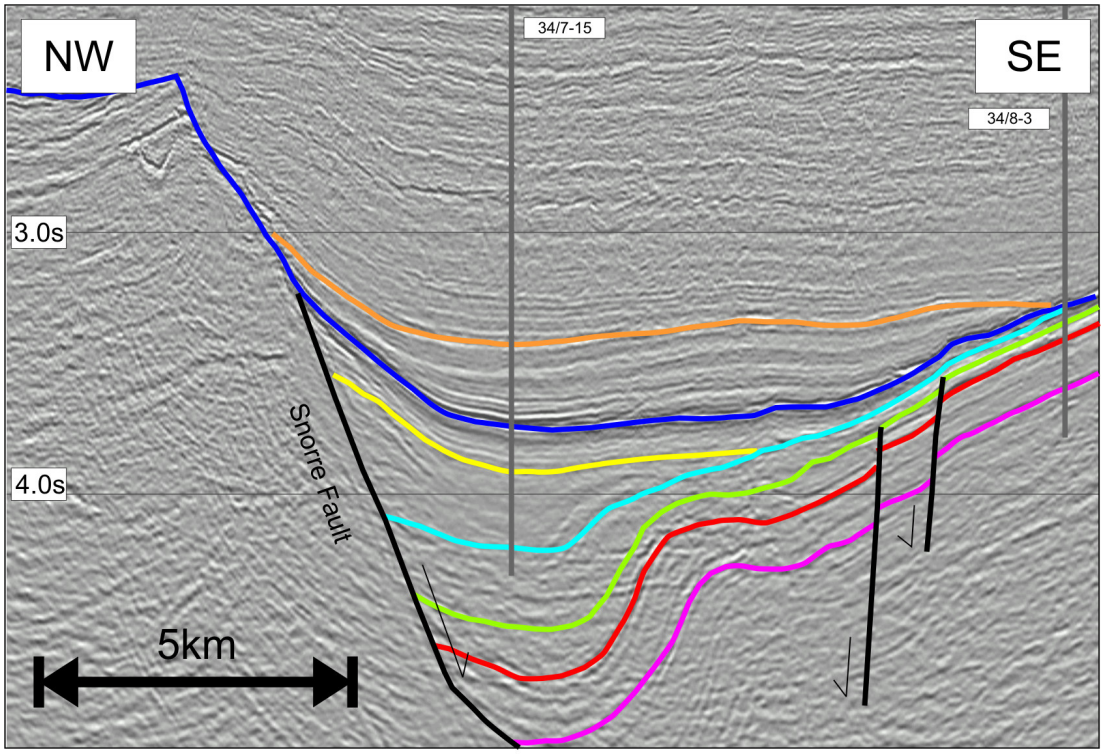

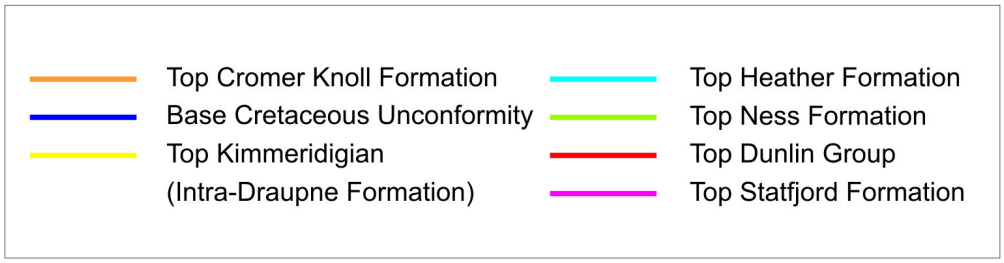

Figure 4.21
Seismic panel showing syn-rift stratigraphy associated with the Snorre Fault
Note thickening of both syn-rift unit 1 (Top Ness Formation to Top Heather Formation) and syn-rift unit 2a (Top Heather Formation to Top Kimmeridgian horizon) into the easterly dipping Snorre Fault. Syn-rift unit 2b (Top Kimmeridgian to Base Cretaceaous Unconformity shows a uniform thickness throughout the hangingwall depocentre to the Snorre Fault.
For location see figure 4.34

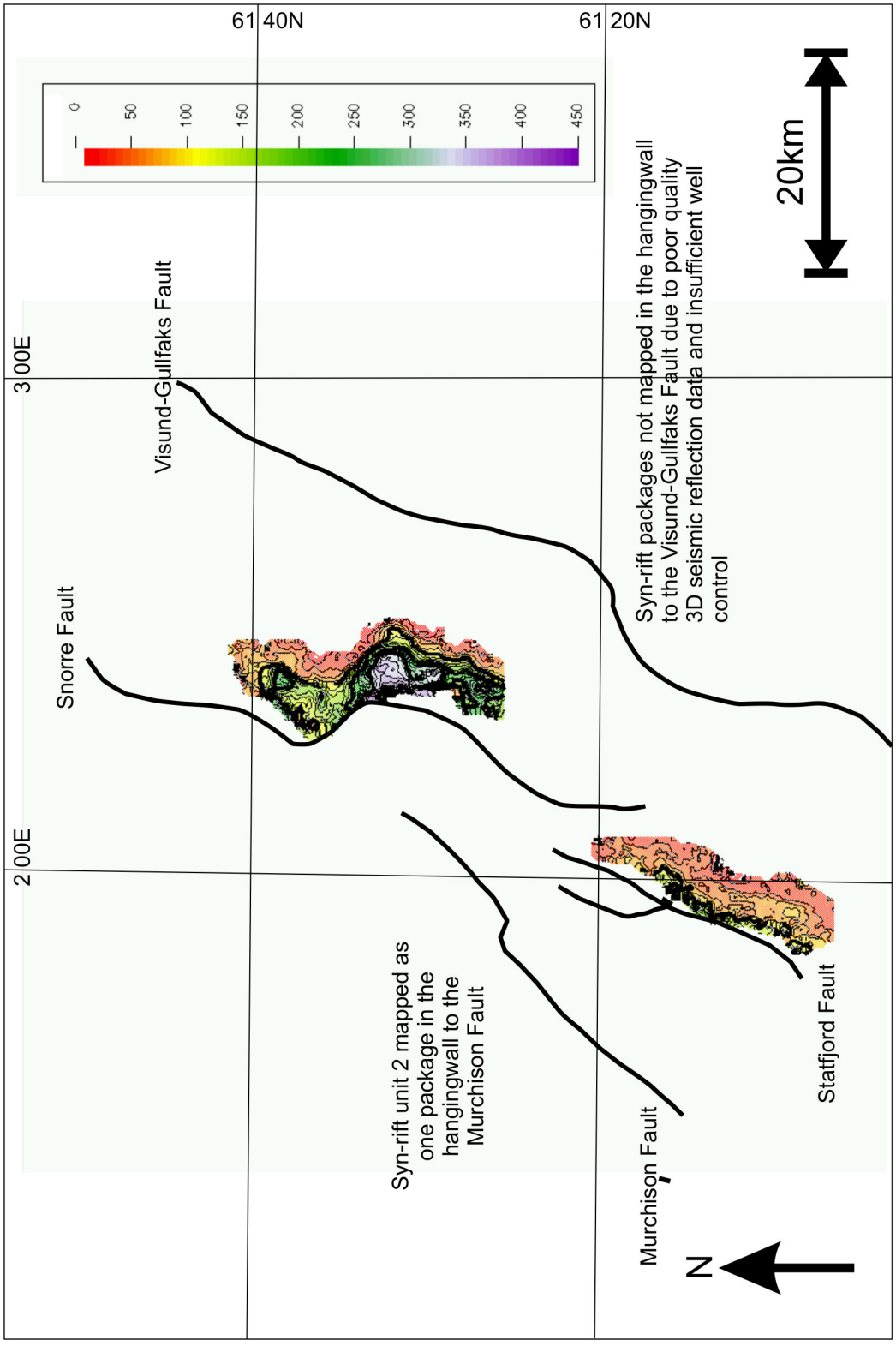

Figure 4.22 Two way time map of syn-rift unit 2a (Top Heather Formation to Top Kimmeridgian)

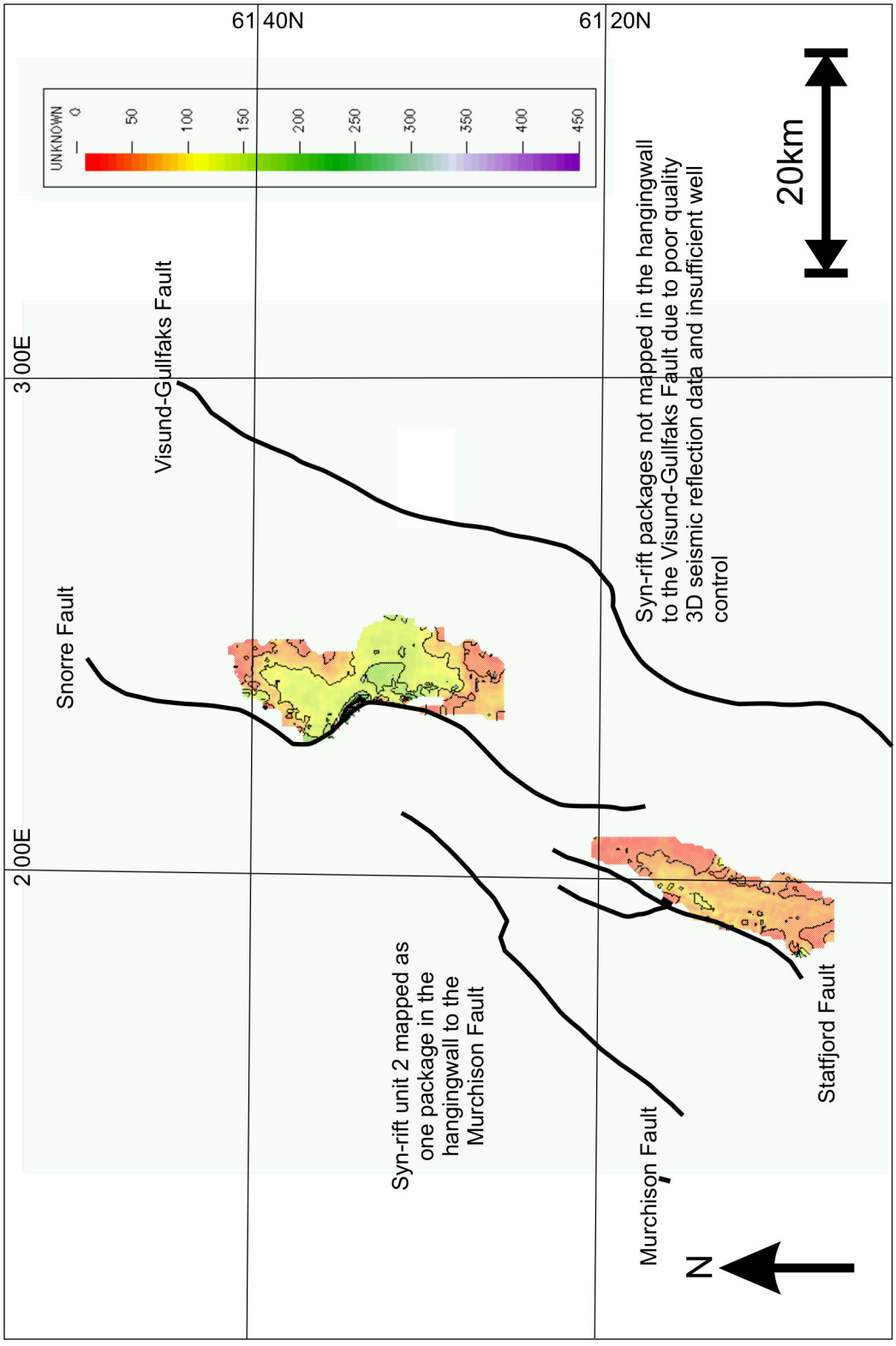

Figure 4.23 Two way time map of syn-rift unit 2b (Top Kimmeridgian to Base Cretaceous Unconformity)

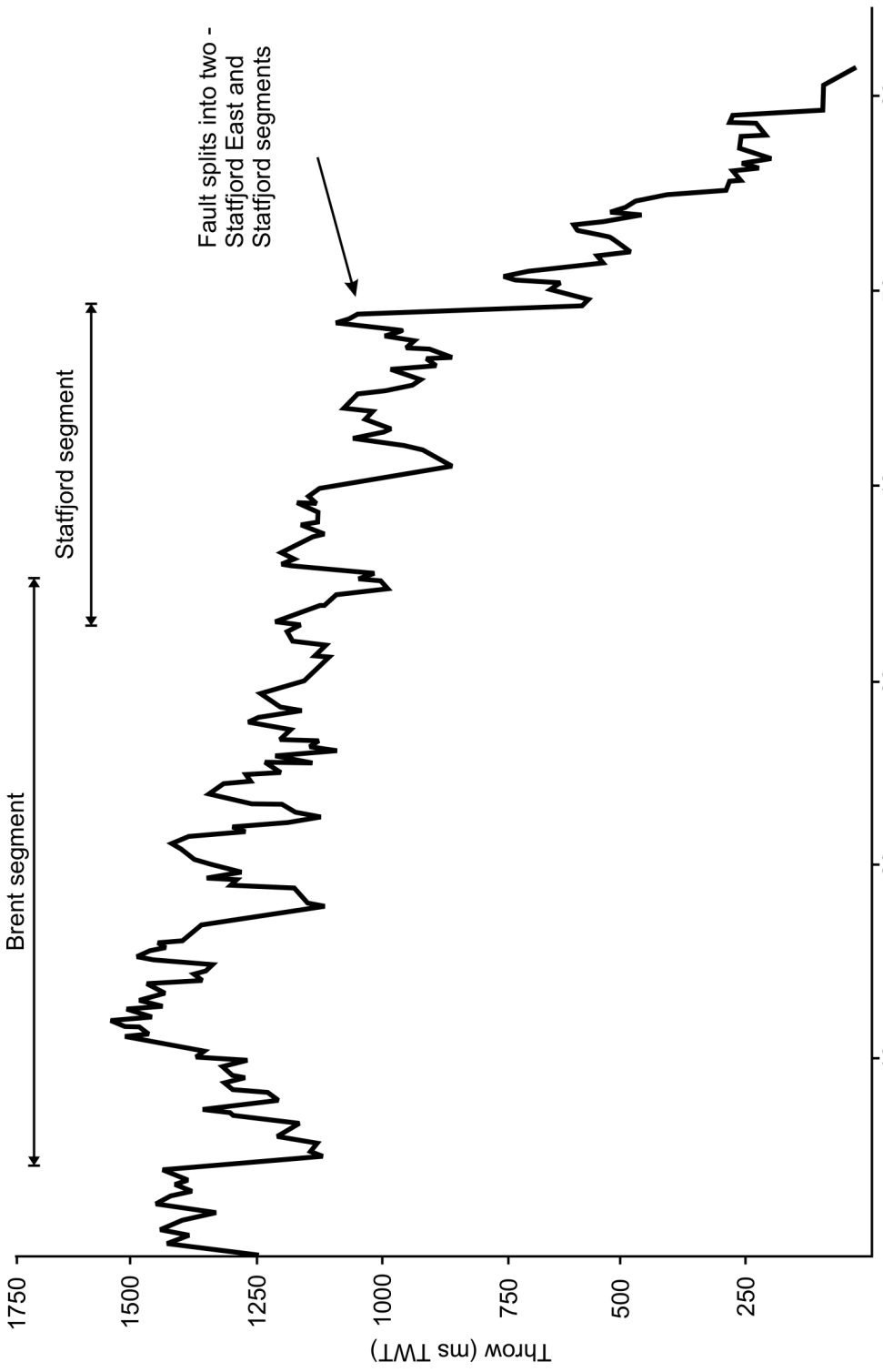

Figure 4.24
Displacement-length profile for the Strathspey-Brent-Statfjord Fault Array After McLeod, 2000.

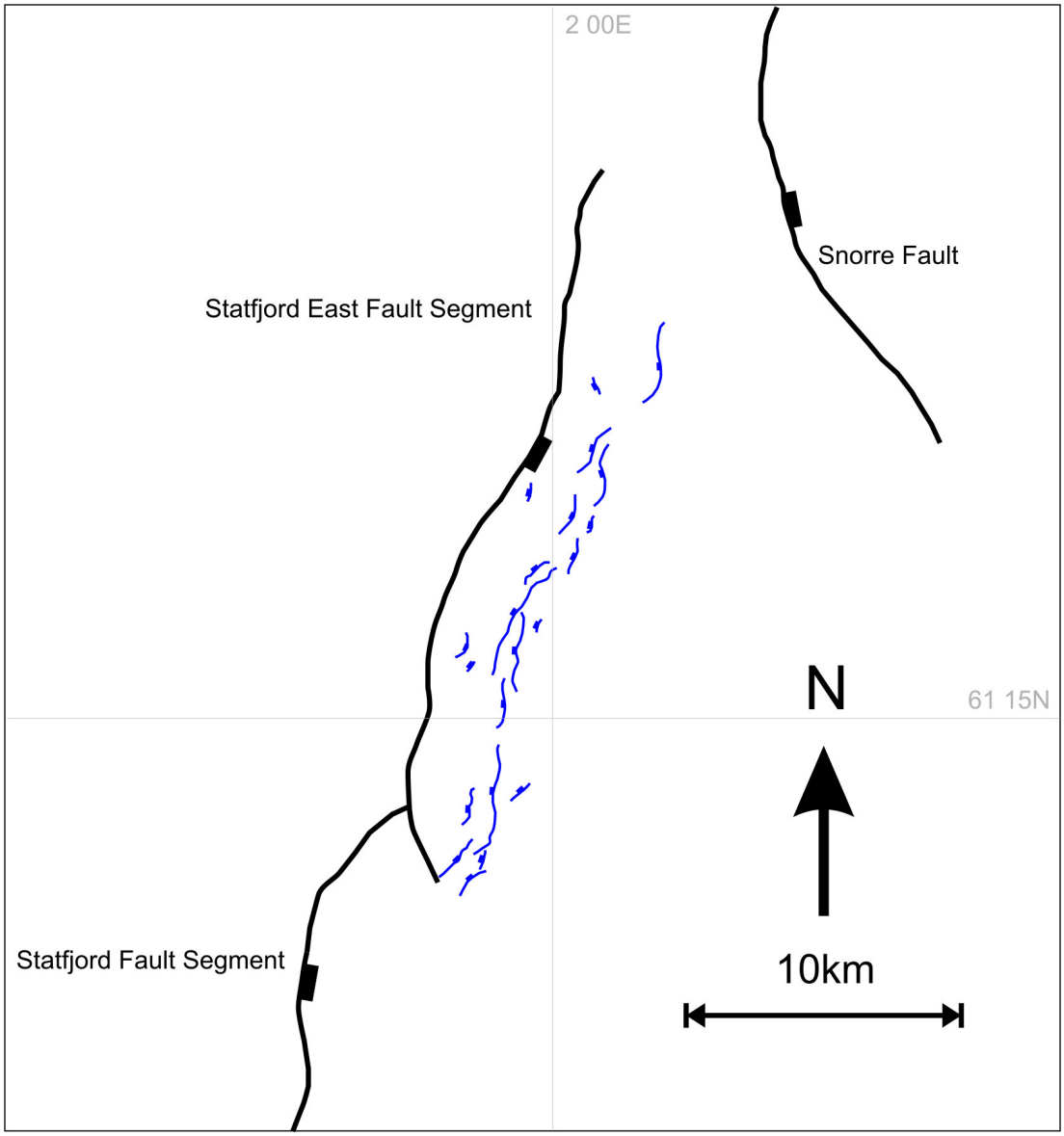

Figure 4.25
Map of the population of antitheitc faults found in the immediate hangingwall to the Statfjord Fault adjacent to the Statfjord East Segment.
After McLeod, 2000.

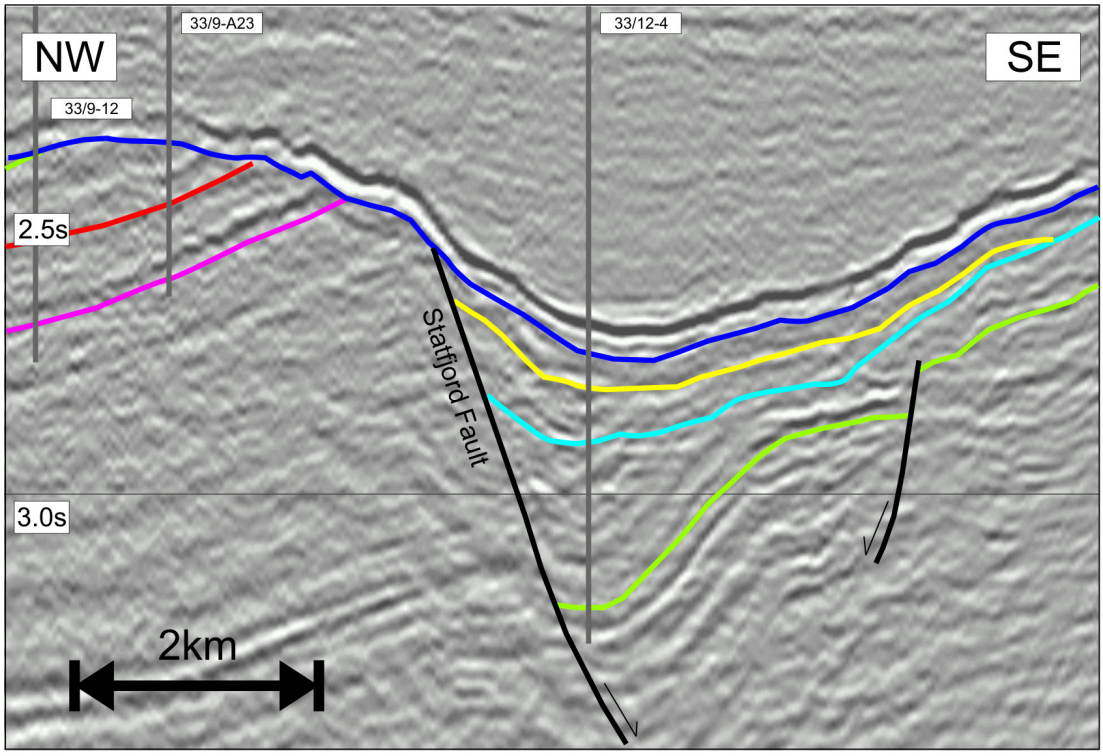

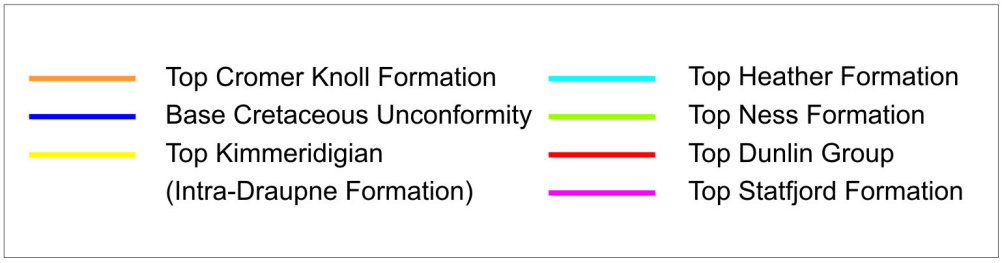

Figure 4.26
Seismic panel showing an antithetic structure in the hangingwall to the Statfjord Fault
Note thickening of syn-rift unit 1 (Top Ness Formation to Top Heather Formation) into the westerly dipping antithetic fault
For location see figure 4.34

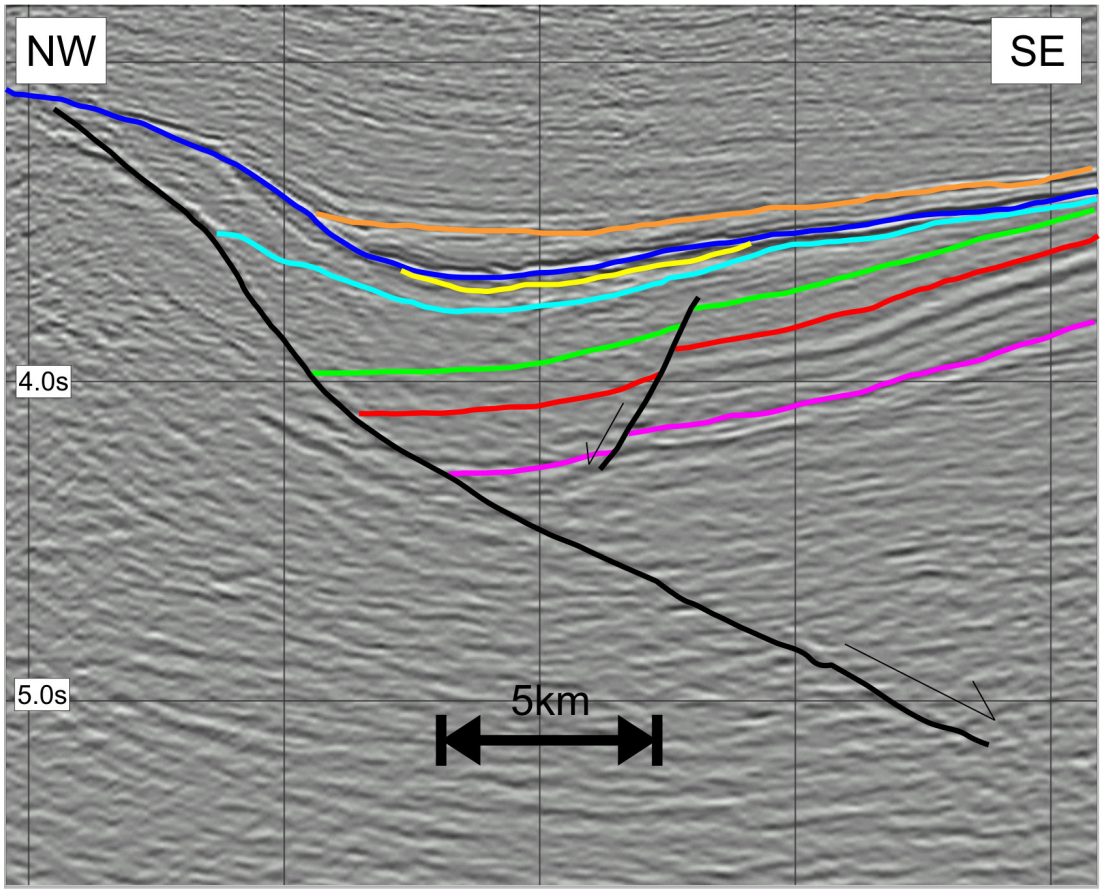

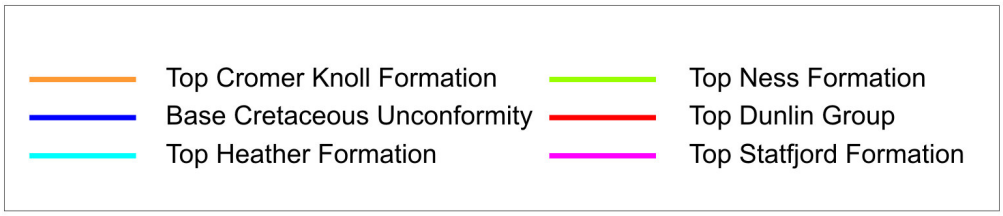

Figure 4.27
Seismic panel over the Snorre Fault showing associated antithetic structure.
Note that antithetic cuts Top Ness Formation but does not cut Top Heather Formation
For location see figure 4.34

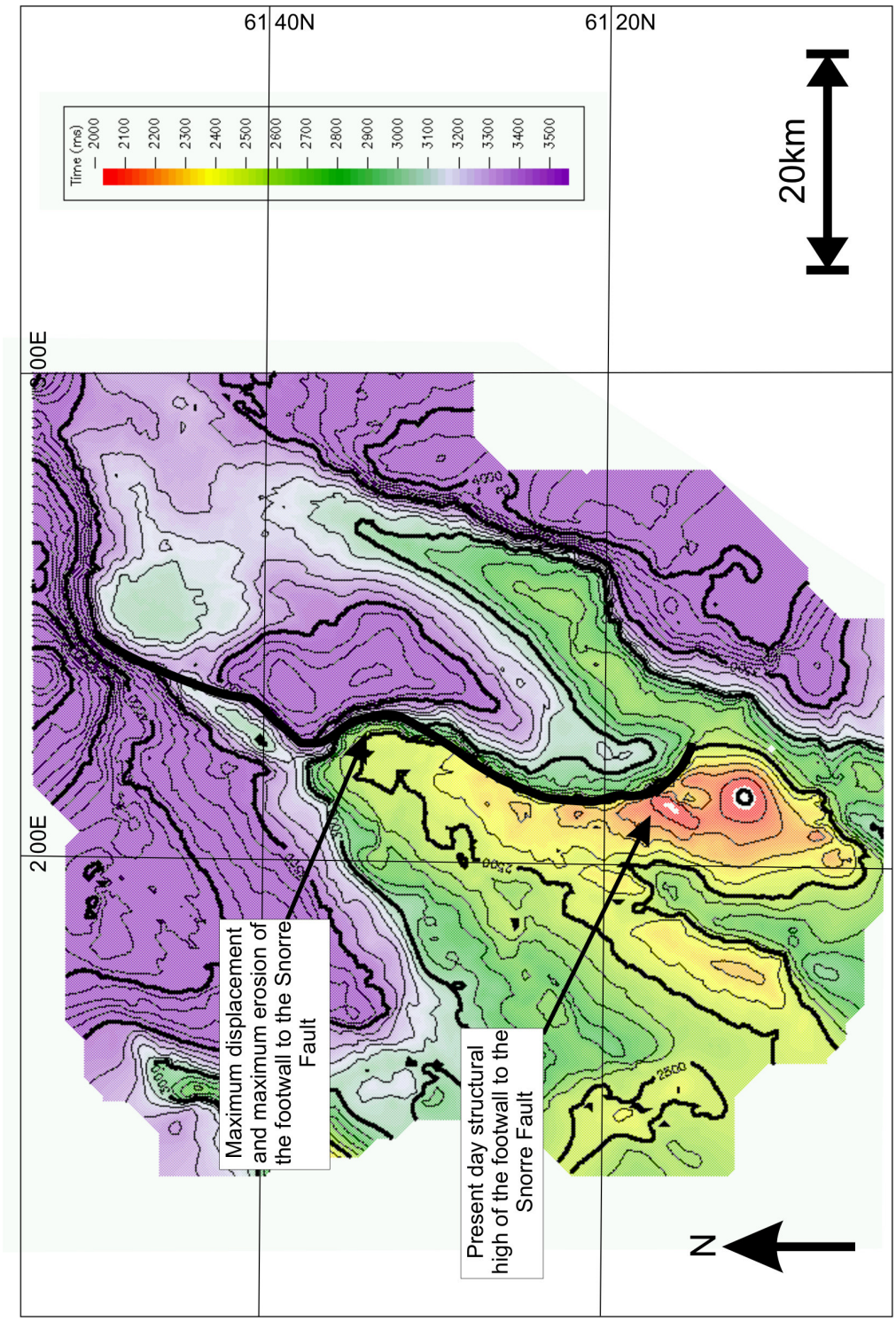

Figure 4.28 Two way time map to Base Cretaceous Unconformity showing points of maximum displacement, maximum footwall erosion and present day structural high on the Snorre Fault

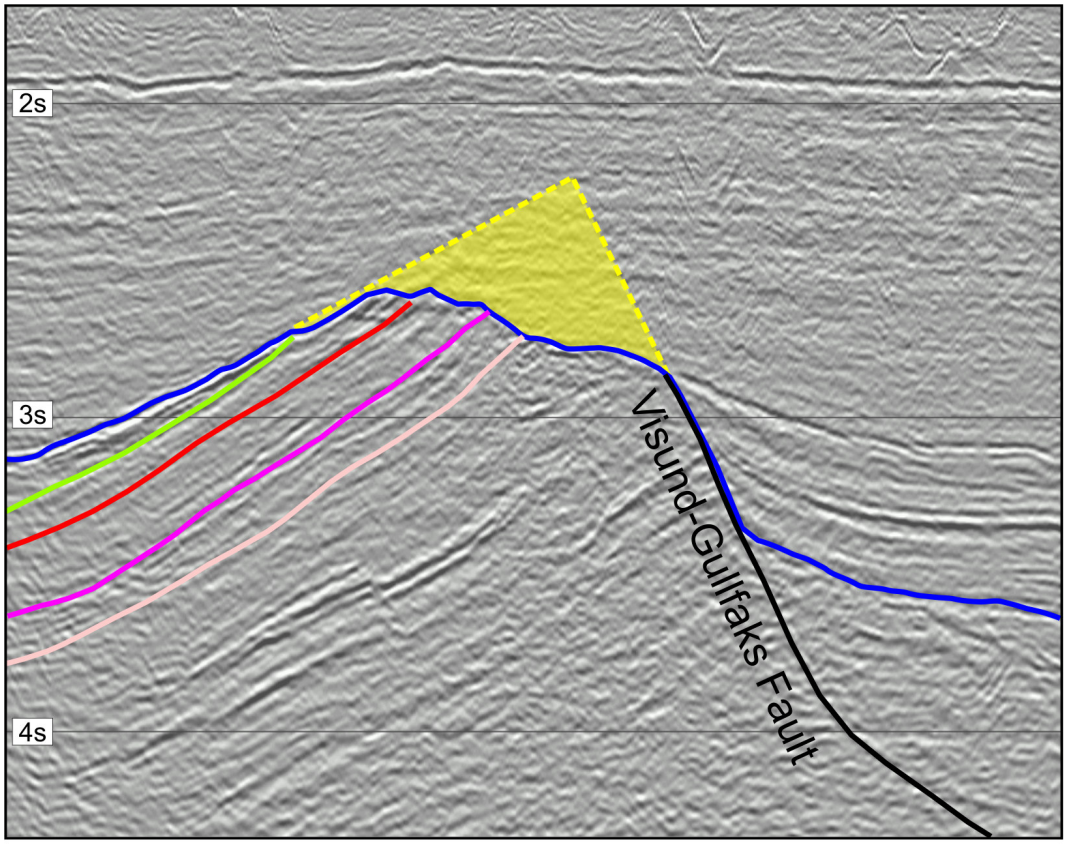

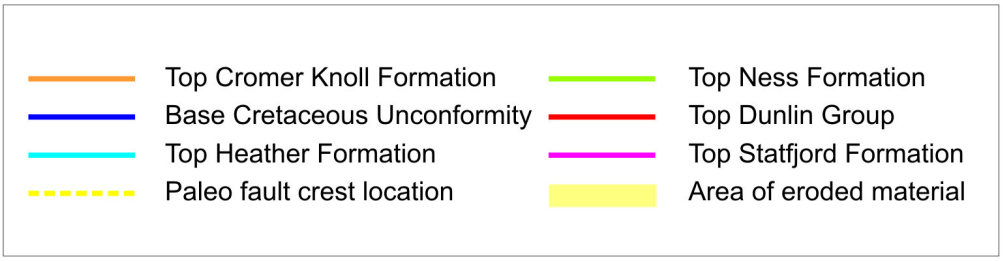

Figure 4.29
Seismic panel showing eroded crest of Visund-Gullfaks Fault Block
For location see figure 4.34

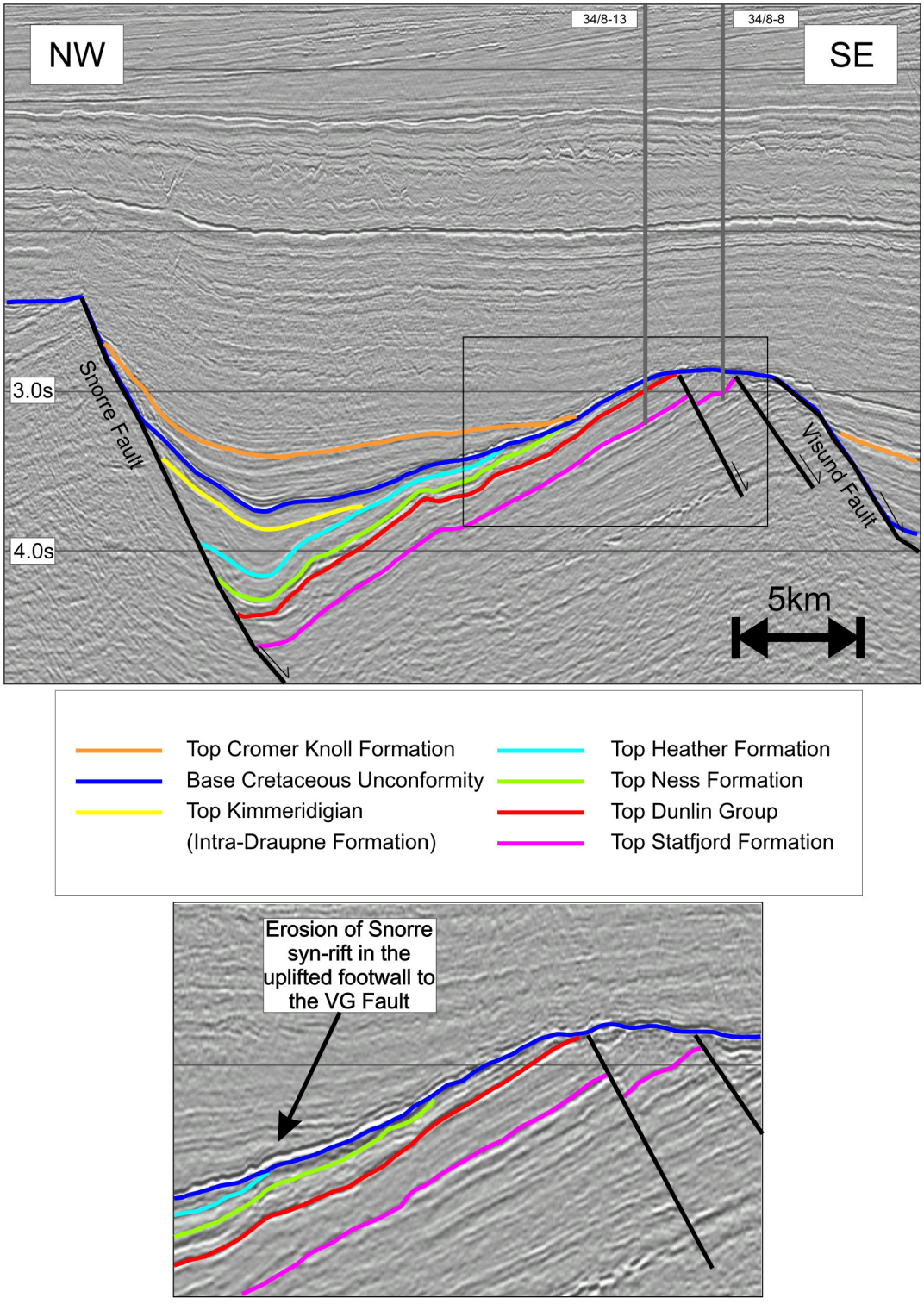

Figure 4.30
Seismic panel showing erosion of syn-rift stratigraphy associated with the Snorre Fault in the uplifted crest of the Visund-Gullfaks fault.
Black box shows position of inset seismic panel (bottom) For location see figure 4.34
Note that displacement on Visund-Gullfaks Fault and magnitude of erosion of the associated footwall scarp are much greater than that on the Snorre Fault. This is the result of a greater slip rate and a longer period of activity experienced by the VG Fault.

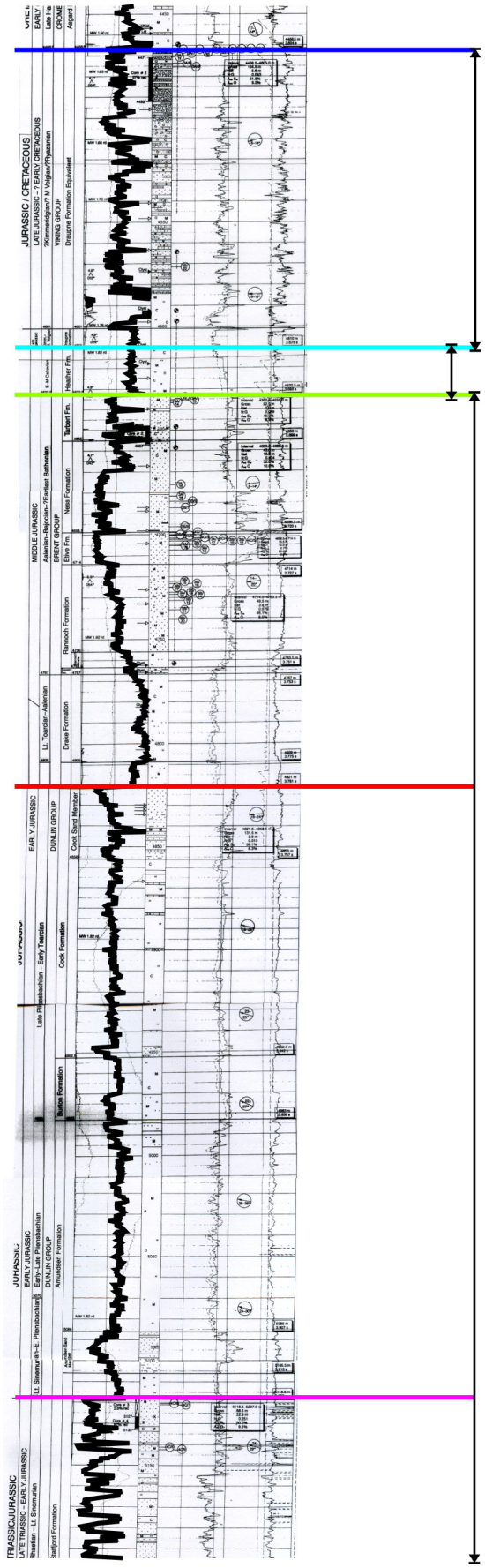

Figure 4.31
Extract from composite log for well 34/8-7 showing complete Jurassic section

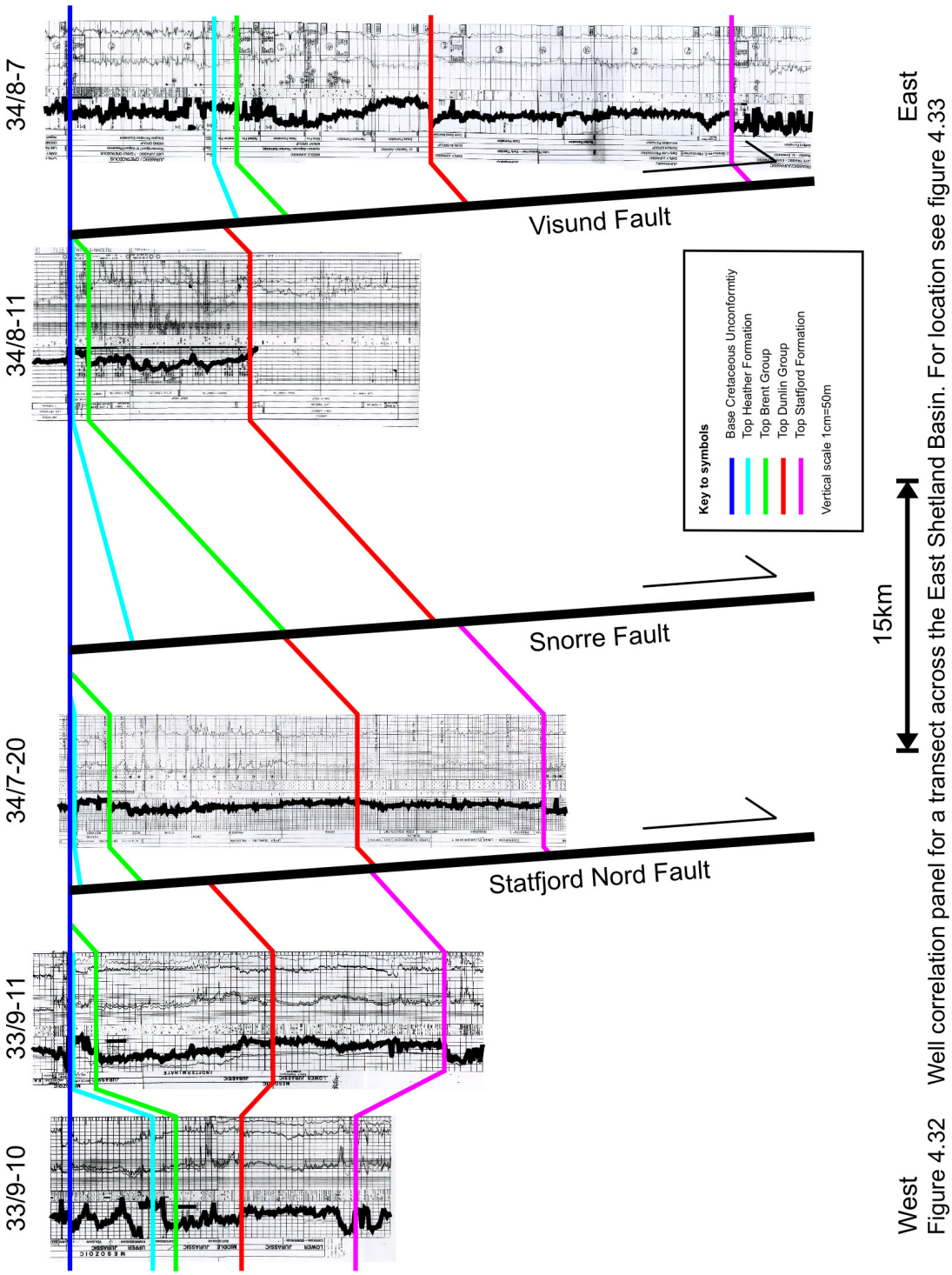

Figure 4.32 Well correlation panel for a transect across the East Shetland Basin. For location see figure 4.33

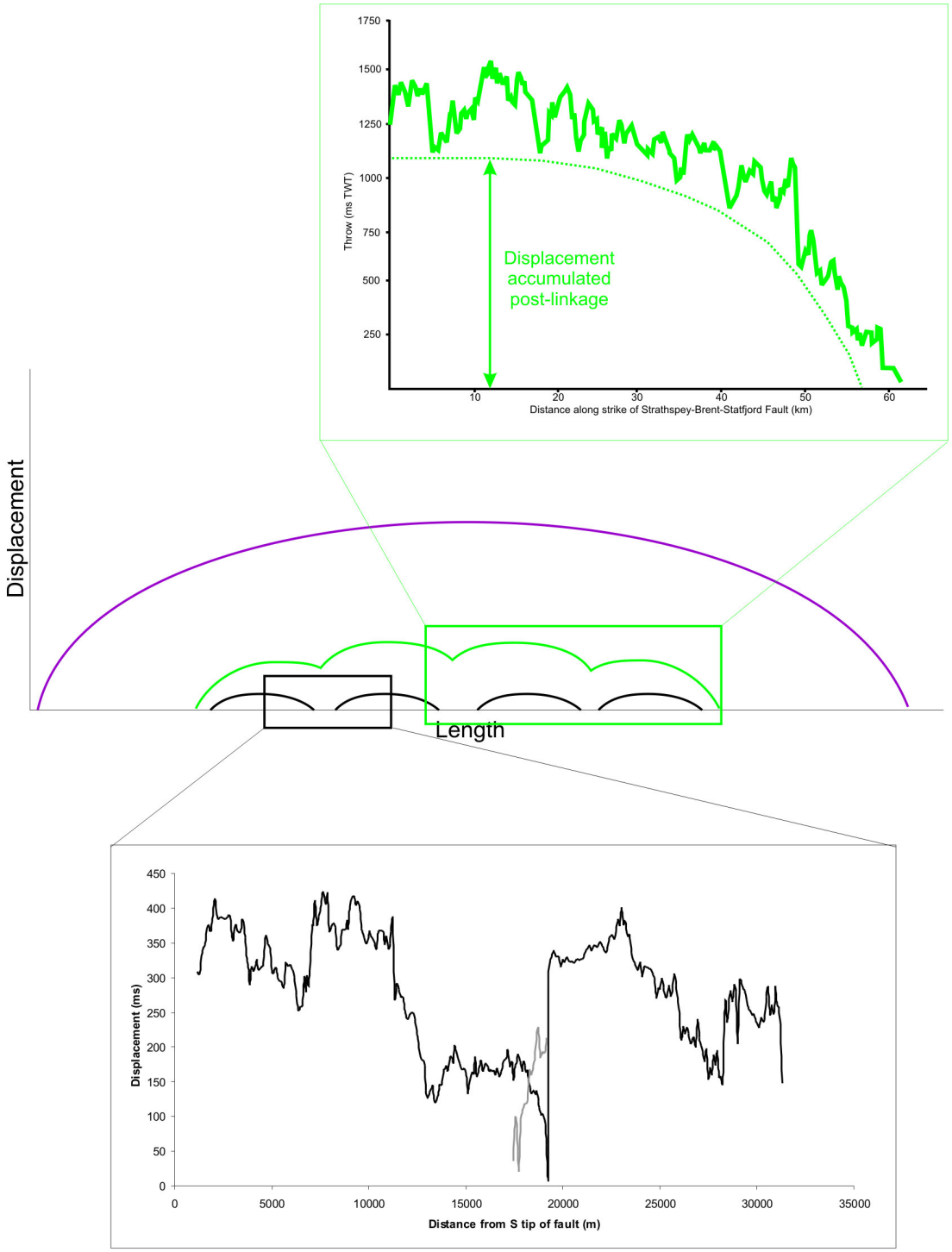

Figure 4.33A
Schematic displacement-length curves for the Murchison (black), Statfjord (green) and Visund-Gullfaks (purple) faults. Insets show real displacement-length curves over specific parts of each of the faults.
Note how the Murchison Fault is at an early stage of linkage as a result of early cessation of activity on the structure. In contrast, the Statfjord Fault is at a more advanced stage of linkage. The predicted displacement-length profile for the Visund-Gullfaks fault is for a fully-equilibrated throughgoing normal fault.

Figure 4.33B
Schematic graph showing accumulation of displacement on faults in different locations within the East Shetland Basin during the Mid to Late Jurassic rift episode.
Initially all faults in the basin are active. The Murchison Fault shows the lowest rate of slip and the Visund-Gullfaks shows the highest rate of slip.
The Murchison fault, becomes inactive at c. 155Ma. The Statfjord Fault becomes inactive at c. 148Ma and the Visund-Gullfaks Fault is active throughout the rift episode.

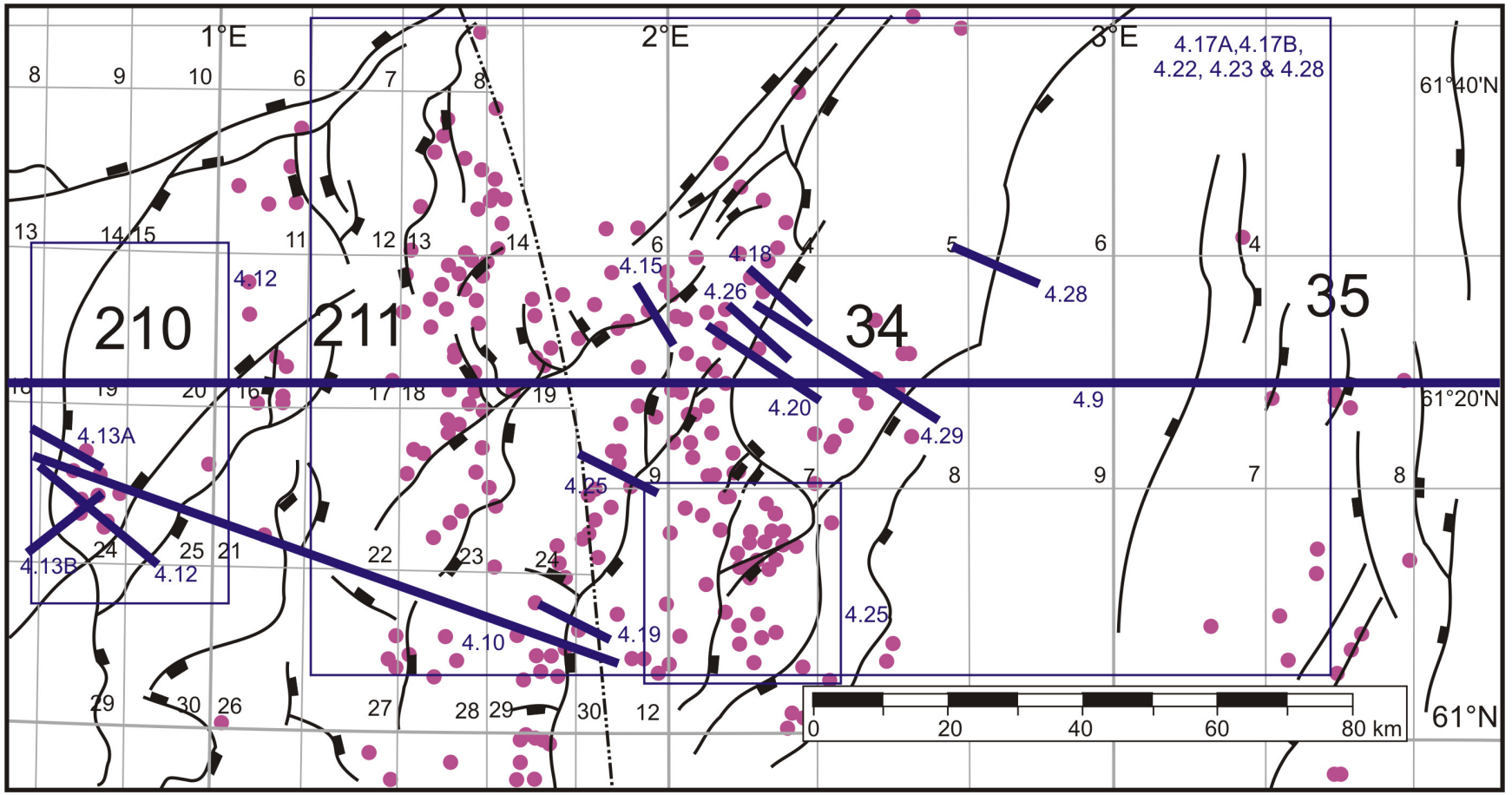

Figure 4.34
Map showing major faults and location of seismic lines and maps presented in chapter 4
Purple circles show positions of exploration, development and appraisal wells with logs available for incorporation into this study

5. Applications to subsurface data 2 – Footwall deformation in the Northern North Sea rift Province

5.1 Introduction

In addition to revealing the role of strain localisation in the development of the Northern North Sea rift system, the subsurface data also highlights the complex nature of deformation that affected the footwalls to the major faults in the area during the Mid to Late Jurassic rift episode. This chapter will examine three types of footwall deformation in detail, none of which has been previously documented. In section 5.2 the role of strike-perpendicular faulting is examined using examples from the Murchison Fault in the western part of the East Shetland Basin (figure 5.1). In section 5.3 the role of strike-parallel faulting is documented using a suite of faults present in the footwall to the Visund-Gullfaks fault, bounding the North Viking Graben (figure 5.1). Finally, in section 5.4, the role of footwall degradation is considered with particular reference to the Visund area and an estimate is made of the volume of material lost as a result of footwall uplift. The chapter concludes with a discussion of the modes of footwall deformation, degradation and consideration of the causes and wider implications of these processes.

5.2 Role of strike-perpendicular faulting

5.2.1 The Murchison Fault

The Murchison Fault is a northeast-southwest trending, east dipping planar normal fault over 40km in length with total accumulated displacement in excess of 400ms (c. 620m) (figure 5.2A). It bounds the Thistle, Murchison and Statfjord-Nord hydrocarbon fields and the Sygma hydrocarbon discovery. Data from these locations are available for incorporation in to this study (figure 5.3). It is thought to comprise a number of paleosegments representing short, precursor fault segments which grew by radial tip propagation and subsequently linked to form the single throughgoing structure observed today (Young et al., 2001). Displacement minima on a displacement length profile have been interpreted as linkage points which never fully equilibrated as a single structure (figure 5.4). This study is concerned with the northern part of the fault bounding the Murchison and Statfjord Nord hydrocarbon fields. The study section comprises two principal paleosegments, the Murchison Fault segment to the south with a length of 15km and maximum displacement 450ms (c. 710m) and the Statfjord Nord Segment to the north with a length of 11km in the study area and a maximum displacement

of 380ms (c. 600m). The two segments are hard linked via a breached relay termed the Jog Fault (Young et al., 2001). Hard linkage occurred late in the history of the Murchison fault and as such expected displacement-length scalings were never re-established at the linkage point.

5.2.2 Structure of Faults

Brittle deformation in the footwall to the Murchison Fault is of two main types: Strike-parallel (abandoned) fault tips and strike-perpendicular footwall transverse faults. Abandoned tips originate from the main fault at positions of former segment linkage. They are 2-4 km in length and show displacement which reaches a maximum at the main fault and decreases towards the fault tip (figure 5.5). The orientation of abandoned fault tips is a continuation along strike of the fault segment with which it was associated prior to segment linkage. The abandoned tips show activity which is restricted to the period before segment linkage occurred on the main fault after which they were abandoned in the footwall to a new, longer, main fault (Dawers and Underhill, 2000). They will not be considered further in this study.

Footwall transverse faults are small scale structures that are often present as back-to-back pairs separating a small horst block, for example Murchison Southwest (MSW) and Murchison Northeast (MNE) faults (figures 5.2B and 5.2C). The faults have a normal sense of displacement along their length and are extensional in character. They are found perpendicular to the main fault (figures 5.3) and tend to be located at the position of former segment boundaries although their displacement accumulation history is not restricted to prior to segment linkage. The length of the faults varies between 4 and 8 km.

The footwall transverse faults terminate at the main Murchison Fault and importantly do not cut the main normal fault plane at any stratigraphic level. Displacement on the faults decreases away from the main Murchison Fault where it is at a maximum (figure 5.5). A displacement – length profile for the Murchison Southwest and Murchison Northeast footwall faults defines one half of a theoretical bell-shaped displacement-length profile (figure 5.5). Maximum displacement varies from 40 to 180 ms (c. 60 to 280 m) between individual footwall release structures and does not correlate well with the overall length of the footwall structures.

5.2.3 Timing of movement

Detailed interpretation of the stratigraphy alongside the footwall faults associated with the Murchison Fault allows quantification of the timing of activity on the structures. This is achieved via incorporation of well-calibrated exploration well data with an extensive and densely-spaced (12.5m line spacing) 3D seismic database. The footwall faults are visible on maps to both Base Cretaceous Unconformity and Top Brent Group (figure 5.6A and 5.6B). In addition, calibration allows construction of well correlation panels (figure 5.7) which show similar geometric relationships with greater resolution.

The syn-rift stratigraphy associated with the Murchison Fault is subdivided into two discrete packages: syn-rift unit 1 and syn-rift unit 2. Syn-rift unit 1 comprises the Tarbert and Heather Formations. It is marked at its base by the Top Ness Formation or Top Pre-rift reflector and at its top by the Top Heather Formation. Syn-rift unit 2 comprises the Kimmeridge Clay Formation (Draupne Formation in Norwegian Waters). It is defined at its base by the Top Heather Formation reflector and at its top by the Base Cretaceous Unconformity. The footwall transverse faults show a wedge of early syn-rift sediment (syn-rift unit 1) situated in their hangingwall which increases in thickness into the fault (figure 5.6C). Expansion of syn-rift unit 1 is greatest in the immediate footwall to the main Murchison Fault and decreases away from the main fault (figures 5.2B and 5.2C). Expansion of the Tarbert and Heather Formations (syn-rift unit 1) into the footwall release faults indicates activity on the structures at the time of deposition of the formation (169-155Ma). In contrast, the upper part of the syn-rift (syn-rift unit 2) shows no expansion into the footwall transverse faults and as such they are interpreted to have become inactive before deposition of syn-rift unit 2. This upper syn-rift was deposited as a drape over the footwall fault system (figure 5.6D).

As the main Murchison Fault became inactive at c. 155Ma it is evident that activity on the footwall release faults ceased at the same time as the Main Murchison Fault.

5.2.4 Relationship to the master faults and to hangingwall faults

Footwall transverse faults terminate abruptly against the Murchison Fault. The hangingwall of the Murchison Fault shows little evidence for along strike brittle deformation (Figure 5.2D). However the hangingwall stratigraphy is folded into open folds with wavelength 2-6 km. These show no positional correlation to the release faults present in the footwall to the Murchison Fault. In addition, the hangingwall shows an overall down-warping along the

length of the Murchison Fault (figure 5.2D). The position of maximum down-warping correlates with the position of maximum displacement on the main fault.

5.2.5 Discussion

Rift cross faults are defined as those structures formed at high angles to the rift axis (Destro et al., 2003). They have been variously interpreted in recent extensional tectonic literature as transfer faults (Gibbs, 1984, 1990), transverse faults (Letouzey, 1986; Colletta et al., 1988), hard-linked transfer faults, (Walsh and Watterson, 1991; McClay and Khalil, 1998), cutoff stretch faults (Stewart, 2001) and release faults (Destro, 1995; Roberts, 1996).

Release faults are defined as those cross faults having predominantly vertical displacement of normal character which are associated with an individual fault and which die out within the hangingwall before connecting to another normal fault (Destro, 1995). Release faults were first identified in the Sergipe-Alagoas Basin, northeast Brazil, where they were termed *'falhas de alivio'* by Destro et al., (1990), (figure 5.8). Since then release faults have been well documented in the hangingwall to major faults for example in the Seripe-Alagoas Basin, Brazil (Destro, 1995) and in the Reconcavo Rift (Destro et al., 2003). They have also been identified in other areas, for example on seismic reflection data in the North Sea where they are shown to be present in both the footwall and hangingwall of the Smith Bank Fault (Stewart, 2001) and in the field in the Gulf of Corinth, Greece, where they are present near fault segment boundaries (Roberts, 1996). A further example of release faults is found in the footwall to major normal faults in Gebel El Zeit and along the offshore "B" Trend, Gulf of Suez, Egypt. The structures were not identified as release faults and are termed cross faults (Helmy, 1990). However, their location perpendicular to the main controlling fault in the immediate footwall to the fault suggests that they are release faults. It is important to distinguish release faults from transfer faults. Release faults do not connect normal faults as transfer faults do, but die out in the individual footwall or hangingwall block.

A release fault forms as a result of varying throws along the strike of a planar normal fault. It is well understood that for an idealised, isolated extensional fault the displacement on the structure is at a minimum at the fault tips and reaches a maximum at the centre of the fault, resulting in a characteristic 'bell-shaped' displacement length profile. As a result of differential vertical displacements along the length of the fault, the stratigraphy in both the footwall and hangingwall are bent and a suite of release faults is necessary in order to take up the extensional stresses in the plane parallel to the fault associated with the differential displacement. Release faults therefore form an integral part of the rift system. Calculations

by Stewart (2001) predict up to 3% of stretch parallel with the trend of the main fault itself, depending on the partitioning of extension between hangingwall and footwall. The total accumulated displacement on a release fault is always less than that on the master fault as they form as a direct response to differential down-dip displacements of the fault blocks on either side of the parent fault block. Release faults do not reflect the orientation of the regional stress field in a basin (Destro et al., 2003).

This extensional deformation of both hangingwall and footwalls of larger extensional faults has also been predicted in three-dimensional elastic dislocation numerical models of subsurface displacement for generalised faults (Ma and Kusznir, 1993). Footwall release faults in the Greater Murchison area are believed to have formed as a direct response to varying throws along the strike of the principal, planar normal fault, the Murchison Fault. They are interpreted to be the brittle manifestation of stress that results from the upward bowing of the footwall scarp during the accumulation of slip on the main Murchison Fault. The accumulation of maximum displacement in the centre of the evolving Murchison Fault introduces stresses to the footwall as it is bowed upwards in the centre by differential along-strike displacements. As such footwall release faults are a geometric requirement, necessary to accommodate variations in along-strike displacements in the footwall to the main Murchison Fault. Footwall release faults are defined as planar faults which are extensional in character. They show little or no component of strike-slip movement and have a maximum displacement at the main fault which decreases to zero in the immediate footwall to the fault. They do not connect adjacent normal faults. Footwall release faults do not cut the main fault plane at any stratigraphic level and as such the accommodation of displacement in the hangingwall to the main fault is decoupled from that which occurs in the footwall.

Footwall release faults preferentially intersect the main Murchison Fault at the position of former segment boundaries. The orderly and predictable fashion with which normal faults are segmented results in a regular distribution of footwall release faults in the footwall to the Murchison Fault. The position of footwall release faults at the position of former segment boundaries may reflect the increased along strike extension resulting from a decrease in displacement on the main fault at segment boundaries. A similar distribution of release faults is observed in the Gulf of Corinth, Greece, and is attributed to positions where a decrease in the displacement on the main fault is observed and consequently where along-strike extension cannot be accommodated by oblique-slip on the main fault (Roberts, 1996).

The relationship between relative magnitudes of footwall uplift and hangingwall subsidence in a fault bounded evolving half-graben has been shown to be dominated by hangingwall

subsidence. As a result, greater along strike extension such as that described above would be predicted to occur in the hangingwall than in the footwall to segmented normal faults (Wu and Bruhn 1994; Ma and Kusznir, 1995). This work suggests that longer release faults, with a larger displacement would be expected to form in the hangingwall to normal faults than in the uplifting footwall. There is no brittle deformation observed in the hangingwall to the Murchison Fault. Observations from other normal fault arrays suggest the ratio of footwall uplift to hangingwall subsidence is 1:6. These data suggest that the amount of deformation to be accommodated in the hangingwall should be six times that accommodated in the footwall to the Murchison Fault. It would therefore be expected that the hangingwall of the Murchison Fault would need to accommodate six times the displacement observed to be accommodated in footwall release faults. The lithologies of the footwall and hangingwall to the Murchison Fault are identical and they are present within the same regional stress regime. The absence of brittle deformational structures in the hangingwall may be a result of one of two processes: either the ratio of footwall uplift to hangingwall subsidence on the Murchison Fault is anomalous, or deformation in the hangingwall is accommodated in a non-brittle regime or in such a way that is beyond seismic resolution. There is little evidence for the first case: the Murchison Fault is a planar, long extensional fault which conforms to models of normal fault evolution in other respects. In the second case, along strike extension in the immediate hangingwall to the Murchison Fault may be accommodated via a fracture network that is beyond seismic resolution. The uplift of the footwall to the Murchison Fault to a structurally higher level during exhumation may result in modification of the rheology of the block via decompression and embrittlement. This is in comparison to the subsiding hangingwall block which is transported to a deeper more ductile regime. This may result in deformation in the footwall being accommodated in the brittle regime whilst in the hangingwall deformation is accommodated in the ductile regime. Alternatively, deformation may be accommodated by faulting at deeper structural levels (i.e. below seismic reflection data) in the hangingwall to the Murchison Fault.

The decoupling of footwall and hangingwall along-strike deformation regimes across the main fault can result in a contrast in deformational styles as observed in the Murchison Fault. The timing of deformation on faults in the footwall to the Murchison Fault corresponds to that of the deformation accommodated on the main fault itself. This is as expected since it is deformation on the main fault that results in differential uplift of the footwall and causes the formation of footwall release faults.

5.3 Role of strike-parallel footwall faulting

5.3.1 The Visund-Gullfaks Fault

The Visund-Gullfaks Fault (VGF) is the largest fault in the East Shetland Basin in terms of length, tilt and a maximum total accumulated displacement in excess of 5km (Faerseth et al., 1995). The structure is the most easterly fault in the East Shetland Basin and as such bounds the North Viking Graben along its western edge (figure 5.1). The VGF plane is a well defined planar feature which is well imaged on seismic reflection data (figure 5.9). It bounds the Visund, Gullfaks and Gullfaks South hydrocarbon fields. The fault is a single throughgoing fault strand which extends from 61˚N in the south to 61˚80'N in the north. It is 150km in total length and comprises a number of paleosegments.

The fault strikes north-south in the northern part of the study area but swings to strike north-north-east to south-south-west towards its southern tip. The change in strike corresponds to a branch in the fault, the westerly branch comprising the main VGF array and the easterly branch comprising the structure bounding the Kvitbjorn Hydrocarbon Field (figure 5.10). The branch delineates a slumped terrace, situated to the southeast of the main fault, which became decoupled from the main Visund-Gullfaks Fault during the Mid to Late Kimmeridgian (Faerseth et al., 1995). Both the southern and northern tips of the VGF are not imaged within the study area, as they are outside the area of 3D seismic data As a direct result of the large accumulated slip, the syn-rift sediments in the hangingwall to the VGF are at average depths of 5 seconds. This results in very poor seismic resolution and it not being possible to carry out detailed mapping of the syn-rift sediments. However, slip magnitude can be estimated from the few exploration wells (for example, 34/8-7) that penetrate the VG hangingwall. In addition, the presence of the Kvitbjorn hydrocarbon field on the slumped terrace in the southern part of the hangingwall to the VGF provides additional well and seismic calibration. It is also not possible to compute a displacement-length profile for the VGF due to both the erosion down to Middle Triassic levels in the footwall and the deep structural burial of the hangingwall stratigraphy as described above.

5.3.2 Footwall Structure

The footwall to the Visund-Gullfaks Fault (VGF) is intensely deformed by a fault population comprising an associated array of dominantly easterly-dipping (synthetic) normal faults located in the immediate footwall and striking parallel to the main fault itself (figure 5.11).

These are visible on maps of two-way time to the Top Statfjord Formation (pre-rift; figure 5.12). The topography seen at the Top Statfjord Formation level reflects the degree to which the footwall has been dissected by this population of short, low displacement normal faults. Overprinting this deformation is an overall shallow dip to the west of the pre-rift sediments. This fault-induced topography is not present at the Base Cretaceous Unconformity (BCU) as the uplifted footwall scarps to the footwall faults have been removed by erosion as a result of larger magnitude uplift of the footwall scarp to the main VGF itself (figure 5.13). Instead the topography seen on the BCU in the footwall to the VGF shows a high in the east, onto the footwall scarp of the main fault, decreasing to the west into the hangingwall of the adjacent Snorre Fault. The northern tip of the study area is uplifted in the footwall to a regional east-west orientated structure.

The footwall fault population associated with the VGF is predominantly synthetic to the main fault although in the south a population of shorter, smaller displacement antithetic structures is present (figure 5.11). Faults are named in the order that they were identified and mapped. Where fault numbers are missing they have been identified as comprising part of a larger fault, being beyond seismic resolution or their displacement is not quantifiable due to erosion in the uplifted footwall to the main Visund-Gullfaks Fault. The structure of the footwall fault population associated with the VGF will be considered in terms of the character of the faults, displacement-length relationships, fault spacing and fault terminations.

The synthetic fault population comprises in excess of thirty faults which range in mapped length from 6-16 km. The antithetic fault population comprises of approximately ten faults which are in general smaller (4-8 km) and have lower displacements than the synthetic fault population.

The total mappable length of each individual fault is shorter than the true length of the fault as the displacement at the fault tips falls below seismic resolution (see section 3.5). Displacement is measured as throw between the footwall and hangingwall cut-offs at Top Statfjord Formation level at 12.5m intervals along the length of the footwall fault (see figure 3.8 for definition of throw). Measurements were taken perpendicular to the strike of the footwall structures.

The strike-parallel faults in the footwall to the VGF show maximum accumulated displacements in the range 42-442 ms (c. 60-700m). There is a positive correlation between maximum displacement on an individual footwall fault and the total mappable length of the fault (figure 5.14). Faults with lengths in the range 6-16 km would be predicted to

accumulate maximum displacement of approximately 200 to 550m (Schlische et al., 1996). Thus, the faults in the footwall to the VGF have accumulated maximum displacements of a magnitude expected considering their total length. They are in general not underdisplaced and activity on these structures is not likely to have been prematurely terminated as observed elsewhere in the basin, for example on the Murchison Fault.

The along-strike displacement-length characteristics of each individual footwall structure associated with the VGF can be extracted along the length of each fault. The faults generally show a maximum displacement near the centre of the fault and displacement reaches a minimum at the fault tips (figure 5.15). This corresponds to a characteristic 'bell-shaped' displacement-length profile observed from normal faults both in the field (Peacock and Sanderson, 1993 and 1994; Dawers et al., 1993) and in numerical models (Cowie and Scholz, 1992b).

Displacement length profiles for individual footwall faults are presented in appendix 4. The profiles in general conform to the characteristic fully equilibriated 'bell-shaped' model, although where one part of the fault lies outside the study area, the complete bell-shaped profile is not mappable and only part of the profile is imaged (for example, Visund Footwall Fault 41 shown in figure 5.16). Faults with total length in excess of 10 – 12 km show a saw-tooth displacement-length profile overprinted upon which a bell-shaped profile can be discerned (figure 5.15). The displacement minima on such curves are likely to represent points of former segment linkage which may not have fully equilibrated to the characteristic bell-shaped profile following a linkage event. Such minima do not affect the overall displacement-length scaling relationships for the larger footwall faults as demonstrated above.

The along-strike total accumulated displacement summed for displacement on all footwall faults at a given location along the main VGF is presented in figure 5.17. The displacement-length relationship shows an overall bell-shaped profile with accentuated displacement in the northern section of the footwall to the VGF. The tips of the main VGF are outside the study area and it is likely that the displacement maxima for the along-strike total accumulated displacement for the footwall faults is as observed and that part of the profile would be located to the north and south of the study area for this thesis. The profile shows a number of local displacement minima. Their origin is related to the presence of footwall faults in differing locations with different amounts of overlap along the length of the main VG.

The along-strike total accumulated footwall fault displacement for the mappable section of the VG reaches a maximum of 988ms (c. 1560m).

Importantly, the footwall fault population shows a systematic relationship between maximum accumulated displacement and distance from the main VGF. Footwall faults located closer to the main VGF show lower maximum displacements than those located more distally (figure 5.18). In addition, footwall faults located more distally tend to be of marginally greater length than those located more proximally to the VGF and would therefore be predicted to have accumulated larger maximum displacement (Schlische et al., 1996).

The spacing between footwall faults and distribution within the footwall to the VGF shows a range of regular and irregular patterns. Along the mappable length of the VGF the strike of adjacent footwall faults is parallel to the strike on the main fault. Thus, in the north faults strike north to south and in the south strike north-north-east to south-south-west. The relative spacings will be considered in two units: The first to the north of 61˚35'N and the second to the south of 61˚35'N.

Strike-parallel footwall faults associated with the VGF in the northern part of the footwall show a regular pattern of spacing between adjacent faults. Faults are present throughout much of the northern part of the footwall from the VGF in the east to within 5km of the Snorre Fault in the west (figure 5.11). The across-strike spacing between faults is generally 2-3 km and fault planes are generally planar and mutually parallel. The resulting deformation dissects the footwall of the VGF into 2-3km thick parallel sided slices (figure 5.19). In the northern part of the study area there is little physical interaction between adjacent faults, the individual strands are isolated and do not tend to branch or terminate at or from each other. Synthetic footwall faults dominate in this part of the footwall to the VGF and antithetic faults, where present, are short (less than 2km), have small magnitude maximum displacements (less than 100m), and tend to be located on the extremities of the footwall fault population.

In the southern part of the VG area, footwall deformation is accommodated on a more distributed array of faults. These are dominantly synthetic in the immediate footwall to the VGF and antithetic in the more distal footwall. The faults are more distributed and are not defined by a regular spacing. The spacing between adjacent footwall faults varies between 2 and 10 km and a large area of the central part of the VGF footwall is largely free of deformational structures (figure 5.20). In addition, the faults tend not be isolated structures but to branch from one another (figure 5.11); for example Visund Footwall Faults 12 and 13 (both antithetic structures) branch from the synthetic Visund Footwall Fault 17.

Strike parallel footwall faults are present in the footwall to the VGF in positions directly adjacent to the fault scarp itself. However, lack of well control and erosion to deeper structural levels (Middle Triassic) results in it not being possible to quantify the amount of displacement accumulated on the structures in the immediate footwall. These structures have been eroded during the degradation of the uplifted footwall scarp and will be considered later in section 5.4.

5.3.3 Timing of movement

The timing of movement on the suite of footwall faults associated with the VGF can be estimated via examination of the structural relationships between the faults and the stratigraphy of the VGF footwall. The footwall faults offset all pre-rift reflectors, namely the Top Triassic, Top Statfjord Formation, Top Dunlin Group and Top Brent Group and do not affect any of the post-rift reflectors associated with the Mid to Late Jurassic rift episode in the Northern North Sea (figure 5.19). They were therefore active between the end of the pre-rift and start of the post-rift i.e. during the syn-rift interval in the latest part of the Jurassic. However, the position of the footwall faults in the immediate footwall to the Visund-Gullfaks Fault and the magnitude of uplift and erosion on the VGF itself prevents any more accurate estimation of timing of movement on the suite of footwall faults. This is because any syn-rift stratigraphy that may once have been associated with the footwall faults has been removed due to uplift on the VGF and subsequent erosion of the footwall and the faults contained within it.

5.3.4 Discussion

The fault sub-parallel planar fault array present in the footwall to the VG fault is unusual and a phenomenon not seen elsewhere in either the Northern North Sea or other rift provinces. The structures are unique to the VGF and as a result demand a new interpretation.

One hypothesis for the origin of the fault population in the footwall to the VGF may be due to the rapid localisation of strain onto the Visund-Gullfaks Fault during the Volgian. The migration of the locus of extension in the East Shetland Basin caused a focussing of strain onto the rift axis and specifically onto the Visund-Gullfaks Fault itself. The VGF itself may not have been able to take up the increasing strain as localisation progressed and as a result the suite of footwall faults formed in order to accommodate the increasing strain on the graben bounding fault.

An alternative hypothesis for the development of the footwall faults is that they may have formed in response to a gravitational collapse of an oversteepened footwall. Gravitational collapse structures may range in scale from centimetres to hundreds of kilometres and affect both loose sediments and consolidated rocks (Hesthammer and Fossen, 1999). Collapse of this type is documented to occur in the footwalls to large extensional fault blocks in areas undergoing regional extension.

Gravitational failure is observed on uplifted footwall scarps elsewhere in the Northern North Sea. For example, the Statfjord Fault is deformed by gravitational collapse which took place as rotational block slides. The fault blocks remained internally rigid. Deformation occurred via polyphase movement on listric faults which detached within soft shales and are associated with several rotated slump blocks which decrease in size away from the break-away zone (Hesthammer and Fossen, 1999). On the footwall scarp to the Brent Field, systematic failure of the scarp has been documented by McLeod and Underhill (1999). Here, a fault scarp degradation complex is recognised to be the remnants of translational-rotational slides which slid on major decollement horizons within the Ness Formation, Dunlin Group and Lower Banks Group. The failure horizons are described as discrete, planar-circular shear surfaces. A further example of gravity-induced failure in the Northern North Sea is the Zeta structure. Located in the footwall to the Snorre Fault, this is interpreted to be a detached gravity slide block, formed by collapse of the uplifted footwall block (Berger and Roberts, 1999).

On the footwalls to the Statfjord, Snorre and Brent faults the area affected by gravitational failure is commonly amphitheatre-like in map view, having a listric and concave upwards detachment surface (Hesthammer and Fossen, 1999). The footwall faults associated with the VG fault are planar in nature and show no evidence for a listric shape geometry in cross section (figure 5.19). Furthermore, they penetrate deeper into the footwall than the superficial slumps described above on the Statfjord and Brent field and as a result are considered unlikely to have been formed by gravitational collapse of an oversteepened footwall.

5.4 Degradation of the Visund-Gullfaks Fault Scarp

5.4.1 Introduction

Normal fault footwall scarps are uplifted as a direct result of slip on the bounding fault. Their elevation is maintained over a significant time period as a result of continual accumulation of

slip in discrete seismic events on the bounding normal fault. Fault scarps are in general steep and are therefore prone to gravity-driven, seismically triggered denudation processes (e.g. Keefer 1984 and 1999). These processes liberate sediment from the uplifted scarp which is then available for redeposition in adjacent hangingwall depocentres.

The VGF in the East Shetland Basin underwent significant footwall uplift during the Mid to Late Jurassic rift episode. As a result, the footwall was extensively degraded by the effects of both submarine and sub-aerial processes, however there is to date no documentation of the effects of fault scarp degradation along the VGF. This section will first consider the structure of the degraded fault scarp before quantitatively assessing the impact of erosion on the footwall to the VGF. Finally, the section will consider the fate of the eroded footwall products by examination of the adjacent hangingwall depocentres.

5.4.2 Fault Scarp Structure

The VGF scarp is a well-defined undulating surface mappable on 3D-seismic data. It is a clear onlap surface onto which post-rift horizons onlap to both the east and west (figure 5.21). The surface is erosional in nature, having resulted from removal of pre-rift stratigraphy in the footwall to the VGF. The surface corresponds with the top syn-rift, or Base Cretaceous Unconformity reflector. The north-south mappable extent of the degraded fault scarp is limited by the availability of 3D seismic reflection data for incorporation into the study. The easterly limit of the scarp is defined by the main VGF plane itself and the westerly extent by the subcrop to Base Cretaceous Unconformity of the top pre-rift horizon, Top Ness Formation. As documented in section 4.6 rapid uplift of the footwall to the VGF during the latest part of the rift episode may have removed some of the syn-rift units associated with the Snorre Fault. In locations where this has visibly occurred the fault scarp is delineated to the west by a higher stratigraphic marker in the Heather Formation.

There is no along-strike marked development of a footwall scarp degradation complex ‘FSDC’ (as defined by Underhill et al., 1997) on the eroded crest of the VGF. This is in contrast to other faults in the Northern North Sea, where such a complex has been located and mapped in detail (for example on the Statfjord Fault; McLeod and Underhill, 1999 and on the Ninian field, Underhill et al., 1997). This could be due to a complete absence of a complex along most of the length of the fault, or a complex may be present but be beyond seismic resolution (see section 3.5). A limited amount of material is present adjacent to the Gullfaks Field in the southern part of the mapped VGF. The external boundaries of the Fault

Scarp Degradation Complex (FSDC) are well defined but the internal structure of the deposit is beyond seismic resolution appearing transparent and where reflectors are discernable to be internally chaotic. The upper boundary of the FSDC is synonymous with the top syn-rift or Base Cretaceous Unconformity in the area. There is seismic onlap of post-rift horizons such as the Cromer Knoll Group onto this surface. The FSDC is therefore designated as part of the syn-rift stratigraphy. The lower boundary is erosional in character and is defined by the erosional truncation of the pre-rift stratigraphy in the footwall to the VGF. It is the amalgamation of these two bounding surfaces that result in it not being possible to regionally map the presence of a fault scarp degradation complex along the length of the VGF.

The FSDC observed in the vicinity of the Gullfaks Field covers a mappable area of c.12km² and shows chaotic internal morphology (figure 2.22). It is elongated along the strike of the VGF and reaches a maximum of c.100 ms in overall thickness. The complex is located on top of the fault scarp and is on the eastern side of the eroded surface.

5.4.3 Impact of erosion

The impact of erosion on the VGF scarp can be quantified within the study area. The uplifted footwall to the VGF has undergone erosion along its full length within the study area and 2D data from outside the study area suggest it has been degraded along its entire length from the fault tip in the north to the Alwyn Field in the south. The along strike length of the fault scarp within the study area which has undergone erosion is approximately 60km. The across strike width of the eroded area varies along the length of the fault. In the north of the study area the area of footwall affected by erosion is much wider (c. 20km) than in the south, (figure 2.22). This is due to a lower gradient on the bounding fault. In contrast, the eroded area is c. 5km wide in the southern part of the study area where the VGF is steeper.

Erosion of the footwall to the VGF resulted in the backstepping of the fault crest during the syn-rift and early post-rift interval. The denuded crestal area of the VGF was reconstructed by extrapolating the trace of the fault and the top pre-rift (Top Ness Formation) markers (figure 2.23). The point of intersection of these two markers was interpreted to give the position of the paleo-fault crest. Crestal reconstruction shows that the position of the VGF crest has been backstepped towards the west by up to 5km as a result of erosion during the Mid to Late Jurassic rift episode (figure 5.23). This value agrees with the published value of 3.5 - 4km for back-stepping of the northern part of the fault crest as a result of Late Jurassic

erosion (Faerseth et al., 1995). Erosion has also removed the upper section of the footwall faults described in section 5.32 above (figure 5.19).

Reconstruction of the paleo-crest of the VGF also allows an estimate to be made of the volume of material removed from the footwall scarp. The seismic surfaces describing the reconstructed footwall crest and the erosion surface were depth converted using data from the Cretaceous interval in well 34/8-7. This technique introduces error due to depth conversion of a large area based upon a single point of time-depth data. The volume contained between the two defining horizons was calculated using Midland Valley 3DMove software.

Erosion of the footwall to the VGF within the study area has removed an estimated c. 65km³ of material. This volume is a lower estimate as it does not take account of uplifted material associated with smaller displacement faults (described in section 5.3 above) in the footwall to the VGF. Extrapolation of this value out of the study area, assuming similar magnitudes of uplift and erosion along the 150km length of the fault predicts that an estimated 200km³ of material has been removed as a result of uplift and subsequent erosion of the footwall to VGF.

5.4.4 Redistribution of eroded sediments

The degradation and erosion of 65km³ of sediment from the footwall of the VGF within the study area results in the redistribution of this volume of material to depositional sinks elsewhere in the basin. The immediate destination for material eroded from an uplifted footwall are the downslope areas located perpendicular to the strike of the principal fault: in the VG area this is the hangingwall depocentre associated with the VGF located to the east of the footwall scarp and the hangingwall depocentre associated with the Snorre and Statfjord faults located down the dip-slope of the footwall to the west of the eroding scarp.

Well 34/7-8 is located in the immediate hangingwall to the VGF (figure 5.25). It is the only well in the study area to contain a complete logged Jurassic section from the hangingwall to the VGF (figure 5.26). The well contains four cored intervals of which three were recovered for examination. The uppermost cored interval (core 1) is from the Latest Jurassic Draupne Formation (Kimmeridge Clay Formation equivalent) (4492m – 4471m). Lithologically, the core is dominated by a breccia or conglomerate which is light brown-grey to olive grey in colour (figure 5.27). It has a sandstone matrix of grey-brown to dusky-brown colour containing transparent quartz grains which are medium to coarse grained, subangular and

moderately well sorted. The matrix is very hard with a siliceous cement, and contains traces of mica and occasional micaceous and carbonate laminations and coal fragments. The clasts are subrounded to subangular and moderately sorted ranging in size from a few millimeters to several centimetres. The clasts are predominately composed of non-calcareous claystone, siltstone and sandstone. There is no visible porosity.

The conglomeratic interval in well 34/8-7 is present in rocks of the Draupne Formation deposited in the latest part of the Middle to Upper Jurassic rift episode in the Northern North Sea. The Draupne Formation is Late Oxfordian to Ryazanian in age. Micropaleontological analyses reveal a suite of fauna that is diagnostic of this interval. In addition, fauna present in the conglomeratic interval are diagnostic of the Middle Callovian.

The clasts present in the conglomerate in the core are interpreted to have been derived from the uplifting footwall of the VGF. Material was removed from the footwall as a result of shallow marine or sub-aerial erosion whilst the footwall was in an uplifted position and redeposited in the hangingwall depocentre.

.

5.4.5 Discussion

In addition to the deformation caused by footwall faulting, the VGF scarp has been significantly degraded by erosion. Normal fault scarps, such as the VGF scarp, are generally steep and are often prone to failure as a result of gravitational instability. This process causes structural degradation and produces sedimentological products for reworking. Normal fault scarps maintain their topography and gradient for a significant period in geological time by repeat movement events on the bounding fault. Normal fault scarp failure has been widely recognised in field settings from currently extending regions, for example the Aegean Region in Greece (Ferentinos et al., 1988; Stewart and Hancock, 1988) and along the Wasatch Front in Utah (Hamblin, 1976). However, in a subsurface setting the low preservation potential of topography on uplifted fault scarps and the rapid rate of sediment transfer into adjacent depocentres results in few ancient examples having been well documented (McLeod and Underhill, 1999). However, the East Shetland Basin in the Northern North Sea preserves a number of degraded footwall scarps that result from Mid to Late Jurassic regional extension. In addition to the scarps themselves, the dense data coverage has also resulted in identification of the products of fault scarp degradation in adjacent hangingwall depocentres, for example in the Ninian Area (Underhill et al., 1997).

The VGF is the largest fault in the East Shetland Basin both in terms of length and total accumulated displacement (see chapter 4). As such, the magnitude of footwall uplift on the VGF is predicted to be greater than any other fault in the East Shetland Basin. Assuming that the conditions needed for erosion of an uplifted footwall were similar throughout the East Shetland Basin during the Mid to Late Jurassic rift interval then the magnitude of erosion predicted to have occurred on the VGF would be greater than that observed on other faults in the basin. In contrast to the VGF, the Statfjord Fault is a 62km long single throughgoing fault strand with a planar easterly dip and maximum displacement in excess of 2km (McLeod et al., 2000). McLeod (2000) records that the total footwall area affected by erosion on the Statfjord Fault is 167.7km² and that the scarp has back-stepped by 2 – 2.5km. The erosion removed a total of 35.24km² of pre-rift lithologies from the uplifted footwall and left an eroded scarp 2.5 – 3.5km wide. The Heather Field is situated in a small fault block on the western edge of the East Shetland Basin. It is estimated to have lost one third of the pre-rift Brent Group deposits as a result of footwall erosion. This corresponds to a vertical height loss of c. 120m at the crest of the footwall scarp (Gray and Barnes, 1981). A comparison of the magnitude of erosion on fault crests located more distally from the North Viking Graben, and those that are therefore assumed to have accumulated less slip than the VGF (see chapter 4) shows that the VGF was subject to a greater degree of erosion than smaller faults with overall shorter fault trace and smaller maximum accumulated displacement. This was manifested in the removal of a larger amount of pre-rift material and the formation of a wider and longer eroded footwall scarp. However, the degree of back-stepping of the footwall crest appears to be largely unaffected by the magnitude of erosion and both the footwalls to the Statfjord and Visund-Gullfaks Faults were eroded along their entire length.

The crest of the VGF is degraded to a predominantly flat surface with low amplitude topography (figure 5.23). This suggests that the dominant mechanism of erosion was peneplanation near to wave base. This interpretation is supported by a similar morphology on the crest of the Snorre Fault, at similar or lower structural elevation, also interpreted to have resulted from erosion at or near sea level (Yielding, 1990). The magnitude of uplift and erosion on the VGF may have resulted in the crest of the footwall forming an elongate emergent area above sea-level. Such features are defined as ‘footwall islands’, (Barr, 1987) and are likely to result in a setting with large original across-strike fault spacing and a steep-initial fault plane. The VGF block is c. 30km in width and is calculated to have had an original pre-compaction dip of 50-60˚ (Faerseth et al., 1995) and therefore is a prime candidate for the development of a footwall island. Examples of footwall islands in extensional provinces are not just predicted from modelling data but can be observed in field

extensional basins: For example, in the southern Gulf of Suez, Egypt, (see section 2.6) Middle Miocene stratigraphy has been uplifted in the footwalls to major normal faults to an elevation 300-500m above present day sea level. Gebel Zeit is a high-standing northwest-southeast trending tilted fault block which is emergent above the present day sea level. The block exposes Precambrian basement and pre-rift sediments on its upper edge which is currently subject to erosion in the present day Gulf of Suez. In addition, the structure of central Greece is dominated by a series of large normal faults, two of which combine to produce the island of Evia in the Aegean Sea. Evia is a footwall island defined by the uplifted footwalls to two opposite polarity normal faults (Leeder and Jackson, 1993).

The VGF shows no marked development of a continuous along strike fault scarp degradation complex mounted on its uplifted footwall. Such a complex has been documented from most of the other major faults in the Northern North Sea Rift Province for example, Alwyn North (Johnson and Eyssantier, 1987), Brent, (Livera and Gdula, 1990; Schulte et al., 1994; Coutts et al., 1996; McLeod and Underhill, 1999), Snorre, (Dahl and Solli, 1992) and Statfjord, (Hesthammer and Fossen, 1999; McLeod, 2000). The absence of a FSDC on the VGF may reflect the magnitude of uplift and erosion experienced by the fault.. The rapid rate at which erosion took place may have precluded the formation of a FSDC as material was eroded and immediately removed from the footwall scarp. In addition, the VGF was subject to rapid uplift during the final part of the Mid to Late Jurassic Rift Episode as a result of strain localisation towards the Viking Graben (see chapter 4). As a result any development of a FSDC on the footwall scarp which may have once been present may have been removed during rapid uplift and erosion, which may have taken the crest of the eroding footwall to at or above wave base (see above). Formation of a well-developed FSDC on the VGF may have been further precluded by the presence and activity of the population of footwall faults present in the immediate crest to the fault (see section 5.3).

Footwall erosion of the type described above is commonly attributed in the literature to pre-rifting doming (Ziegler, 1982), heterogeneous stretching (Coward, 1986), local transpression (Beach, 1985) or regional compression (Frost, 1987). As shown above, tilted fault blocks in the Northern North Sea show varying degrees of erosion with varying amounts of Middle and Lower Jurassic and Upper Triassic section being removed. Footwall erosion in an extensional province is predicted by the domino model (see section 2.2.1) of extension in which rigid fault blocks progressively rotate as extension proceeds (Yielding, 1990). Uplift and degradation of the footwalls in the Northern North Sea is a direct consequence of Mid to Late Jurassic normal faulting and fault-block rotation. Yielding (1990) uses the domino

model to predict the magnitude of footwall uplift on three Late Jurassic extensional faults from the East Shetland Basin. The work shows that the major control on the degree of erosion or degradation at the crest of a tilted fault block is the width of the block: large fault blocks will typically show greater erosion. The northern section of the Visund-Gullfaks Fault Block is 30km wide. In contrast, the Statfjord Fault Block is c. 18km, the Snorre Fault Block 12km and the Murchison Fault Block 10km. The Visund-Gullfaks Fault is therefore the largest fault block in the area by across-strike distance and therefore would have been expected to have undergone the largest magnitude erosion according to Yielding (1990).

The conglomeratic interval in well 34/8-7 contains subangular, poorly sorted clasts of mixed composition. Deposition of these clasts is likely to have occurred in close proximity to the source due to the low degree of rounding and the poorly sorted nature of the sample. The closest and most accessible source during the latest part of the Jurassic rift interval was the uplifting footwall to the VGF. The transport direction for the conglomeratic clasts is to the east and the distance travelled a minimum of 10km.

The composition of the clasts incorporated into the conglomerates may reflect the varied composition of the pre-rift deposits in the footwall to the VGF. The Brent Group comprises sandstones, coals, siltstones and claystones, all lithologies present as clasts in the cored conglomerate. The eroding Brent Formation, uplifted and tilted during Mid to Late Jurassic extension and largely removed by erosion from the VGF scarp, may have been the source for many of the conglomerate clasts. A similar relationship is seen adjacent to the Brent Fault, south of the study area. Here, well 211/29-8 penetrates the immediate hangingwall to the Brent Fault where it encounters a chaotic band of allochthonous Brent Group sediments and in situ Humber Group (McLeod and Underhill, 1999). This talus of degraded syn-rift sediment located adjacent to the Brent Fault is also visible as divergent reflectors on seismic data.

The age of the conglomeratic interval cored in well 34/8-7 is Callovian to Ryzanian. This time corresponds to the final part of the Mid to Late Jurassic rift episode. The source for this clastic material has been identified to be the footwall scarp associated with the VGF which was therefore still being actively degraded at the end of the rift episode. This further supports the evidence presented in Chapter 4 that the VGF was active at the end of the rift episode.

5.5 Conclusions

Deformation of the uplifted footwalls to the major faults associated with the Northern North Sea Mid to Late Jurassic rift episode has been documented to have occurred in different ways at different locations, with different timescales and with different implications. In the central East Shetland Basin, the footwall to the Murchison Fault has been dissected by footwall release faults, formed as a result of differential uplift along the strike of the bounding master fault. On the edge of the Viking Graben the footwall to the Visund-Gullfaks Fault has been sliced up by regularly spaced, strike-parallel faults formed in response to strain localisation onto the rift axis. In addition, the footwall to the Visund-Gullfaks Fault has been significantly degraded by erosion. The wider implications of the deformation, in particular the effects on potential hydrocarbon prospectivity in the uplifted footwalls, will be considered further in chapter 6.

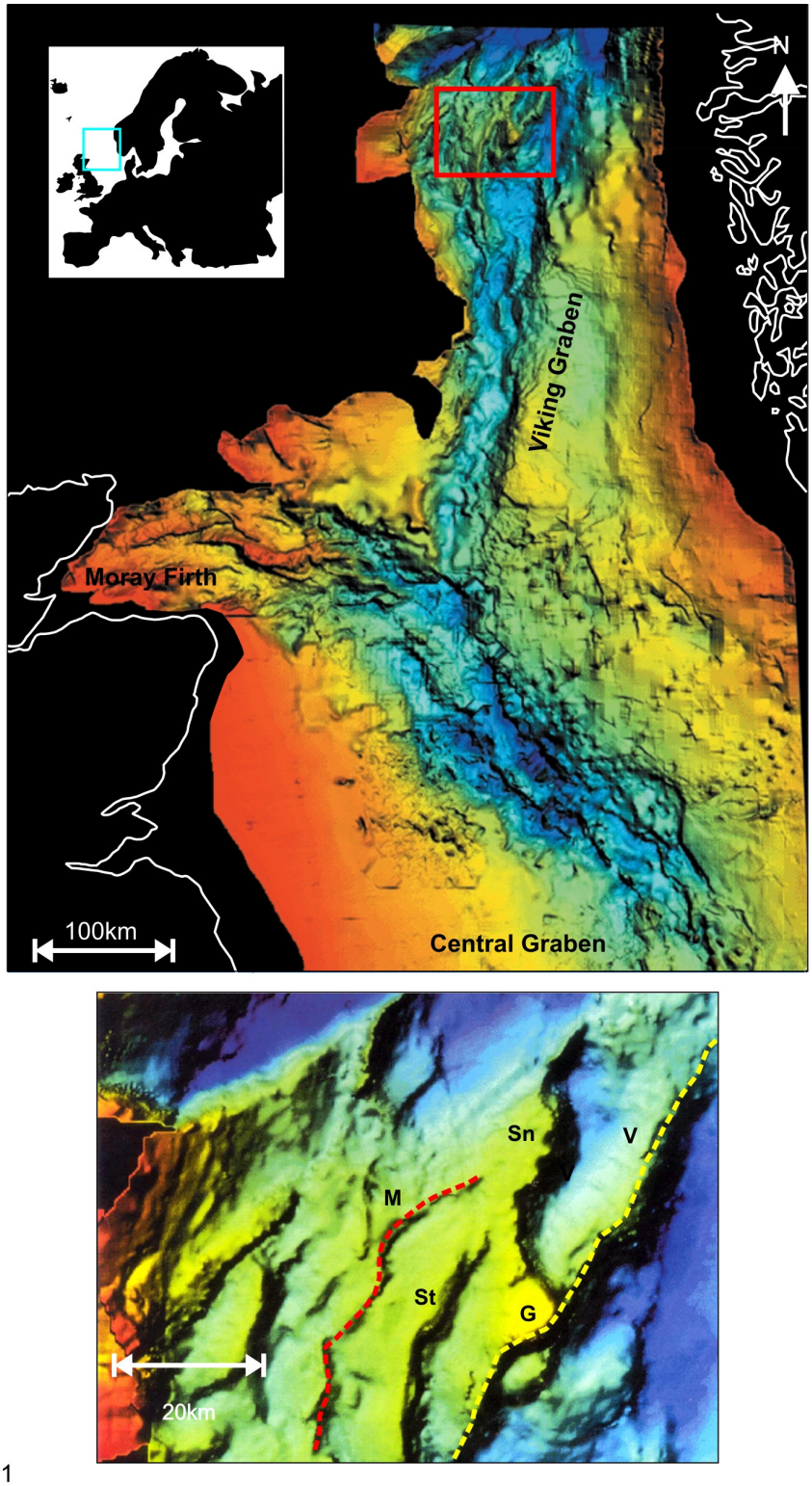

Figure 5.1
Time map to Base Cretaceous Unconformity.
Red box shows area of enlarged map (bottom).
M=Murchison Field, St= Statfjord Field, Sn=Snorre Field, G=Gullfaks Field, V=Visund Field
Murchison Fault shown in red dashed line. Visund-Gullfaks Fault shown in yellow dashed line
After Fraser et al., 2003.

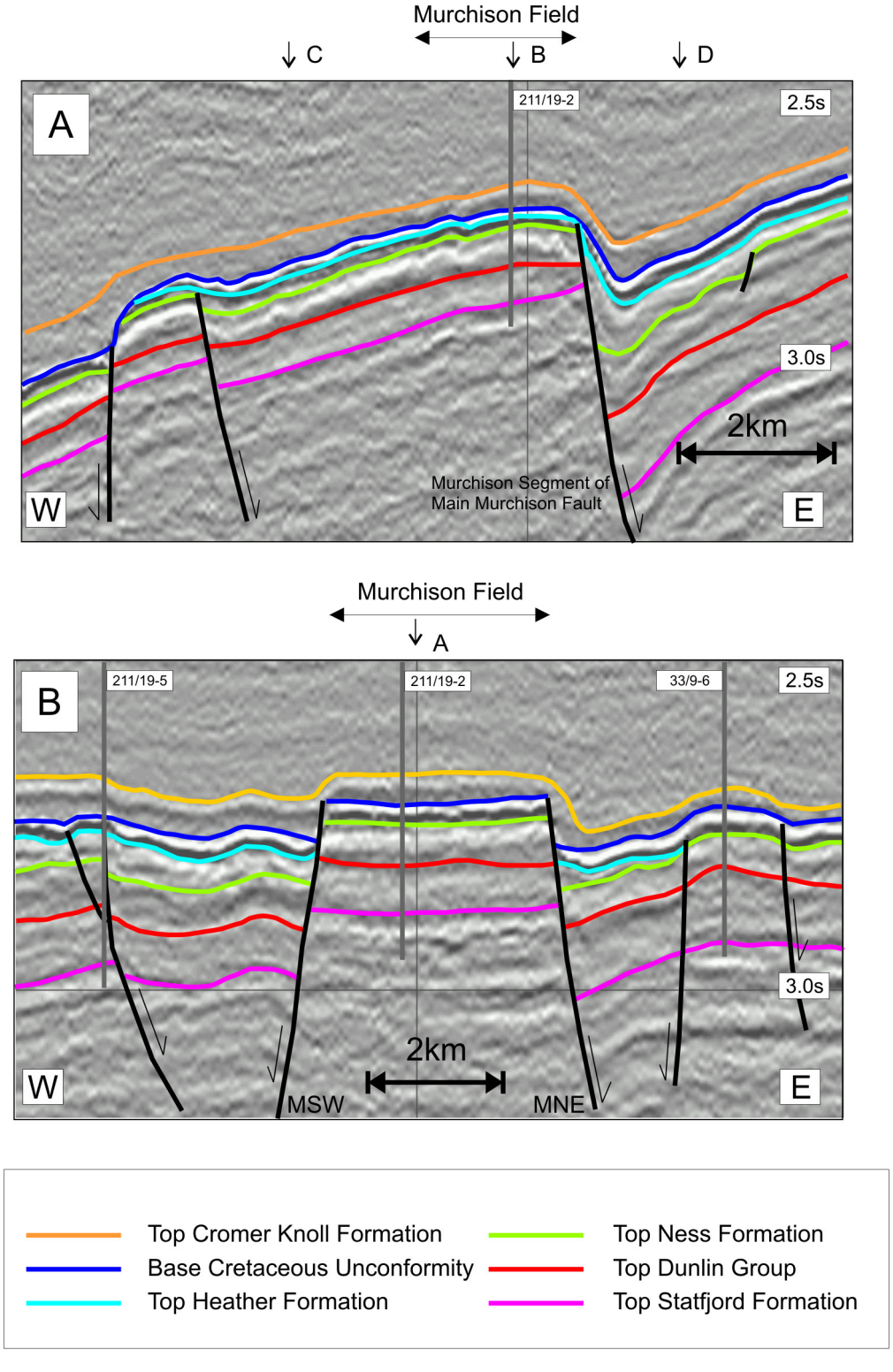

Figure 5.2
Seismic panels from the Greater Murchison Area
Panel A: Strike perpendicular section showing main Murchison Fault
Panel B: Strike parallel section in immediate footwall to Murchison Fault showing footwall release faults Murchison Southest (MSW) and Murchison Northeast MNE).
Locations of seismic lines are shown on figure 5.3

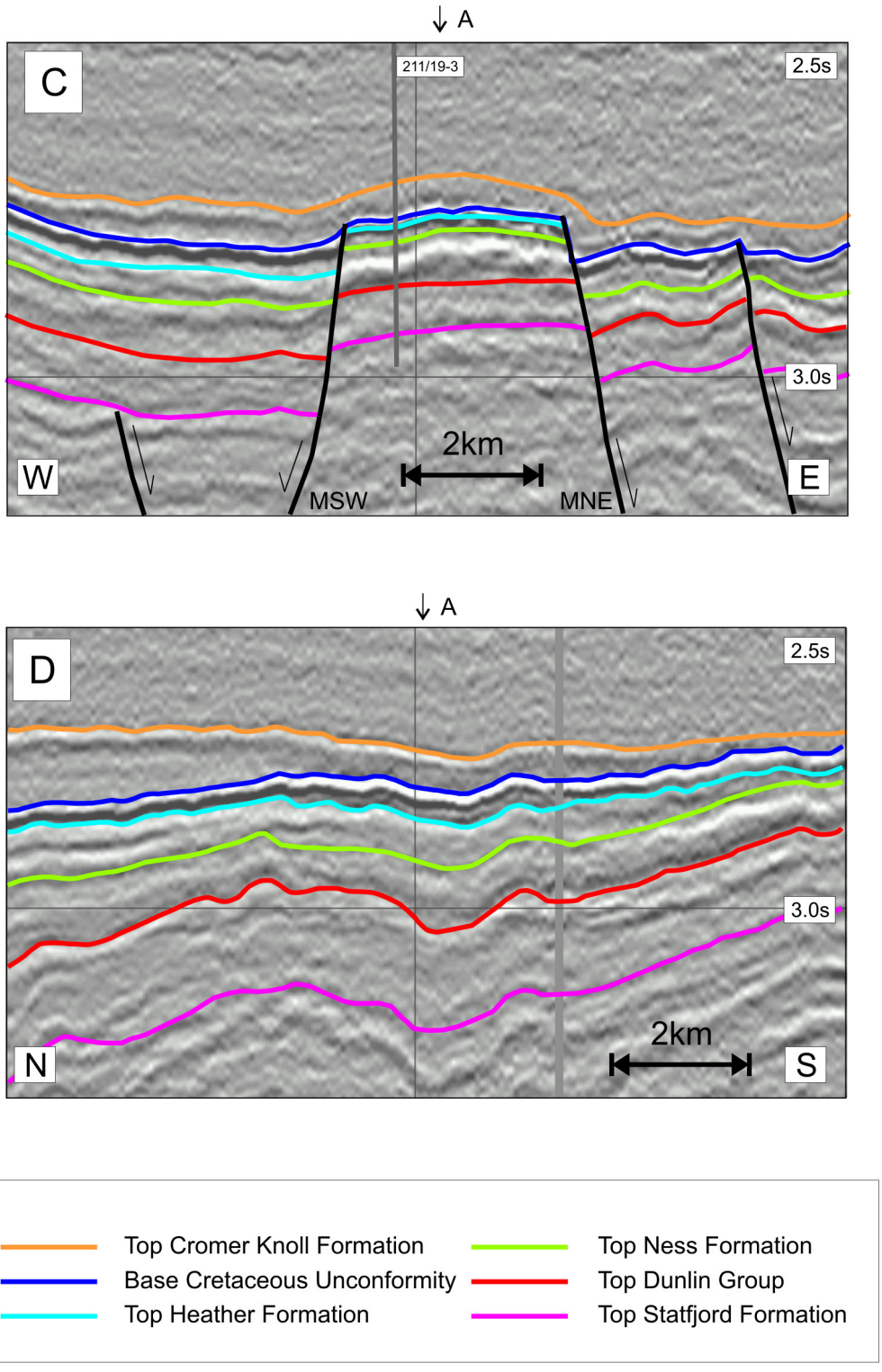

Figure 5.2 continued
Seismic panels from the Greater Murchison Area
Panel C: Strike parallel section located 4km into the footwall of the Murchison Fault
Panel D: Strike parallel section in the hangingwall to the Murchison Fault.
Locations of seismic lines are shown on figure 5.3

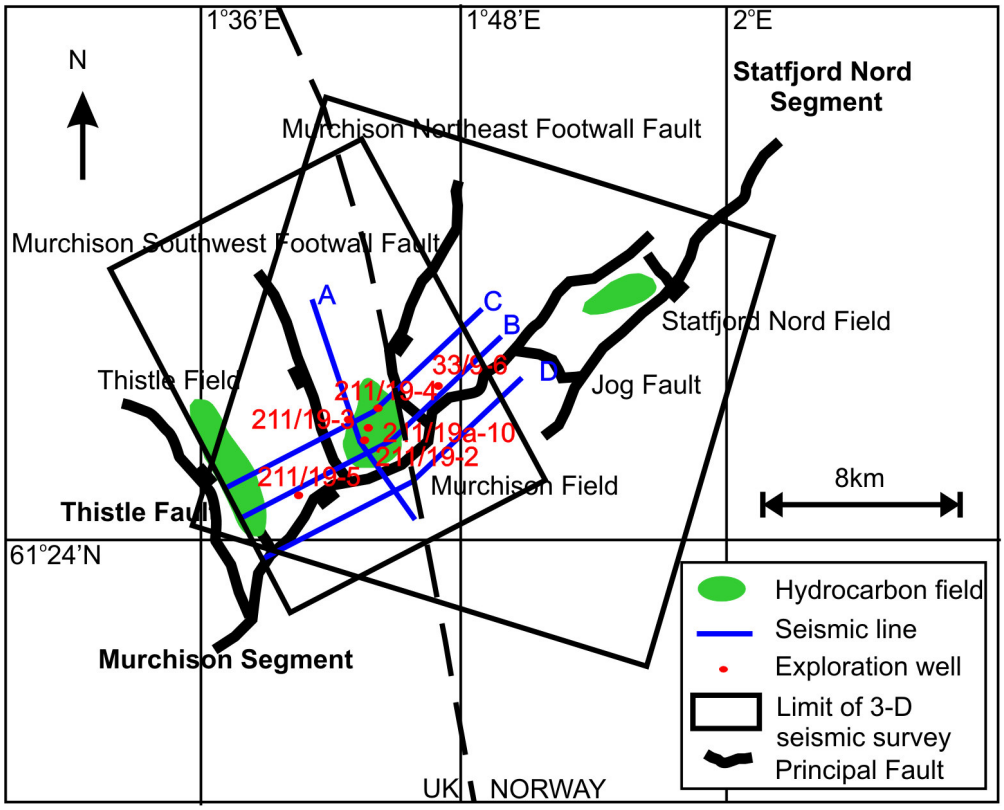

Figure 5.3
Map showing location of data incorporated into the study with reference to major faults
Blue lines show the location of seismic lines shown in figure 5.2

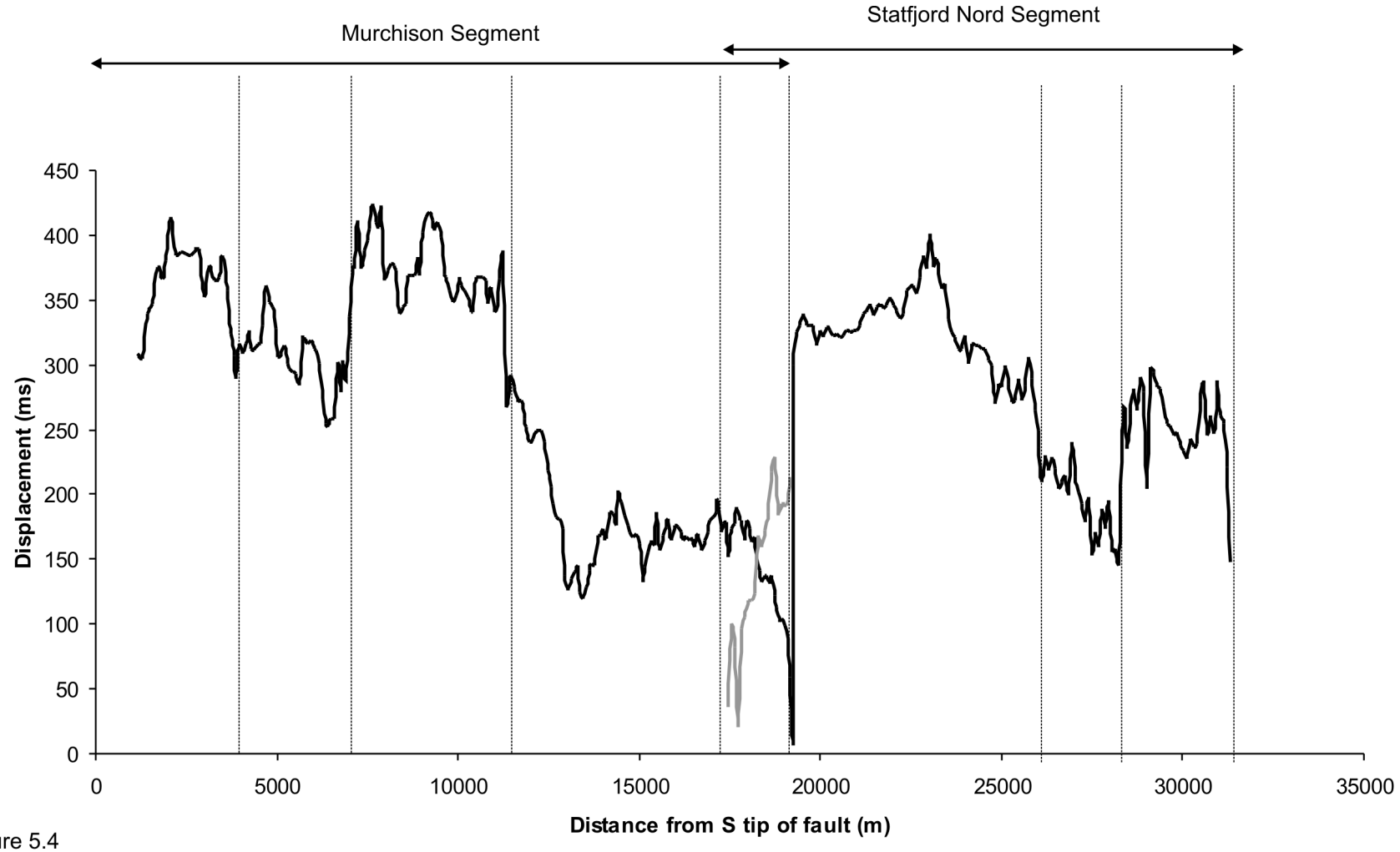

Figure 5.4
Displacement-length profile for Murchison Fault. Dotted lines show positions of former segment boundaries. Constructed from footwall and hangingwall cutoffs at Top Statfjord (intra-prerift) level. Grey profile shows abandoned tip in hangingwall to main fault. Southern tip of fault outside study area

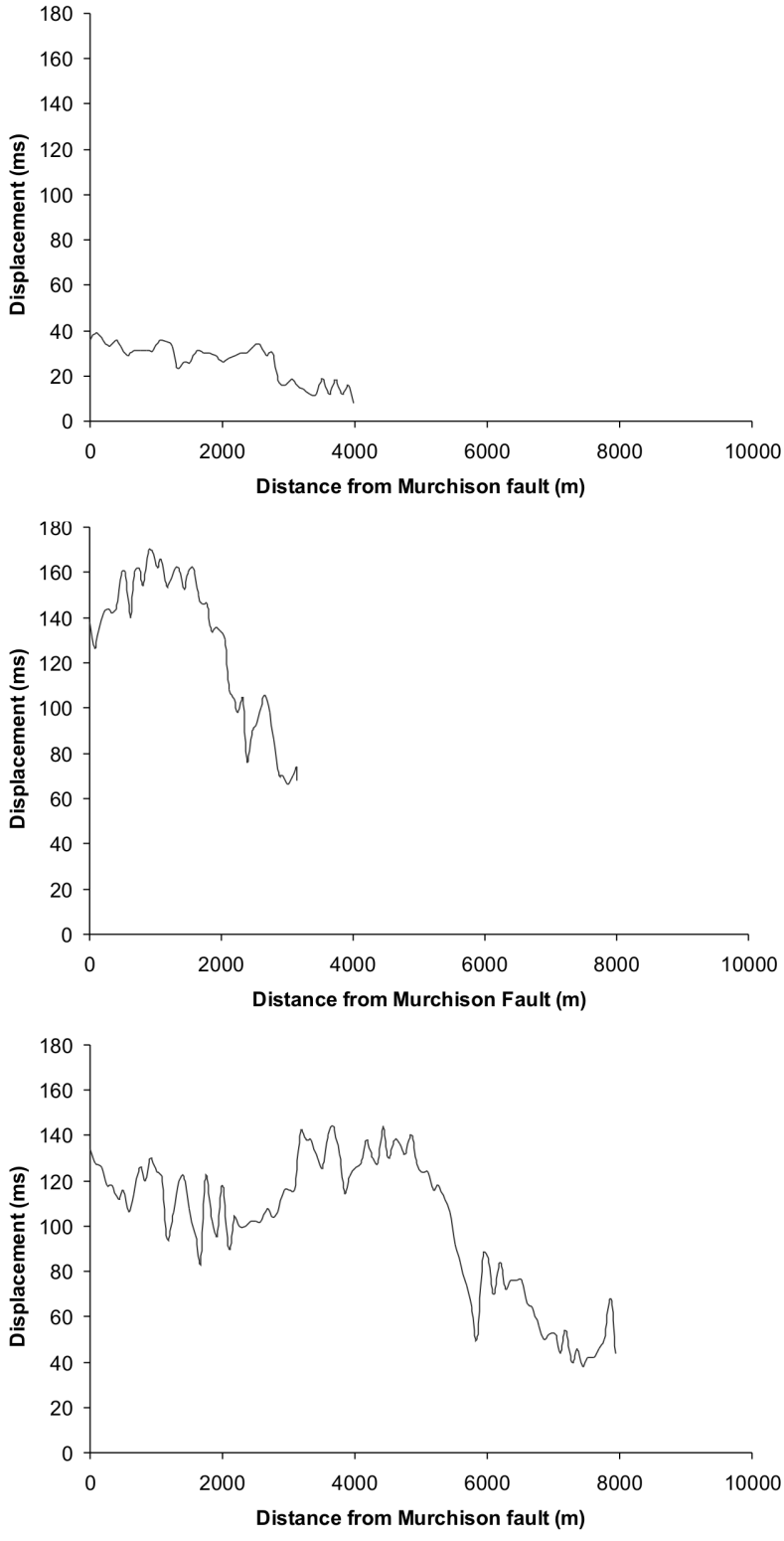

Figure 5.5
Displacement-length profiles for one abandoned tip (FF6 - top) and two footwall release faults perpendicular to the Murchison Fault, MSW (centre) and MNE (bottom). All show a decrease in displacement away from the main Murchison Fault.

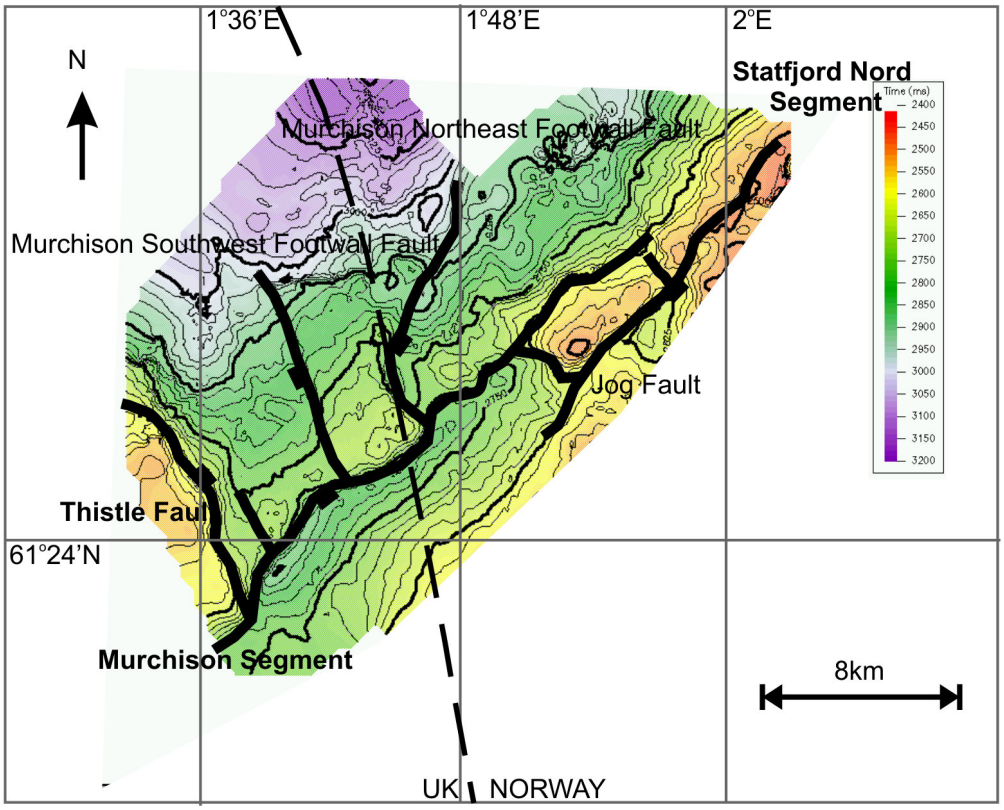

Figure 5.6A Two way time map to Base Cretaceous Unconformity in the Greater Murchison Area

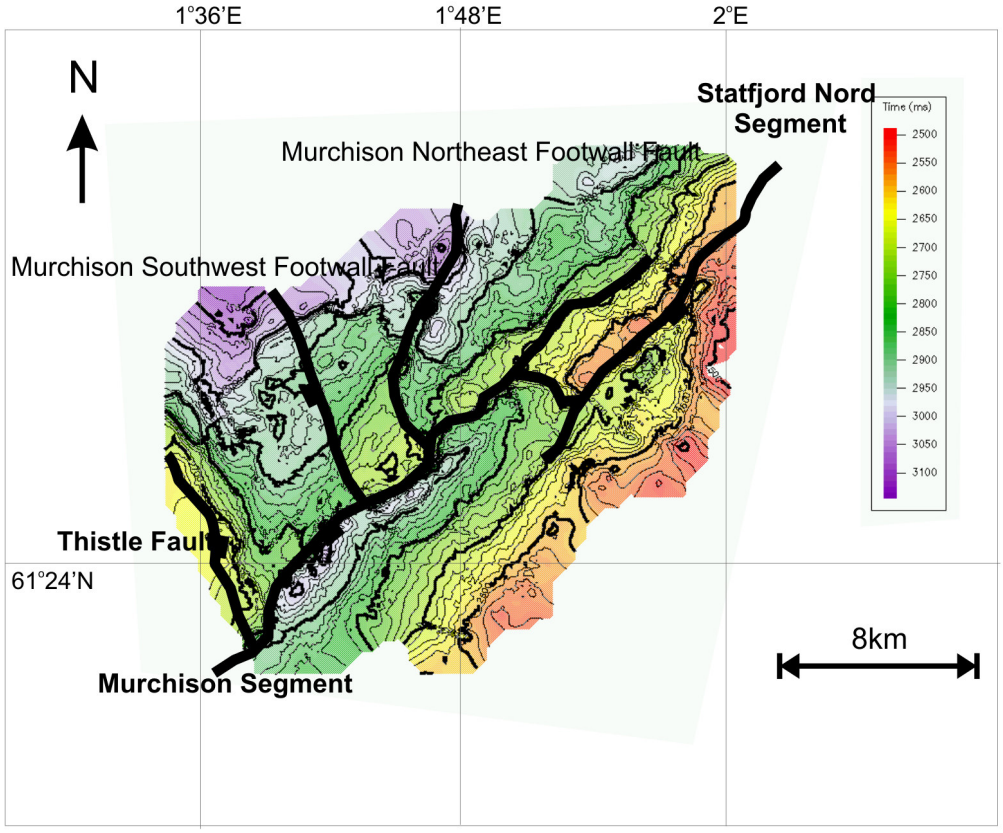

Figure 5.6B Two way time map to Top Brent (Top Prerift) in the Greater Murchison Area

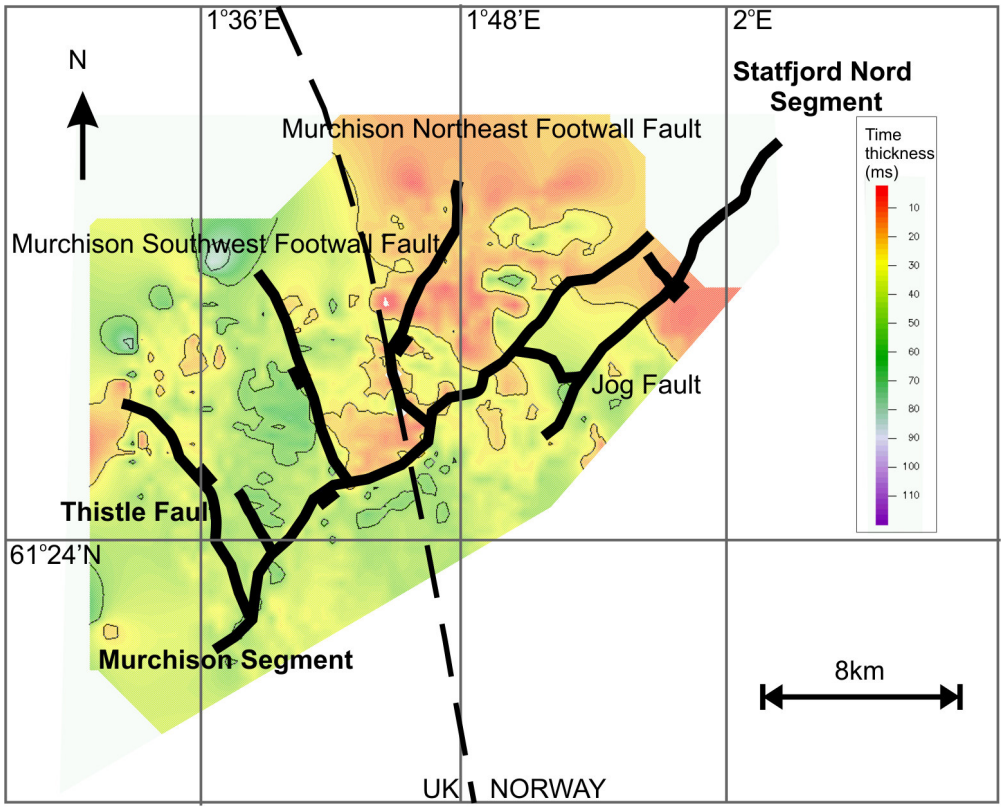

Figure 5.6C Isochron map of syn-rift unit 2

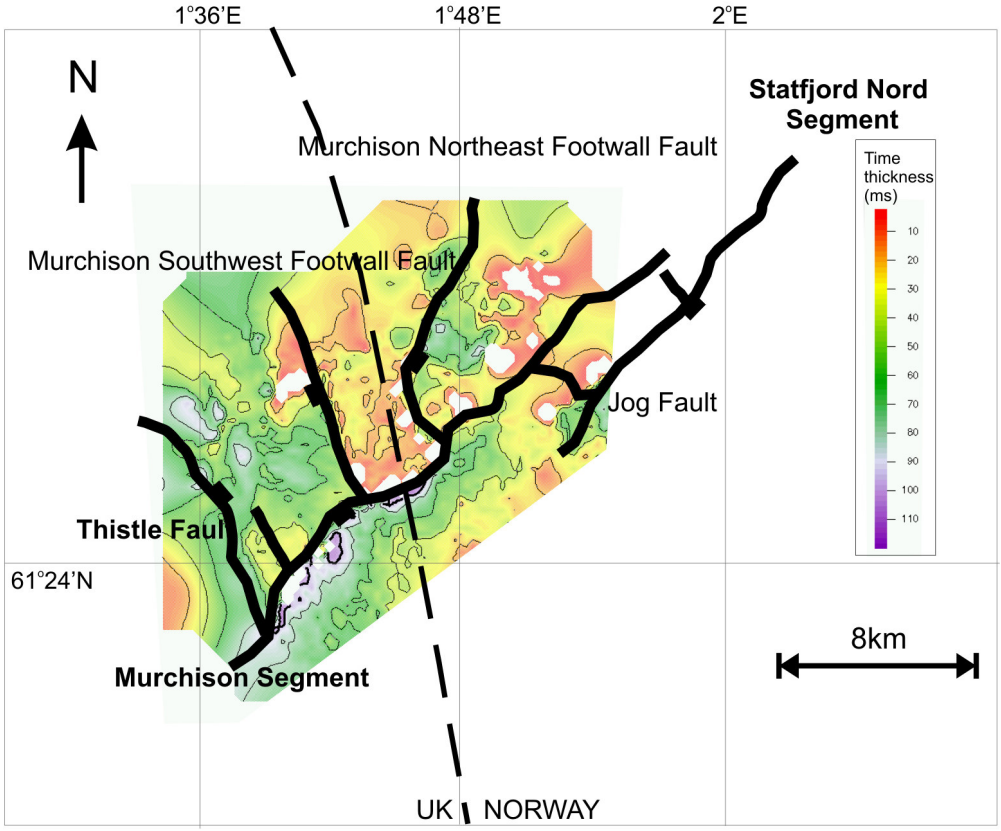

Figure 5.6D Isochron map of syn-rift unit 1

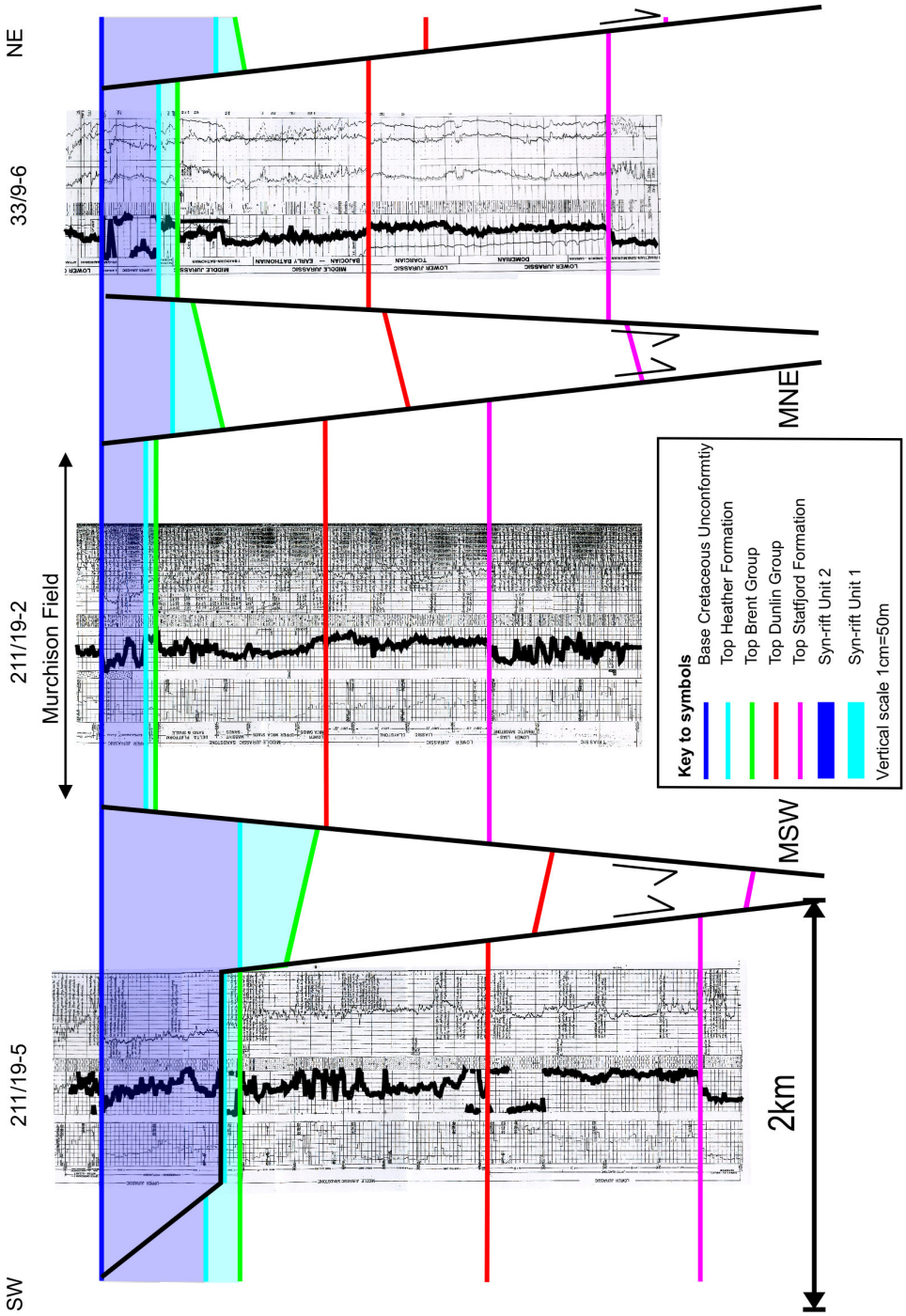

Figure 5.7
Well correlation across the Murchison Field showing thickening of syn-rift package 2 (Heather Formation) into the footwall release faults

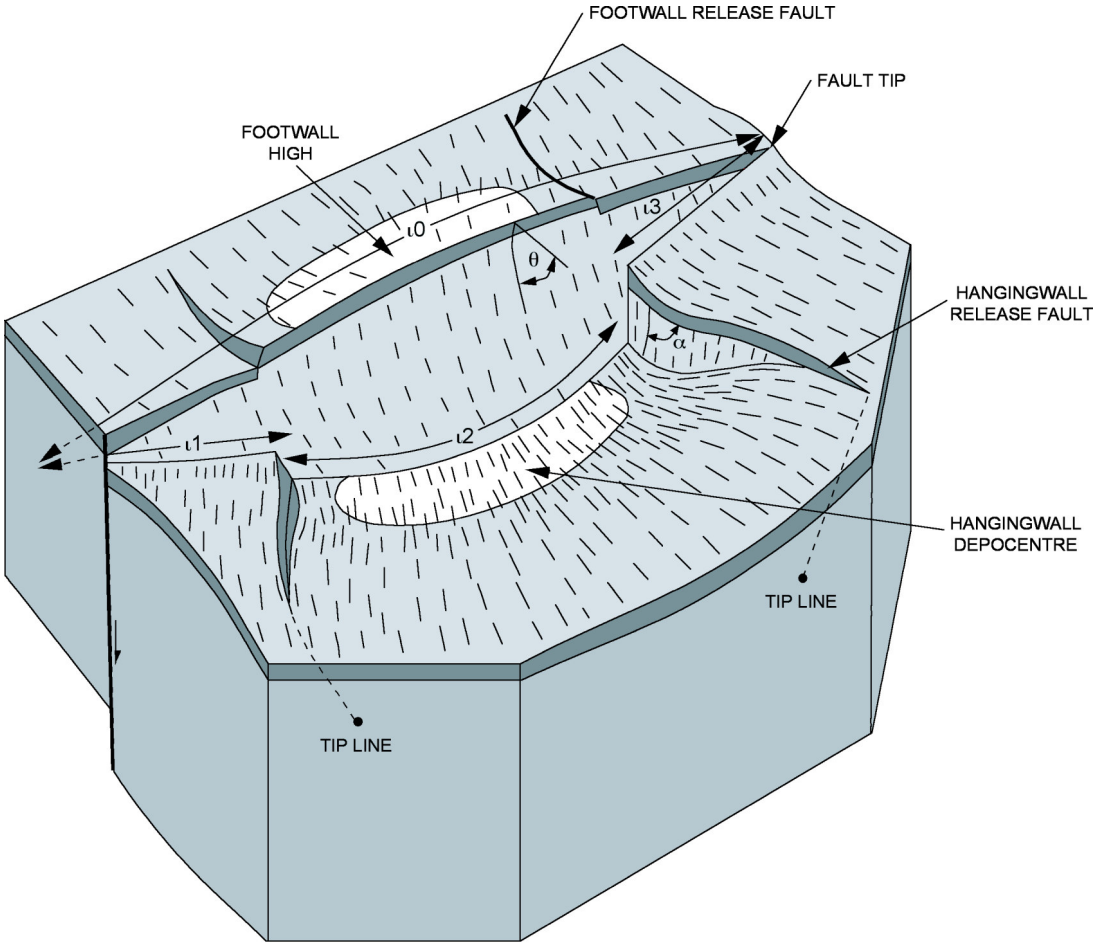

Figure 5.8
Block diagram showing the displacement variation along the strike of a normal fault. Release faults form in both the footwall and hangingwall as a direct result of displacement variations along the strike of the fault.
After Destro et al, 2003.

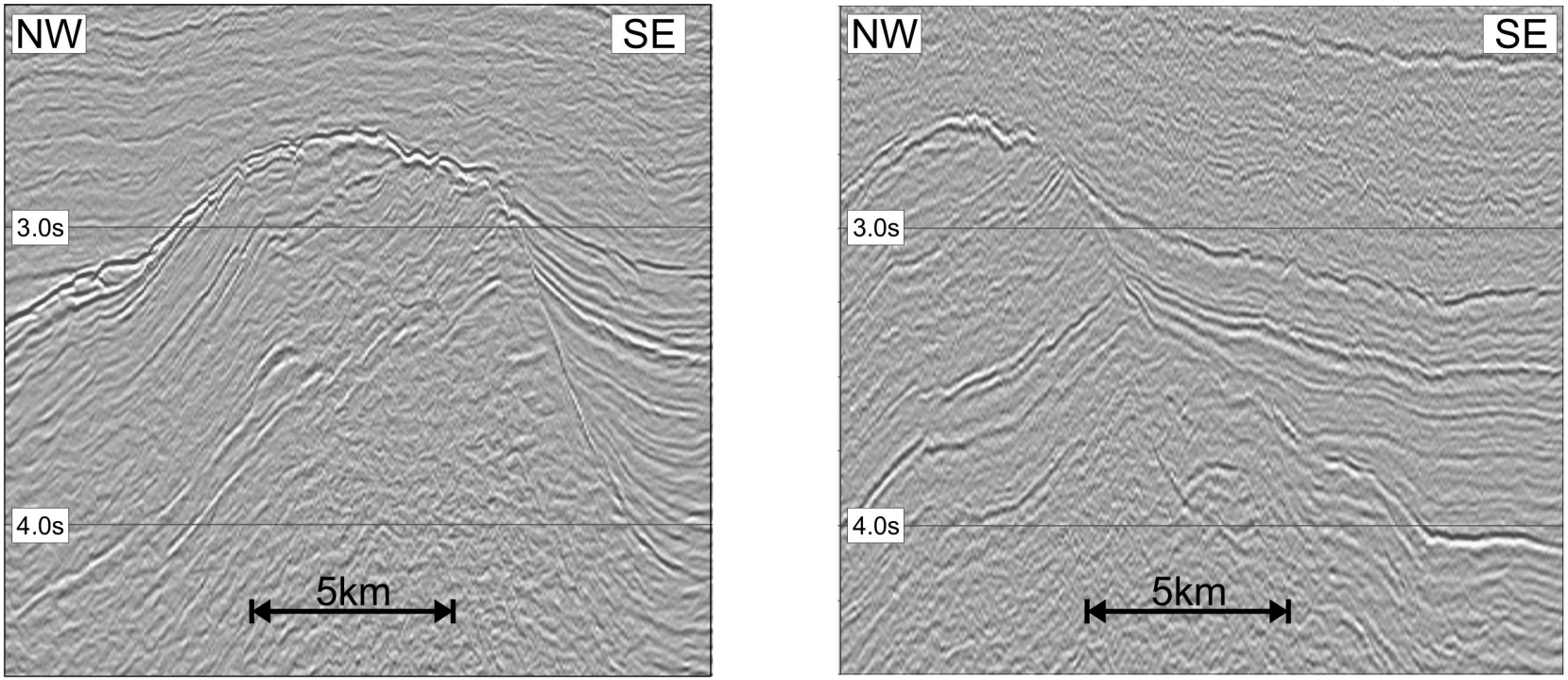

Figure 5.9
Two seismic lines over the Visund-Gullfaks Fault showing well-imaged fault plane

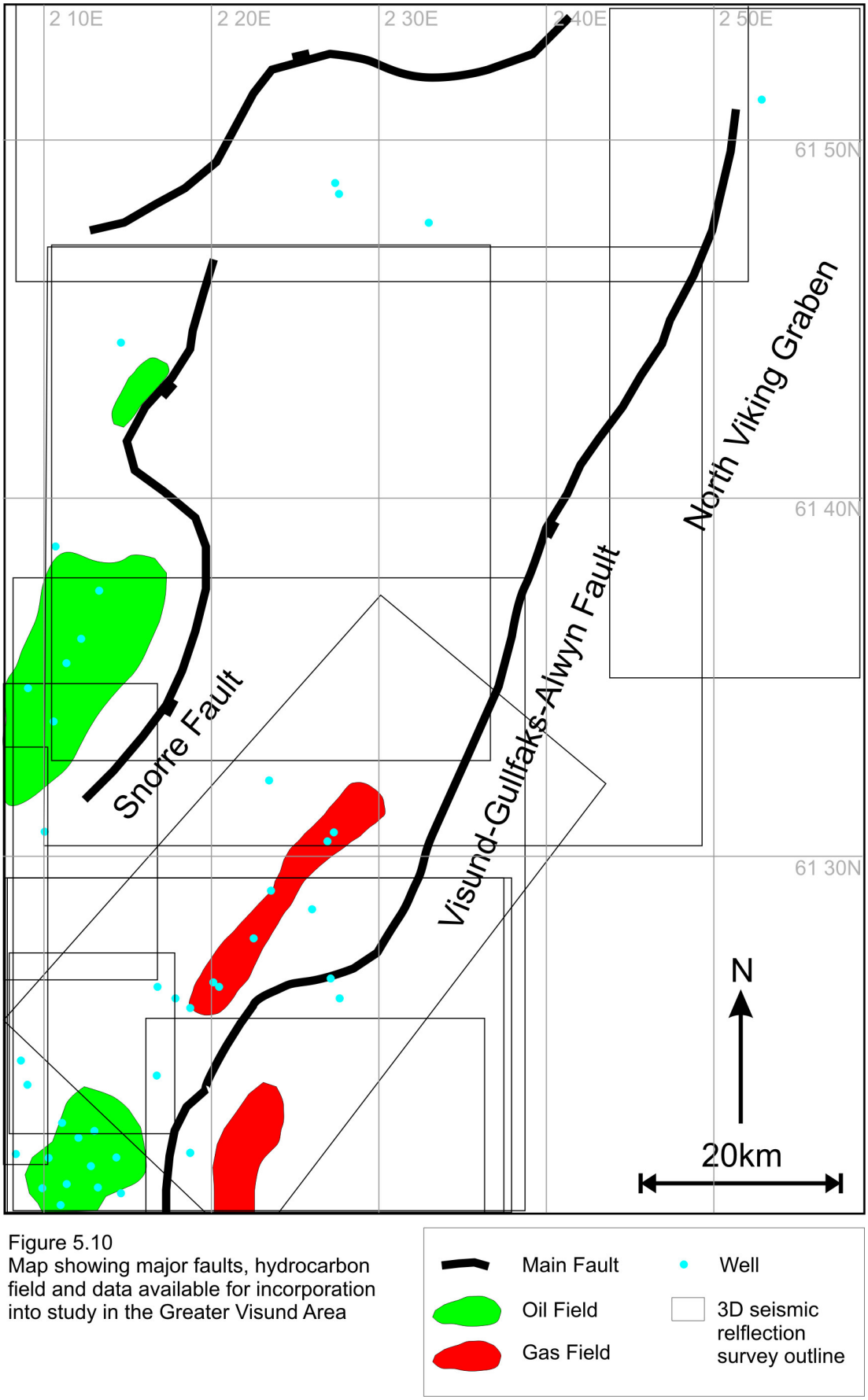

Figure 5.10
Map showing major faults, hydrocarbon field and data available for incorporation into study in the Greater Visund Area

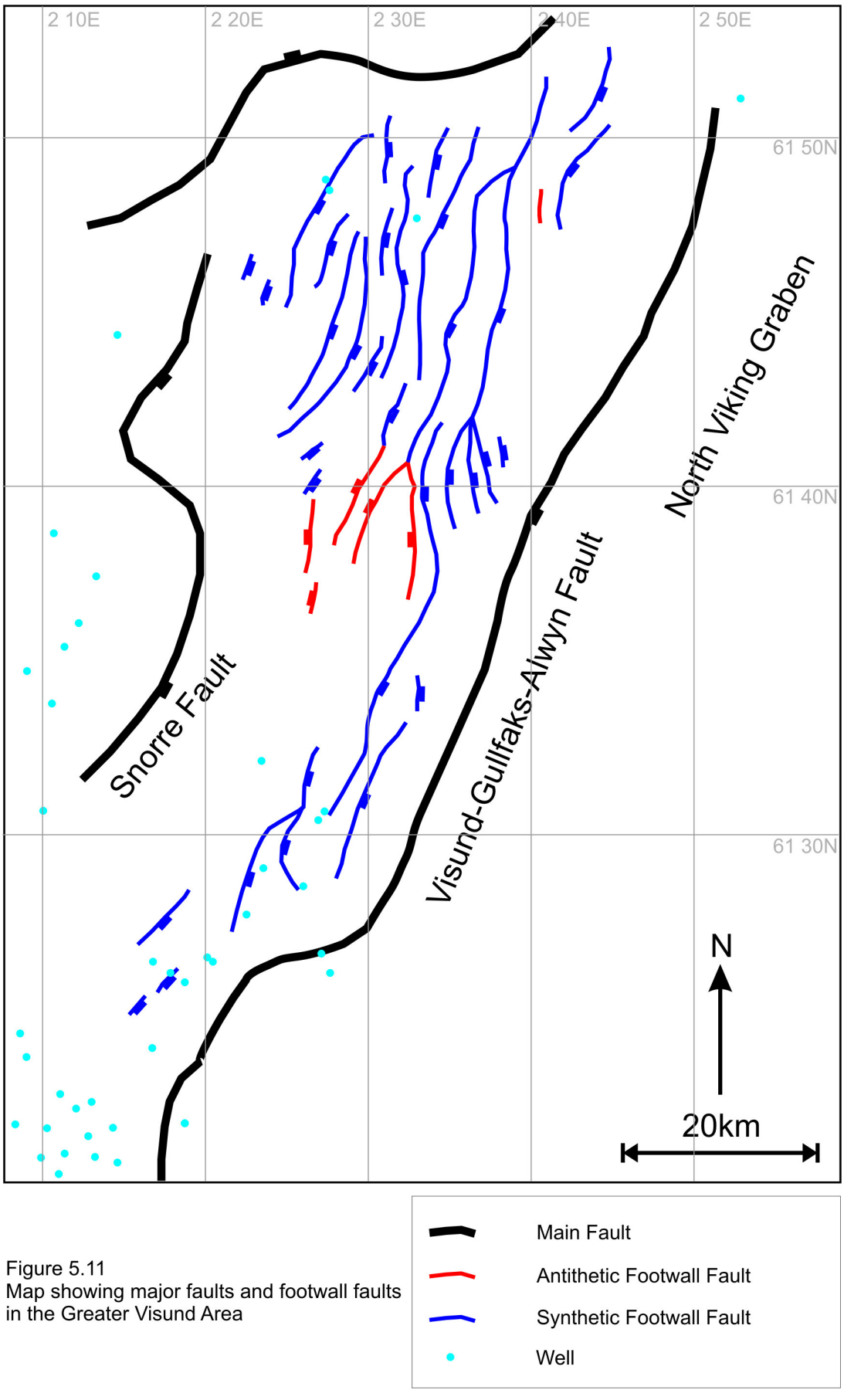

Figure 5.11
Map showing major faults and footwall faults in the Greater Visund Area

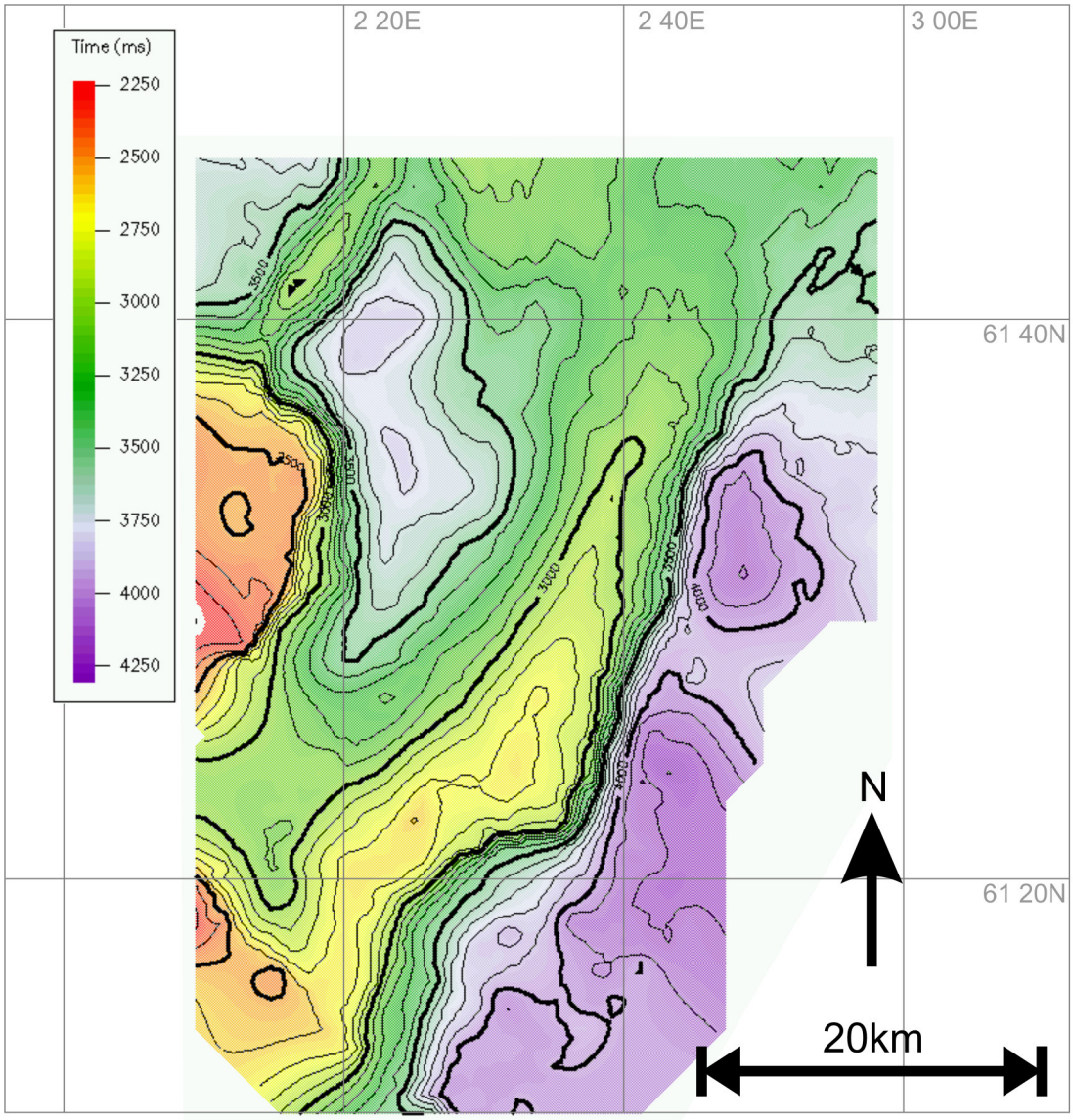

Figure 5.12
Two way time map to Base Cretaceous Unconformity in the Greater Visund area.

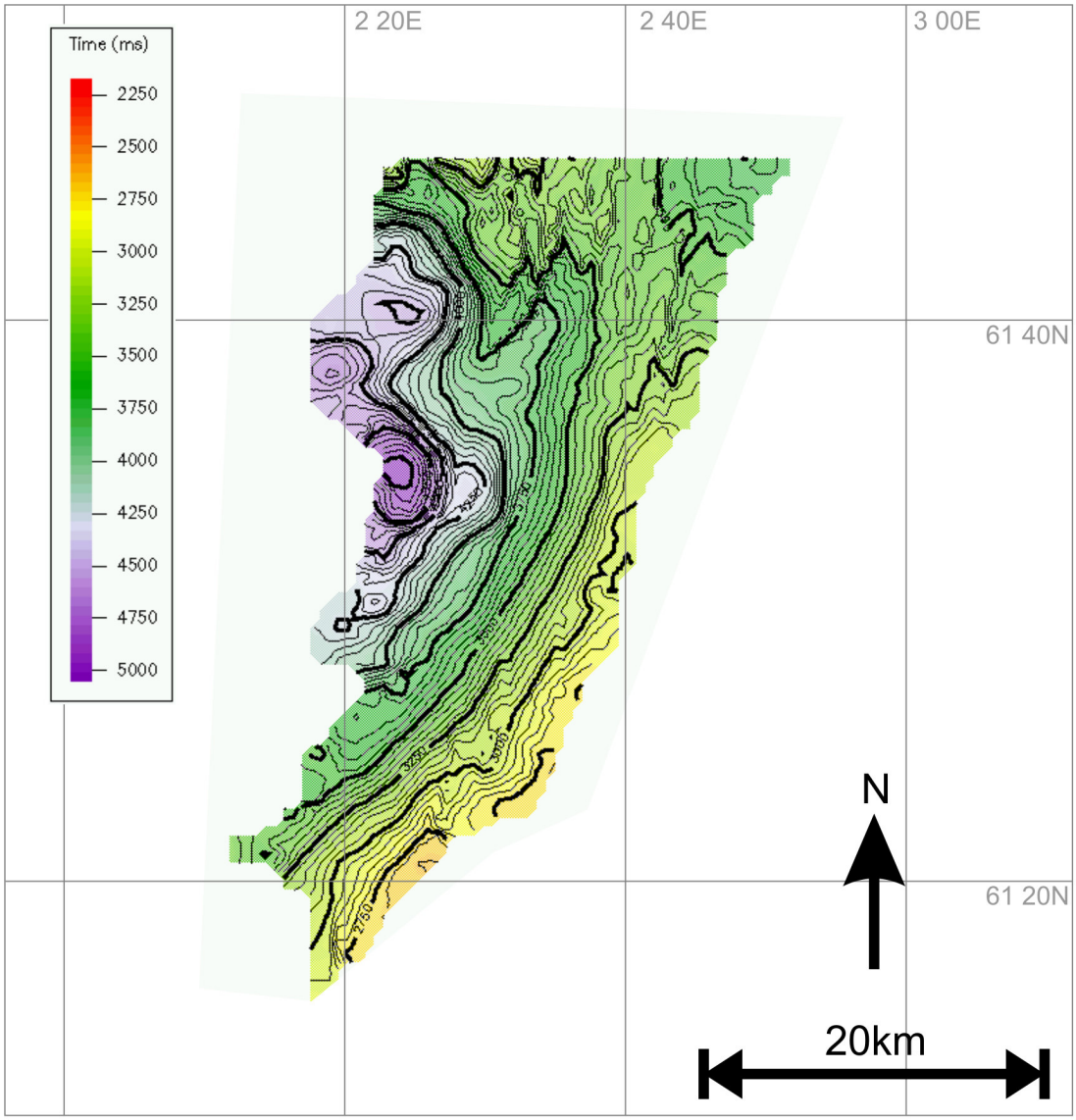

Figure 5.13
Two way time map to Top Statfjord Formation in the Greater Visund area.

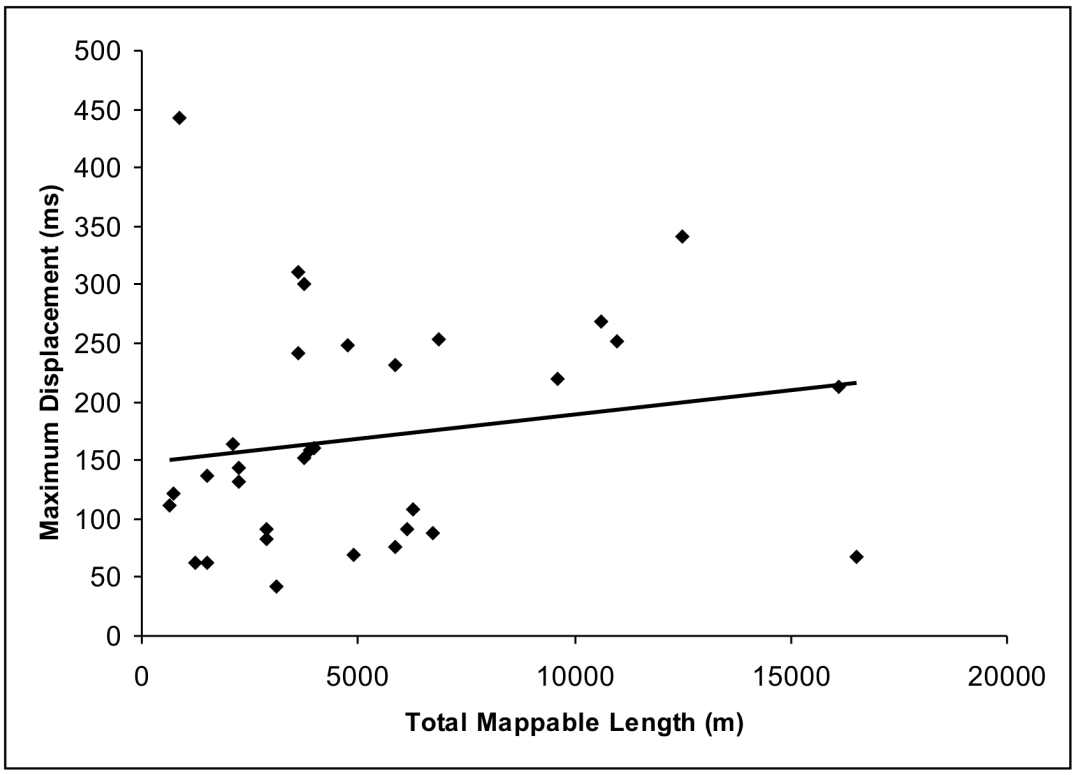

Figure 5.14
Graph showing positive correlation between displacement and length for strike-parallel faults in the immediate footwall to the Visund-Gullfaks Fault

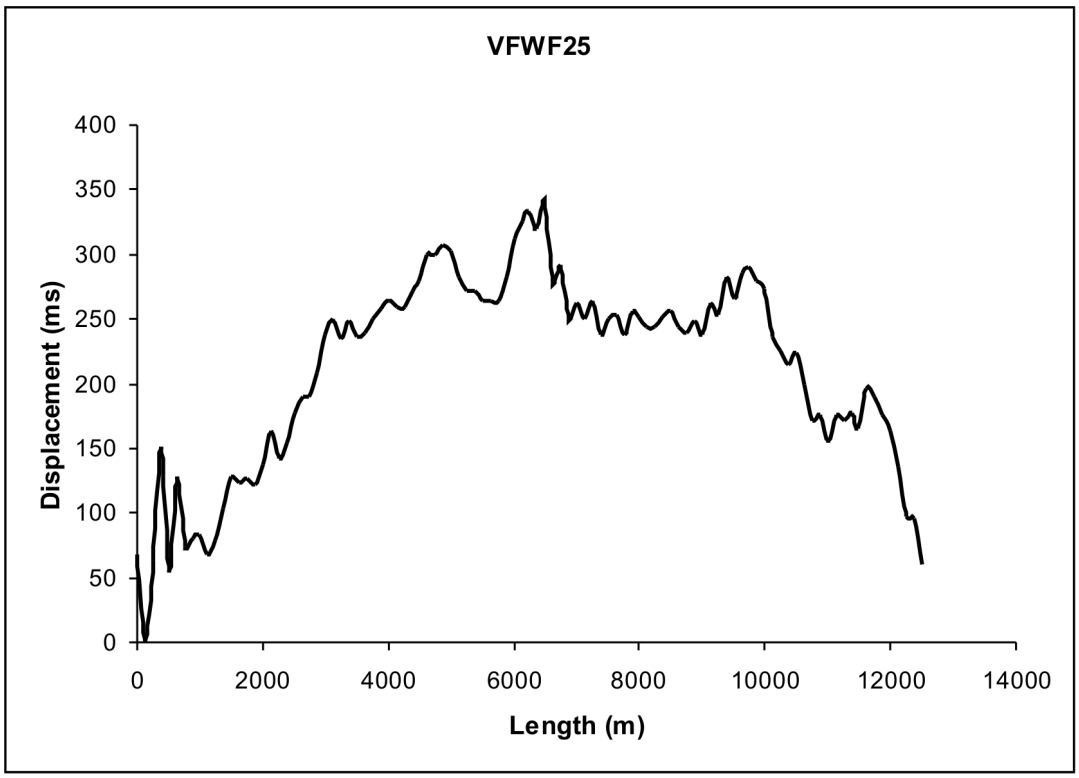

Figure 5.15
Displacement-length profile for Viisund Footwall Fault 25 showing characteristic 'bell-shaped' profile

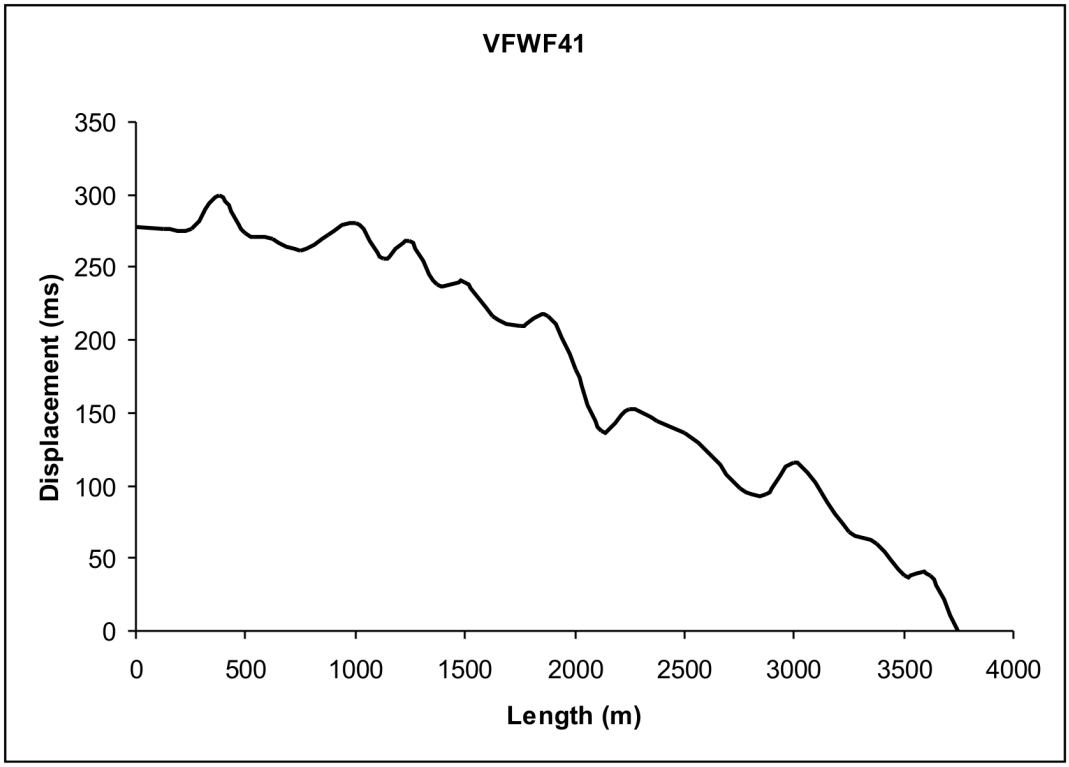

Figure 5.16
Displacement-length profile for Viisund Footwall Fault 41 showing incomplete 'bell-shaped' profile

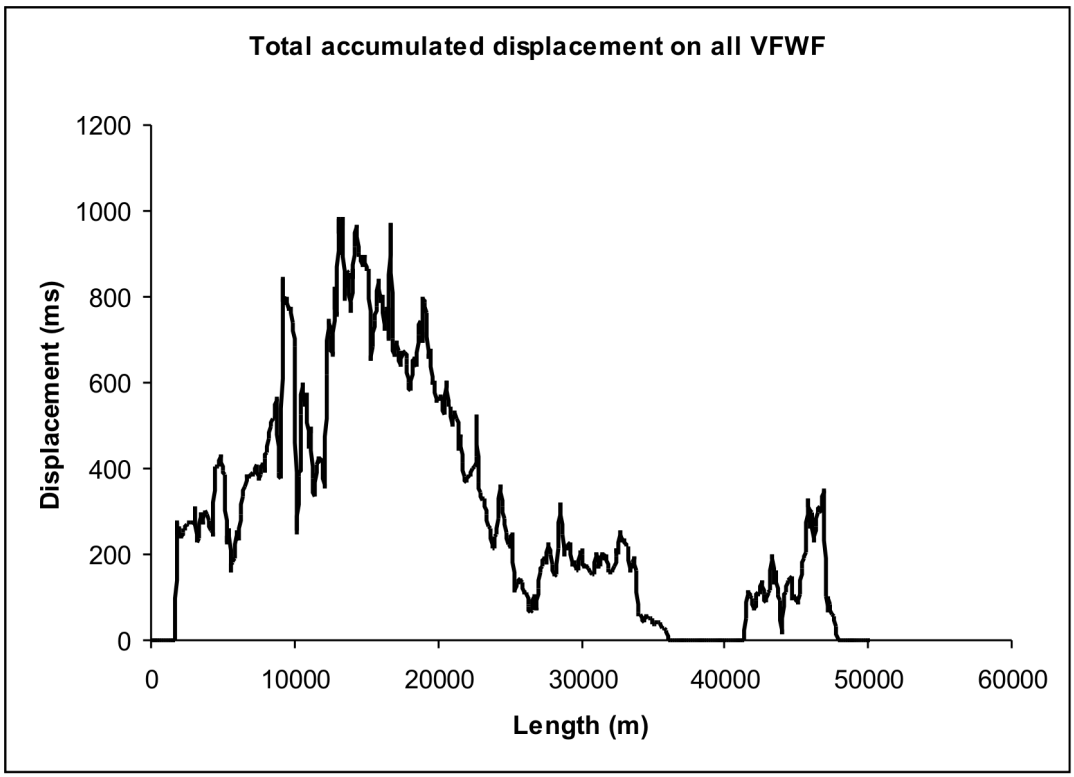

Figure 5.17
Graph showing total accumulated throw, across-strike of faults in the immediate footwall to the Visund-Gullfaks Fault

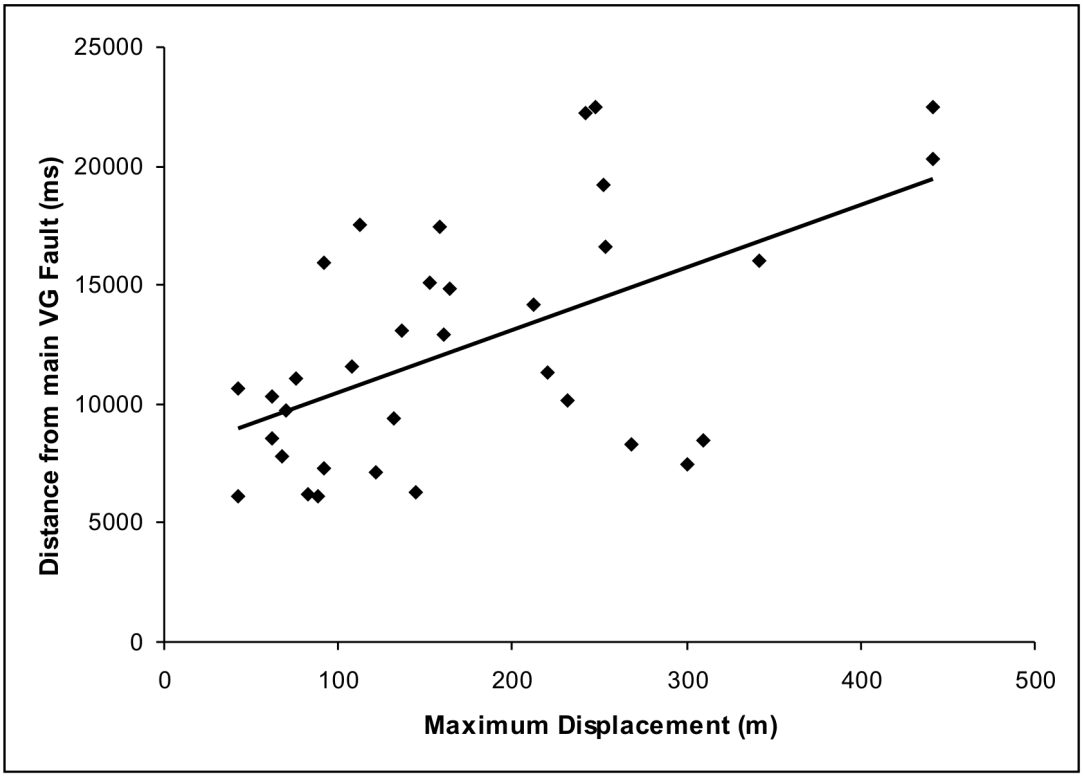

Figure 5.18
Graph showing positive correlation between maximum displacement on footwall faults and distance from the main Visund-Gullfaks Fault

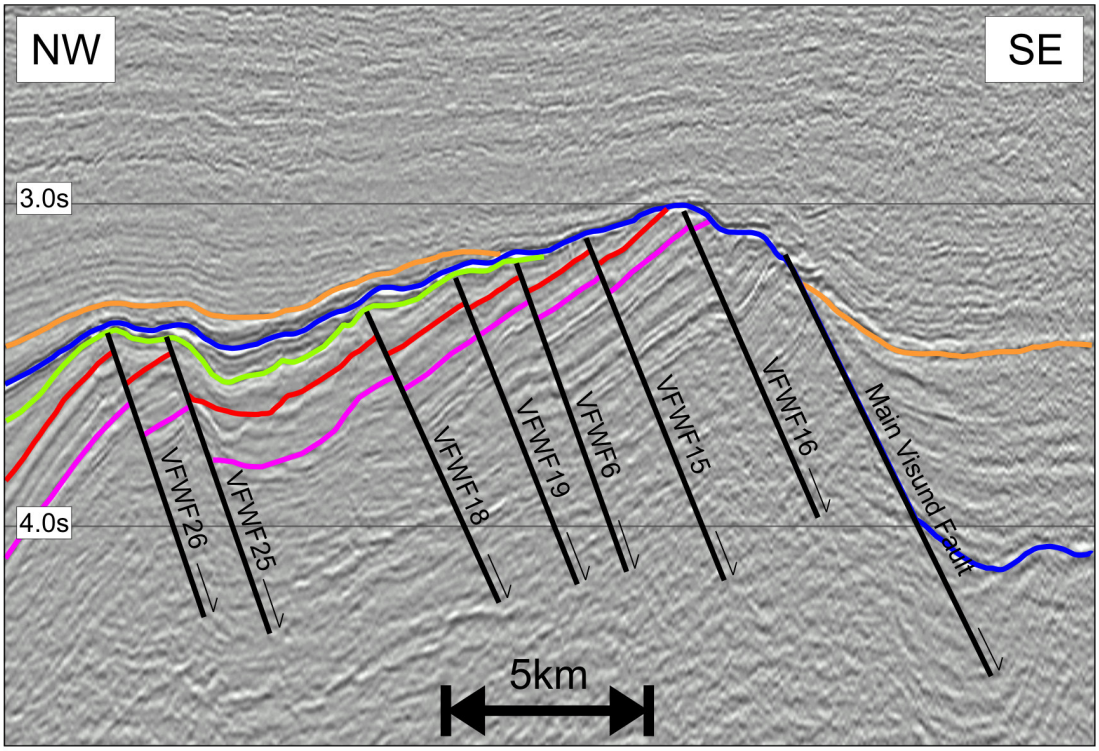

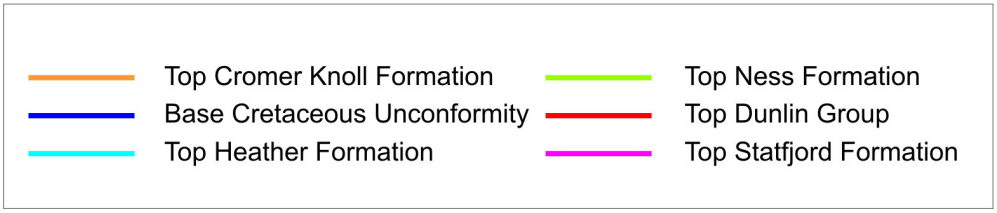

Figure 5.19
Seismic panel showing regular across-strike spacing of footwall faults associated with the main Visund-Gullfaks Fault
For location see figure 5.28

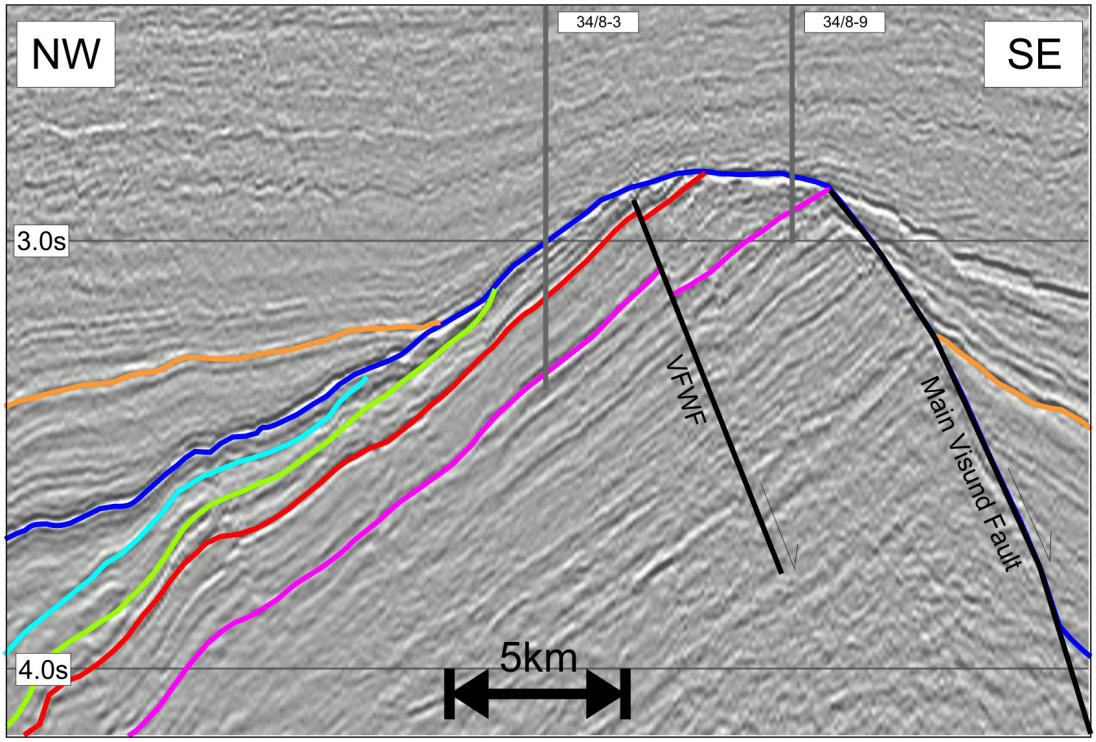

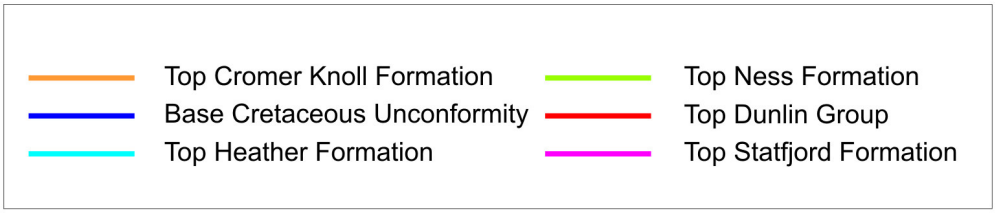

Figure 5.20
Seismic panel showing the southern section of the footwall of the Visund-Gullfaks Fault. This area is largely free of footwall faults.
For location see figure 5.28

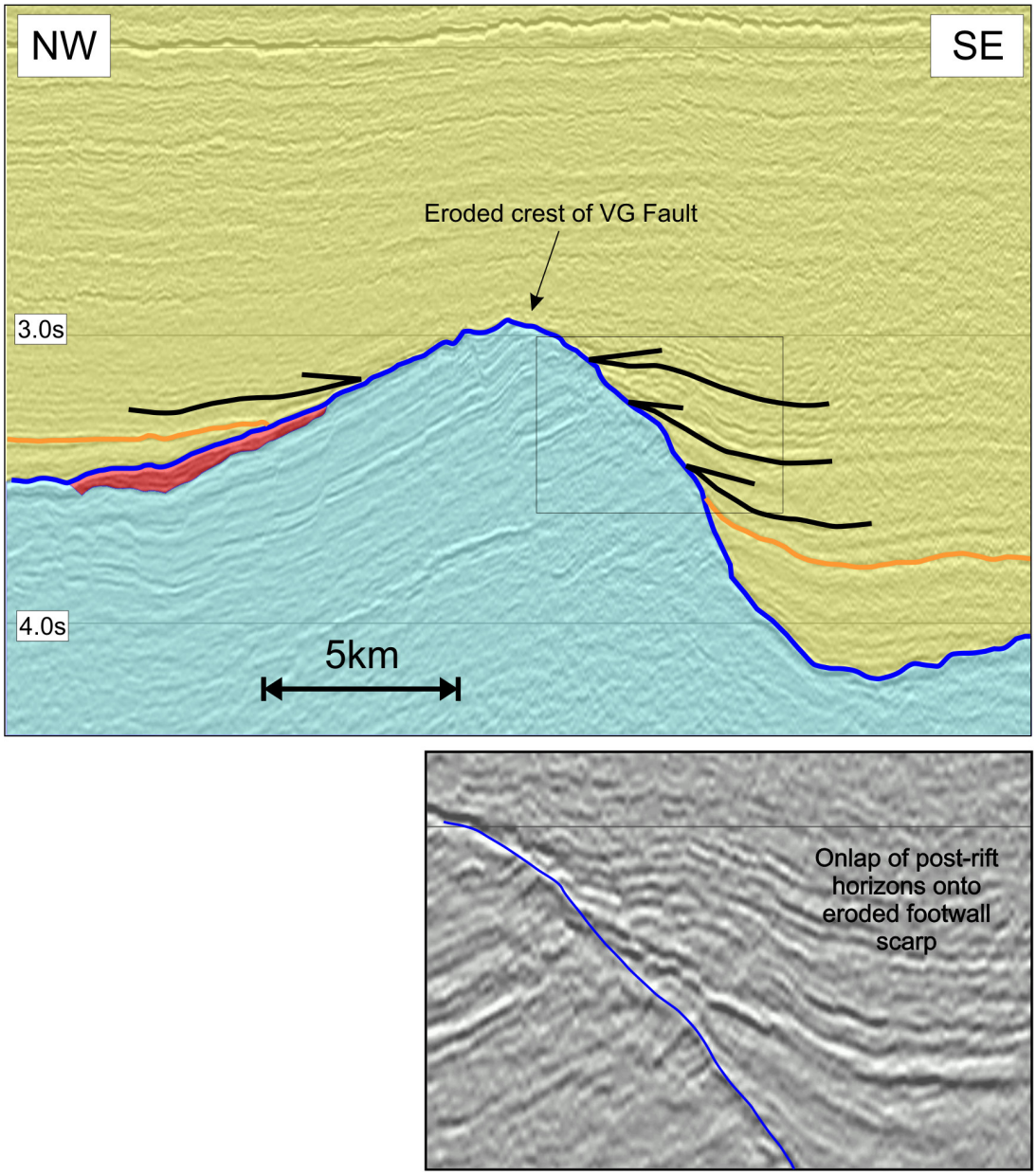

Figure 5.21
Seismic panel showing the eroded crest of the Visund-Gullfaks Fault footwall scarp as an onlap surface.
Post-rift reflectors onlap onto the scarp from both the east and the west.
For location see figure 5.28

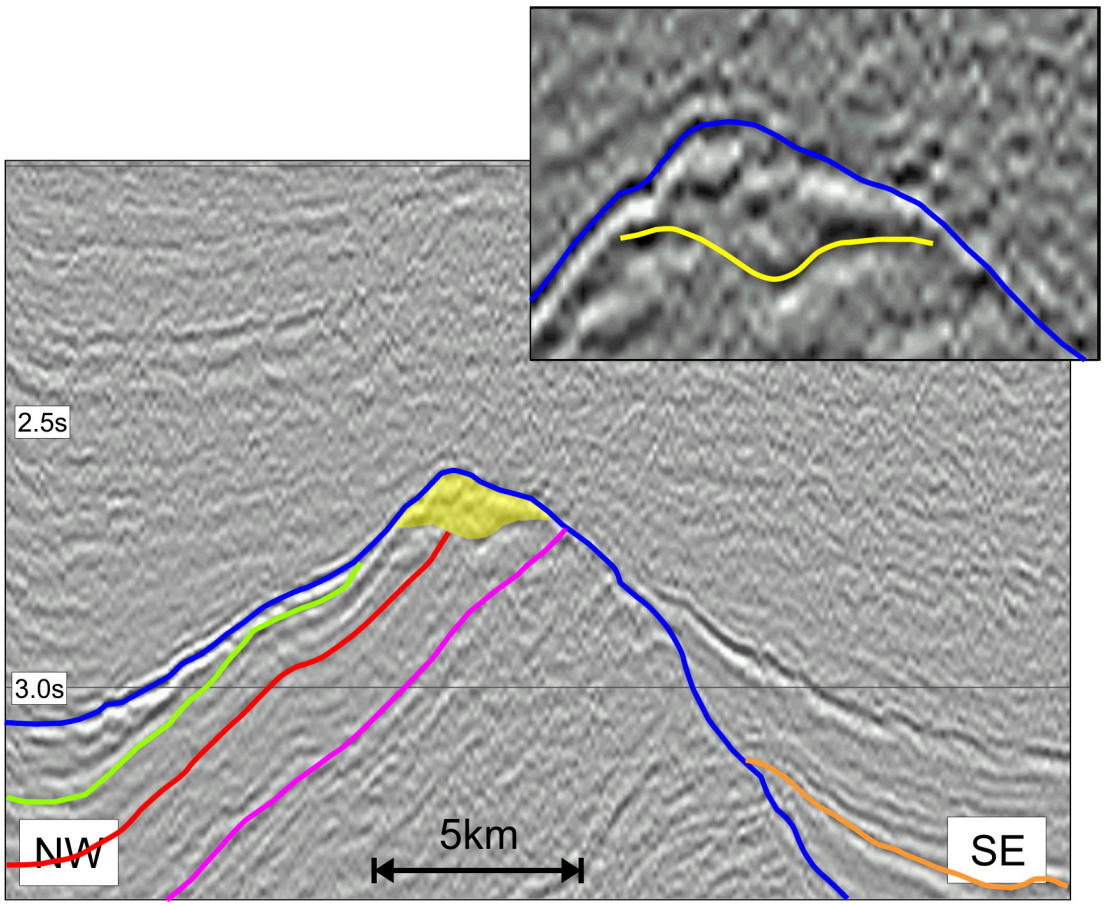

Figure 5.22
Seismic panel showing development of a fault scarp degradation complex on the crest of the Gullfaks Fault.
Inset shows transparent and where discernable, chaotic nature of internal reflectors
For location see figure 5.28

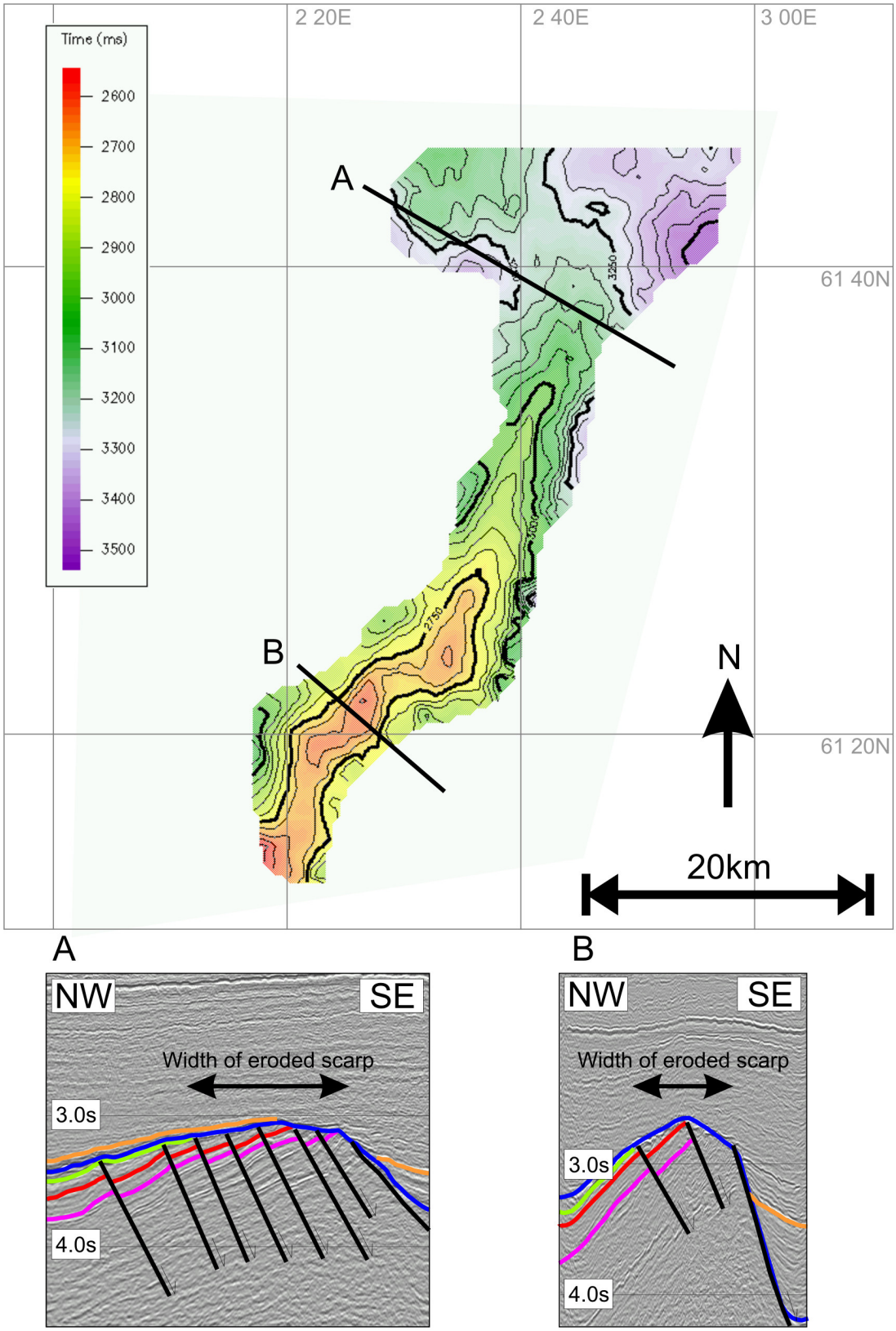

Figure 5.23
Two way time map showing the eroded area on the scarp to the Visund-Gullfaks Fault
Insets show contrasting width of eroded scarp along the length of the fault.
For key to seismic interpretation see figure 5.22

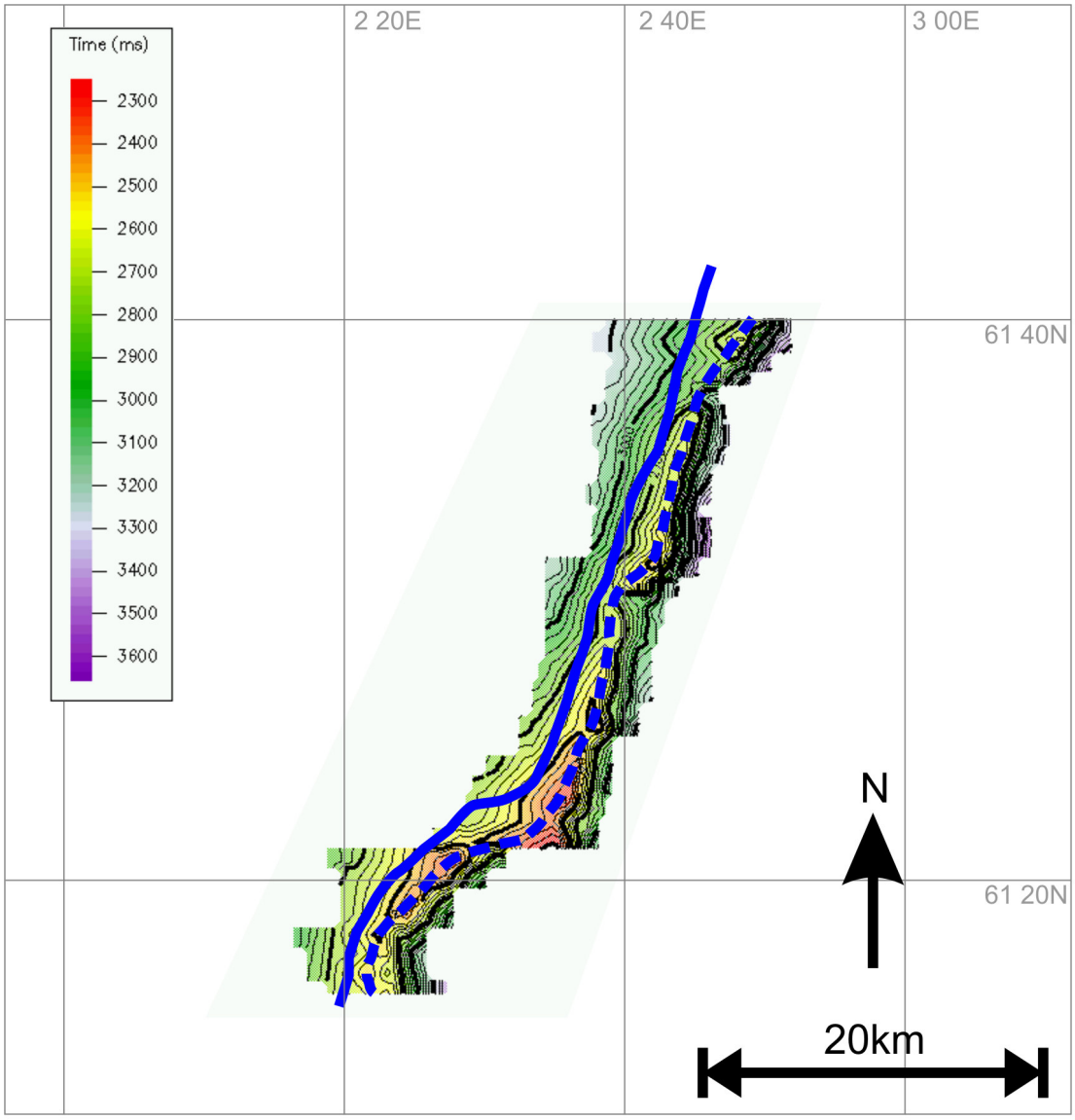

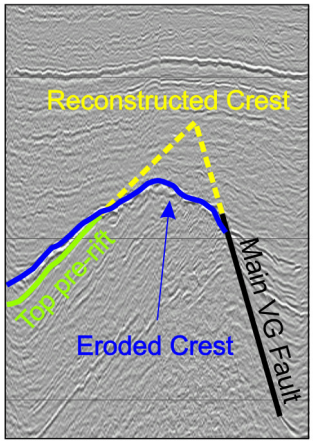

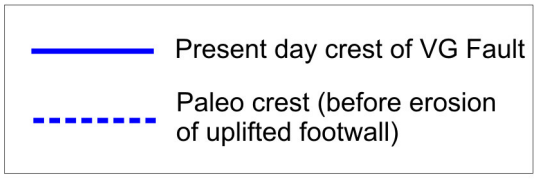

Figure 5.24
Two way time map showing reconstucted crest of Visund-Gullfaks Fault prior to erosion
Inset shows method of reconstruction

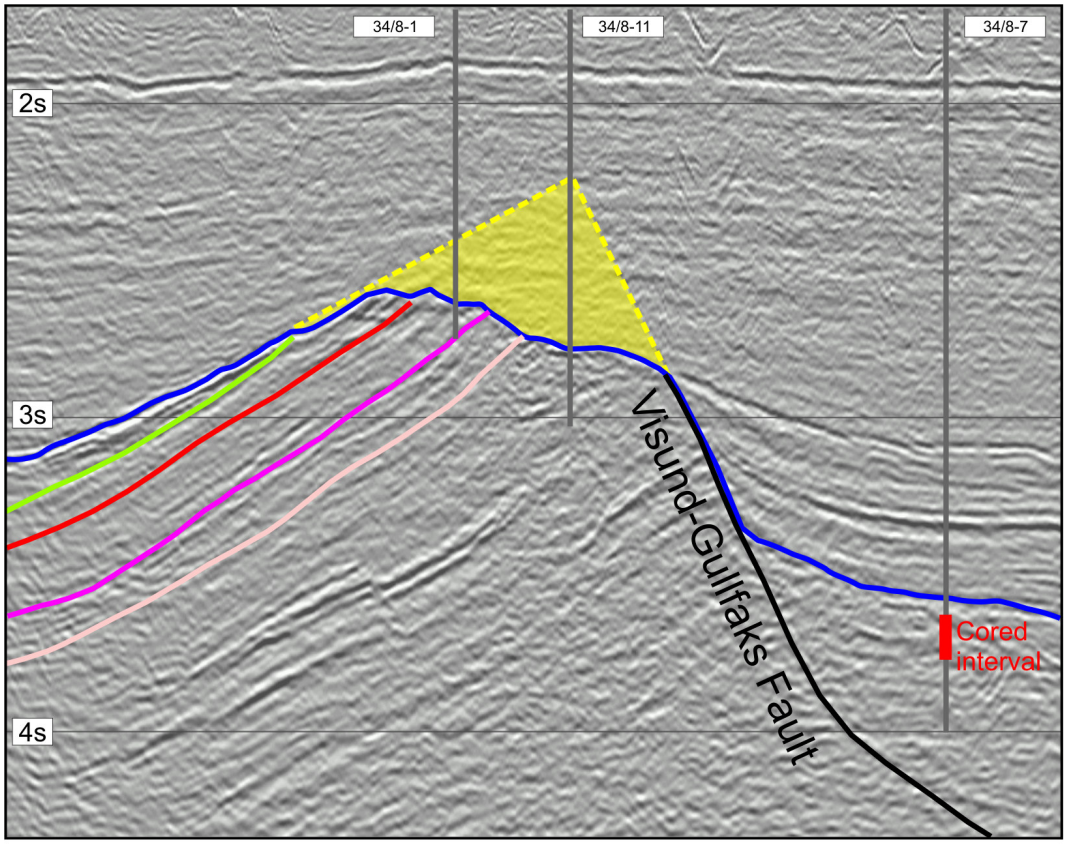

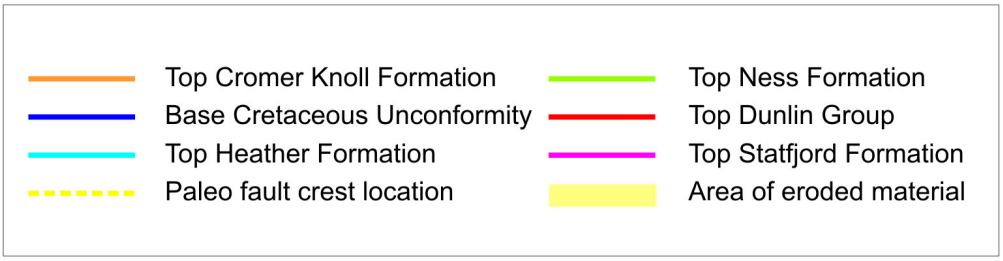

Figure 5.25
Seismic panel showing reconstructed crest of Visund-Gullfaks Fault and position of well containing cored interval.
For location see figure 5.28

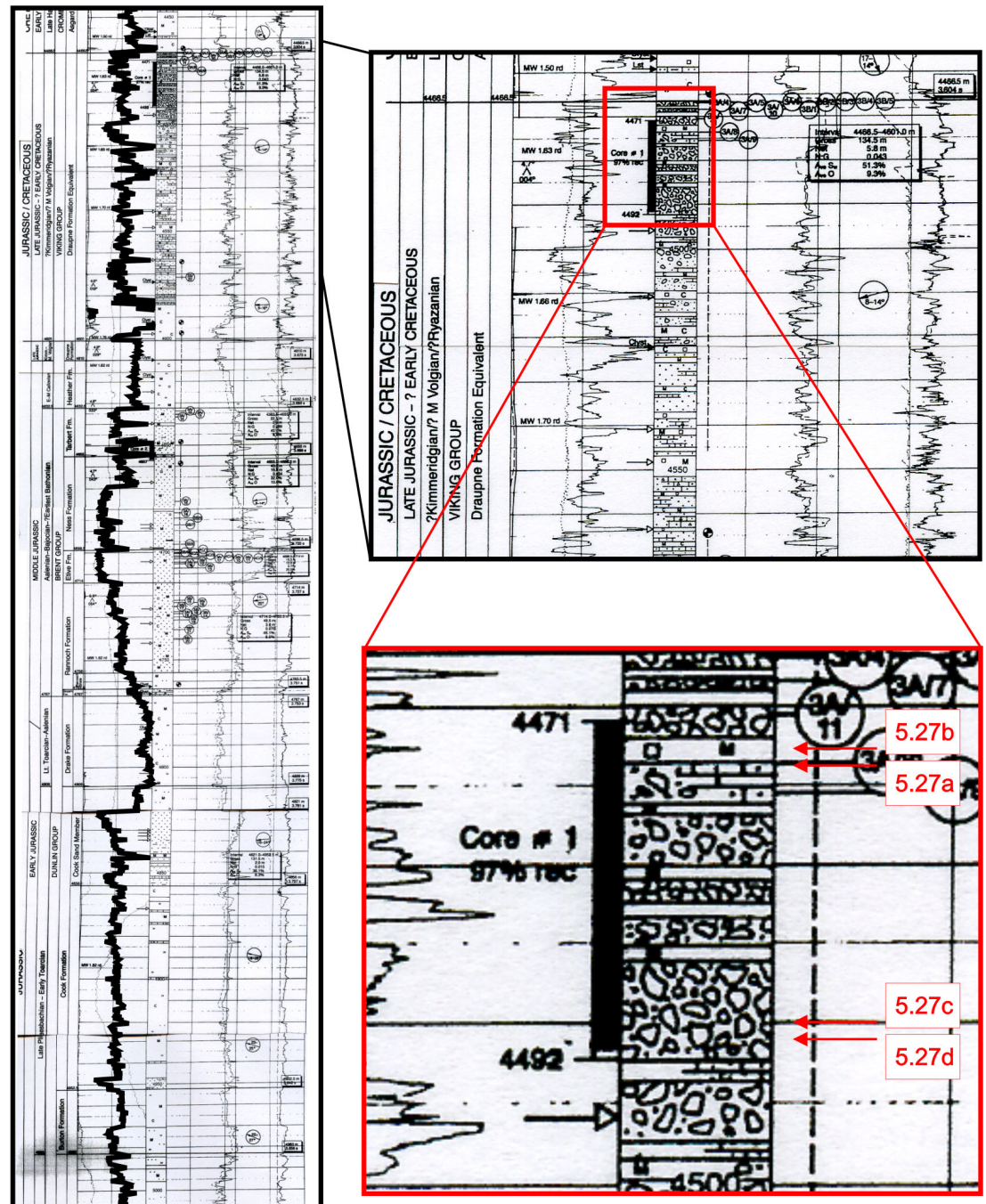

Figure 5.26
Well correlation log excerpt from exploration well 34/8-7 showing position of cored interval.
Insert shows location of core photographs shown in figures 5.27 a-d

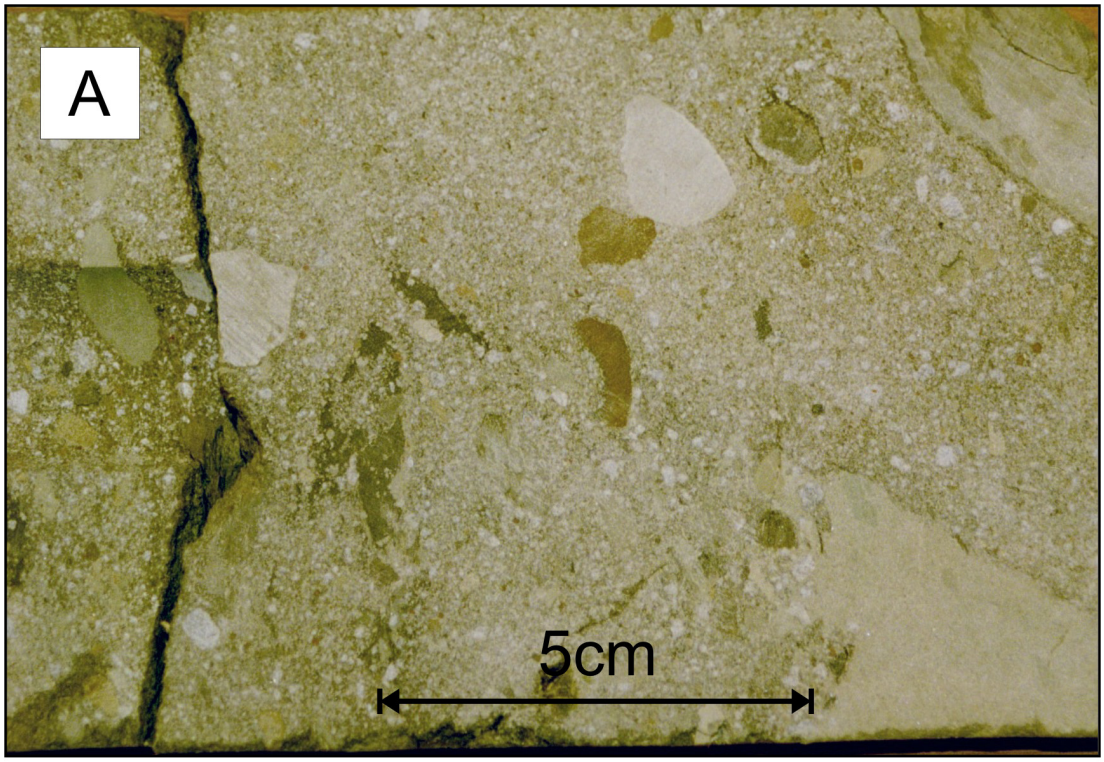

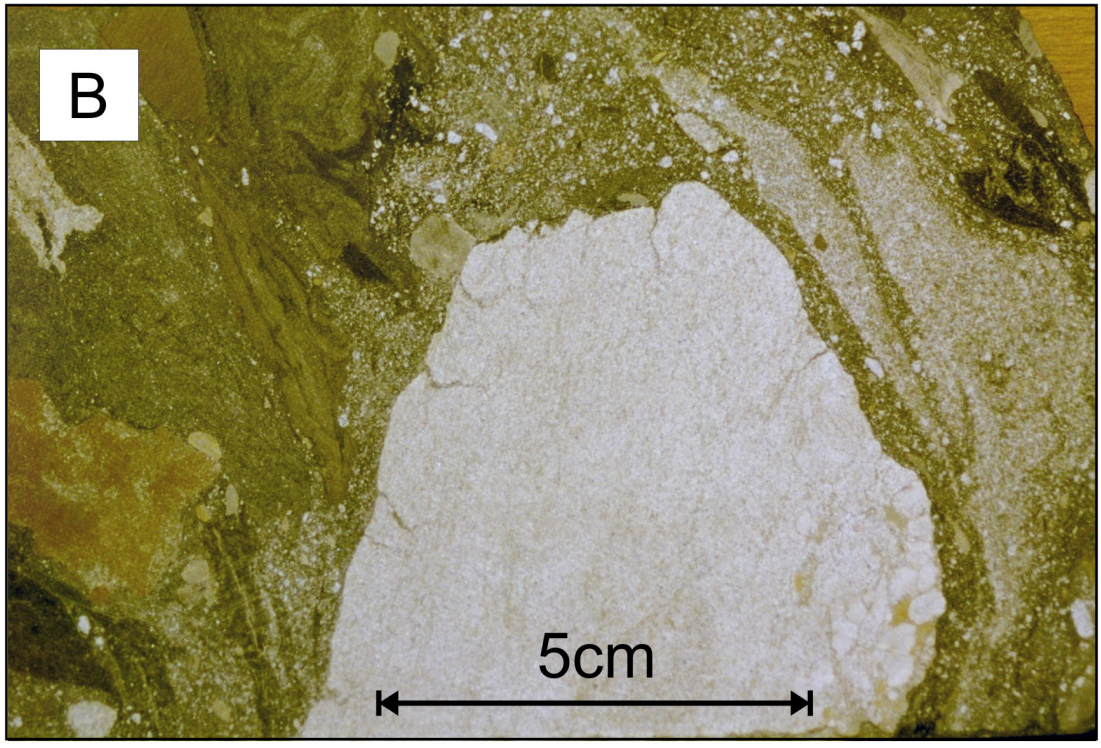

Figure 5.27
Core photographs showing conglomerate/breccia present in well 34/8-7.
For location see figure 5.26

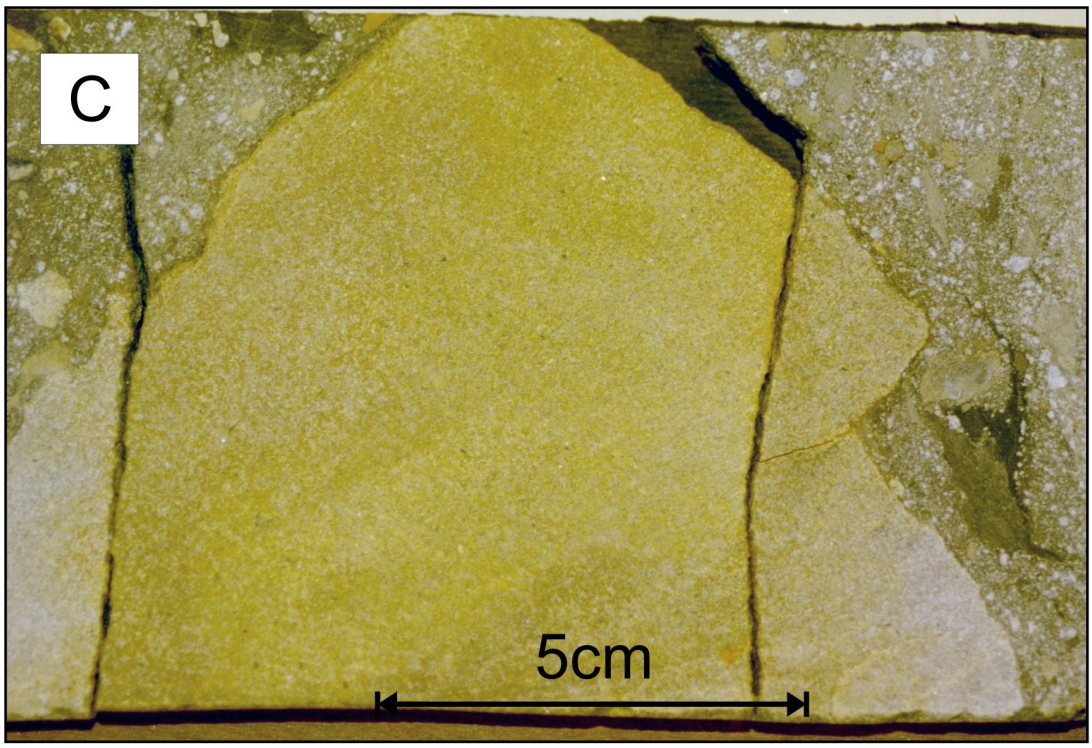

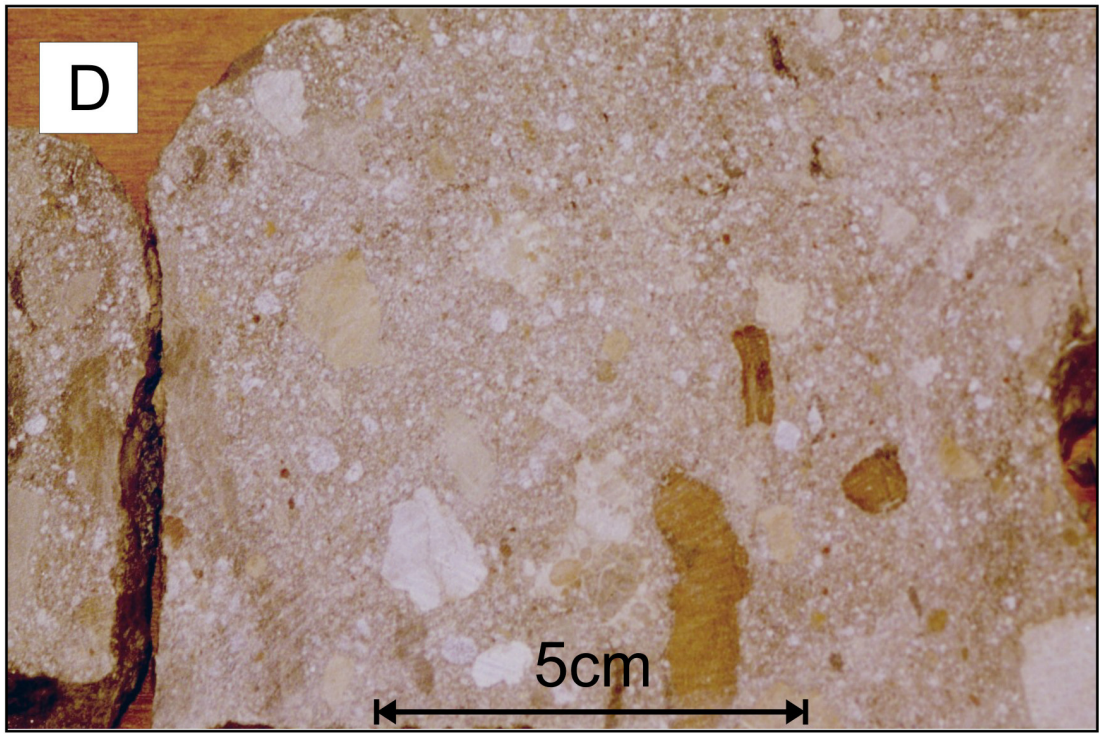

Figure 5.27 continued.
Core photographs showing conglomerate/breccia present in well 34/8-7.
For location see figure 5.26

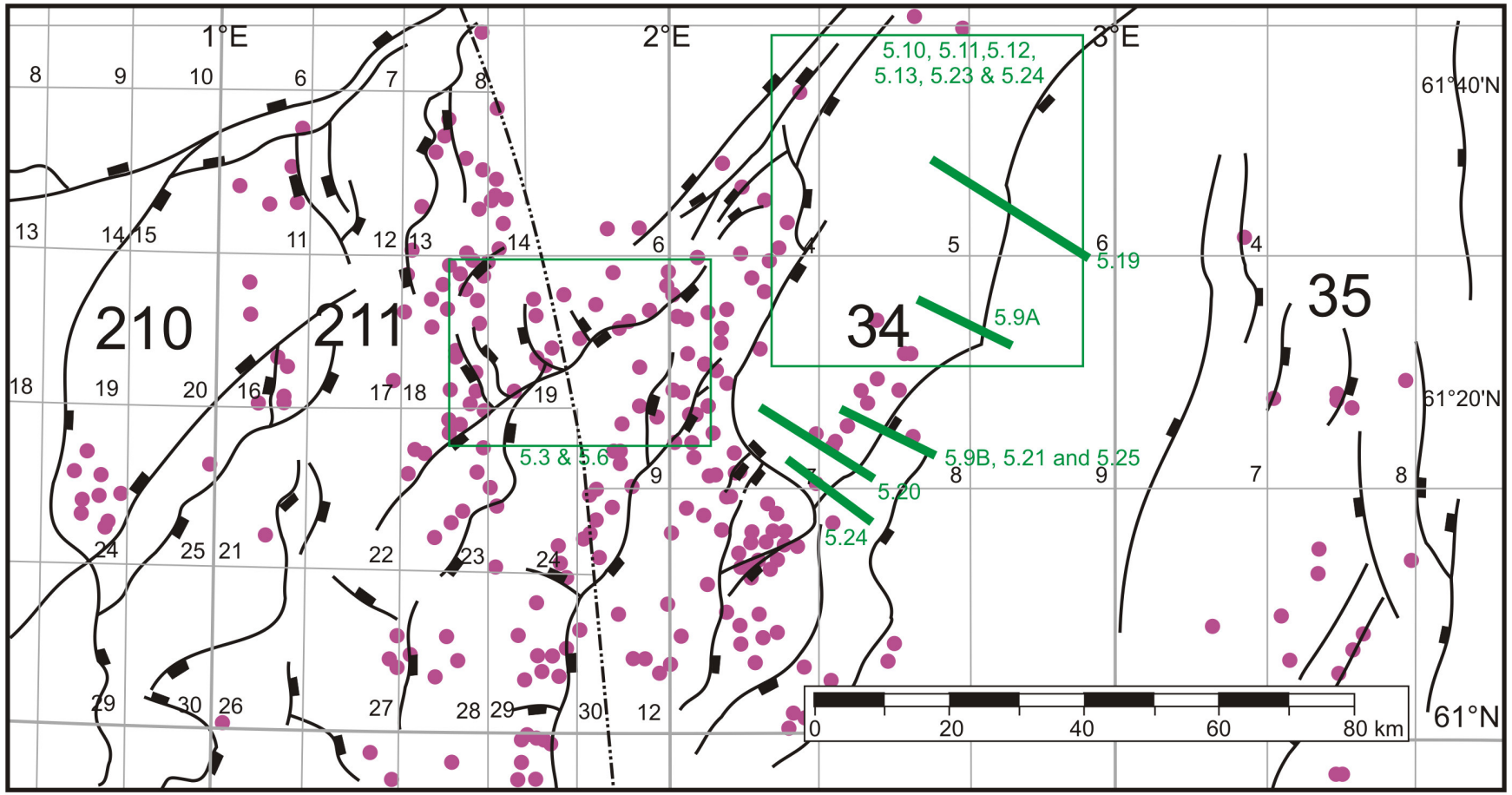

Figure 5.28
Map showing major faults and location of seismic lines and maps presented in chapter 5
Purple circles show positions of exploration, development and appraisal wells with logs available for incorporation into this study

6. Discussion and Conclusions

6.1 Introduction

This study has addressed two key issues relating to the evolution of rift provinces: firstly, the role of strain localisation in the development of a rift province and secondly, the diverse nature of footwall deformation resulting directly from normal fault growth and linkage. The aims of the study have been met through the integration of a large volume of subsurface data from the East Shetland Basin, Northern North Sea and with field data from the Gulf of Corinth in Greece. In particular, the study has presented a new and original interpretation for the distribution of strain in the Northern North Sea during the Mid to Late Jurassic rift episode.

This chapter will first consider a holistic model for the development of the Northern North Sea rift province. The model described aims to unify data presented in earlier chapters of this thesis in order to present a detailed interpretation of the temporal and spatial variability in the location and rate of strain accumulation during Mid to Late Jurassic rifting. Section 6.3 aims to apply the model of rift basin development to other rifts and considers the appropriateness of existing models which describe the generic evolution of rift provinces in the light of new interpretation. Section 6.4 will consider the implications of strain localisation and footwall deformation for hydrocarbon prospectivity in the Northern North Sea before consideration of the implications of this study for future work.

6.2 The role of strain localisation in the evolution of the Northern North Sea and other rift systems

The development and evolution of the Northern North Sea during the Mid to Late Jurassic rift event can be described using a holistic model which may be applicable to other rift systems. The model is subdivided into six stages documenting the temporal and spatial evolution of the rift province and partitioning of strain within the evolving basin (figure 6.1).

1. The onset of extension in the Northern North Sea rift province occurred c. 167Ma. It is characterised by the nucleation and initiation of activity on large numbers of isolated fault segments which grow by radial tip propagation. The segments are short and have small displacements. The structures have no preferred dip directions and

are orientated sub-perpendicular to the maximum extension direction. Isolated depocentres develop next to these bilaterally propagating segments in which syn-rift stratigraphy shows expansion into the active faults. The majority of these small structures became inactive within the first 10-15My of rifting.

2. The Bathonian (167-164Ma) is a composite stage in the development of the rift province when nucleation continues to occur alongside the onset of segment interaction and linkage. Segment linkage is thought to occur where faults are optimally located along-strike and adjacent to one another (Cowie, 1998). Where linkage occurs between adjacent along strike fault segments, the associated depocentres coalesce and form large depocentres which are initially underfilled. As linkage occurs the dominance of synthetic, inward-facing faults gradually becomes established over antithetic, outward-facing faults, resulting in cessation of activity on the smaller, less optimally placed antithetic structures. The dominance of the larger synthetic faults at the expense of the smaller antithetic faults can be explained by fault interaction at depth resulting in one fault becoming inactive at the expense of the other (Jackson, 1987; Scholz and Contreras, 1998). Faults have been shown to be preferentially enhanced if they dip towards the region of highest strain, i.e. those dipping towards the rift axis, (Hardacre and Cowie, 2003). This stage in the development of the rift province is recorded by the deposition of the lower part of the Heather Formation as syn-rift units which are predominantly present in discrete depocentres associated with medium length normal faults. As with stage 1, the syn-rift units show expansion into active normal faults.

3. During the Callovian and Lower Oxfordian (164-155 Ma) the rift basin underwent the dominant stage of fault segment interaction and subsequent linkage. There is a marked decrease in the nucleation rate of new faults. Fault segment hard linkage results in the formation of large coalesced depocentres which extend along the entire length of the now throughgoing normal faults. The formation of fully-linked fault arrays and their associated half-grabens occurs as strain is preferentially localised onto optimally positioned structures at the expense of other faults. At this stage, fault linkage results in many faults being underdisplaced for their length and having newly-formed underfilled hangingwall depocentres. Each of these newly-formed large fault systems has a single isolated hangingwall depocentre associated with it: these are the result of coalescence of remnant depocentres that formed associated with the earlier, shorter precursor fault segments. The upper part of the Heather Formation was deposited in these newly formed, coalesced depocentres. The linkage

to form long throughgoing fault systems results in more uniform subsidence along the strike of the normal faults. The formation of large, throughgoing normal fault systems and the distribution of slip from zero at the fault tips to a maximum at the centre of the fault strand may result in the formation of release faults both in the hangingwall and in the footwall. These short, small displacement structures form perpendicular to the main block-bounding faults and are often located at the position of former segment linkage where a large amount of displacement is accumulated following a linkage event. As a result of differential vertical displacements along the length of the fault, the deformation of the stratigraphy in both the footwall and hangingwall result in the formation of a suite of release faults. These are necessary in order to take up the extensional stresses in the plane parallel to the fault associated with the differential displacement.

4. The onset of basin-wide strain localisation during the Kimmeridgian (155 – 148 Ma) saw the previously distributed strain in the basin begin to focus towards the centre of the rift province. This process is recorded in the syn-rift sediments and fault morphology by the cessation of activity on those faults furthest away from the rift axis and a focussing of strain and subsequent increase in slip rates on more proximally located structures. An increase in slip rates may result in the uplifting footwalls to some normal faults being in relatively shallow water or becoming emergent above sea level. This may result in erosion by wave action and sub-aerial processes, removing the crest of the footwall and redepositing material elsewhere in the basin. Redeposition may occur in the shallow environment as beach and shelf deposits or material may be transported to deeper hangingwall depocentres. The denuded footwall may develop a fault scarp degradation complex mounted on its crest as a result of scarp erosion (Underhill et al., 1997; McLeod and Underhill, 1999) and the results of gravity-driven slope failure and shallow sediment flows (McLeod, 2000). The syn-rift sediments of the Lower Kimmeridge Clay Formation were deposited during this interval. This unit is draped over inactive faults, such as the Murchison Fault but thickens into the hangingwall depocentres of active faults such as the Snorre Fault.

5. Continued focussing of strain towards the rift axis results in the cessation of activity on all faults in the basin except the most proximal normal fault, i.e. the structure bounding the rift axis, the Visund-Gullfaks Fault during the Volgian (c.148Ma). More distal structures are abandoned and despite having linked to form full length fault arrays, never acquire enough slip to become a fully equilibrated fault system.

This disequilibrium is reflected in both the displacement-length profiles of the underdisplaced structures which preserve segment linkage points as displacement lows and also as topographical highs in their underfilled hangingwall depocentres. The syn-rift deposits of the Upper Kimmeridge Clay Formation associated with the distal suite of faults show a uniform thickness drape of sediment over both uplifted footwalls and hangingwall depocentres indicating inactivity for the duration of this period. This stage represents the climax of the rift event which is dominated by full focussing of strain onto a single throughgoing normal fault, bounding the rift axis. All other faults in the basin have become inactive and some are passively uplifted, rotated and eroded in the footwall to larger, more proximal structures. The rate of slip on this graben-bounding fault reaches its maximum in the rift climax stage and may become more than can be accommodated on a single fault strand. Where this occurs, strain may be taken up in a suite of faults present in the immediate footwall to the rift axis bounding fault. These structures are sub-parallel to the main fault and overlap each other along strike. The total accumulated across-strike displacement on these structures mirrors the displacement-length relationships of the main fault.

6. The rift climax is followed by the transition into the post-rift stage of basin evolution when slip rates diminish rapidly and active faulting eventually ceases in the Early Cretaceous. Early post-rift stratigraphy onlaps the structures resulting from the rift episode and any topographic lows, such as underfilled depocentres, are passively infilled. On a basin-wide scale accommodation space is generated by regional thermal subsidence. Some fault displacement is seen, however, but is interpreted to be the result of sediment compaction that preferentially affects the hangingwall syn-rift package (figure 6.2).

In summary, detailed interpretation of the syn-rift architecture associated with four major faults on a transect across the East Shetland Basin allows the development of a holistic model in which the evolution of the Northern North Sea Mid to Late Jurassic rift basin is considered. Initially, extension was characterised by a large number of small faults which grew by radial tip propagation and linkage. Strain was initially focussed onto a small number of throughgoing fault arrays at the expense of less optimally positioned structures. The rift episode culminated in complete regional localisation of strain when activity was primarily confined to a single thoroughgoing fault defining the western edge of the North Viking Graben.

The focussing of strain onto large, crustal-scale normal faults and then onto the rift axis is a phenomenon observed in other major rift provinces. The major half graben bounding faults in the East Shetland Basin grew by radial tip propagation and subsequent linkage of a hierarchy of paleosegments. This process of localisation of deformation from a distributed area onto individual through-going normal fault systems is also observed in the Gulf of Suez, Egypt. The Hamman Faraun fault population evolved from an initial stage where deformation was distributed across the fault block on several isolated to weakly linked fault segments, through a stage of fault segment linkage to a situation where deformation was localised on major fault block border faults (Gawthorpe et al., 2003). As observed in the Northern North Sea, the localisation of displacement onto the crustal-scale border faults bounding the Hamman Faraun fault block was associated with a reduction in the number of active faults due to the cessation of activity on many of the intra-block faults. A similar process is also seen in the Timor Sea (Meyer et al., 2002) and can be reproduced using numerical models (see section 6.3 below). The process of regional strain localisation onto the rift axis (such as is observed in the Northern North Sea) can also be seen in the Gulf of Corinth, Greece. The area to the south of the Gulf of Corinth comprises a sub-parallel array of normal faults. The basin has narrowed over time as fault controlled subsidence has migrated north. As a result segmented, linked normal faults have been progressively abandoned and passively rotated in the footwalls of younger faults and thick Pliocene lacrustine sequences and Quaternary terrestrial sediments have been rapidly uplifted above sea level in the footwalls to active normal faults (Gawthorpe et al., 1994).

Strain rate within the Northern North Sea rift basin during Mid to Late Jurassic extension was consistently very low ($< 3 \times 10^{-16}$ s^{-1} ; Bellingham and White, 2000) and there is no evidence for a significant change in overall strain rate as the rift episode progressed. The observed pattern of strain localisation is therefore likely to have been as a result of the regional evolution of the Northern North Sea Basin rather than a change in global-scale stress fields. A strain rate of 3×10^{-16} s^{-1} (Bellingham and White, 2000) is 30% strain in 3×10^{15} sec, or 31.7My. Taken as 20% strain over the 20My of Mid Jurassic rifting this is consistent with a β factor of 1.2 during the rift event.

There is a proposed relationship between effective elastic thickness (T_e) and the maximum length that can be reached by a normal fault (Jackson and White, 1989; Hayward and Ebinger, 1996; Scholz and Contreras, 1998; Ebinger et al., 1999) provided it penetrates to the base of the seismogenic zone. The major Late Jurassic structures in the Northern North Sea are near planar to depths of 20km and show continuous reflection through the crust on

seismic data (figure 4.10; Christiansson et al., 2000). The faults dissect both the upper and lower crust. The holistic model presented in this thesis documents a decrease in the number of active faults over time as strain is localised towards the centre of the basin. In addition, it shows a systematic increase in the length and total accumulated displacement on faults moving towards the rift axis. For example, the largest fault in the East Shetland Basin both in terms of length and maximum displacement is the Visund-Gullfaks Fault which bounds the North Viking Graben. The North Viking Graben, located at the centre of the rift province, is the area that would be expected to have undergone most extension and therefore to have the highest geothermal gradient and lowest effective elastic thickness of anywhere in the basin. To use elastic thickness as a proxy for the maximum length of faults requires therefore that there is a systematic variation in effective elastic thickness across the East Shetland Basin. There is no published evidence for such a systematic variation from back-stripping studies which have successfully modelled this area using a constant T_e of 1.5km (Roberts et al., 1998). The proposed relationship between maximum elastic thickness and maximum fault size, either in terms of length or displacement is therefore not valid in the Northern North Sea.

An alternative approach to predict the effective elastic thickness in a given basin based on the maximum fault length was proposed by Ebinger et al. (1999). This work predicts a relationship between the length of a normal fault and the effective elastic thickness in which it has formed based upon data from the active East African Rift. Applying this relationship to the Visund-Gullfaks Fault (which has a total length in excess of 150km) gives an elastic thickness greater than 50km. This is much greater than all other estimates of effective elastic thickness in the Northern North Sea, which are typically in the range 1-5km (Bellingham and White, 2000). The model proposed by Ebinger et al., 1999 also predicts that the longest faults will form in the coldest, strongest lithosphere. Since the longest fault in the East Shetland Basin occurs at the rift axis then this relationship can also be shown not to be applicable to the Northern North Sea.

6.3 Modelling the development of rift systems

There are a large number of numerical and analogue models which successfully reproduce the generic response of continental lithosphere to instantaneous stretching. The development of a generic model that accurately reproduces the structures observed in any one rift province is an overwhelming challenge as a result of the wide variety of rift morphology visible at the

earth's surface today. Rifts may be passive or active, they may form slowly or quickly and may be symmetric or asymmetric. The range of models appears to be bi-polar: At one end are those that emphasise the role of brittle deformation in extension (e.g. Kusznir et al., 1991) and at the other end are those models that adopt a basin-wide approach and emphasise the role of ductile deformation during extension (e.g. Bellingham and White, 2000). The role of normal faulting in each of these end-members is either inflated or ignored and a large number of intermediate models have been developed in order to describe the temporal and spatial evolution of rift provinces.

Scaled analogue sandbox models are a powerful tool for simulating the development of extensional structures in rift systems through simulation of the brittle extensional deformation of sedimentary rocks in the upper crust (figure 6.3). McClay (1990), has applied a variety of sandbox models to the development of normal fault arrays in rift systems. Many of these are not applicable to the Northern North Sea due to a difference in boundary conditions or style of faulting (e.g. McClay, 1990). The only models that are applicable to the development of the northern North Sea Mid to Late Jurassic rift province are those that are characterised by steep, planar normal faults. Analogue models simulate development of structures on a number of scales within an evolving rift province. For example, sandbox models have been shown to predict the segmented nature of faults in an evolving rift province and the way in which they interact via relay ramps and subsequently link (McClay and White, 1995).

Numerical models are more flexible than analogue sandbox models due to the range of parameters (e.g. rheology and boundary conditions) which they can incorporate. The models are based upon a conceptual framework that describes mathematically how rocks deform in response to applied loads. Brittle-elastic and elasto-plastic conceptual models are most common as the deformation of elasto-plastic solids is similar to the deformation seen in rocks. Numerical models have successfully reproduced the displacement-length characteristics of an isolated normal fault (Cowie and Scholz, 1992a), the variation in slip rates and spacings for active normal faults (Cowie and Roberts, 2001), the feedback controls on the growth rate of normal faults (Cowie, 1998) and how the formation of extensional basins is controlled by the development of large, linked normal fault arrays (Cowie et al., 2000).

The migration of the locus of extension towards the rift axis with time has profound implications for modelling the evolution of the Northern North Sea and other rift provinces.

The mechanism presented in section 6.2 above for the evolution of the rift province requires that the onset of rifting is synchronous in the latest Bajocian (Ravnas et al., 1997; Davies et al., 2000) but that the cessation of activity is not synchronous and instead occurs in a step-wise fashion beginning in the west of the East Shetland Basin and sequentially ceasing activity on faults towards the east. The latest primary motion occurs on the axis-bounding fault.

Chapter 2 introduced the domino model of extensional faulting in which the geometry of fault blocks in a rift province is approximated to a set of rotating dominos (Barr, 1987). As extension progresses all faults achieve extension together by the same amount, rotating the intervening blocks to the same angle. The domino model therefore requires that all major normal faults in a rift province are active for the entire duration of the rift episode. This has been widely applied to structures relating from the Northern North Sea Mid to Late Jurassic rift episode (Barr, 1987a, 1987b, 1991; White, 1990; Yielding, 1990; Roberts et al., 1993). The strain localisation model described in section 6.2 above does not allow simultaneous movement of all faults in the rift province for the entire duration of the rift episode. The domino model is therefore not applicable to the Northern North Sea Mid to Late Jurassic rift episode.

The localisation of strain within an individual fault block onto major throughgoing fault strands bounding individual fault blocks has been modelled using analogue and numerical models. The models attempt to reproduce the transition in a fault population as it evolves from an initial stage when deformation is distributed across the fault block on several isolated to weakly interacting fault segments, through a stage of fault segment linkage, to a situation where deformation is localised onto major, crustal-scale, block bounding faults. Analogue models have successfully reproduced this pattern of strain localisation in the laboratory. For example, Mansfield and Cartwright (2001) used a deforming crystacal plaster and barite mud sequence as an analogue for the development of extensional fault systems. In addition, Ackermann et al., (2001) used wet clay to show the increasing dominance of large faults when extension was applied to an analogue model. Ackermann et al., (2001) suggest that this trend reflects the control that mechanical layer thickness may exert on fault interaction. Numerical models, such as the healing-reloading feedback model of Cowie (1998) have successfully reproduced the development of large, crustal-scale normal faults. The model shows that the temporal development of an individual normal fault is dependant on whether or not it maintains an optimal geometry. A fault may become inactive or be re-

activated at any stage due to its position and orientation relative to other active faults (Cowie, 1998).

The numerical and analogue models which successfully model strain localisation onto throughgoing crustal-scale normal faults are valid in a larger, more holistic model in which strain is also localised towards the centre of the rift with time. The growth and development of each individual fault strand as a result of strain localisation within each individual fault block can occur within the auspices of strain localisation onto the rift axis. However, the localisation of strain on a basin-wide scale within the rift province as a whole is a progression from existing models in which strain becomes localised on an individual fault strand during formation of a half-graben.

The transition from a basin in which there is no dominant direction of dip to that dominated by large, inward-dipping synthetic faults has also been reproduced using analogue and numerical models. Ishikawa and Otsuki (1995) used sandbox experiments to investigate the influence of horizontal strain gradients on the asymmetry of normal fault systems in regions of crustal extension. They showed that faults facing in the direction of highest strain were preferentially developed at the expense of structures with an opposite sense of dip. Since the holistic model described above shows a focussing of strain onto the rift axis as the extensional episode progresses then faults that dip towards the rift axis would be expected to gradually dominate in the basin. In addition, numerical models have also successfully shown the increasing dominance of inward-dipping synthetic faults over outward-dipping antithetic faults as the rift episode proceeds. Models show that when a lateral strain gradient is imposed as an initial condition, faults that dip towards the region of highest strain, synthetic faults, will emerge as the dominant set at the expense of outward-dipping, antithetic faults (Hardacre and Cowie, 2003).

The migration of the locus of extension towards the centre of the rift province over time has been successfully reproduced using numerical models but has not been replicated using analogue models. Kusznir and Park (1987) investigated the response of the lithosphere to an applied tectonic tensile force and analysed the resulting stress distribution using a mathematical model incorporating the elastic, plastic and brittle behaviour of lithospheric material. Their model showed the extensional strength of the intraplate continental lithosphere was critically dependant on the geothermal gradient, crustal composition and thickness. Work which aims to reconstruct the migration of the locus of extension has to date concentrated on modelling the effects of the evolving thermal structure of the lithosphere on

faulting. The model uses a visco-plastic rheology in a finite element model to investigate the effects of crustal rheology and thermal structure on the development of normal faults in 2D (Behn et al., 2002). In this approach, the effective viscosity of the lithosphere depends on temperature, strain rate and plastic yielding criteria (Cowie et al., 2005). Input values include published values of strain rates, layer thicknesses and thermal structure for the Northern North Sea. The model reproduces the pattern of faulting described above in the Northern North Sea . When a weak lateral temperature gradient is imposed, deformation is distributed between sets of conjugate normal faults with similar strain rates. Active faulting extends up to c. 75km either side of the rift axis. As the lateral temperature gradient becomes more pronounced, active faults dip preferentially towards the area where the geothermal gradient is highest and the highest strain rates occur where the lithosphere is thinnest. The total width of the zone of active faulting narrows from c. 150km to c. 50km (Cowie et al., 2005). The model therefore predicts a mechanism for the strain localisation which depends on coupling between the brittle fault growth and temperature dependant viscous deformation. A relatively small perturbation to the thermal structure of the lithosphere is shown to exert an important control on fault development and strain localisation within the brittle layer, very similar both spatially and temporally to what is observed in the Northern North Sea Late Jurassic rift province.

6.4 Implications for petroleum prospectivity

After thirty-five years of hydrocarbon exploration, the Northern North Sea has become a mature basin in terms of hydrocarbon exploration. The majority of the large structural plays have been in production for in excess of 15 years (Underhill, 1998). The search for hydrocarbons has turned to new and innovative ways in which to exploit existing reserves in the Northern North Sea. These are generally smaller and more numerous than the large fields that dominated the industry during the last century. A detailed knowledge of the history of the hydrocarbon province will provide an important insight into the maturation, migration and accumulation history of potentially economic reserves of oil and gas.

The holistic model presented above in which strain was localised onto the rift axis during the Late Jurassic rift episode in the Northern North Sea provides new insights into the activity histories of normal faults at designated locations within the East Shetland Basin. Detailed knowledge of which faults were active and when in the duration of the rift episode allows

reconstruction of not simply fault movement histories, but also uplift and possible sub-aerial exposure of footwall fault-blocks, the formation of footwall islands and reconstruction of clastic sediment dispersal pathways.

The implications for petroleum prospectivity described below with respect to the Northern North Sea are applicable to prospectivity in other basins. The structural configuration and sedimentological evolution of the Northern North Sea has been shown to be comparable with a number of other rift provinces, some of which contain exploitable hydrocarbon plays, (e.g. Gulf of Suez, Egypt). The implications for petroleum prospectivity described above are therefore expected to play an important role in other comparable rift provinces.

6.4.1 Fault Movement Histories

The model presented above for the development of the East Shetland Basin during Mid to Late Jurassic rifting provides new constraints on the record of fault activity in the basin. Traditionally all faults in the basin are thought to have been active from the onset of extension until the early Cretaceous when extension ceased. This is shown above not to be the case. Faults on the edge of the rift province are shown to have become inactive first, with cessation of activity occurring progressively across the East Shetland Basin, from west to east with latest primary motion occurring on the axis bounding fault. Knowledge of which faults were active and when in the duration of the rift episode is vital to a reconstruction of sediment dispersal pathways, the formation and subsequent erosion and redeposition of footwall islands and the formation of fault scarp degradation complexes. These aspects are discussed in detail below.

6.4.2 Sediment dispersal pathways

In addition, the model for the development and evolution of the East Shetland Basin during Mid to Late Jurassic rifting has a profound effect on the spatial and temporal evolution of pathways available for sediment dispersal.

During initial rifting subsidence rates and structural relief in rift basins are generally low and have little impact on sediment dispersal pathways (figure 6.4A). As faults grow and interact many faults became inactive as strain is localized onto a small number of larger structures. The dominant basin-floor topography at this time was a series of half-grabens which formed as a response to footwall tilting and uplift and hangingwall subsidence. The segment linkage

to form major, crustal-scale, throughgoing normal faults with half graben morphology may have limited sediment transfer in the basin to transverse pathways running north and south within the East Shetland Basin. This restriction is maximized by the emergence of uplifted footwall scarps to form islands (see section 6.4.3 below). During development of this morphology, along-strike variations in the uplift and subsidence of footwall and hangingwall blocks respectively may generate contrasting sedimentation patterns along the length of the fault (Gawthorpe and Leeder, 2000).

The migration of the locus of extension towards the rift axis with time results in the cessation of activity on more distal faults prior to the end of the rift episode. As a result these faults are likely to have passively subsided, and their topography to have gradually declined in the latest part of the rift episode. Erosion of the uplifted scarps may have initially provided material for redeposition elsewhere in the basin (See section 6.4.4 below) and a lowering of topography may have removed both a sediment source and restrictions on sediment transfer in the basin. However, the rift-bounding fault (the Visund-Gullfaks Fault) was active until late in the rift episode and was characterized by an emergent footwall scarp. This 150km long structure was a significant barrier to east-west movement of sediment into the North Viking Graben and as such is likely to have channelled sediment in a north-south direction towards the end of the rift episode.

Gawthorpe and Leeder (2000) recognise that there are important structural controls upon sedimentary sequences exerted by the episodicity and migration of the locus of active faulting. For example, on the southern side of the Gulf of Corinth, Greece, successive gilbert-type fan deltas have formed in response to northward migration of fault activity over time (Dart et al., 1994; Gawthorpe et al., 1994). Modern fan-deltas in the area are linked via submarine channels to submarine fans (Ferrentinos et al., 1988). Therefore in the Gulf of Corinth a migration of sedimentary environments can be seen to accompany the migration of the locus of activity towards the rift axis. In addition, reworking of sedimentary architectures, such as is occurring in the Keranitis Fan Delta (see figures 2.19 and 2.20), may be an important source of material to present day depocentres. Although the Gulf of Corinth (as a predominantly sub-ariel rift basin) may not be a direct comparison with the Northern North Sea rift basin, the temporal and spatial controls on fault activity can be seen to have a profound effect on sediment dispersal pathways, and are likely to be to some extent comparable with the submarine setting of the Northern North Sea in the Mid to Late Jurassic rift episode.

The cessation of activity on more distal faults results in the fault and their hangingwall depocentres being passively uplifted in the footwalls to larger, still active, faults situated

more proximally to the North Viking Graben. As a result, the sedimentary succession in the hangingwall depocentres of these faults are characterised by the transition from deep-water into to a shallower water setting over time.

Analysis of petroleum prospectivity in a rift basin requires knowledge of sediment dispersal pathways in order to evaluate which sediment was available as a source, reservoir or seal during the evolution of the rift province. Understanding of the migration of the locus of extension in the Northern North Sea rift basin will allow development of a more detailed model in which sediment dispersal pathways can be modified in the light of a dominant axial fault and periods of inactivity on more distal structures.

6.4.3 Footwall Islands

Strain localization towards the centre of the rift province with time and increased slip rates on more proximal faults are likely to have resulted in the uplift of footwalls above sea level in the Mid to Late Jurassic to form 'footwall islands'.

The uplift and sub-aerial exposure of footwall crests in the Mid to Late Jurassic Northern North Sea rift province may have affected hydrocarbon prospectivity of the structures. The majority of large hydrocarbon fields in the East Shetland Basin are of 'Brent-type' tilted fault block style. In these fields, the hydrocarbon accumulation is in the crest of a back-tilted footwall block. Knowledge of the erosion, diagenesis and burial history of these tilted footwall blocks will provide a valuable insight into the petroleum system.

Sub-aerial exposure as a footwall island may have a number of effects on the uplifted footwall crest. Firstly, the island is subject to sub-aerial processes, such as diagenesis by meteoric water. This may result in a change in reservoir quality through dissolution of a calcareous cement or alteration of permeability or porosity. In addition, sub-aerial processes may erode the uplifted block, modifying its shape, and therefore its trapping potential.

Application of models of strain localisation to the reconstruction of footwall islands in the Mid to Late Jurassic Northern North Sea rift province results in the need for consideration of individual footwall uplift dependant on position within the basin. For example, the Visund-Gullfaks fault is known to have been active throughout the rift episode at gradually increasing slip rate. Thus, it is likely to have maintained a sub-aerial position for longer, and therefore been altered to a greater degree than the Snorre Fault which became inactive before the end of the rift episode.

Finally, footwall islands provide an important intrabasinal source of sediment. Footwall islands are known to frequently be rimmed with a series of prograding shoreface sequences which form during the time the footwall is an emergent island. For example, several episodes of marine sands are recorded in wells to have prograded from the emergent footwall to the Snorre fault during the Late Jurassic rift episode (Dahl and Solli, 1993). The implications for petroleum prospectivity of footwall islands as an important source of intrabasinal sediment is considered in section 6.4.4 below.

6.4.4 Erosion of Uplifted Footwall Islands

A well-documented effect of synsedimentary footwall uplift of the tilted fault-block structures resulting from Mid to Late Jurassic rifting in the Northern North Sea rift province was not only to cause incision but also to promote resedimentation of the erosional products down-flank from the crest of the structures (Underhill, 1998).

The processes by which material is eroded from the crest of an uplifted footwall are various and complex. Some footwall crests in the East Shetland Basin are known to have been uplifted to a sub-aerial setting during the Late Jurassic therefore rendering them susceptible to erosion by meteoric water and fluvial processes in addition to those of a marine setting (e.g. Snorre (figure 6.5; Dahl and Solli, 1993) and Statfjord (McLeod, 2000)). In contrast, others may have been uplifted to a shallow marine setting at or near wave base. The process by which material was removed from the crest of the uplifted footwall block is therefore various, but uniformly involves peneplanation of the crest at or near wave base at some point in its history. This results in a general decrease in slope angle of the uplifted scarp with the crest and footslope area enlarging at the expense of the mid-slope area (Peterson, 1985). Transportation of eroded material may be down dip, away from the rift axis, or may be over the fault into the hangingwall depocentre (figure 6.4).

The deposits resulting from erosion of an uplifted footwall crest in the East Shetland Basin are in general clean sands such as the Kimmeridge Clay Sandstone Member and Munin Sands (see Chapter 3 for a detailed discussion), which are present as isolated units in the mud-dominated Kimmeridge Clay Formation. The abrupt decrease of gradient from the footwall uplands to the hangingwall depositional basin causes rapid deposition and the construction of fan deltas and submarine fans (Gawthorpe and Leeder, 2000), for example the Magnus Sandstone Member, in the deeper marine environment. In the shallow marine and sub-aerial environment they are deposited as beaches, talus cones, alluvial fans and shelves.

During the early 1990's reservoirs resulting from redeposition of eroded material were actively targeted during exploration, largely as a method by which to utilize existing oil field infrastructure (Underhill, 1998). Petroleum prospectivity of these sands is dependent on a number of factors: the reservoir quality of the sand, the age of the deposit and its post-depositional history. These factors are in turn dependant on the processes of erosion, deposition and subsequent burial history of the sand unit. An increased knowledge of the processes by which the unit was eroded and subsequently redeposited, such as is developed in the holistic model of section 6.2 above, will aid understanding of these processes and aid the search for subtle accumulations of hydrocarbons. However, despite the importance of this process it should be noted that footwall highs which formed intrabasinal sediment sources were of limited size compared with both the volume of the adjacent depositional sinks (Ravnas and Bondevik, 1997) and the more traditional 'Brent-type' tilted fault block reservoirs.

6.4.5 Fault Scarp Degradation Complexes

In the Northern North Sea rift province the footwall mounted fault scarp degradation complexes (FSDC) are hydrocarbon bearing, and hence form important secondary reservoirs. For example, the Ninian Field is producing from at least two major degradation complexes (Underhill et al., 1997). The high structural elevation of the FSDC, their hydrocarbon fill and the advanced state of exploitation of in-situ Brent Group reservoirs in all these fields results in the potential for a large amount of remaining undiscovered reserves to be present in the FSDC of the East Shetland Basin (Underhill et al., 1997). In fact, it has been estimated that fault scarp degradation complexes may contain at least one third of the remaining reserves in the East Shetland Basin (Schulte et al, 1994; Coutts et al, 1996). Identification and mapping of such complexes is therefore vital in the deliberate search for more subtle accumulations of hydrocarbons.

The lack of a significant FSDC on much of the Visund-Gullfaks fault scarp may be interpreted to be the result of complete localisation of strain onto this fault during the climax of Late Jurassic rifting in the Northern North Sea. If the lack of a well developed, laterally continuous FSDC is indicative of an axial fault onto which strain is partitioned in the latest part of the rift episode than FSDC exploration targets on similarly placed faults in other rift systems would be futile.

6.4.6 Footwall Compartmentalisation

The dissection and tilting of footwalls to the major faults in the East Shetland Basin acts to compartmentalise the footwall structure, resulting in the formation of hydrocarbon fields which are not restricted to the structural high point of each individual footwall crest. For example, the strike-perpendicular footwall faults associated with the Murchison Fault partition the footwall creating individual compartments in which the Thistle, Murchison and Zeta hydrocarbon accumulations are located (figure 6.6). An absence of footwall faulting in the Greater Murchison area would result in the migration of all hydrocarbons up dip to the crest of the Murchison structure, located near the Murchison Field itself. A similar compartmentalisation is seen in offshore "B" trend, Gulf of Suez, Egypt. Here, structures resembling footwall release faults result in the formation of the GS 365, Sidki, East Zeit and Hilal hydrocarbon fields (Helmy, 1990). A detailed knowledge of the structural history associated with the footwall to each major fault in the rift province provides valuable information on the likely migration pathways and traps of the petroleum system.

6.5 Implications for further work

The migration of the locus of extension towards the centre of the Late Jurassic Northern North Sea rift province over time has been presented by the detailed interpretation of syn-rift deposits associated with the Murchison, Statfjord and Snorre faults. Further quantification of strain localisation onto the rift axis could be achieved by interpretation of the syn-rift stratigraphy in the hangingwall to the Visund-Gullfaks Fault. This data is in the North Viking Graben and therefore at greater than five seconds two way time on seismic reflection data. Seismic reflection data quality decreases with depth and the data is not preferentially enhanced to resolve stratigraphy in the deep North Viking Graben: as a result it has not been possible in this study to undertake a detailed interpretation. In addition, the North Viking Graben is not an active target for exploration: as a result well penetrations in the area are sparse and lateral correlation of reflectors is not possible. It may be possible in the future to quantify the movement on the Visund-Gullfaks Fault using seismic and well data over the Kvitbjorn Field to the south. This field is located in the North Viking Graben and in the hangingwall to the VG Fault and interpretation may therefore provide a more detailed history of the VG fault. Furthermore, the model of strain localisation could be tested by examination of the detailed syn-rift stratigraphy associated with faults that are the along-strike lateral equivalents of the structures examined in this study. For example, the Hutton and Ninian

faults are the along strike lateral equivalents of the Murchison Fault and a wealth of data exists in this area.

The evidence presented from the East Shetland Basin for the evolution of a population of faults from a large number of short, distributed fault segments to a single throughgoing fault situated on the rift axis may be applicable to other rift dominated settings for example the Gulf of Corinth, Greece and the Gulf of Suez, Egypt.

The Gulf of Corinth is an ensilac marginal basin developed due to north-south directed rollback-related extension in the forearc area behind an active subduction zone located along the outer Hellenic arc (figure 2.16). The onset of rifting in the Gulf of Corinth occurred during the latest Miocene to earliest Pliocene (Kelletat et al 1976). Present day extension in the back arc to the Hellenic trough is 10-20mm/yr (Billiriset et al 1991) and is characterised by zones of high extension separating more slowly deforming blocks (Jackson and McKenzie, 1988). The Gulf is an asymmetric half graben bounded by a major normal fault located on its southern edge.

North-south extension in the Gulf of Corinth is expressed as a series of predominately right stepping north-dipping normal faults and south-dipping antithetic faults which produce an asymmetric half graben with larger faults and thicker syn-rift deposits located on the southern margin of the Gulf, on the northern edge of the Peloponnese Peninsular (McNeill and Collier, 2004). The present day fault configuration on the southern side of the Gulf of Corinth is dominated by a single active fault (the Gulf of Corinth master fault) located offshore in the present day gulf.

Application of the strain localisation model developed for the East Shetland Basin would assume that the suite of sub parallel, east-west striking normal faults extending southwards from the present day gulf into the Northern Peloponnesus peninsular were once all active and that as rifting progressed they became inactive in a stepwise progression as strain was gradually localised towards the centre of the Gulf of Corinth rift. This model is in conflict with existing models for the development of the Gulf of Corinth in which only a single fault is active at any one time and in which the position of active faulting has stepped northward over time (e.g. Dart et al, 1995, Goldsworthy and Jackson, 2001) leaving inactive faults abandoned in the footwall to younger faults. This requires cessation of activity on an older more distal fault before the onset of activity on a newer fault more proximal to the rift axis. In this model, strain is progressively localised onto the rift axis over time but the rift axis is

never characterised by an early population of large numbers of discrete, short fault segments. Instead, it requires individual short fault segments to develop in preferential locations, i.e. in front of (north of) an active fault, in order for them to be precursors to a throughgoing fault strand to the north of an active fault. Further work would aim to address this question.

Further work to apply the holistic model of strain localisation to other basins would enable testing of the model. This work may however be limited by the lack of such an extensive, densely-spaced dataset such as is available from the East Shetland Basin.

For more than 70 years geologists have used experimental models with wet clay, dry sand and wet plaster to simulate normal faulting (e.g. Cloos, 1928, 1930, 1968; Oertel, 1965; Withjack and Jamison, 1986; Vendeville, 1987; Kautz and Sclater, 1988; Ellis and McClay, 1988; Withjack et al., 1995), (Ackermann et al., 2001). Analogue models have provided a valuable insight into the development and evolution of normal fault populations in extensional basins. However, strain localisation on a basin-wide scale has not been successfully modelled to date. The primary limitation on modelling of the migration of the locus of extension towards the rift axis over time using analogue models is that they are incapable of stimulating strain hardening and strain rate hardening. It is necessary to simulate these processes in order for cessation of activity on more distally located faults early in the rift episode to be modelled and hence reproduce the process of strain localisation. This process has been suggested to be due to the evolving thermal structure of the lithosphere (Cowie et al., 2005) which cannot yet be modelled using sandbox experiments. Further work concerned with the development of our understanding of strain localisation would concentrate on a method by which faults on the edge of the rift province could be 'locked' in some way so as to progressively concentrate strain onto the rift axis.

6.6 Conclusions

6.6.1 The migration of the locus of extension

Detailed documentation of the syn-rift stratigraphy associated with a suite of faults in the Mid to Late Jurassic Northern North Sea rift province shows that the locus of extension migrated towards the centre of the rift during the extensional episode.

- The rift basin was initially dominated by large numbers of short, small displacement faults which grew by radial tip propagation, and subsequently linked as a result of strain localisation onto major, crustal-scale, block-bounding faults
- After formation of these major through-going fault systems the dominant method of strain localisation became a regional focussing of activity towards the North Viking Graben. The major structures in the East Shetland Basin show a systematic increase in length and maximum accumulated displacement towards the rift axis, the North Viking Graben. Strain was progressively localised onto an increasingly smaller number of active normal faults located increasingly more proximally to the North Viking Graben. As the number of active faults in the basin decreased so the slip rate on the remaining active structures increased. The across strike width of the active rift basin has therefore narrowed over time. In addition, an increasing dominance of synthetic over antithetic faults occurred during the rift episode.
- Three key observations provide evidence for the localisation of strain towards the North Viking Graben over time and the establishment of a lateral strain gradient across the East Shetland Basin. Firstly, the magnitude of total accumulated slip on faults across the basin varies systematically from a minimum furthest away from the North Viking Graben to a maximum at the rift axis itself. Secondly, the activity histories of the faults show a progressive cessation of activity with the faults furthest away from the rift axis becoming inactive first and the fault bounding the rift axis being active last and therefore longest. Thirdly, the increasing dominance over time of large inward-dipping synthetic faults.
- Strain localisation onto major, crustal-scale, block bounding faults can be modelled using both analogue and numerical models. The regional migration of the locus of extension towards the rift axis with time can be modelled using a numerical model in which a small thermal perturbation to the lithosphere is introduced. This process has not been modelled using sandbox experiments due to the inability of the method to allow faults to be locked.

6.6.2 Footwall deformation

A variety of styles and scales of footwall deformation can be documented within the East Shetland Basin, Northern North Sea.

- *Strike-perpendicular* footwall release faults, associated with the Murchison Fault, form as a result of differential vertical displacements along the length of the fault. The structures are extensional in character and form perpendicular to the block bounding fault, often at the position of former segment linkage. They are generally short (4– 8 km) and have small total accumulated displacements (40 - 180 ms). Footwall release faults appear to be a very important, integral part of the rift structure and are an effective means by which hydrocarbon closures area created.

- *Strike-parallel* footwall faults form when localisation of strain onto the graben-bounding fault results in a greater slip rate than can be accommodated by a single fault. The structures are 6-16 km in length, have displacements ranging from 60 to 700m and form in the immediate footwall to the Visund-Gullfaks Fault.

- Footwalls to the major faults in the East Shetland Basin show denudation as a result of erosion at, above or near to wave base. The length of the denuded scarp of the Visund-Gullfaks Fault is c. 60km and the width ranges from 20km in the north of the study area to 5km in the south. The footwall crest has been backstepped by up to 5km. The total volume of sediment removed is estimated to be 65km³. A similar process of denudation is known to have occurred on the Statfjord Fault and is thought to have occurred on the footwall to the Snorre Fault.

- Redistribution of eroded sediment from the eroded footwall crest was limited to restricted sediment pathways by the presence of footwall islands and was redeposited in both shallow and deep marine settings in fan, debris flow, beach, shelf and deltaic deposits.

6.6.3 Generic Implications

The development of a new holistic model in which the evolution of the Northern North Sea rift province is shown to be dominated by strain localisation onto the rift axis has implications for other rift provinces

- The model of strain localisation is shown to be applicable to other rift provinces, for example the Gulf of Corinth, Greece and the Gulf of Suez, Egypt

- The model may be applicable to other rift provinces where data are currently sparse or absent

- The model has profound implications for hydrocarbon prospectivity in the Northern North Sea and where applicable to other rift provinces may aid the search for subtle hydrocarbon accumulations be they structural or stratigraphic in nature

- The interpretation of a unique and high-quality data set has shown that existing models of rift basin development and the assumptions derived from old, 2D seismic data on which they are based, may not be correct. The approach to such areas should be open-minded and aim to make use of all the data available.

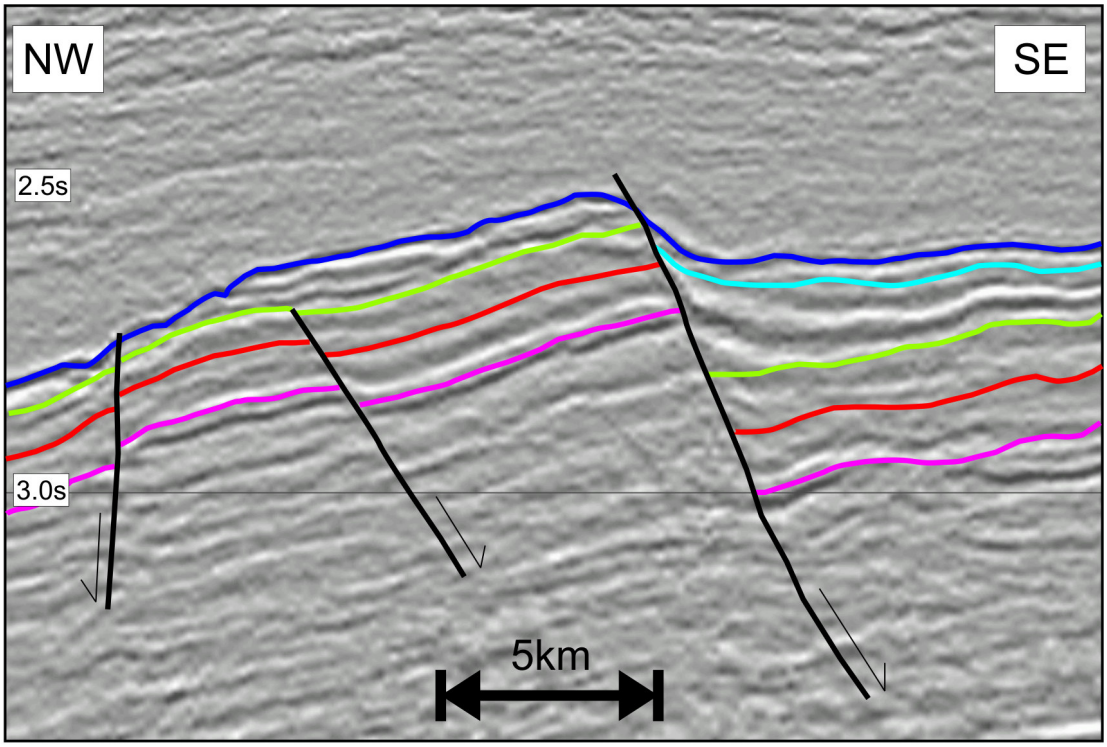

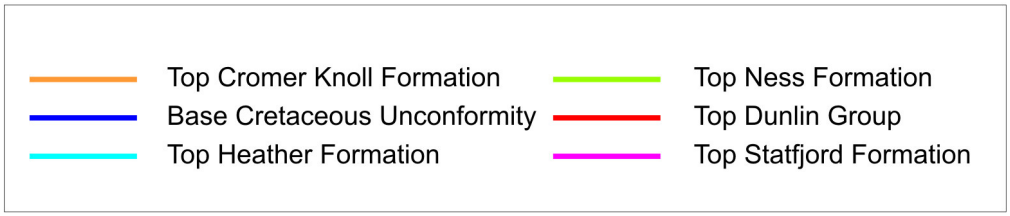

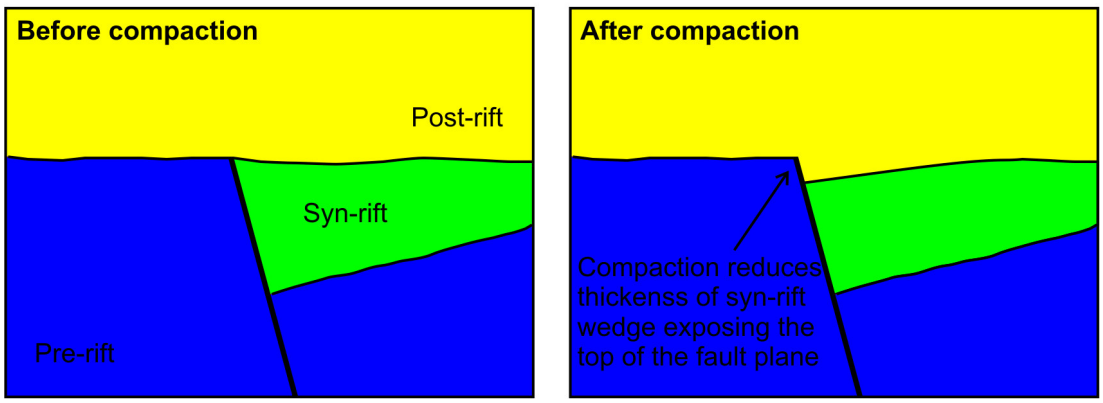

Figure 6.2
Top : Seismic line showing how compaction preferentially affects the syn-rift units.
Bottom : Schematic representation of how compaction affects the syn-rift units

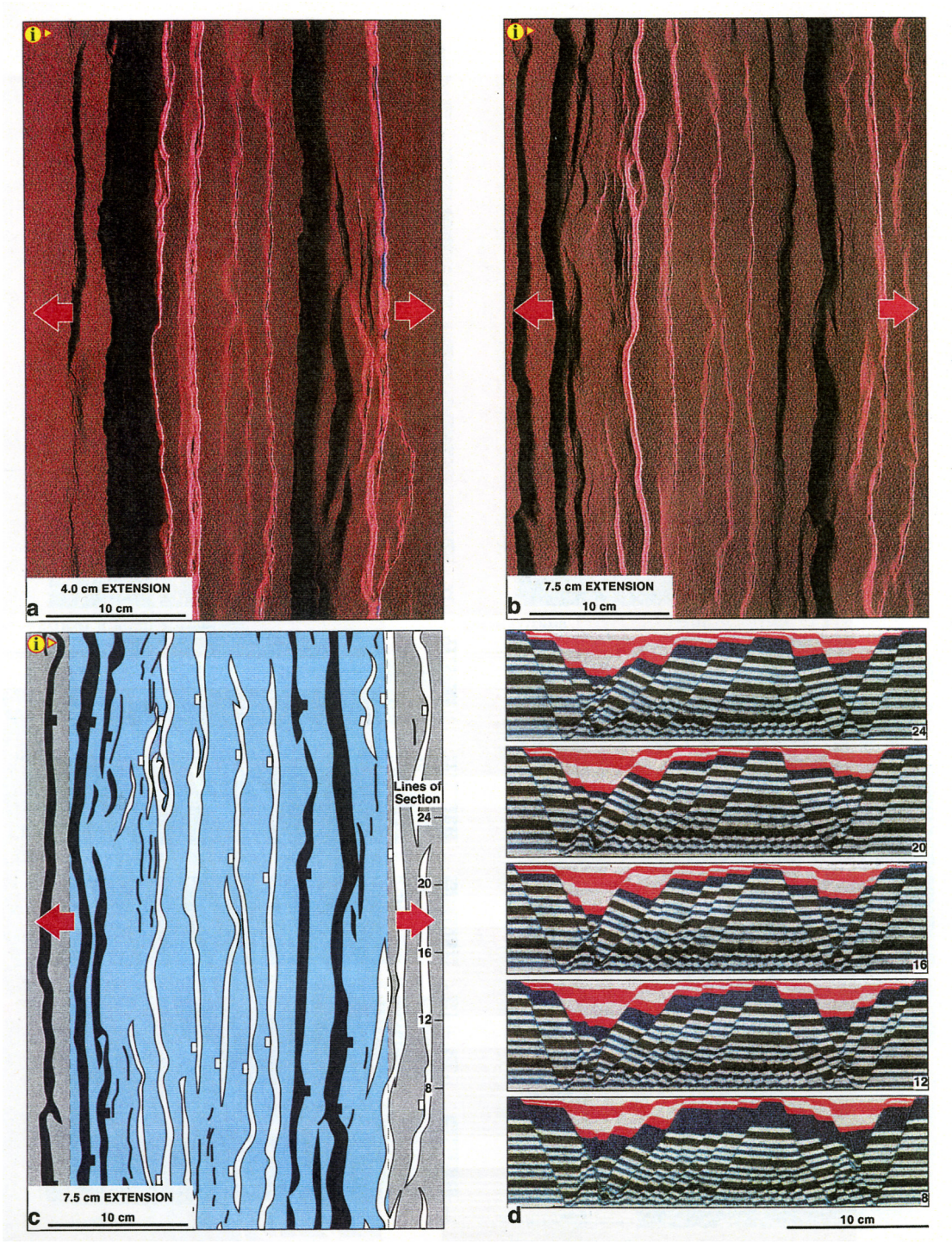

Figure 6.3
Example of an analogue model for orthogonal stretching
a. Overhead view of model after 4cm extension
b. Overhead views of model after 7.5cm extension
c. Line diagram interpretation of surface fault pattern at the end of extension. Dark bands are faults dipping to the rift and light bands are faults dipping to the left.
D. Serial sections through the model. Synkinematic strata are the red and white layers at the top of the grabens on either side of the central intra-rift horst block. Location of sections shown on c.
From McClay et al., 2002

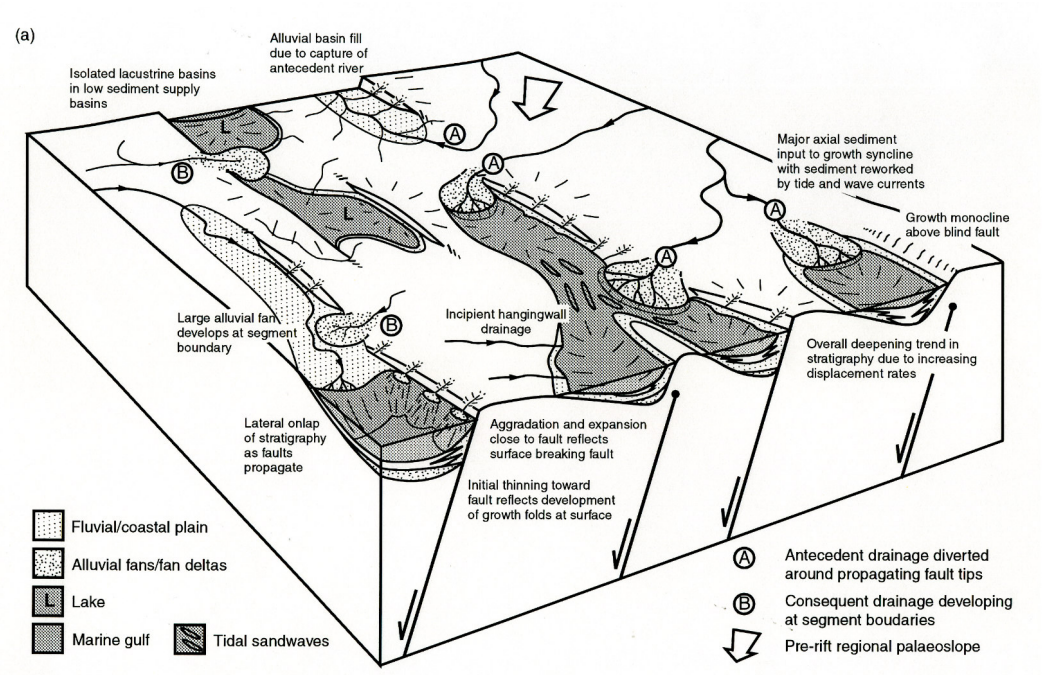

Figure 6.4A
Tectono-sedimentary evolution of a normal fault array in a coastal or marine setting
(a) Initiation Stage:
Early formed fault segments and growth folds form low-lying topography and define numerous isolated depocentres partly linked at highstands of sea level to form shallow, elongate marine gulfs and lakes. Antecedent drainage, locally modified by the evolving fault and fold topography, forms major sediment transport pathways. These early syn-rift depocentres display a marked variation in sedimentary fill, depending on their position with repect to sea level, sediment sources and the relationship between topography and sea level.
From Gawthorpe and Leeder, 2000

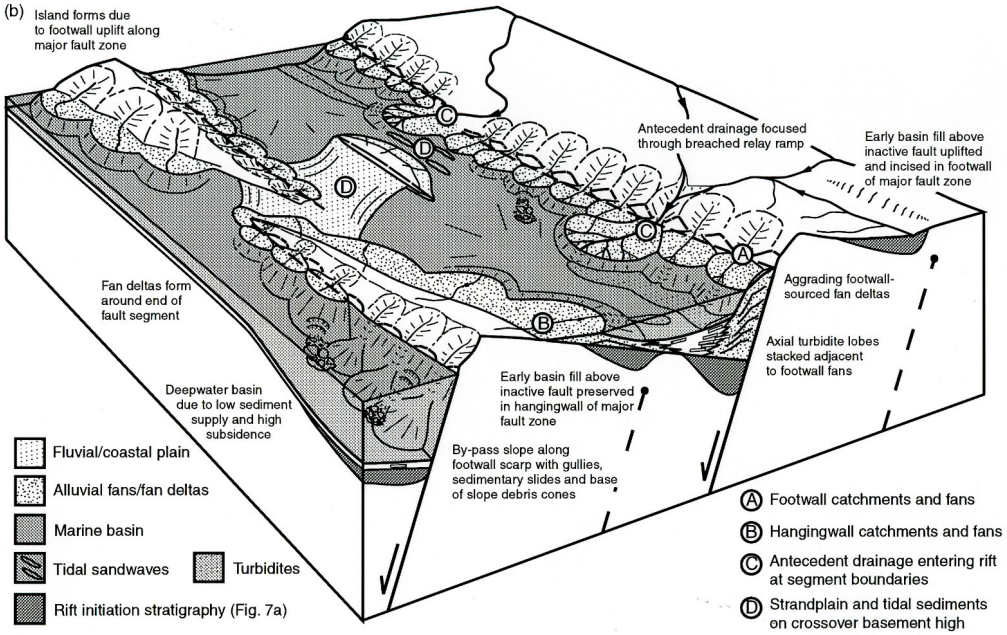

Figure 6.4B
Tectono-sedimentary evolution of a normal fault array in a coastal or marine setting
(B) Interaction and Linkage Stage during sea level highstand:
Lateral propagation and interaction between fault segments leads to enlargement and coalescence of early fault depocentres, whilst other faults become inactive (dashed lines). Development of drainage catchments along uplifting footwalls leads to the development of transverse sediment supply to footwall and hangingwall derived deltas. Right-hand fault zones along the rift shoulder are supplied by antecedent drainage that enters the rift through topogrpahically low segment boundaries. Left-handed faul zones form isolated footwall islands. Limited transverse sediment supply from these islands leads to the development of shallow marine and tidal sedimentation.Tilting of the basin floor promotes axial transport of turbidites that stack and interfinger with the toes of footwall-derived deposits. Localisation of deformation along major fault zones leads to increased subsidence rates that may outpace sediment supply and result in an overdeepening upward trend in the basin fill.
From Gawthorpe and Leeder, 2000

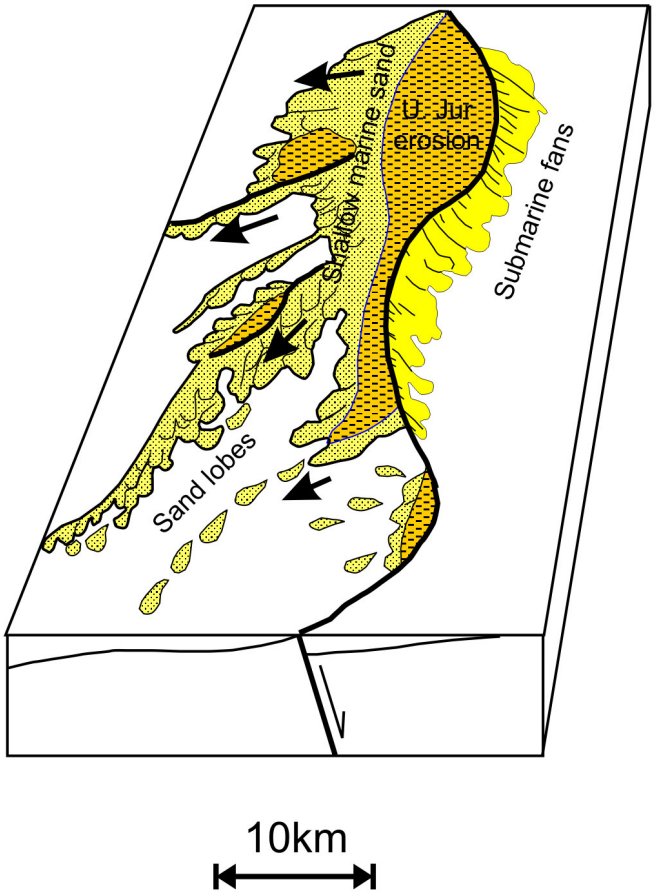

Figure 6.5
A schematic presentation of the Upper Jurassic sand developments in the Snorre Area
After Dahl and Solli, 1993

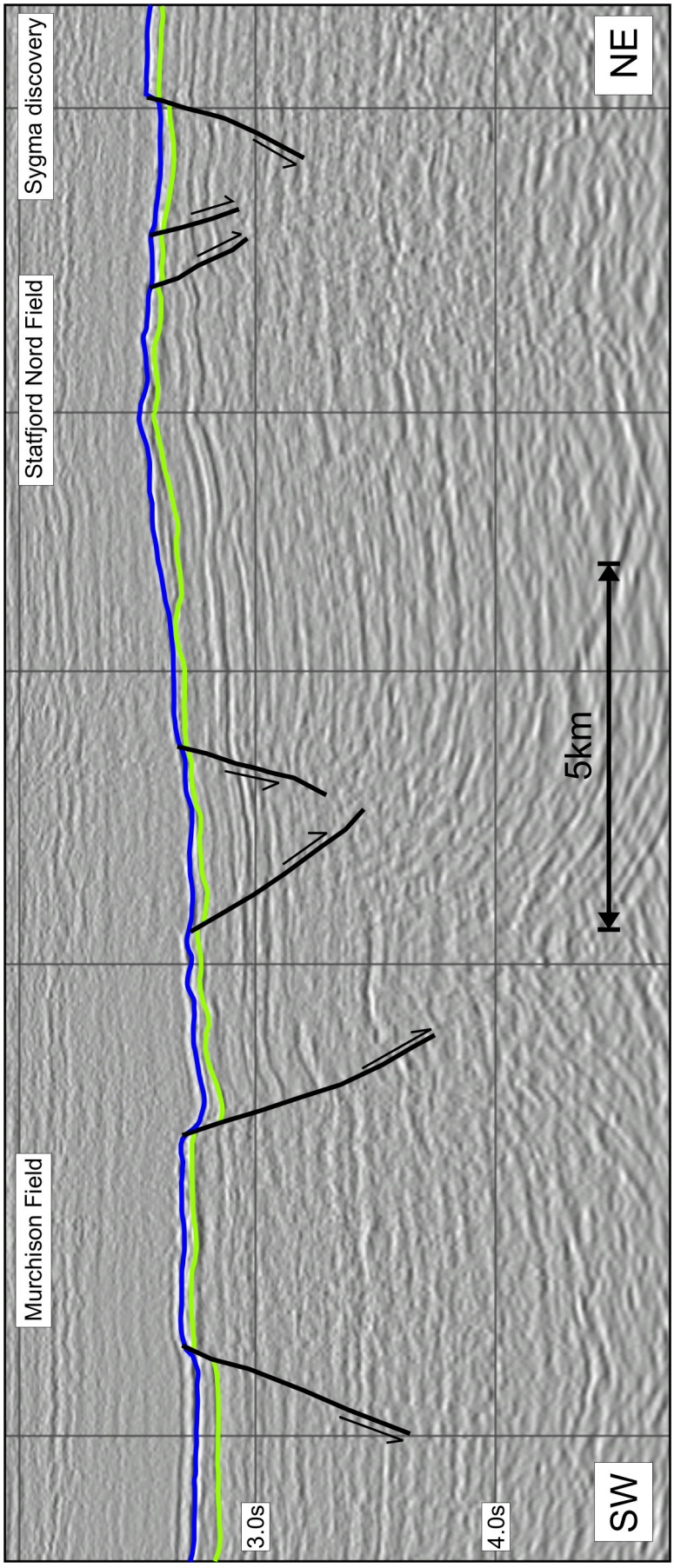

Figure 6.6
Seismic line through the footwall to the Murchison Fault showing compartmentalisation of the footwall by a variety of footwall faults
Blue line shows Base Cretaceous Unconformity. Green line shows top Brent Group (Top reservoir)

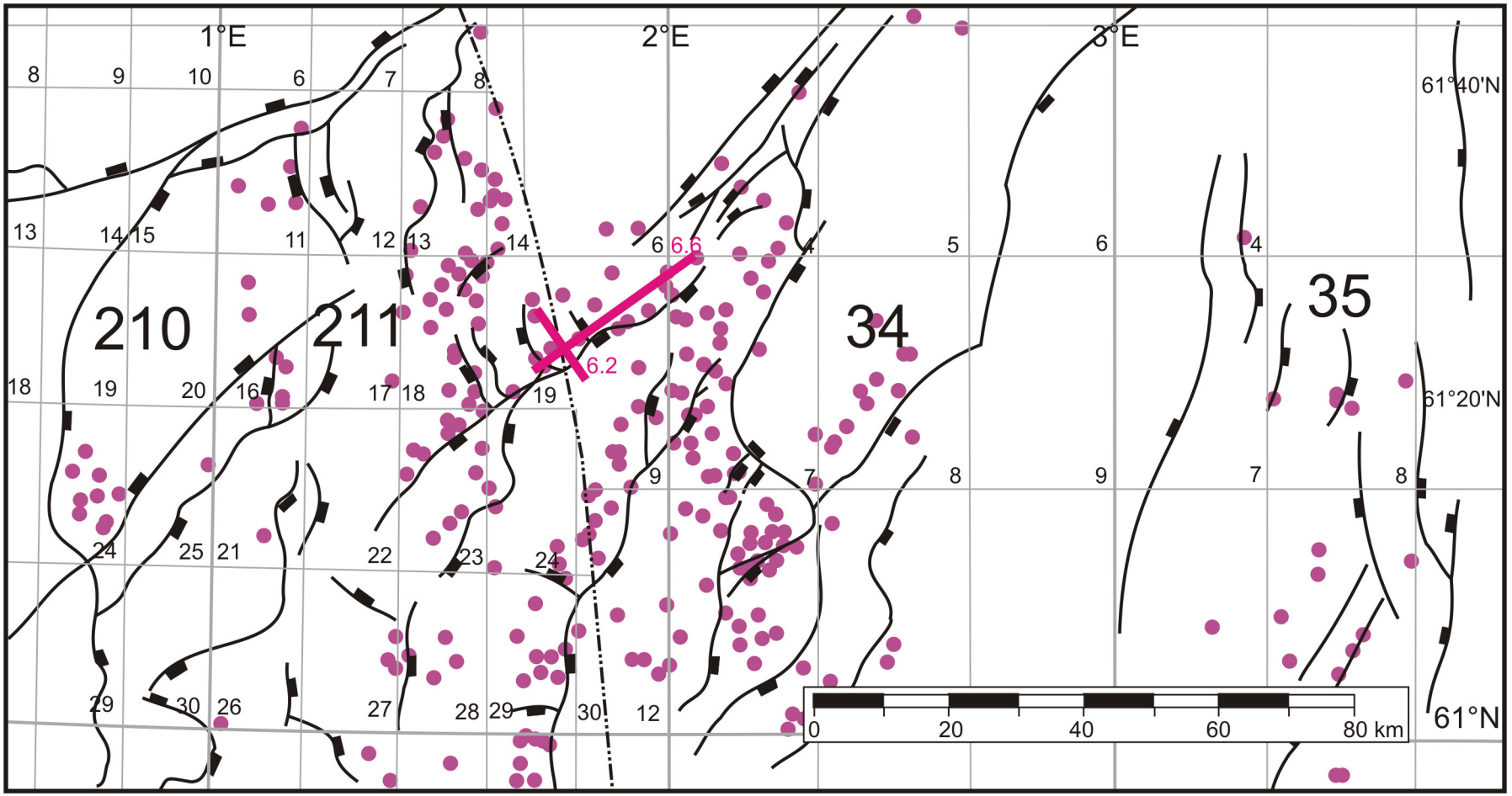

Figure 6.7
Map showing major faults and location of seismic lines presented in chapter 6
Purple circles show positions of exploration, development and appraisal wells with logs available for incorporation into this study

7. References

Ackermann, R.V., Schlische, R.W. & Withjack, M.O. 2001. The geometric and statistical evolution of normal fault systems: an experimental study of the effects of mechanical layer thickness on scaling laws. *Journal of Structural Geology,* **23**, 1803-1819.

Allen, P.A. & Allen, J.R. 2005. *Basin Analysis: Principles and Applications, 2nd Edition.* Blackwell Science Limited. 549pp.

Anders, M.H. & Schlische, R.W. 1994. Overlapping faults, intrabasin highs, and the growth of normal faults. *Journal of Geology,* **102**, 165-180.

Angelier, J. 1985. Extension and rifting: the Zeit region, Gulf of Suez. *Journal of Structural Geology,* **7**, 605-612.

Armijo, R., Meyer, B., King, G.C.P., Rigo, A. & Papanastassiou, D. 1996. Quaternary evolution of the Corinth Rift and its implications for Late Cenozoic evolution of the Aegean. *Geophysical Journal International,* **126**, 11-53.

Badley, J.D., Price, J.D., Rambech Dahl, C. & Agdestein, T. 1988. The structural evolution of the northern Viking Graben and its bearing upon extensional modes of basin formation. *Journal of the Geological Society, London,* **145**, 455-472.

Badley, M.E. 1985. *Practical Seismic Interpretation*. D. Reidel Publishing Company, Boston.

Badley, M.E., Freeman, B., Roberts, A.M., Thatcher, J.S., Walsh, J., Watterson, J. & Yielding, G. 1990. Fault interpretation during seismic interpretation and reservoir evaluation. *Proceedings of the first Archie Conference,* 224-241.

Ball, J. 1916. *The geology and geography of west central Sinai*. Egyptian Survey Department, Cairo.

Banbury, N.J. & Underhill, J.R. 2002. Structural controls on the Triassic prospectivity of the greater Tern-Eider-Cormorant area (East Shetland Basin). University of Edinburgh Internal Report for Shell Expro.

Barnet, J.A.M., Mortimer, J., Rippon, J.H., Walsh, J.J. & Watterson, J. 1987. Displacement geometry in the volume containing a single normal fault. *Bulletin of the American Association of Petroleum Geologists,* **71**, 925-937.

Barr, D. 1987a. Lithospheric stretching, detached normal faulting and footwall uplift. In: Coward, M.P., Dewey, J.F. & Hancock, P.L. (eds.) *Continental Extensional Tectonics.* Special Publication of the Geological Society, London, **28**, 75-94.

Barr, D. 1987b. Structural/stratigraphic models for extensional basins of half-graben type. *Journal of Structural Geology,* **9,** 491-500.

Barr, D. 1991. Subsidence and sedimentation in semi-starved half-graben: a model based on North Sea data. In: Roberts, A.M., Yielding, G. & Freeman, B. (eds.). *The Geometry of Normal Faults,* Special Publication of the Geological Society, London, **56**, 17-28.

Barron, T. 1917. *The topography and geology of the peninsula of Sinai (western portion).* Egyptian Survey Department, Cairo.

Bartholomew, I.D., Peters, J.M. & Powell, C.M. 1993. Regional structural evolution of the North Sea: oblique slip and the reactivation of basement lineaments. In: Parker, J.R. (ed.) *Petroleum Geology of Northwest Europe: Proceedings of the 4th Conference,* 1109-1122.

Bartov, Y., Steinitz, G., Eyal, M & Eyal, Y. 1980. Sinistral movement along the Gulf of Aqaba – its age and relation to the opening of the Red Sea. *Nature,* **285**, 220-222.

Beach, A. 1985. Some comments on sedimentary basin development in the Northern North Sea. *Scottish Journal of Geology,* **21**, 493-512.

Behn, M.D., Lin, J. & Zuber, M.T. 2002. A continuum mechanics model for normal faulting using a strain-rate softening rheology: implications for thermal and rheological controls on continental and oceanic rifting. *Earth and Planetary Science Letters***, 202**, 725-740.

Bellingham, P. & White, N. 2000. A general inverse method for modelling extensional sedimentary basins. *Basin Research,* **12**, 219-226.

Berger, M. & Roberts, A.M. 1999. The Zeta Structure: a footwall degradation complex formed by gravity sliding on the western margin of the Tampen Spur, Northern North Sea. In: Fleet, A.J. & Boldy, S.A.R. (eds.) *Petroleum Geology of Northwest Europe: Proceedings of the 5th Conference,* 107-116.

Bertram, G.T. & Milton, N.J. 1989. Reconstructing basin evolution from sedimentary thickness; the importance of paleobathymetric control with reference to the North Sea. *Basin Research,* **1**, 247-257.

Billiris, H., Paradissis, D., Veis, G., England, P., Featherstone, W., Parsons, B., Cross, P., Rands, P., Rayson, M., Sellers, P., Ashkenazi, V., Davison, M., Jackson, J. & Ambraseys, N. 1991. Geodetic determination of tectonic deformation in central Greece from 1900 to 1988. *Nature,* **350**, 124-129.

Bosworth, W. 1985. Geometry of propagating continental rifts. *Nature,* **316**, 625-627.

Brooks, M. & Ferentinous, G. 1984. Tectonics and sedimentation in the Gulf of Corinth and the Zakynthos and Kefallinia Channels, Western Greece. *Tectonophysics,* **101**, 25-54.

Brown, S., Richards, P.C. & Thompson, A.R. 1987. Patterns in the deposition of the Brent Group (Middle Jurassic) UK North Sea. In: Brooks, J. & Glennie, K. (eds.) *Petroleum Geology of Northwest Europe,* 899-913.

Buddings, M.C. & Inglin, H.F. 1981. A reservoir geological model of the Brent Sands in southern Cormorant. In: Illing, L.V. & Hobson, G.D. (eds.), *Petroleum Geology of the continental shelf of northwest Europe*, 326-334.

Bulat, J. 2005. Some considerations on the interpretation of seabed images based on commercial 3D seismic in the Faroe-Shetland Channel. *Basin Research,* **17**, 21-42.

Burke, K. 1977. Aulacogens and continental break-up. *Annual Review - Earth Planetary Science,* **5**, 371-396.

Burke K. & Dewey, J.F. 1973. Plume-generated triple junctions – Key indicators in applying plate tectonics to old rocks. *Journal of Geology,* **81**, 406-433.

Busk, H.G. 1929. *Earth Flexures*. Cambridge University Press.

Cartwright. J.A. 1991. The kinematic evolution of the Coffee Soil Fault. In: Roberts, A.M. & Yielding, G. & Freeman, B. (eds.). *The Geometry of Normal Faults,* Special Publication of the Geological Society, London, **56**, 29-40.

Cartwright. J.A., Trudgill, B.D. & Mansfield, C.S. 1995. Fault growth by segment linkage: and explanation for scatter in maximum displacement and trace length data from the Canyonlands Graben of SE Utah. *Journal of Structural Geology,* **17**, 1319-1326.

Cartwright. J.A., Mansfield, C.S. & Trudgill, B.D. 1996. The growth of normal faults by segment linkage. In: Buchanan, P.G. & Nieuwland, D.A. (eds.) *Modern Developments in Structural Interpretation, Validation and Modelling.* Special Publication of the Geological Society, London, **99***,* 163-177.

Chauvin, A.L. & Valachi, L.Z. 1980. Sedimentology of the Brent and Statfjord Formation of Statfjord Field. In: *The sedimentation of North Sea reservoir rocks*. Norsk Petroleumsforening, Geilo.

Childs, C., Watterson J. & Walsh J.J. 1995. Fault overlap zones within developing normal-fault systems. *Journal of the Geological Society, London***, 152**, 535-549.

Chénet, P.Y. & Letouzey, J. 1983. Tectonique de la zone comprise entre Abu Durba et Gebel Mezzazat (Sinai Egypte) dans le contexte de evolution du rift de Suez. *Bulletin Centres Recherche Exploration-Production, Elf-Aquitaine,* **7**, 201-215.

Christiansson, P., Faleide, J.I. & Berge, A.M. 2000. Crustal structure in the northern North Sea: an integrated geophysical study, In: Nøttvedt, A. (ed.), *Dynamics of the Norwegian Margin*. Special Publication of the Geological Society, London, **167**, 15-40.

Clarke, P.J., Davies, R.R., England, P.C., Parsons, B.E., Billiris, H., Paradissis, D., Veis, G., Denys, P.H., Cross, P.A., Ashkenazi, V. & Bingley, H. 1997. Geodetic estimate of seismic hazard in the Gulf of Korinthos. *Geophysical Research Letters,* **24**, 1303-1306.

Cloos, H. 1928. Experimente zur inneren tektonik. *Centralblatt fur Mineralogie,* **Abt. B**, 609-621.

Cloos, H. 1930. Kunstliche gebirge, II. *Natur und Museum,* **60**, 258-269.

Cloos, E. 1968. Experimental analysis of Gulf Coast fracture patterns. *American Association of Petroleum Geologists Bulletin,* **52**, 420-444.

Cochran, J.R. 1983. A model for Development of the Red Sea. *American Association of Petroleum Geologists Bulletin,* **67**, 41-69.

Colletta, B., Le Quellec, P., Letouzey, J. & Moretti, I. 1988. Longitudinal evolution of the Suez rift structure (Egypt). *Tectonophysics,* **153**, 221-233.

Contreras, J., Scholz, C.H. & King, G.C.P. 1997. A model of rift basin evolution constrained by first-order stratigraphic observations. *Journal of Geophysical Research,* **102**, 7673-7690.

Contreras J., Anders M.H. & Scholz C.H. 2000. Growth of a normal fault system: observations from the Lake Malawi basin of the east African rift. *Journal of Structural Geology,* **22**, 159-168.

Corfield, S. & Sharp, I.R. 2000. Structural Style and stratigraphic architecture of fault propagation folding in extensional settings: a seismic example from the Smørbukk area, Halten Terrace, Mid-Norway. *Basin Research,* **12**, 329-341.

Cornford, C. 1990. Source rocks and hydrocarbons of the North Sea. In: Glennie, K.W. (ed.) Introduction to the Petroleum Geology of the North Sea. 376-462.

Coutts, S.D., Larsson, S.Y. & Rosman, R. 1996. Development of the slumped crestal area of the Brent Reservoir, Brent Field: an integrated approach. *Petroleum Geoscience*, **2**, 219-229.

Coward, M.P. 1986. Heterogeneous stretching, simple shear and basin development. *Earth and Planetary Science Letters,* **80**, 325-336.

Coward, M.P., Dewey, J.F., Hempton, M. & Holroyd, J. 2003. Chapter 2 – Tectonic Evolution. In: Evans, D., Graham, C., Amour, A. & Bathurst, P. (eds.), *The Millennium Atlas: Petroleum Geology of the Central and Northern North Sea.* The Geological Society, London. 17-34.

Cowie, P.A., 1998. A healing-reloading feedback control on the growth rate of seismogenic faults. *Journal of Structural Geology,* **20**, 1075-1087

Cowie, P.A., Gupta, S. & Dawers, N.H. 2000. Implications of fault array evolution for synrift depocentre development: insights from a numerical fault growth model. *Basin Research,* **12**, 241-261.

Cowie, P.A. & Scholz, C.H. 1992a. Physical explanation for the displacement-length relationship of faults using a post-yield fracture mechanics model. *Journal of Structural Geology,* **14**, 1133-1148.

Cowie, P.A. & Scholz, C.H. 1992b. Displacement-length scaling relationship for faults: data synthesis and discussion. *Journal of Structural Geology,* **14**, 1149-1156.

Cowie, P.A. & Roberts, G.P. 2001. Constraining slip rates and spacings for active normal faults. *Journal of Structural Geology,* **23**, 1901-1915.

Cowie, P.A., Underhill, J.R., Behn, M., Lin, J. & Gill, C.E. 2005. Spatio-temporal evolution of strain accumulation derived from multi-scale observations of Late Jurassic rifting in the northern North Sea: A critical test of models for lithospheric extension. *Earth and Planetary Science Letters,* In press.

Dahl, N. & Solli, T. 1993. The structural evolution of the Snorre Field and surrounding areas. In: Parker, J.R. (ed.) *Petroleum Geology of Northwest Europe: Proceedings of the 4th Conference,* 1159-1166.

Dart, C.J., Collier, R.E.Ll., Gawthorpe, R.L. Keller, J.V.A. & Nichols, G. 1994. Sequence stratigraphy of (?)Pliocene-Quaternary synrift Gilbert-type fan deltas, northern Peloponnesus, Greece. *Marine and Petroleum Geology,* **11**, 543-560.

Dart, C., Cohen, H., Akyuz, H. & Barka, A. 1995. Basinward migration of rift-border faults: implications for facies distributions and preservation potential. *Geology,* **23**, 69-72.

Davies, S.J., Turner, J.D. & Underhill, J.R. 2001. Sequential dip-slip fault movement during rifting: a new model for the evolution of the Jurassic trilete North Sea rift system. *Petroleum Geoscience,* **7**, 371-388.

Davies, S.J., Dawers, N.H., McLeod, A.E. & Underhill, J.R. 2000. The structural and sedimentological evolution of early synrift successions: The middle Jurassic Tarbet Formation, North Sea. *Basin Research,* **12**, 343-365.

Davison, I. 1989. Extensional domino fault tectonics: Kinematics and geometrical constraints. *Annales Tectonicae,* **III**, 12-24.

Dawers, N. H., Anders, M. H. & Scholz, C. H. 1993 Growth Of Normal Faults - Displacement-Length Scaling, *Geology*, **21**, 1107-1110.

Dawers, N.H. & Anders, M.H. 1995. Displacement-length scaling and fault linkage. *Journal of Structural Geology,* **17**, 607-614.

Dawers, N.H. & Underhill, J.R. 2000. The role of Fault Interaction and Linkage in Controlling Synrift Stratigraphic Sequences: Late Jurassic, Statfjord East Area, Northern North Sea. *American Association of Petroleum Geologists Bulletin,* **84**, 45-64.

De'ath, N.G. & Schuyleman, S.F. 1981. The geology of the Magnus oilfield. In: Illing, L.V. & Hobson, G.D. (eds.), *Petroleum Geology of Northwest Europe*, 342-351.

Deegan, C.E. & Scull, B.J. 1977. A proposed standard lithostratigraphic nomenclature for the central and northern North Sea. *Report of the Institute of Geological Sciences,* No 77/25; *Bulletin of the Norwegian Petroleum Directorate,* No 1.

Destro, N., Chagas, L.S., Chiossi, D.S.N., Machado, E.C.V. & Masiero, G.H.N. 1990. Sistema em relay assiado a regime extensional na borda oeste da Bacia de Sergipe-Alagoas: *Thirty-sixth Congresso Brasilerio de Geologia, Natal, SBG-Núcleo Nordeste,* **5**, 2226-2237.

Destro, N. 1995. Release Fault: A variety of cross fault in linked extensional faults systems, in the Sergipe-Alagoas Basin, NE Brazil. *Journal of Structural Geology*, **17**, 615-629.

Destro, N., Szatmari, P., Alkmim, F.F. & Magnavita, L.P. 2003. Release faults, associated structures, and their control on petroleum trends in the Recôncavo rift, northeast Brazil. *American Association of Petroleum Geologists Bulletin,* **87**, 1123-1144.

Doré, A.G., Hamar, G.P., Lilleng, T., Shaw, N.D., Skarpnes, O. & Vollset, J. 1984. In: Vollset, J. & Doré, A.G. (eds.). *A revised Triassic and Jurassic lithostratigraphic nomenclature for the Norwegian North Sea.* Norwegian Petroleum Directorate Bulletin, Number 3.

Doutsos, T., Kontopoulos, N. & Poulimenos, G. 1988. The Corinth-Patras rift as the initial stage of continental fragmentation behind an active island arc (Greece). *Basin Research* **1**, 177-190.

Ebinger, C.J., Jackson, J.A., Foster, A.N. & Hayward, N.J. 1999. Extensional basin geometry and the elastic lithosphere. *Philosophical Transactions of the Royal Society of London,* **357,** 741-765.

Ellis, P.G. & McClay, K.R. 1988. Listric extensional fault systems – results of analogue model experiments. *Basin Research*, **1**, 55-70.

Engelstad, N. 1987. Murchison. In: Spencer, A.M. (ed.) Geology of the Norwegian Oil and Gas Fields. Graham and Trotman, London. 295-306.

Eynon, G. 1981. Basin development and sedimentation in the Middle Jurassic of the northern North Sea. In: Illing, L.V. & Hobson, G.D. (eds.) *Petroleum Geology of the continental shelf of Northwest Europe,* 196-204.

Faerseth, R.B., Sjøblom, T.S., Steel, R.J., Liljedahl, T., Sauar, B.E. & Tjelland, T. 1995. Tectonic controls on Bathonian-Volgian syn-rift successions on the Visund fault block, northern North Sea. In: Steel, R.J. (ed). *Sequence Stratigraphy on the Northwest European Margin.* Norwegian Petroleum Society Special Publication, **5**, 325-346.

Faerseth, R.B. 1996. Interaction of Permo-Triassic and Jurassic extensional fault-blocks during the development of the northern North Sea. *Journal of the Geological Society, London,* **153**, 931-944.

Faerseth, R.B. & Ravnas, R. 1998. Evolution of the Oseberg Fault-Block in context of the northern North Sea structural framework. *Marine and Petroleum Geology,* **15**, 467-490.

Ferentinos, G., Papatheodorou, G. & Collins, M.B. 1988. Sediment transport processes on an active submarine fault escarpment: Gulf of Corinth, Greece. *Marine Geology,* **83**, 43-61.

Fraser, S.A., Robinson, A.M., Johnson, H.D., Underhill, J.R., Kadolsky, D.G., Connell, R., Johannssen, P. & Ravnas, R. 2003. Chapter 11 – Upper Jurassic. In: Evans, D., Graham, C., Amour, A. & Bathurst, P. (eds.), *The Millennium Atlas: Petroleum Geology of the Central and Northern North Sea.* The Geological Society, London. 157-190

Frost, R.E. 1987. The evolution of the Viking Graben tilted fault block structures: a compressional origin. In: Brooks, J. & Glennie, K. (eds.), *Petroleum Geology of Northwest Europe,* 1009-1024.

Galloway, W.E. 1989. Genetic sequence stratigraphic sequences in basin analysis 1. Architecture and genesis of flooding-surface bounded depositional units. *American Association of Petroleum Geologists Bulletin,* **73,** 125-142.

Garfunkel, Z. 1981. Internal structure of the Dead Sea leaky transform (rift) in relation to plate kinematics. *Tectonophysics,* **80**, 81-108.

Garfunkel, Z. & Bartov, Y. 1977. The tectonics of the Suez Rift. *Geological Survey of Israel Bulletin,* **71**, 1-44.

Gawthorpe, R.L., Fraser, A.J. & Collier, R.E. 1994. Sequence stratigraphy in active extensional basins: implications for the interpretations of ancient basin fills. *Marine and Petroleum Geology,* **11**, 642-658.

Gawthorpe, R.L., Sharp, I., Underhill, J.R. & Gupta, S. 1997. Linked sequence stratigraphic and structural evolution of propagating normal faults. *Geology,* **25**, 795-798.

Gawthorpe, R.L. & Leeder, M.R. 2000. Tectono-sedimentary evolution of active extensional basins. *Basin Research,* **12**, 195-218.

Gawthorpe, R.L., Jackson, C.A.-L., Young, M.J., Sharp, I.R., Moustafa, A.R. & Leppard, C.W. 2003. Normal fault growth, displacement localisation and the evolution of normal fault populations: the Hammam Faraun fault block, Suez Rift, Egypt. *Journal of Structural Geology,* **25**, 883-895.

Gibbs, A.D. 1983. Balanced cross-section construction from seismic lines in areas of extensional tectonics. *Journal of Structural Geology,* **5**, 153-160.

Gibbs, A.D. 1984. Structural evolution of extensional basin margins. *Journal of the Geological Society, London,* **141**, 609-620.

Gibbs, A.D. 1990. Linked Fault tectonics of the North Sea. In: Blundell, D.J. &. Gibbs, A.D. *Tectonic Evolution of the North Sea rifts*. 145-157.

Glennie, K.W. & Underhill, J.R. 1998. Origin, Development and Evolution of Structural Styles. In: Glennie, K.W. (ed.). *Petroleum geology of the North Sea: basic concepts and recent advances.* 4th ed. Oxford: Blackwell Science. 42-84.

Glennie, K.W., Higham, J. & Stemmerik, L. 2003. Chapter 8 - Permian. In: Evans, D., Graham, C., Amour, A. & Bathurst, P. (eds.), *The Millennium Atlas: Petroleum Geology of the Central and Northern North Sea.* The Geological Society, London. 91-104.

Goldsworthy, M. & Jackson, J.A. 2000. Active normal fault evolution in Greece revealed by geomorphology and drainage patterns. *Journal of the Geological Society, London,* **157**, 967-981.

Goldsworthy, M. & Jackson, J.A. 2001. Migration of activity within normal fault systems: examples from the Quarternary of mainland Greece. *Journal of Structural Geology,* **23**, 489-506.

Gradstein, F.M., Ogg, J.G. & Smith, A.G. (eds.) 2005. *A Geologic Timescale 2004*. Cambridge University Press.

Graue, E., Helland-Hanson, W., Johnsen, J., Lømo, L., Nøttvedt, A., Rønning, K., Ryseth, A. & Steel, R. 1987. Advance and retreat of the Brent Delta System, Norwegian North Sea. In: Brooks, J. & Glennie, K. (eds.) *Petroleum Geology of Northwest Europe,* 915-937.

Gray, W.D.T. & Barnes, G. 1981. The Heather Oil Field. In: Illing, L.V. & Hobson, G.D. *Petroleum Geology of the continental shelf of North-West Europe; Proceedings of the second conference*, 335-341.

Gupta, S., Cowie, P.A., Dawers, N.H. & Underhill, J.R. 1998. A mechanism to explain rift-basin subsidence and stratigraphic patterns through fault-array evolution. *Geology,* **26**, 595-598

Gupta, S., Underhill, J.R., Sharp, I.R. & Gawthorpe, R.L. 1999. Role of fault interactions in controlling synrift sediment dispersal patterns: Miocene, Abu Alaqa Group, Suez Rift, Sinai, Egypt. *Basin Research,* **11**, 167-189.

Gupta, S. & Cowie, P.A. 2000. Processes and controls in the stratigraphic development of extensional basins, *Basin Research,* **12**, 185-194.

Haq, B.U., Hardenbol, J. & Vail, P.R. 1988. Chronology of fluctuating sea levels since the Triassic (250 million years ago to present). *Science,* **235**, 1156-1167.

Hay, J.T.C. 1978. Structural development in the northern North Sea. *Journal of Petroleum Geology,* **1**, 65-77.

Hamblin, W.K. 1976. Patterns of displacement along the Wasatch Front. *Geology,* **4**, 619-622.

Hayward, N.J. & Ebinger, C.J. 1996. Variations in the along-axis segmentation of the Afar Rift system. *Tectonics,* **15**, 244-257.

Helland-Hansen, W., Steel, R., Nakayama, K. & Kendel, C.G.St C. 1989. Review and computer modelling of the Brent Group stratigraphy, In: Whateley, M.K.G. & Pickering, K.T. (eds.), *Deltas: sites and traps for fossil fuels*, Special Publication of the Geological Society, London*,* **41**, 237-252.

Helland-Hansen, W., Ashton, M., Lomo, L. & Steel, R. 1992. Advance and retreat of the Brent Delta. In: Morton, A.C., Haszeldine, R.S., Giles, M.R. & Broom, S. (eds.). *Geology of the Brent Group*. Special Publication of the Geological Society, London*,* **61**, 109-127.

Helmy, H.M. 1990. Southern Gulf of Suez, Egypt: structural geology of the B-trend oil fields. In: Brooks, J. (ed.) *Classic Petroleum Provinces,* Special Publication of the Geological Society, London, **50**, 353-363.

Hesjedal, A. & Hamar, G.P. 1083. Lower Cretaceous stratigraphy and tectonic of the south-southeastern Norwegian offshore. In: Kaasschieter, J.P.H. & Reijers, T.J.A (eds.), Petroleum Geology of the southeastern North Sea and the adjacent onshore areas. *Geologie et Mijnbouw,* **62**, 135-144.

Hesthammer, J. & Fossen, H. 1999. Evolution and geometries of gravitational collapse structures with examples from the Stafjord Field, northern North Sea. *Marine and Petroleum Geology,* **16**, 259-281.

Higgs, B. 1988. Syn-sedimentary structural controls on basin deformation in the Gulf of Corinth, Greece. *Basin Research,* **1**, 155-165.

Hodgkinson, K.M., Stein, R.S. & King, G.C.P. 1996. The 1954 Rainbow Mountain-Fairview Peak-Dixie Valley earthquakes: A triggered normal faulting sequence. *Journal of Geophysical Research,* **101**¸ 25459-25471.

Isaksen, D. & Tonstad, K (editors) 1989. A revised Cretaceous and Tertiary lithostratigraphic nomenclature for the Norwegian North Sea. *Bulletin of the Norwegian Petroleum Directorate,* No 5.

Ishikawa, M. & Otsuki, K. 1995. Effects of strain gradients on asymmetry of experimental normal faults systems. *Journal of Structural Geology,* **17**, 1047-1053.

Jackson, C.A.-L., Gawthorpe, R.L. & Sharp, I.R. 2002. Growth and linkage of the East Tanka fault zone, Suez rift: structural style and syn-rift stratigraphic response. *Journal of the Geological Society, London,* **159**, 175-187.

Jackson, J.A. 1987. Active normal faulting and crustal extension. In: Coward, M.P., Dewey, J.F. & Hancock, P.L. (eds.), *Continental Extensional Tectonics*, Special Publication of the Geological Society, London, **28**, 3-18.

Jackson, J.A. & McKenzie, D. 1983. The geometrical evolution of normal fault systems. *Journal of Structural Geology,* **5**, 471-482.

Jackson, J.A. & McKenzie, D. 1988. Rates of active deformation in the Aegean Sea and surrounding regions. *Basin Research,* **1**, 121-128.

Jackson, J.A., White, N.J., Garfunkel, Z. & Anderson, H. 1988. Relations between normal-fault geometry, tilting and vertical motions in extensional terrains: an example from the southern Gulf of Suez. *Journal of Structural Geology,* **10**, 155-170.

Jackson, J.A. & White, N.J. 1989. Normal faulting in the upper continental crust: observations from regions of active extension. *Journal of Structural Geology,* **11**, 15-36.

Jackson, J.A., King, G. & Vita-Finzi, C. 1982. The neotectonics of the Aegean: an alternative view. *Earth and Planetary Science Letters,* **61**, 303-318.

Jackson, J.A. and Blenkinsop, T. 1997. The Bilila-Mtakataka fault in Malawi: An active, 100km long, normal fault segment in thick seismogenic crust. *Tectonics,* **16**, 137-150

Jarvis, G.T. & McKenzie, D.P. 1980. Sedimentary basin formation with finite extension rates. *Earth and Planetary Science Letters,* **48**, 42-52.

Johnson, A. & Eyssautier, M. 1987. Alwyn North Field and its regional geological context. In: Brooks, J. & Glennie, K. (eds.) *Petroleum Geology of Northwest Europe.* 963-977.

Johnson, H., Richards, P.C., Long, D. & Graham, C.C. 1993. *United Kingdom offshore regional report: the geology of the Northern North Sea.*

Kautz, S.A. & Schlater, J.G. 1988. Internal deformation in clay models of extension by block faulting. *Tectonics*, **7**, 823-832.

Kearey, P. & Brooks, M. 1991. *An introduction to Geophysical Exploration*. Blackwell Science, Oxford.

Keefer, D.K. 1984. Landslides caused by earthquakes. *Geological Society of America Bulletin,* **95**, 406-421.

Keefer, D.K. 1999. Earthquake-induced landslides and their effects on alluvial fans. *Journal of Sedimentary Research,* **69***,* 84-104.

Kirk, R.J. 1980. Statfjord Field: a North Sea giant. In: Halbouty, M.T. (ed) Giant oil and gas fields of the decade. *American Association of Petroleum Geologists* Memoir*,* **30**, 95-116.

Kissel, C. & Laj, C. 1988. The Tertiary geodynamic evolution of the Aegean Arc: a paleomagnetic reconstruction. *Tectonophysics,* **146**, 183-201.

Kusznir, N.J. & Park, R.G. 1987. The extensional strength of the continental lithosphere: its dependence on geothermal gradient, and crustal composition and thickness. In: Coward, M.P., Dewey, J.F. & Hancock, P.L. (eds.), *Continental Extensional Tectonics,* Special Publication of the Geological Society, London*,* **28**, 35-52.

Kusznir, N.J., Marsden, G. & Egan, S.S. 1991. A flexural-cantilever simple-shear/pure-shear model of continental lithosphere extension: applications to the Jeanne d'Arc Basins, Grand Banks and Viking Graben North Sea. In: Roberts, A.M., Yielding, G. & Freeman, B. (eds.), *The Geometry of Normal Faults,* Special Publication of the Geological Society, London*,* **56**, 41-60.

Leeder, M.R., Seger, M. & Stark, C.P. 1991. Sedimentology and tectonic geomorphology adjacent to active and inactive normal faults in the Megara Basin and Alykonides Gulf, Central Greece. *Journal of the Geological Society London,* **148**, 331-343.

Leeder, M.R. & Jackson, J.A. 1993. The interaction between normal faulting and drainage in active extensional basins, with examples from the western United States and central Greece. *Basin Research,* **5**, 79-102.

Le Pichon, X. & Angelier, J. 1979. The Hellenic are and trench system: a key to the neotectonic evolution of the eastern Mediterranean area. *Tectonophysics,* **60**, 1-42.

Letouzey, J. 1986. Cenozoic paleostress pattern in the Alpine Foreland and structural interpretation in a platform basin, *Tectonophysics,* **132**, 215-231.

Livera, S.E. & Gdula, J.E. 1990. Brent Oil Field. In: Beaumont, E.A. & Foster, N.H. (eds.) *Structural traps II, Traps associated with tectonic faulting.* Atlas of Oil and Gas Fields, *American Association of Petroleum Geologists Memoir,* 21-63.

Loomis, K.B. & Ingle, J.C. 1994. Subsidence and uplift of the Late Cretaceous-Cenozoic margin of California: New evidence from the Gualala and Point Arena basins. *Geological Society of America Bulletin,* **106**, 915-931.

Ma, X.Q. & Kusznir, N.J. 1993. Modelling of near-field subsurface displacements for generalised faults and fault arrays. *Journal of Structural Geology,* **15**, 1471-1484.

Ma, X.Q. & Kusznir, N.J. 1995. Coseismic and postseismic subsurface displacements and strains for a dip-slip normal fault in a three-dimensional clastic gravitational medium. *Journal of Geophysical Research,* **100**, 12813-12828.

Mansfield, C. & Cartwright, J. 2001. Fault growth by linkage: observations and implications from analogue models. *Journal of Structural Geology,* **23**, 745-763.

McClay, K.R. 1990. Extensional fault systems in sedimentary basins – A review of analogue model studies. *Marine and Petroleum Geology,* **7**, 206-238.

McClay, K. & White, M. 1995. Analogue models of orthogonal and oblique rifting. *Marine and Petroleum Geology,* **12**, 137-151.

McClay K. & Khalil S. 1998. Extensional hard linkages, eastern Gulf of Suez, Egypt *Geology,* **26**, 563-566.

McClay, K., Dooley, T., Whitehouse, P. & Mills, M. 2002. 4-D evolution of rift systems: Insights from scaled physical models. *American Association of Petroleum Geologists Bulletin***, 86**, 935-959.

McKenzie, D.P. 1978. Some remarks on the development of sedimentary basins. *Earth and Planetary Science Letters,* **40**, 25-32.

McLeod, A.E. 2000. The control of fault array evolution on sediment dispersal and footwall degradation in rift systems. *University of Edinburgh PhD thesis.*

McLeod, A.E., Dawers, N.H. & Underhill, J.R. 2000. The propagation and linkage of normal faults: insights from the Strathspey-Brent-Statfjord fault array, northern North Sea. *Basin Research,* **12**, 263-284.

McLeod, A.E. & Underhill, J.R. 1999. Processes and products of footwall degradation, northern Brent Field, Northern North Sea. In: Fleet, A.J. & Boldy, S.A.R. (eds.) *Petroleum Geology of Northwest Europe: Proceedings of the 5th conference,* 91-106.

McLeod, A.E., Underhill, J.R., Davies, S.J. & Dawers, N. H. 2002. The influence of fault array evolution on synrift sedimentation patterns: Controls on deposition in the Strathspey-Brent-Statfjord half graben, northern North Sea. *American Association of Petroleum Geologists Bulletin,* **86**, 1061-1093.

McMurray, L.S. & Gawthorpe, R.L. 2000. Along-strike variability of forced regressive deposits: late Quarternary, northern Peloponnesus, Greece. In: Hunt, D. & Gawthorpe, R.L. (eds.). *Sedimentary Responses to Forced Regressions.* Special Publication of the Geological Society, London, **172**, 363-377.

McNeill, L. C. & Collier, R. E. L., 2004. Uplift and slip rates of the eastern Eliki fault segment, Gulf of Corinth, Greece, inferred from Holocene and Pleistocene terraces, *Journal of the Geological Society*, London, **161**, 81-92.

Meinesz, F.A.V. 1950.Les grabens africains, résultat de compression ou le tension dans la croûte terrestre? *A.V. Koninki. Belg. Kol. Inst. Bull*., **21,** 539-552

Meyer, V., Nicol, A., Childs, C., Walsh, J.J. & Watterson, J. 2002. Progressive localisation of strain during the evolution of a normal fault population. *Journal of Structural Geology.* **24**, 1215-1251.

Morton, A.C. 1985. A new approach to provenance studies: electron microprobe analysis of detrital grains from Middle Jurassic sandstones of the northern North Sea. *Sedimentology,* **32**, 553-566.

Morton, W.H. & Black, R. 1975. Crustal attenuation in Afar. In: Pilgar, A. & Roslier, A. (eds.). Afar depression of Ethiopia, Inter-Union Commission on Geodynamics. Proceedings of International Symposium on the Afar Region and related rift problems. E. Schweizerbart'sche Verlagsbuchhandlung. Stuttgart. Germany. Scientific Report No. 14, 55-65.

Moustafa, A.M. 1976. Block faulting in the Gulf of Suez. *Egyptian General Petroleum Corporation, Fifth Exploration Seminar.*

Moustafa, A.R. 2002. Controls on the geometry of transfer zones in the Suez rift and northwest Red Sea: Implications for the structural geometry of rift systems. *American Association of Petroleum Geologists Bulletin,* **86**, 979-1002.

Moustafa, A.R. 1993. Structural characteristics and tectonic evolution of the east-margin blocks of the Suez rift. *Tectonophysics,* **223**, 381-399.

Odinsen, T., Christiansson, P., Gabrielsen, R.H., Faleide, J.J. & Berge, A.M. 2000. The geometries and deep structure of the northern North Sea rift system. In: Nøttvedt (ed), *Dynamics of the Norwegian Margin.* Special Publication of the Geological Society, London, **167**, 41-57.

Oertel, G. 1965. The mechanism of faulting in clay experiments. *Tectonophysics,* **2**, 1-20.

Parsons, T. 2002. Global Omori law decay of triggered earthquakes: Large aftershocks outside the classical aftershock zone. *Journal of Geophysical Research,* **107**, 2199-2219.

Partington, M.A., Mitchener, B.C., Milton, N.J. & Fraser, A.J. 1993a. Genetic sequence stratigraphy for the North Sea Late Jurassic and early Cretaceous: distribution and prediction of Kimmeridgian-Late Ryazanian reservoirs in the North Sea and adjacent areas. In: Parker, J.R. (ed), *Petroleum Geology of Northwest Europe: Proceedings of the 4th Conference,* 347-370.

Partington, M.A., Copestake, P., Mitchener, B.C. & Underhill, J.R. 1993b. Biostratigraphic calibration of genetic stratigraphic sequences in the Jurassic-lowermost Cretaceous Hettangian to Ryazanian of the North Sea and adjacent areas. In: Parker, J.R. (ed), *Petroleum Geology of Northwest Europe: Proceedings of the 4th Conference,* 371-386.

Patton, T.L. & Nelson, R.A. 1988. Rift offsets, Gulf of Suez, Egypt. *American Association of Petroleum Geologists Bulletin,* **72**, 233-233.

Patton, T.L., Moustafa, A.R., Nelson, R.A. & Abdine, S.A. 1994. Tectonic evolution and Structural Setting of the Suez Rift. *American Association of Petroleum Geologists Memoir,* **59**, 9-55.

Peacock, D.C.P & Sanderson, D.J. 1993**.** Estimating strain using a line sample. *Journal of Structural Geology,* **15**, 1513-1516.

Peacock, D.C.P & Sanderson, D.J. 1994. Geometry and development of relay ramps in normal fault systems. *American Association of Petroleum Geologists Bulletin,* **78**, 147-165.

Peterson, F. 1985. Equilibrium tendency in piedmont scarp denudation, Watatch Front, Utah. In: Morisawa, M. & Hack, J.T. *Tectonic Geomorphology,* Allen and Unwin, Boston. 209-233.

Pickering, G., Peacock, D.C.P., Sanderson, D.J. & Bull, J.M. 1997. Modelling tip zones to predict the throw and length characteristics of faults. *American Association of Petroleum Geologists Bulletin,* **81**, 82-99.

Poulsen, N.E. & Riding, J.B. 2003. The Jurassic dinoflagellate cyst zonation of subboreal northwest Europe. In: Ineson, J.R. & Surlyk, F. (eds.). *The Jurassic of Denmark and Greenland, Geological Survey of Denmark and Greenland Bulletin,* **1**, 115-144.

Proffert, J.M. 1987. Cenozoic geology of the Yerington District, Nevada, and implications for the nature and origin of Basin and Range faulting. *Geological Society of America Bulletin,* **88**, 247-266.

Prosser, S. 1993. Rift-related linked depositional systems and their seismic expression. In: Williams, G.D. & Dobb, A. (eds.). *Tectonics and Sequence Stratigraphy,* Special Publication of the Geological Society, London, **71**, 35-66.

Quennell, A.M.1958. The structural and geomorphic evolution of the Dead Sea rift: *Quarterly Journal of the Geological Society, London,* **114**, 1-24.

Ramberg, A.B. & Morgan, P. 1984. Physical characteristics and evolutionary trends of continental rifts. *Proceedings of the 27th International Geological Congress,* **7**, 165-216.

Ransome, F.L., Emmons, W.H. & Garrey, G.H. 1910. Geology and ore deposits of the Bullfrog District, Nevada. *United States Geological Society Bulletin,* **407**, 1-130.

Rattey, R.P. & Hayward, A.B. 1993. Sequence stratigraphy of a failed rift system: the middle Jurassic to Cretaceous basin evolution of the Central and Northern North Sea. In: Parker, J.K. (ed), *Petroleum Geology of Northwest Europe: Proceedings of the 4th Conference,* 215-249.

Ravnås, R. & Bondevik, K. 1997. Architecture and controls on Bathonian-Kimmeridgian shallow-marine synrift wedges of the Oseberg-Brage area, northern North Sea. *Basin Research,* **9**, 197-226.

Ravnås, R., Bondevik, K., Helland-Hansen, W., Lømo, L., Ryseth, A. & Steel, R.J. 1997. Sedimentation history as an indicator of rift initiation and development: the late Bajocian-Bathonian evolution of the Oseberg-Brage area, northern North Sea. *Norske Geologica Tiddsk.,* **77**, 205-232.

Rawson, P.F. & Riley, L.A. 1982. Latest Jurassic-Early Cretaceous events and the "Late Cimmerian Unconformity" in the North Sea area. *American Association of Petroleum Geologists Bulletin,* **66**, 2628-2648.

Richards, P.C. 1990. The early to mid-Jurassic evolution of the Northern North Sea. In: Hardman, R.F.P. & Brooks, J. (eds.). *Tectonic events responsible for Britain's Oil and Gas Reserves,* Special Publication of the Geological Society, London, **55**, 191-205.

Rippon, J.H. 1985. Contoured patterns of the throw and hade of normal faults in the Coal Measures (Westphalian) of north-east Derbyshire. *Proceedings of the Yorkshire Geological Society,* **45**, 147-161.

Roberts, A.M. & Yielding, G. 1991. Deformation around basin-margin faults in the North Sea/mid-Norway rift. In: Roberts, A.M., Yielding, G. & Freeman, B. (eds.) 1991. *The Geometry of Normal Faults,* Special Publication of the Geological Society, London*,* **56**, 61-78.

Roberts, A.M., Yielding, G. & Badley, M.E. 1993. Tectonic and bathymetric controls on stratigraphic sequences within evolving half-graben. In: Williams, G.D. & Dobb, A. (eds.) *Tectonics and Sequence Stratigraphy.* Special Publication of the Geological Society, London*,* **71**, 87-121.

Roberts, A.M. & Yielding, G. 1994. Continental Extension Tectonics. In: Hancock, P.L. (ed). *Continental Deformation*, Permagon Press, Oxford. pp 233-250.

Roberts, G.P. 1996. Non characteristic normal faulting surface ruptures from the Gulf of Corinth, Greece. *Journal of Geophysical Research,* **101,** 25255-25267.

Roberts, S. & Jackson, J.A. 1991. Active normal faulting in central Greece: an overview. In: Roberts, A.M., Yielding, G. & Freeman, B. (eds.), *The Geometry of normal faults*, Special Publication of the Geological Society, London*,* **56**, 125-142.

Robson, D.A. 1971. The structure of the Gulf of Suez (Clysmic) rift, with special reference to the eastern side. *Quarterly Journal of the Geological Society, London,* ***127***, 247-253.

Røe, S.L. & Steel, R. 1985. Sedimentation, sea-level rise and tectonics at the Triassic-Jurassic boundary: Statfjord Formation, Tampen Spur, northern North Sea. *Journal of Petroleum Geology,* **8,** 163-186.

Ryseth, A. 1989. Correlation of depositional patterns in the Ness Formation, Oseberg area. In: Collinson, J.D. (ed), *Correlation in hydrocarbon exploration,* 313-326.

Schlische, R.W. 1991. Half-graben basin filling models: New constraints on continental extensional basin development. *Basin Research,* **3**, 123-141.

Schlische, R.W., Young, S.S., Ackermann, R.V. & Gupta, A. 1996. Geometry and scaling relations of a population of very small rift-related normal faults. *Geology,* **24**, 683-686.

Scholz, C.H. 1990. *The mechanics of earthquakes and faulting.* Cambridge University Press.

Scholz, C.H. & Contreras, J.C. 1998. Mechanics of continental rift architecture. *Geology,* **26** 967-970.

Schulte, W.M., Van Rossem, P.A.H. & Van de Vijver, W. 1994. Current challenges in the Brent Field. *Journal of Petroleum Technology,* **46**, 1073-1079.

Selwood, B.W. & Netherwood, R.E. 1984. Facies evolution in the Gulf of Suez area: Sedimentation history as an indicator of rift initiation and development. *Modern Geology,* **9**, 43-69.

Schimazaki, K. 1986. Small and large earthquakes: the effects of the thickness of the seismogenic layer and the free surface. In: Das, S., Boatwright, J. & Scholz, C.H. (eds.), *Earthquake Source Mechanics. American Geophysical Union, Geophysical Monographs*, **37**, 209-216.

Sheriff, R.E. 1985. Aspects of seismic resolution. In: Berg, O.R. & Woolverton, D.G. (eds.), *Seismic Stratigraphy II; an integrated approach to hydrocarbon exploration. American Association of Petroleum Geologists Memoir,* **39**, 1-10.

Sorel, D. 2000. A Pleistocene and still-active detachment fault and the origin of the Corinth-Patras rift, Greece. *Geology*, **28**, 83-86.

Steckler, M.S. & Ten Brink, U.S. 1986. Lithospheric strength as a control on new plate boundaries: examples from the northern Red Sea region. *Earth and Planetary Science Letters*, **79**, 120-132.

Steel, R.J. 1993. Triassic-Jurassic megasequence stratigraphy in the northern North Sea: rift to post-rift evolution. In: Parker, J.R. (ed), *Petroleum Geology of Northwest Europe: Proceedings of the 4th conference,* 299-315.

Stein, R.S. & Barrientos, S.E., 1985. Planar high-angle faulting in the Basin and Range: Geodetic analysis of the 1983 Borah Peak, Idaho, Earthquake. *Journal of Geophysical Research,* **90**, 11355-11366.

Stewart, I.S. & Hancock, P.L. 1988. Normal fault zone evolution and fault scarp degradation in the Aegean region. *Basin Research,* **1**, 139-153.

Stewart, S.A. 2001. Displacement distributions on extensional faults: Implications for fault stretch, linkage, and seal. *American Association of Petroleum Geologists Bulletin,* **85**, 587-599.

Stow, D.A.V. & Atkin, B. 1987. Sediment facies and geochemistry of Upper Jurassic mudrocks in the central North Sea area. In: Brooks, J. & Glennie, K.W. (eds.) *Petroleum Geology of Northwest Europe,* 797-808.

Taymaz, T, Jackson, J.A. & McKenzie, D. 1991. Active tectonics of the north and central Aegean Sea. *Geophysical Journal International,* **106**, 433-490.

Thomson, K. & Underhill, J.R. 1993. Controls on the development and evolution of structural styles in the Inner Moray Firth Basin. In: Parker, J.R. (ed.), *Petroleum Geology of Northwest Europe: Proceedings of the 4th Conference,* 1167-1178.

Tomasso, M., Underhill, J.R., Hodgkinson, R.A. & Young, M.J. In Press. Structural styles and depositional architecture in the Triassic of the Ninian and Alwyn North Fields:

Implications for basin development and prospectivity in the Northern North Sea. *Marine and Petroleum Geology.*

Trudgill, B.D. & Cartwright, J.A. 1994. Relay ramp forms and normal fault linkages – Canyonlands National Park, Utah. *Bulletin of the Geological Society of America,* **106**, 1143-1157.

Underhill, J.R. 1991. Implications of Mesozoic-Recent basin development in the western Inner Moray Firth, UK. *Marine and Petroleum Geology,* **8**, 377-380.

Underhill, J.R. 1991. Controls on Late Jurassic seismic sequences, Inner Moray Firth, UK North Sea: a critical test of a key segment of Exxon's original global cycle chart. *Basin Research,* **3**, 79-98.

Underhill, J.R.1998. Jurassic. In: Glennie, K.W. (ed.). Petroleum geology of the North Sea: basic concepts and recent advances. 4th ed. Blackwell Science, Oxford. 245-293.

Underhill, J.R. 2003. The tectonic and stratigraphic framework of the United Kingdom's oil and gas fields. In: Gluyas, J.G. & Hichens, H.M. (eds.). *United Kingdom Oil and Gas Fields, Commemorative Millennium Volume.* Geological Society of London, Memoir, **20**, 17-59.

Underhill, J.R. & Partington, M.A. 1993. Jurassic thermal doming and deflation in the North Sea: implications of the sequence stratigraphic evidence. In: Parker. J.R. (ed.), *Petroleum Geology of Northwest Europe; Proceedings of the 4th Conference,* 337-345.

Underhill, J.R. & Partington, M.A. 1994. Use of maximum flooding surfaces in determining a regional control on the Intra-Aalenian Mid Cimmerian sequence boundary: implications of North Sea basin development and Exxon's Sea-Level chart. In: Posamentier, H.W. & Wiemer, P.J. (eds.), *Recent advances in siliciclastic sequence stratigraphy, American Association of Petroleum Geologists Memoir,* **58**, 449-484.

Underhill, J.R., Sawyer, M.J., Hodgson, P., Sahllcross, M.D. & Gawthorpe, R.L. 1997. Implications of fault scarp degradation for Brent Group prospectivity, Ninian Field, Northern North Sea. *American Association of Petroleum Geologists Bulletin,* **81**, 999-1022.

Vendeville, B. 1987. Champs de failles et tectonique en extension: modélisation expérimentale. PhD thesis. Université de Rennes (France).

Walsh, J.J.& Watterson, J. 1991. Geometric and kinematic coherence and scale effects in normal fault systems. In: Roberts, A.M., Yielding, G. & Freeman, B. (eds.), 1991, *The Geometry of normal faults* Special Publication of the Geological Society, London, **56**, 193-206.

Watterson, J. 1986. Fault dimensions, displacements and growth. *Pure and applied Geophysics,* **124**, 365-393.

White, N.J. 1990. Does the uniform stretching model work in the North Sea? In: Blundell, D.J. & Gibbs, A.D. (eds.), *Tectonic Evolution of the North Sea Rifts*, Oxford University Press.

Withjack, M.O. & Jamison, W.R. 1986. Deformation produced by oblique rifting. *Tectonophysics,* **126**, 99-124.

Withjack, M.O., Islam, Q. & LaPointe, P. 1995. Normal faults and their hangingwall deformation – an experimental study. *American Association of Petroleum Geologists Bulletin*, **79**, 1-18.

Woodworth, P.L., Tsimplis, M.N., Flather, R.A. & Shennan, I. 1999. A review of the trends observed in British Isles mean sea level data measured by tide gauges. Geophysical Journal International, 136, 651-670.

Woolam, R. & Riding, J.B. 1983. *Dinoflagellate Cyst Zonation of the British Jurassic.* Report No. **83/2**, Institute of Geological Science.

Wu, D. & Bruhn, R.L. 1994. Geometry and kinematics of active normal faults, South Quirrh Mountains, Utah: implications for fault growth. *Journal of Structural Geology,* **16**, 1061-1076.

Yielding, G. 1990. Footwall uplift associated with Late Jurassic normal faulting in the northern North Sea. *Journal of the Geological Society, London,* **147**, 219-222.

Yielding, G., Badley, M.E. & Roberts, A.M. 1992. The structural evolution of the Brent Group. In: Morton, A.C., Haszeldine, R.S., Giles, M.R. & Brown, S. (eds.), 1992, *Geology of the Brent Group.* Special Publication of the Geological Society, London, **61**, 27-43.

Young, M.J., Gawthorpe, R.L. & Hardy, S. 2001. Growth and linkage of a segmented normal fault zone: the Late Jurassic Murchison-Statfjord North Fault, northern North Sea. *Journal of Structural Geology,* **23**, 1933-1952.

Zanella, E. & Coward, M.P. 2003. Chapter 4 - Structural Framework. In: Evans, D., Graham, C., Amour, A. & Bathurst, P. (eds.), *The Millennium Atlas: Petroleum Geology of the Central and Northern North Sea.* The Geological Society, London. 45-60.

Zanella, E., Coward, M.P. & McGrandle, A. 2003. Chapter 4 – Crustal Structure. In: Evans, D., Graham, C., Amour, A. & Bathurst, P. (eds.), *The Millennium Atlas: Petroleum Geology of the Central and Northern North Sea.* The Geological Society, London. 35-44.

Ziegler, P.A. 1990. Tectonic and paleogeographic development of the North Sea rift system. In: Blundell, D.J. &. Gibbs, A.D, Tectonic Evolution of the North Sea rifts. 1-36.

Ziegler, P.A. 1982. *Geological Atlas of Western and Central Europe.* Shell International Petroleum Maatachappij B.V. 130pp.

www[1]: http://www.uga.edu/~strata/sequence/seqStrat.html

Technical file note prepared for: ConocoPhillips

Project Number 543/03

Biostratigraphic analysis of selected core samples from Norsk Hydro well 34/8-7.

Date: 07.02.03

Analysts: Stephen Packer (micropalaeontology) and Martin Pearce (palynology)

Notes:

- **Aims of study:** The cored interval in 34/8-7 has been previously examined in some detail by Paleo Services in the 1990's as part of a single well biostratigraphic study for Norsk Hydro.The relevant section was broken down as follows:

  4466.5m (log) to 4601.0m (log): Early Cretaceous? - Late Jurassic, Ryzanian? - Volgian (Draupne equivalent).

  4601.0m (log) to 4610.0m (log): Middle Volgian - Kimmeridgian. (Draupne).

  4610.0m (log) to 4632.5m (log): Middle - Early Callovian. (Heather).

  The primary aim of the current re-study is to attempt to date the cored conglomeratic interval, assigned to Draupne equivalent by Paleo Services.

- **Samples:** 5 core samples (listed below) were analysed for micropalaeontology & palynology. Samples were collected by ConocoPhillips. Finer grained lithologies were preferentially selected during sampling.

- **Recovery:** A summary of the new data generated herein is listed as Table 2. Micropalaeontological recovery comprises rare to abundant miscellaneous microfossils, comprising burrow infill and bivalve spat. Rare agglutinating foraminifera were also noted. Palynological recovery is good, with assemblages composed almost entirely of *in situ* terrestrially-derived palynomorphs with abundant structured humic debris in all samples. Preservation is variable from poor to moderate. A single specimen of the acritarch *Micrhystridium* spp. at 4489.80m is the only *in situ* palynological evidence of *marine* conditions.

- **Age interpretation:** No reliable (first order) chronostratigraphic markers were recovered from the 5 samples examined. However the occurrence of bivalve spat in the sample at 4471.60m and the possible sequence of events within the Late – Middle Jurassic section, derived from combining the data generated herein and the Paleo Services data (see Table 1) may suggest a level within the **Kimmeridgian JM7 Biozone (Cymodoce ammonite zone)** at the top of the section studied. (The interpretation of JM7 should be treated with caution however, as a good sequence of biostratigraphic events that normally overly the bivalve spat horizon cannot be recognised, and occurrences of bivalve debris may occur at deeper stratigraphic horizons in a regional context).

  The presence of a palynoflora composed almost entirely of long-ranging terrestrially derived taxa, with the absence of any identifiable *in situ* dinoflagellate cysts, precludes a meaningful biostratigraphic interpretation.

When the original Paleo Services data is combined with the new data generated herein the following sequence of events (in terms of Millennia Micropalaeontological Biozones) (Table 1)appear to present:

TABLE 1	**Combined data interpretation**			
Depth	**Event**	**Data Source**	**Zone**	**Interpreted age**
4471.60m	Bivalve spat	Millennia data	JM7?	Kimmeridgian
4582m	Rare *Haplophragmoides* spp.	Paleo Services data	JM8?	Kimmeridgian - Late Oxfordian
4602m	*?Parvicingula* and *Stichocapsa* spp. (*in situ?*)	Paleo Services data	?	These faunas were thought to be Volgian to Kimmerigian by Paleo Services, whilst this is possible they may also be derived from Callovian were similar assemblages can occur. The problems with depths for particular cuttings samples should also be noted (see Paleo Services).
4610m	*Verneuilinoides* sp. 1 *H. infracalloviensis*	Paleo Services data	JM13	Middle Callovian

TABLE 2	**New data (Millennia)**		
Depth (m)	**Age**	**Zone**	**Biostratigraphic comments**
4471.60	?Kimmeridgian	**M:** ?JM7 **P:** Unassigned	**M:** Sparse microfaunal assemblage comprising rare agglutinating foraminifera and pyritised bivalve spat. **P:** Bisaccate pollen dominates, with common *Baculatisporites comaumensis* and frequent *Cerebropollenites* cf. *thiergartii*, *Inaperturopollenites* spp., *Cyathidites australis*? and *Araucariacites australis*?. The combined presence of *Nannoceratopsis gracilis/senex* and *Chasmatosporites hians* suggests Middle Jurassic reworking.
4478.40	Indeterminate	**M:** Unassigned **P:** Unassigned	**M:** Sparse microfaunal assemblage comprising abundant pyritised burrow infill. **P:** Bisaccate pollen dominates, with common *Baculatisporites comaumensis* and *Cyathidites australis*, and frequent *Inaperturopollenites* spp., *Araucariacites australis*, *Perinopollenites elatoides* and *Cyathidites australis*. The combined presence of *Nannoceratopsis gracilis/senex*, *Chasmatosporites hians* and *Lycopodiacidites rugulatus* suggests broadly Middle Jurassic reworking. Carboniferous reworking is also indicated by the presence of *Densosporites* spp.
4478.60	Indeterminate	**M:** Indeterminate **P:** Unassigned	**M:** Very sparse microfaunal assemblage comprising rare pyritised burrow infill. **P:** (As above).
4485.80	Indeterminate	**M:** Indeterminate **P:** Unassigned	**M:** Very sparse microfaunal assemblage comprising rare pyritised burrow infill. **P:** Bisaccate pollen dominates, with abundant *Baculatisporites comaumensis*, common *Cerebropollenites* cf. *thiergartii* and frequent *Inaperturopollenites* spp., ?*Araucariacites* spp., *Perinopollenites elatoides*, *Cyathidites australis*.
4489.80	Indeterminate	**M:** Unassigned **P:** Unassigned	**M:** Sparse microfaunal assemblage comprising rare pyritised burrow infill. **P:** Bisaccate pollen dominates, with common *Baculatisporites comaumensis* and *Inaperturopollenites* spp. *Perinopollenites*

			elatoides and *Cerebropollenites* cf. *thiergartii* frequently occur. A specimen of *Micrhystridium* spp. is the only *in situ* evidence of marine conditions. The combined presence of *Nannoceratopsis gracilis/senex* and *Chasmatosporites hians* suggests Middle Jurassic reworking, while Carboniferous reworking is evident from the presence of *Densosporites* spp.

Key:

M = Micropalaeontology
P = Palynology

Available online at www.sciencedirect.com

SCIENCE DIRECT®

Earth and Planetary Science Letters 234 (2005) 401–419

EPSL

www.elsevier.com/locate/epsl

Spatio-temporal evolution of strain accumulation derived from multi-scale observations of Late Jurassic rifting in the northern North Sea: A critical test of models for lithospheric extension

Patience A. Cowie[a,*], John R. Underhill[a], Mark D. Behn[b,c], Jian Lin[c], Caroline E. Gill[a]

[a]*Grant Institute of Earth Science, School of GeoSciences, Edinburgh University, Edinburgh EH9 3JW, UK*
[b]*Department of Terrestrial Magnetism, Carnegie Institution of Washington, Washington, DC 20015, USA*
[c]*Department of Geology and Geophysics, Woods Hole Oceanographic Institution, Woods Hole, MA 02543, USA*

Received 3 September 2004; received in revised form 14 January 2005; accepted 23 January 2005
Available online 13 April 2005

Abstract

We integrate observations of lithospheric extension over a wide range of spatial and temporal scales within the northern North Sea basin and critically review the extent to which existing theories of lithospheric deformation can account for these observations. Data obtained through a prolonged period of hydrocarbon exploration and production has yielded a dense and diverse data set over the entire Viking Graben and its flanking platform areas. These data show how syn-rift accommodation within the basin varied in space and time with sub-kilometer-scale spatial resolution and a temporal resolution of 2–3 Myr. Regional interpretations of 2D seismic reflection, refraction and gravity data for this area have also been published and provide an image of total basin wide stretching for the entire crust. These image data are combined with published strain rate inversion results obtained from tectonic subsidence patterns to constrain the spatio-temporal evolution of strain accumulation throughout the lithosphere during the 40 Myr (170–130 Ma) period of Late Jurassic extension across this basin. For the first 25–30 Myr, strain localisation dominated basin development with strain rates at the eventual rift axis increasing while strain rates over the flanking areas declined. As strain rates across the whole basin were consistently very low ($<3\times10^{-16}$ s^{-1}), thermally induced strength loss cannot explain this phenomenon. The strain localisation is manifest in the near-surface by a systematic migration of fault activity. The pattern and timing of this migration are inconsistent with flexural bending stresses exerting an underlying control, especially when estimates of flexural rigidity for this area are considered. The best explanation for what is observed in this time period is a coupling between near-surface strain localisation, driven by brittle (or plastic) failure, and the evolving thermal structure of the lithosphere. We demonstrate this process using a continuum mechanics model for normal fault growth that incorporates the strain rate-dependence of frictional strength observed in

* Corresponding author.
E-mail address: patience.cowie@ed.ac.uk (P.A. Cowie).

doi:10.1016/j.epsl.2005.01.039

laboratory studies. During the final 10 Myr of basin formation, strain accumulation was focused within the axis and strain rates declined rapidly. Replacement of weak crust by stronger mantle material plus crustal buoyancy forces can adequately explain this decline.

Keywords: lithospheric extension; strain accumulation; normal faulting; numerical modeling; basin formation

1. Introduction

Extensional basin geometry, and the sedimentary sequences that fill the basin, record the amount, style and duration of lithospheric thinning. These data may be used to determine the way in which the rheology of the lithosphere controls the details of the extension process. Many studies of lithospheric extension already exist and have reached, superficially at least, the same conclusion: i.e., that rheology plays a key role in controlling the rate, duration, magnitude and style of extension (see [1] for review). Depending on the observations being considered, however, a single property of the lithosphere's complex rheology is often highlighted while other aspects are assumed to be less important. At one extreme are models that emphasize the role of near-surface brittle deformation in extension; such models typically pre-define one or more fault surfaces, and proscribe the strain that they accommodate (e.g. [2–6]). At the other extreme are models that consider basin-wide patterns of thinning using a continuum approach. These models typically emphasize the role of deep-seated ductile deformation, and largely ignore structural discontinuities within the basin (e.g., [7–10]).

More complex and holistic thermo-mechanical models for extension of the lithosphere have been developed as increased computational power has become available (e.g. [11–19]). The degree of complexity in current theoretical understanding of the process is evident from a review paper by Buck et al. [1], which quantifies and discusses the competing effects of at least six different factors that may control the style of extension that occurs. Many papers are able to explain generic features and gross variations in rift and/or passive margin geometry, such as overall width or degree of asymmetry (e.g., [12,14,1,17,19]). However, for specific rifts it is difficult to determine with certainty which factors may be more important than others and which ones may be ignored. Moreover, the increased complexity of more recent models for lithospheric extension has not been matched by an increased level of observational detail used to test these results.

Here we bring together, for the first time, a wide range of published observations of rift evolution during a 40 Myr rift event and assess the extent to which existing models of lithospheric stretching can

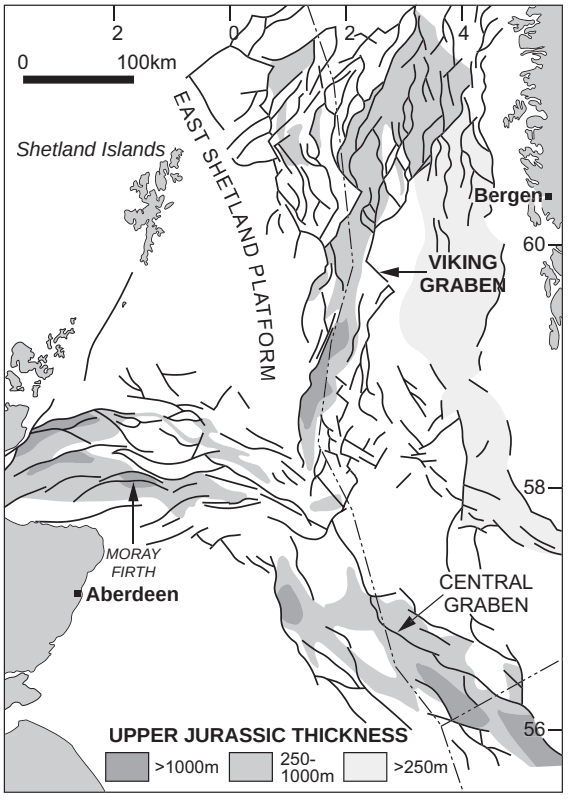

Fig. 1. (a) The North Sea rift system. Location of Fig. 2(a) shown by dashed box. Grey shading indicates thickness of Upper Jurassic sediment accumulation and reflects complexity of accommodation creation across the basin.

explain these observations. The basin studied is the Late Jurassic northern North Sea rift system (Fig. 1). For this area, a subsurface data set comprising 2D seismic reflection and refraction images, high-resolution 3D seismic surveys and biostratigraphically constrained well data has been used to document (a) temporal and spatial variability in the location and rate of strain accumulation during rifting as recorded by the fault population (e.g., [20,5,21–23]), and (b) the regional syn-rift strain rate variations derived from a 2D numerical inversion of tectonic subsidence patterns [24]. These data extend over the entire width of the basin (~200 km) for an along-strike distance of ~100 km. To our knowledge, this study is the first to integrate such a wide variety of observational data, over different spatial and temporal scales, for an individual extensional province. We use these data to determine which mechanical properties of the lithosphere regulated strain accumulation through time across this basin.

2. Multi-scale observations of Late Jurassic extension of the northern North Sea

During the Mesozoic, the northern North Sea basin experienced two, approximately E-W oriented phases of stretching: the Permo-Triassic and the Late Jurassic extensional episodes (e.g., [25–31]). We focus on the Late Jurassic extension event as this is particularly well documented. Extension during this episode began ~170 Ma, in the Aalenian (mid-Jurassic), and finally ceased ~130 Ma, in the Ryazanian (early Cretaceous). A central N-S trending low developed, the Viking Graben (VG), that is flanked in the west by the East Shetland Basin (ESB), and in the east by the Horda Platform (HP) (Fig. 2a). The width of the axial Viking Graben (sensu stricto) is ~35–50 km whereas when the flanking platform areas are included the overall basin width is up to ~250 km wide (Figs. 1 and 2). Maximum stretching during the Late Jurassic occurred at the rift axis ($\beta > 1.3$), i.e., within the VG

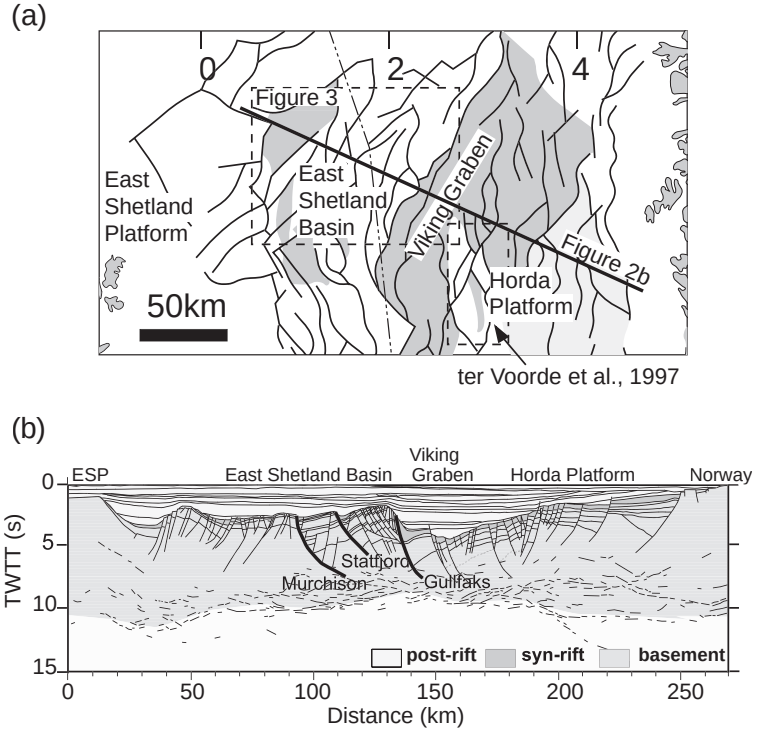

Fig. 2. (a) Map of north Viking Graben with same shading as Fig. 1. Dashed boxes show locations of Fig. 3(a) and detailed study of Horda Platform by ter Voorde et al. [5]. (b) Line drawing interpretation of deep-seismic profile NSDP84-1 oriented NW–SE across the northern North Sea basin (Modified from [63]). For location of line see (a).

itself, and lower amounts of extension occurred across the ESB and HP (see details below). The Late Jurassic extensional faults have accumulated up to several kilometers of throw and have steep to moderate dips, the angle of dip decreasing within the lower crust (Fig. 2b). Following the cessation of rifting in the early Cretaceous, the basin has largely undergone passive thermal subsidence with the development of classic "steer's head" basin geometry (Fig. 2b).

Several recent studies have shown that for large areas of the northern North Sea basin many Late Jurassic faults cross-cut pre-existing Permo-Triassic structures (e.g., [32–34]). Moreover the variation in β-factors for the two rifting events are uncorrelated over most of the area [35]. It has also been shown that the thermal effects of Permo-Triassic rifting had dissipated prior to the onset of Late Jurassic extension [6]. Thus although pre-existing structure may have influenced Late Jurassic rift development the relationship is not one of straightforward inherited structural control.

There are essentially two types of data available for this area: (a) "high-resolution" data, i.e., a dense grid of 3D reflection seismic and numerous cores, and (b) "low-resolution" data, i.e., regional 2D seismic reflection and refraction and gravity data. Thus, high-resolution observations in this area consist of interpreted 3D seismic combined with sedimentary facies analyses from cores to reconstruct depocentre evolution in 3D at sub-kilometer-scale resolution (e.g., [21,22,36,37,23]). The temporal control on these high-resolution studies is ~2–3 Myr, which allows patterns of displacement accumulation on individual faults to be resolved to a few tens of meters. Interpretations of Late Jurassic basin formation for large areas of the ESB and HP now exist to this level of detail (e.g., Figs. 3 and 4). These high-resolution studies only relate to the structural evolution of, at most, the top 5–8 km of the crustal structure.

At a lower resolution, the regional seismic reflection, seismic refraction and gravity data reveal the deeper basin and upper mantle structure down to depths of 30–40 km. The image of overall crustal thinning across the entire rift, from Shetland to Norway, is thus available at a resolution of 10 km (Fig. 2b). These data can constrain the total amount of extension at the end of rifting. White [38]

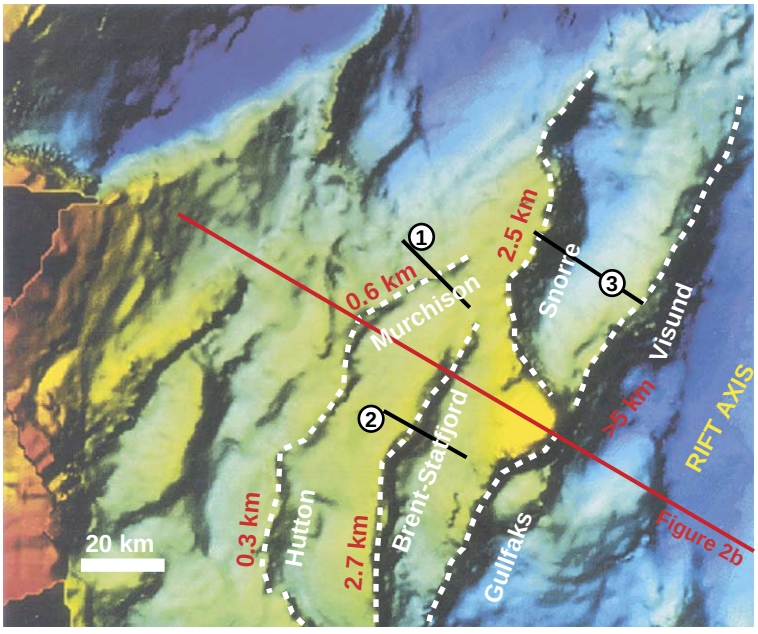

Fig. 3. Structural map of the East Shetland Basin area located in Fig. 2(a). Colors represent depth to top syn-rift (base Cretaceous reflector): blue-purples are deep, and red-yellows are shallow. This surface represents the basin bathymetry at the end of Late Jurassic extension. Image is illuminated from the NW; easterly-dipping faults are shown in shadow. Numbers refer to the seismic sections shown in Fig. 4.

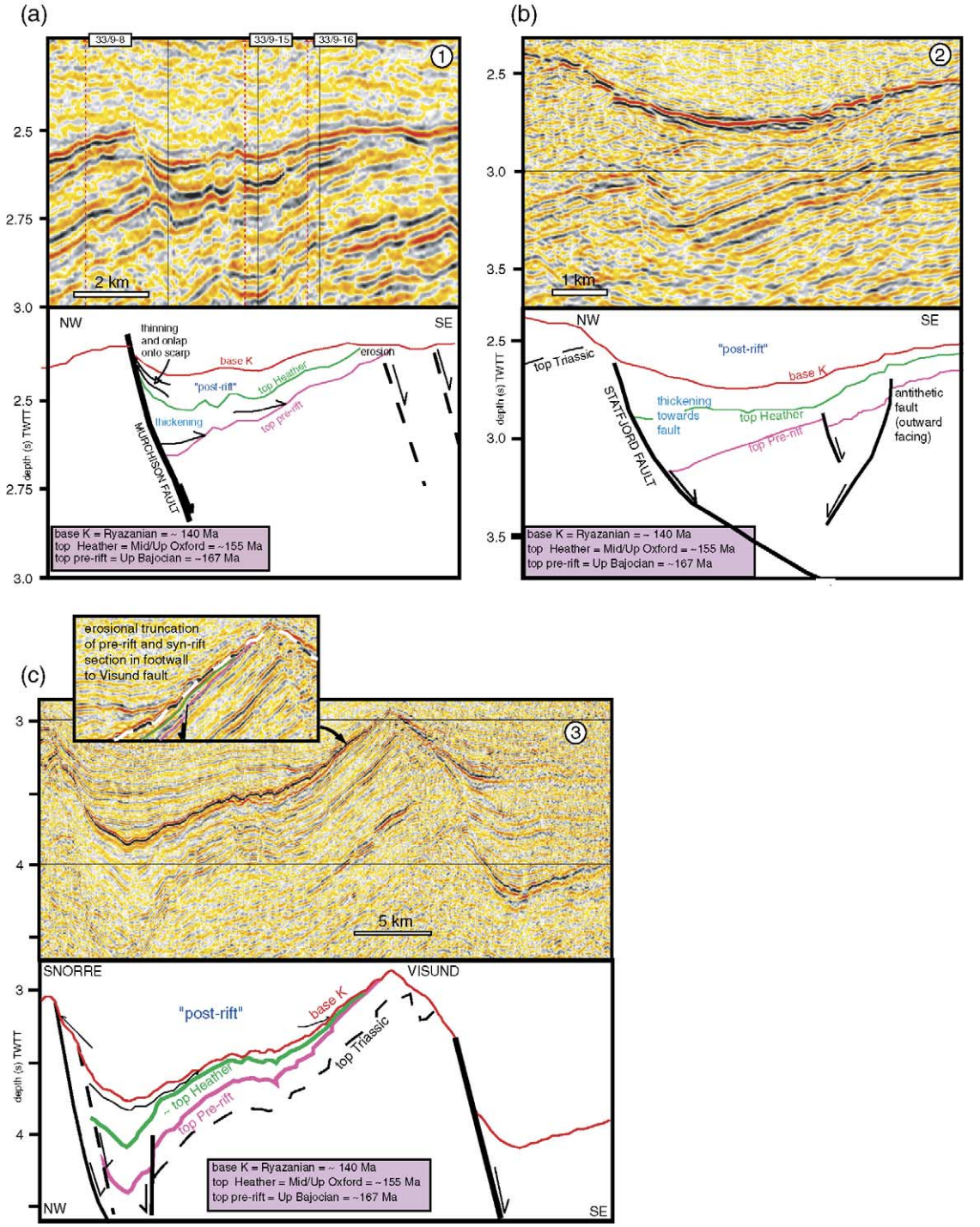

Fig. 4. Seismic reflection profiles and interpretations across (a) Murchison fault (line l), (b) Brent–Statfjord fault (line 2; modified from [21]), and (c) Snorre–Visund faults (line 3) (see Fig. 3 for location of profiles and text for explanation).

introduced a method for inverting basin subsidence curves to obtain the strain rate history during extension. Bellingham and White [24] extended the 1D method to 2D and presented the inversion result they obtained for this area of the northern North Sea. The spatial resolution of the Bellingham and White study [24] is ≈10 km and the temporal resolution is 10–20 Myr.

Compared to the 3D seismic and well core observations the strain rate inversion of Bellingham and White [24] is at least a factor of 10 lower in both spatial and temporal resolution. However, it provides different and independent information because their inversion also uses data from the thermal subsidence (i.e., post-rift) phase of basin development. In other words the extension history they obtain is derived from the record of thermal perturbation and re-equilibration on a lithospheric scale. Thus two obvious questions to ask are (1) what key characteristics of the extension history are revealed by the near-surface ("high-resolution") versus whole lithosphere ("low-resolution") data sets? and (2) to what extent are these characteristics common to both data sets, i.e., do they agree or disagree?

3. Combined interpretation of the multi-scale data set

3.1. Extension history inferred from 2-D strain rate inversion

The strain rate inversion results of Bellingham and White [24] show three main results for this area. Firstly, throughout the whole rift event the maximum strain rate was lower over the flanking basin margin areas ($\sim 1 \times 10^{-16}$ s^{-1}) compared to the rift axis ($\sim 3 \times 10^{-16}$ s^{-1}). Although the difference in strain rate is less than an order of magnitude it is well resolved and, as we show below, it is significant for constraining the controlling mechanism(s). Secondly, extension ceased earlier on the basin margins (~140 Ma) than it did at the rift axis (~130 Ma), although this is less well constrained by their inversion procedure. Thirdly, the distribution of total strain (β-factor) is slightly asymmetric about the rift axis, i.e., on the ESB $\beta \approx 1.3$, within the VG, $\beta \approx 1.5$, and across the HP $\beta \approx 1.15$. The smaller amounts of total extension recorded for the basin margins are therefore due to *both* shorter duration of extension *and* lower strain rates. Note that the strain rate inversion method gives systematically higher values of β than previous workers had obtained for the shallow basin structure (e.g., [39]), possibly due to finite seismic resolution [40]. In this study we are not so interested in the absolute value of β as in the lateral variation of β.

3.2. Extension history inferred from 3-D seismic and core interpretation

The most detailed 3D observations are available for the ESB and thus we focus on this area below. However, we also summarise interpretations of "high-resolution", largely 2D, observations for the HP [34]. Note that quoted fault throws have all been determined by measuring the offset of the pre-rift (i.e., pre-Late Jurassic) stratigraphy across each fault.

3.2.1. Initiation of extension (170–155 Ma)

The higher-resolution near-surface data sets place, first of all, a more precise constraint on the onset of extension, at least for the flanking basin margin areas (the earliest syn-rift at the rift axis is less well-resolved seismically). The first evidence for fault-controlled accommodation creation seen in the reflection data is ~167 Ma on the ESB [37]. On the HP extension initiated ~170 Ma [20]. During the initial phase of extension, sediment supply outpaced the rate of tectonic subsidence so that a true measure of fault activity can be inferred from the coeval syn-rift stratigraphy [21]. Thus formation of early fault segments and their adjacent depocentres is clearly resolved (e.g., [21]).

The first ~10 Myr of extension was associated with a broad zone of diffuse deformation, at least 200 km wide, i.e. extending from the western ESB across the VG to the eastern HP. The first Late Jurassic faults to initiate dipped both towards and away from the eventual rift axis and fault spacing was of the order of a few kilometers (e.g., Stage 1; Fig. 5a). Maximum fault throws of a few hundred meters at slip rates of ≤0.1 mm/yr accrued during this period [21,5]. However, by ~155 Ma, the faults

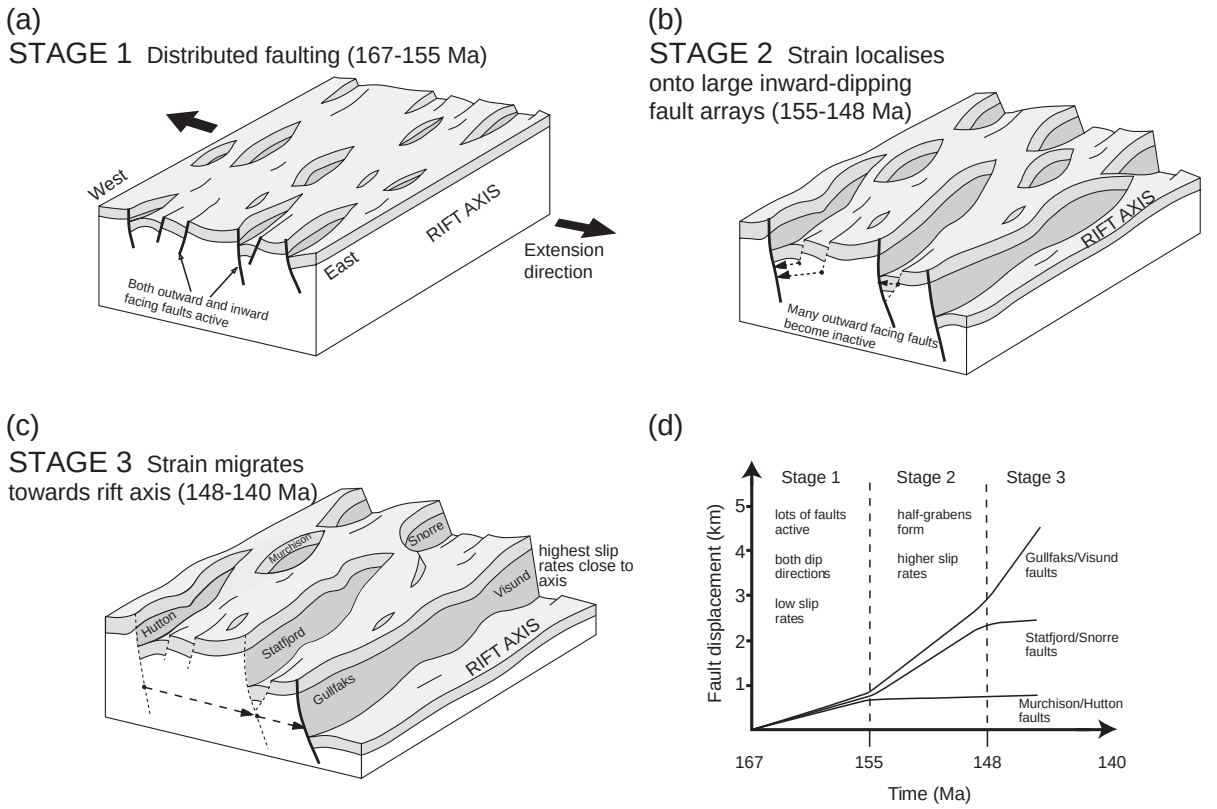

Fig. 5. Cartoon illustration of the migration in fault activity through time across the ESB. In Stage 1 (a) both inward and outward facing faults develop with similar slip rates. In Stage 2 (after 11–12 Myr; b) the outward dipping faults become inactive and the inward dipping faults develop higher slip rates. Dashed arrows indicate strain localising onto inward dipping faults in Stage 2. In Stage 3 (c) the highest rates of fault slip occur on the Gullfaks–Visund fault and faults further off-axis switch off (direction of strain localisation indicated by dashed arrows). The graph in (d) summarises fault throw versus time for the three main fault systems.

that dipped towards the proto rift axis began to emerge as the dominant set controlling subsequent depocentre development on the ESB ([21]; Figs. 4b and 5b). Similary, strain localised at ~160 Ma onto the inward-dipping (i.e., westward-dipping) Brage fault, which is located approximately 25–30 km to the east of the VG on the HP [34]. At this time strain also localised onto the inward dipping fault that forms the eastern boundary of the VG. Activity on these inward-dipping faults resulted in the formation of half grabens comprised of fault blocks, 15–20 km wide, tilting away from the eventual rift axis. The basin also narrowed to ~100 km wide by ~155 Ma, with the Hutton–Murchison fault trend on the ESB defining the approximate western extent of active extension and the Brage fault on the HP defining approximately the eastern extent.

3.2.2. Evolution of extension (155–140 Ma)

The present day pattern of faulting across the ESB clearly shows the dominant inward-dipping (i.e., eastward dipping) faults and the back-tilted half-graben between them (Fig. 3). Fig. 3 also shows that the Visund–Gullfaks fault, which forms the western boundary to the VG, accumulated in excess of 5 km of throw during the Late Jurassic (e.g., [6]). The Brent–Statfjord fault, lying 20–30 km west of the axis has a maximum throw of only 2.7 km [21]. The Inner Snorre fault, at a similar position with respect to the rift axis as the Brent–Statfjord fault, has a comparable throw of ~2.5 km (Fig. 3; [41]). The Murchison fault, which lies 40–50 km to the west of the axis has only 600 m maximum throw [23] and the Hutton fault on the same trend has ~300 m of throw (Fig. 3; [42]).

Faults located further west have even smaller maximum throws [43].

The decrease in maximum fault throw away from the rift axis on the ESB (Fig. 3) could be explained by either a shorter duration of fault activity or a slower rate of slip on faults located further away from the axis. Comparison of the Mcleod et al. [21] study of the Brent–Statfjord fault with our own study of the Murchison fault clearly shows that both of these faults initiated as similarly segmented structures at approximately the same time (~167 Ma). However, when the geometry of the syn-rift fill is examined in detail the evolution of these two faults differs. Whereas the earliest part of the syn-rift stratigraphy (~167 Ma to ~155 Ma) shows thickening into both faults, the younger syn-rift interval thins and onlaps towards the Murchison fault (Fig. 4a, b). Thus, while the Brent–Statfjord fault experienced an increased rate of slip (by a factor of $\sim\times 2$) later in the syn-rift (subsequent to 155 Ma; [21,22,44]; Fig. 4b), the Murchison fault appears to have experienced declining rates or cessation of activity during the same time interval (Fig. 5c,d).

There is also substantial evidence for migration of fault activity from the Inner Snorre fault to the Visund–Gullfaks fault. The Visund–Gullfaks fault experienced its maximum rate of slip between ~148 Ma and ~140 Ma [22,45] whereas the Inner Snorre fault was most active between ~155 Ma and ~148 Ma (Figs. 4c and 5d, [44]). The degree of thickening of the syn-rift wedge into the Inner Snorre fault decreases up-section, indicating that this fault is becoming less active during the latest synrift (Fig. 4c). Furthermore, the inset to Fig. 4(c) shows erosional truncation of both syn-and pre-rift strata in the footwall crest of the Visund–Gullfaks fault. This pattern of erosion indicates that the rate of footwall uplift along the Visund–Gullfaks fault exceeded the rate of hangingwall subsidence along the Inner Snorre fault in the latest syn-rift (~148–140 Ma). McLeod et al. [22] reconstructed the syn-rift paleogeography and sediment dispersal patterns to show that there was a progressive migration of fault activity from the Brent–Statfjord to the Inner Snorre fault and finally to the Visund–Gullfaks fault over a period of 15 Myr (Fig. 5).

In summary, the decrease in maximum fault throw away from the rift axis across the ESB results from the fact that *both* the duration *and* maximum slip rate decreased systematically from the rift axis (Fig. 5d). A similar pattern of fault growth is also observed on the HP. According to [34], the Brage fault on the HP was most active between ~160 Ma and ~153 Ma, but it ceased to be active at ~153 Ma and has a maximum throw of only ~700 m. The fault that forms the eastern margin of the VG continued to be active for the remainder of the rift event [6].

3.3. Conclusions of the combined interpretation

The conclusions drawn from the near-surface versus whole lithosphere studies broadly agree. Both data sets indicate that, if the whole basin is considered, the duration of extension and the maximum strain rate (or maximum fault slip rate) are directly correlated. The greater resolution of the near surface data allows this correlation to be roughly quantified. For example, in areas that experienced ≤10–12 Myr of extension (Murchison–Hutton trend and Brage fault) the maximum fault slip rates were typically ~0.05 mm/yr [21,5]. Faults that were active for ~20–25 Myr (Brent–Statfjord and Inner Snorre faults) experienced maximum slip rates of ~0.15–0.2 mm/yr [21]. The maximum fault slip rate on the Visund–Gullfaks fault, which was most likely active for the entire rift event, i.e., ~40 Myr, is estimated to be 0.3 mm/yr (based on the age and maximum displacement of this fault).

The correlation between extension rate and duration also relates to the spatial evolution of the rift structure. For the first 10–15 Myr of extension (~170–155 Ma) the zone of active faulting was ~200 km wide with many low-slip rate faults active. During this interval faults dipping both towards and away from the eventual rift axis were accommodating strain (e.g., Fig. 5a). The available data cannot rule out the possibility that there was some preferential strain accumulation within a proto-Viking Graben during this initial phase of distributed deformation. Subsequently (between ~155 Ma and ~148 Ma), the zone of active faulting narrowed to ~100 km, with large areas of the HP and the western ESB becoming inactive (Fig. 5b). During this phase the faults that dipped towards the eventual rift axis became dominant and fault slip rates increased on these faults. At this stage the asymmetry of the rift also emerged,

with the eastward dipping Visund–Gullfaks fault gradually becoming a more dominant structure (Fig. 2b). Between ~148–140 Ma many of the inward dipping faults on the basin margins became inactive as strain accumulation localised within in a narrow zone, <50 km wide, right at the axis. The final 10 Myr of extension (140–130 Ma) was focused entirely within the rift axis. During this final phase, crustal deformation may have been largely localised onto a single major shear zone, i.e., the Visund–Gullfaks fault, with the fault bounding the eastern margin of the VG representing a secondary antithetic structure.

4. Comparison between the Late Jurassic strain accumulation pattern and existing models of lithospheric extension

4.1. To what extent does flexural rigidity play a role in controlling the rift evolution?

The effective elastic thickness of the lithosphere (T_e) is thought to be a key factor determining how large an extensional fault can grow and when it will cease to be active (e.g., [46,47,1]. We can compare the temporal evolution of faulting observed in this area with numerical models that explore the role of T_e in controlling how extensional faults grow (e.g., [48,49]). These models assume that flexural strength is concentrated in the brittle upper layer and they predict that new faults will initiate to take up further strain if/when flexural forces associated with existing faults become too great for continued motion to occur (Fig. 6a). The seismic reflection data, summarised here, clearly indicate that the number of active faults actually decreased through time and the width of the active rift zone narrowed as the extension progressed. In particular, the timing of movement on antithetic (outward-dipping) faults relative to the larger inward-dipping faults, as seen in this area, is not explained by the flexural model. (i.e., compare Fig. 6a with Fig. 4b). Moreover, the gradual emergence of the preferred inward dip-direction of the largest faults (and cessation of activity on outward dipping faults) cannot be accounted for by this mechanism.

The overall narrowing of the basin through time might be attributed to lateral variations in T_e, i.e., offset occurs preferentially on faults formed in low T_e areas. Note that the above models assume constant T_e. The flexural force, ΔF, resisting motion on a normal fault with up to a few kilometers of displacement, as observed in this area, is given approximately by $\Delta F = \rho g \alpha w$, where ρ is density, g is acceleration due to gravity, and w is fault offset. The flexural parameter α is related to T_e by $\alpha \propto T_e^{3/4}$. Thus, according to these relationships, larger offset faults are likely to develop in areas where T_e is lower. The increase in maximum fault throw towards the Viking Graben axis, documented above, implies a corresponding decrease in T_e, from the basin margins towards the axis. Although T_e is expected to be lower in areas of greater lithospheric thinning and heating, i.e., at the rift axis, the $>\times 5$ variation in fault throw that we observe implies a significant variation in T_e. Such a large variation is inconsistent with the results of flexural back-stripping studies, which have successfully modeled this area assuming a constant, albeit low, value of $T_e = 1.5$ km [50]. Thus the fault pattern may be reflecting a lateral variation in T_e, but the magnitude of the variation is unlikely to be as large as simple plate flexure theory predicts.

4.2. To what extent does viscosity-controlled extension play a role in determining the observed rift evolution?

An alternative explanation for the pattern of strain accumulation and fault activity is that the viscous lower layers within the lithosphere are regulating the timing and magnitude of faulting. It has been shown that, if the lithosphere has a non-linear temperature-dependent rheology, then the total amount of stretching, the duration of stretching, and the maximum strain rate are all related [7,9,51,10]. Takeshita and Tamaji [51] and Newman and White [10] use a 1D model with a homogeneous non-linear viscous rheology and a constant force boundary condition to show how the extension history varies for different levels of applied force. For initial strain rates $>10^{-15}$ s^{-1} (high applied force) a thermomechanical instability occurs and rifting proceeds to full seafloor spreading. For initial strain rates $<10^{-15}$ s^{-1} (low applied force) finite extension occurs, i.e., a rift basin (or failed rift) is formed. For the latter case the total amount of stretching (β-factor) and the maximum strain rate are correlated. Furthermore, the

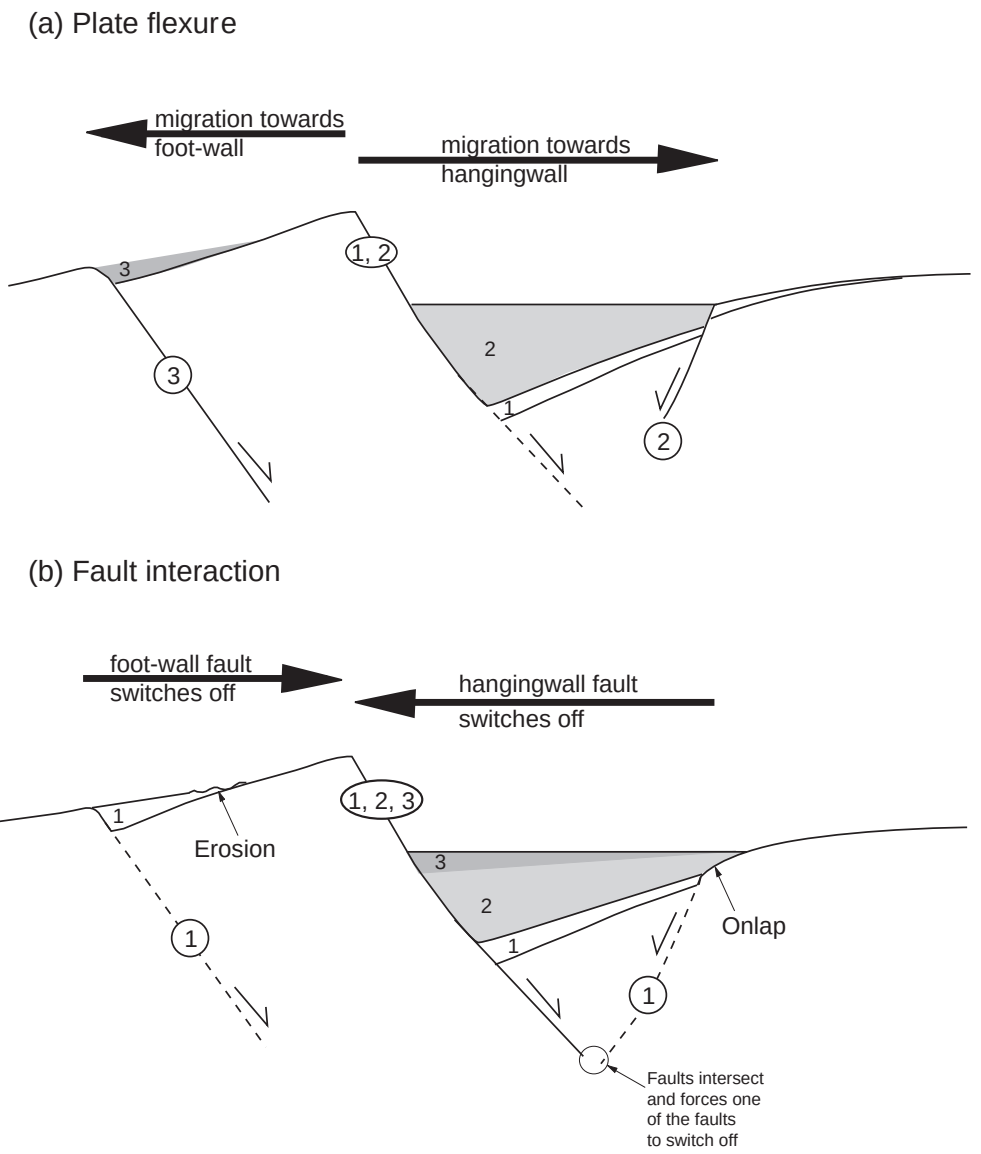

Fig. 6. Comparing the different fault migration patterns predicted by (a) plate flexure, versus (b) fault interaction. Numbers indicate order of fault evolution. In (a), the initiation of secondary fault 2 is caused by plate bending adjacent to high-angle fault 1. Ultimately the cessation of movement on fault 1 forces another fault to form (fault 3) most likely in the footwall [49]. In (b) a number of faults initiate simultaneously (all faults labeled 1). Due to fault interaction one fault emerges as the dominant structure (fault 1,2,3) and faults in the foot-wall and hanging-wall areas become inactive as extension progresses. Grey shading indicates sediment packages associated with different time periods of fault movement.

duration of stretching and the maximum strain rate are inversely related, i.e., areas that extend slowly continue to extend for longer periods of time. The cessation of extension in this model is due to the gradual replacement of weak crust by stronger mantle material as the lithosphere thins. Hence the same strengthening effect occurs after a longer time delay in lower strain rate areas. A constant force boundary condition is the most reasonable for modelling large-scale continental deformation when

buoyancy forces are generated that are comparable to tectonic forces [52].

This model is the basis for what Newman and White refer to as "viscosity-controlled" extension. The apparent agreement between the near-surface seismic reflection observations and the strain rate inversion results suggests that a 1D model may indeed be appropriate for understanding the evolution of this basin. However, while the first of the model predictions is consistent with what is observed, the latter is not (Fig. 7). According to Newman and White [10], the predicted duration of extension across the low-strain-rate platform areas (ESB and HP) is approximately 60 Myr, whereas the observed duration is <25–30 Myr in these areas (Fig. 7). The axis of the rift (the VG sensu stricto) experienced both the highest strain rate and the longest duration of extension (Fig. 7b).

The observations show that, for the first ~30 Myr of the rift history (~170–140 Ma), strain progressively localised at the rift axis (Fig. 5; Fig. 7b). In other words, the increasing rate at the axis was balanced by declining strain accumulation over the HP and the ESB during this interval of time. Thus constant strain rate could have been maintained overall, across the entire basin, even if a constant force was driving the deformation. During the final 10 Myr of extension (140–130 Ma), once strain accumulation had localised within the VG, the strain rate declined from $\sim 3 \times 10^{-16}$ s^{-1} to $<10^{-17}$ s^{-1}.

It is possible that the late-stage decline in strain rate and the ultimate cessation of rifting were externally controlled, i.e., there was a change in the plate driving forces. Alternatively, it can be explained by strengthening of the lithosphere, assuming the applied force remained constant as Newman and White [10] suggest. Crustal buoyancy forces are also likely to have contributed to the cessation of rifting [1]. For example, a β-factor of 1.2 produces a buoyancy force of $\sim 5 \times 10^{11}$ N/m in 25–30 km thick crust, which is comparable (within an order or magnitude) to the

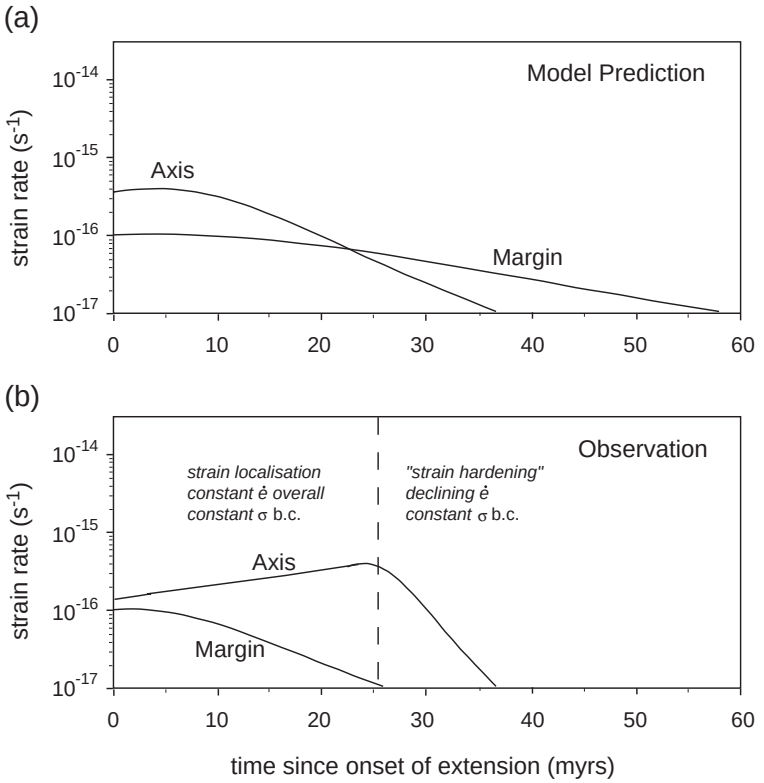

Fig. 7. Comparison between (a) the prediction of 1D "viscosity-controlled" extension [10], and (b) observations based on the combined interpretation (see Section 3). Note that part (b) is derived from estimates of rates and durations based on data available and is partly schematic.

force likely to be available for rifting (see [1] for discussion). However, the strain localisation behaviour of the first 25–30 Myr of extension cannot be explained in terms of viscosity controlled extension because the strain rates in this basin ($<3\times10^{-16}$ s^{-1}) were consistently below the threshold needed for thermally induced strength loss to be significant. Other controls are therefore required to explain this phase.

4.3. To what extent does fault interaction play a role in determining the observed rift evolution?

Many of the observations of fault evolution in the ESB during the first 25–30 Myr of the extension history may be explained in terms of fault interaction. For example, the simultaneous increase in displacement rate on the inward dipping faults and cessation of activity on the outward dipping faults, as seen in Fig. 4b is easily explained by this process (Fig. 6b). Intersection of two faults with opposing dips causes one fault to become inactive and the strain to be taken up by the remaining active fault [53,54]. A fault may also become inactive if it lies in the stress shadow of a neighboring, more active, fault even if the two faults do not intersect [55]. A typical feature of numerical models in which growing faults interact through time is the development of a wide range of fault sizes, similar to that seen in the northern North Sea area (e.g., [55]).

Hardacre and Cowie [56] modelled the spontaneous nucleation and growth of dipping extensional faults in a 2D cross-section. These authors show that when a lateral strain gradient is imposed as an initial condition across the model, faults that dip toward the region of highest strain emerge as the dominant fault set, while those that dip away cease to be active. Ishikawa and Otsuki [57] also found a correlation between the magnitude of the lateral strain gradient and a dominant fault dip-direction. Thus, if a strain gradient existed from the basin margin towards the rift axis, we can explain both the observed emergence of the major inward dipping faults and the highest rates of slip on the faults proximal to the axis.

There are two key observations that suggest that the strain gradient became gradually more pronounced through time. First of all, on the ESB at least, outward facing faults initiated early on and only became inactive after about 11–12 Myr of extension. This would suggest that early in the extensional history there was not a well-developed strain gradient. Second, we observe a gradual but significant narrowing of the zone of active faulting (from ~200 km to <50 km) over the 40 Myr of rifting. The strain gradient will of course increase if the mechanical thickness variation from the basin margins to the axis increases. As the thickness of the lithosphere is thermally controlled, a higher geothermal gradient at the axis will reduce the mechanical thickness and thus enhance the strain in that area relative to the margins.

4.4. Localisation of faulting in response to varying thermal structure

In order investigate the effect of thermal structure on faulting we model the deformation using the 2-D finite-element approach of Behn et al. [17], which is described in detail in the Appendix. Figs. 8 and 9 show the results of using this model to reproduce the pattern of faulting seen in the northern North Sea. We used published values of strain rates, layer thicknesses and thermal structure for the late Jurassic rift event in this area (e.g., [6,10], see Fig. 8 caption). The three panels shown in Fig. 8 represent separate model runs with independent starting conditions designed to illustrate the 3 sequential stages of rift evolution shown in Fig. 5. Although this approach does not explicitly calculate the advection and diffusion of heat associated with finite duration extension, it provides a first order prediction of the style of deformation that will develop for a given thermal regime.

In Fig. 8, the top panel corresponds to Stage 1 of Fig. 5 and shows that when a weak lateral temperature gradient is imposed, deformation is distributed between sets of conjugate normal faults with similar strain rates. Active faulting extends to distances of up to ~75 km either side of the rift axis. The lower two panels of Fig. 8 correspond to Stages 2 and 3 of Fig. 5. As the lateral temperature gradient becomes more pronounced, *active* faults dip preferentially towards the area where the geothermal gradient is highest (half-graben development of Stage 2; Fig. 5) and the highest strain rates occur where the lithosphere is thinnest. The total width of the zone of active faulting narrows from ~150 km to ~50 km (Stage 3) (Figs. 8 and 9). We found that the depth extent and horizontal

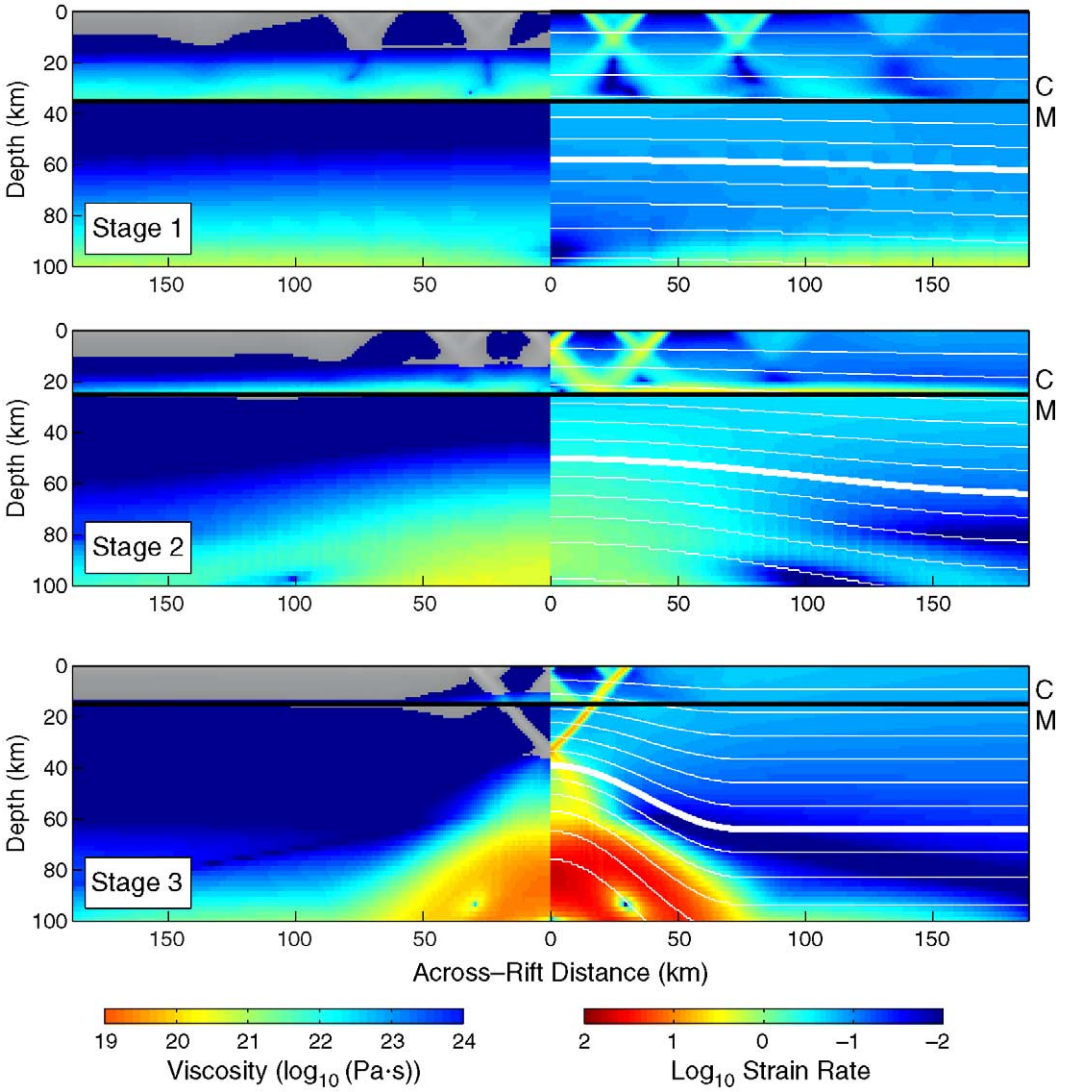

Fig. 8. Simulating the 3 stages of fault evolution (Fig. 5) using the model of Behn et al. [17]. Each panel shows the instantaneous strain rate (right half of diagram) and viscosity structure (left hand side of diagram) calculated for a given set of thermal and rheological input parameters. Strain rates are shown relative to a reference strain rate of 10^{-16} s^{-1}. Viscosities shown in grey shade indicate brittle failure, whiter shades indicate lower effective viscosities. Thick white line = 700 °C isotherm, C=crust, M=mantle. The panels approximate the gross late Jurassic extension history and each one represents a separate model run; the evolution is not modelled explicitly. From top to bottom, the total crustal thickness decreases from 35 km (top panel) to 15 km (bottom panel) while there is a corresponding increase in the geothermal gradient at the rift axis from 12 °C/km (top panel) to 18 °C/km (bottom panel). Thicknesses of upper and lower crust for each run are as follows: upper crust=20 km, lower crust=15 km (top panel); upper crust=15 km, lower crust=10 km (middle panel); upper crust=10 km, lower crust=5 km (bottom panel). The increase in crustal thickness towards rift margins does not significantly influence the result and is ignored. Estimates of extensional strain rate, thermal structure, crustal thickness and lithospheric rheology specific to this area for the late Jurassic are taken from [6,24]. The following flow law parameters were used for all the experiments (Eq. (A1)): upper crust (Q = 172.6 kJ/mol, $A = 3.165 \times 10^{-2}$ $MPa^{-n}s^{-1}$, n = 1.9); lower crust (Q = 172.6 kJ/mol, $A = 3.165 \times 10^{-2}$ $MPa^{-n}s^{-1}$, n = 2.4); mantle (Q = 510 kJ/mol, $A = 7 \times 10^{4}$ $MPa^{-n}s^{-1}$, n = 3). A cosine-bell function is used to define the isotherm geometry and the vertical dimension of the model space = 120 km.

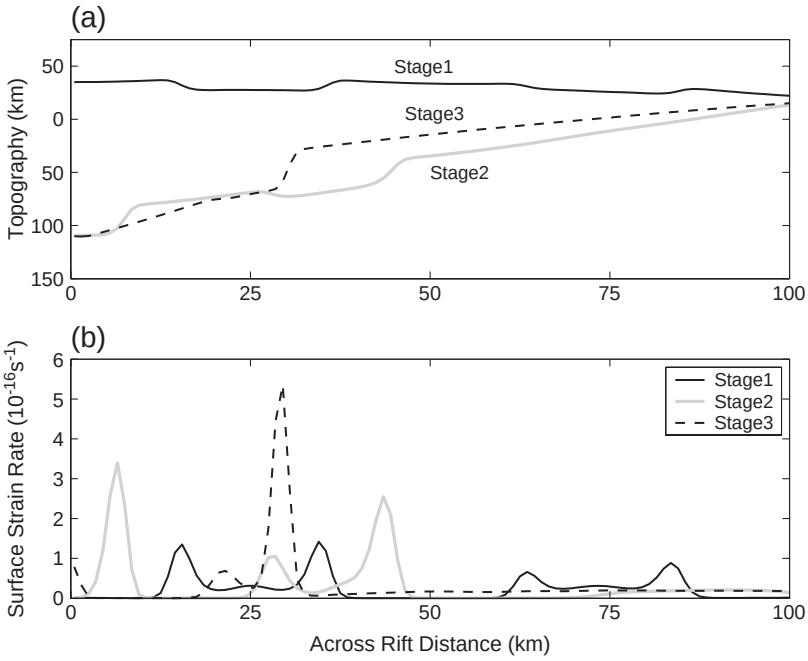

Fig. 9. (a) Surface topography and (b) surface strain rate extracted for the 3 simulations shown in Fig. 8.

pattern of faulting were very sensitive to the imposed thermal structure and horizontal strain rate. The relatively cool geotherm assumed for this area in the Late Jurassic (12–18 °C/km) could cause brittle faulting to penetrate to greater depth. However, the very low strain rate (10^{-16} s^{-1}) offsets the effect of a cool thermal structure because it allows the lower crust and upper mantle to deform by flow to higher levels of stress (e.g., [1]).

The model developed by Behn et al. [17] is also able to account for the fact that the overall width of the basin narrows from ~250 km in west-east width at a latitude of 61 °N, to ~75 km in west-east width further south (59 °N; Fig. 1). A narrower rift is formed if there is either thicker crust or a higher axial geothermal gradient compared to the basin margins, but the along-strike variation in either of these quantities need not necessarily be large. At low geothermal gradients of ≤ 25 °C/km the width is very sensitive to relatively small changes in either of these parameters.

The predicted fault pattern (Figs. 8 and 9) is much simpler than the observed pattern. This is due to the fact that there is no heterogeneity in yield strength included in this model. Models in which random heterogeneity is included produce a wide range of fault sizes and the periodic spacing of the faults disappears [56]. Pre-existing structures will contribute to a strongly heterogeneous crustal strength distribution. Much of the detailed (i.e. kilometer-scale) rift geometry, e.g., complex fault patterns and along-strike variations in rift asymmetry, may be due to this heterogeneity.

5. Discussion and conclusions

Based on the combined data interpretation a number of key observations have been made: (1) a wide range of fault sizes formed during the extensional episode; (2) present-day maximum fault throw increases towards rift axis; (3) a preferred inward dip direction of large faults emerged as extension progressed and was accompanied by cessation of activity on outward dipping smaller-scale faults; (4) maximum fault slip rate (or maximum strain rate) correlates with fault displacement (or stretching factor, β) as well as with the duration of extension; and finally, (6) the zone of active extension narrowed through time (from ~200 km to <50 km over 40 Myr). Such systematic

spatio–temporal relationships would not be predicted if Late Jurassic extension was entirely controlled by the pre-existing (i.e., Permo-Triassic) structure of this area. We have therefore evaluated these observations in the light of existing theory of lithospheric deformation and reached the following conclusions.

1) The lack of a characteristic fault size and the systematic increase in fault throw and length towards the axis implies that the value of T_e varies significantly ($>\times 5$) across the basin. There is no independent evidence for a large lateral variation in T_e; previous workers have successfully modelled the basin stratigraphy assuming a constant value. Thus, although the fault pattern may be reflecting a lateral variation in T_e, the magnitude of the variation is probably much smaller than simple plate flexure theory would predict. In any case, existing plate flexure models for fault evolution assume a constant T_e and they are unable to explain the migration of fault activity through time seen in this area.
2) The gradual emergence of the dominant inward-dipping fault set, the higher slip rates on the faults closest to the rift axis and cessation of fault activity away from the axis, are all consistent with fault growth in the presence of a regional strain gradient. We infer that this pattern of deformation is a response to an evolving thermal structure in the thinning lithosphere. The mechanical lithosphere is thinner (and T_e lower) where the geothermal gradient is higher, i.e., at the rift axis. Faults develop with a preferential dip-direction, and slip-rates increasing, towards the region of highest geothermal gradient. Detailed field observations of modern rifts have documented a similar pattern of "migrating" fault activity through time, e.g., the Gulf of Corinth [58] and the Gulf of Suez [59]. In each case the migration sense is towards the locus of maximum extension.
3) The observed patterns of strain rate, strain (β) and rift duration indicate that the first 25–30 Myr of extension in this area (170–140 Ma) was dominated by strain localisation. The strain rate at the rift axis gradually increased during this time interval while strain rates across the basin margins declined. During the final phase of basin development (140–130 Ma) strain accumulation was focused within the rift axis but the strain rate declined rapidly from $\sim 3\times 10^{-16}$ s^{-1} to $<10^{-17}$ s^{-1}. Strain localisation implies a strain-softening effect within the lithosphere, while the eventual cessation of rifting implies that strain hardening became more important through time (assuming no change in external forces may be invoked). Existing models for "viscosity-controlled" extension (e.g., [10]) are unable to explain this dual behaviour because, at strain rates of the order of 10^{-16} s^{-1}, thermally induced strength loss is insignificant.
4) The model presented in section 4.3.1 illustrates an alternative mechanism for the strain localisation, which depends on a coupling between brittle fault growth and temperature-dependent viscous deformation. A relatively small perturbation to the thermal structure of the lithosphere is shown to exert an important control on fault development and strain localisation within the brittle layer, very similar to what is observed (see (2)). We argue that, due to strain (and/or strain rate) softening along these faults, a feedback will develop between the evolving thermal structure and the growing faults. In other words, extension on faults further focuses lithospheric thinning and heating, resulting in localisation on a lithospheric scale even at low strain rates. Our observations suggest that this process takes several tens of millions of years and results in the bulk of the total extension occurring within an axial zone only 35–50 km wide within a basin that is 200–250 km wide overall. As the strain localises, the loss of heat will increase due to increased lateral heat diffusion. Furthermore, replacement of weak crust by stronger mantle material will become progressively more important during the latter phases of the extension history when crustal buoyancy effects are also larger. Thus the coupled mechanism that we propose can explain why the deformation is initially strongly localising but also, ultimately, self-limiting without having to invoke a change in external boundary conditions.
5) Following from (3) and (4), the method proposed by Newman and White [10] for deriving the parameters of power-law creep within the lithospheric mantle from the subsidence history of wells is not applicable to wells located on the basin margins (e.g., ESB and HP). The only wells that

may actually record deep-seated viscous strain rate variations are those that penetrate the synrift section at the rift axis and thus record the entire extension history. Such wells are extremely rare.

6) The observation of progressive strain localization is not unique to the northern North Sea but can be observed in many modern rifts. For example, in East Africa the ~15 km wide zone of active rifting in the north is more mature than the 65 km wide rift system to the south [60]. Gupta and Scholz [61] interpret this to mean distributed strain occurring in the southern part of the rift, whereas strain has localized at the rift axis in the north. Another example is the Gulf of Suez which has evolved through time, from a zone ~100 km wide when it first formed (~20 Ma; mid-Miocene) to a zone only ~50 km wide during the Pliocene [62]. Thus we believe that the conclusions of this study are likely to be generally applicable.

Acknowledgements

This collaboration initiated while PAC was a Visiting Guest Investigator at WHOI. The idea emerged from discussions with A. McLeod. PAC was partially supported by a University Research Fellowship from the Royal Society of London and travel funds from WHOI. Useful discussions with J. Maclen-nan, N. White, R. Buck, J. Hopper, R. Huismans significantly improved this manuscript. Comments by L. Geoffroy and an anonymous reviewer helped clarify several aspects of the text. WHO1 contribution number 11207.

Appendix A. Finite Element Model

The results shown in Fig. 8 and described in section 4.4 were obtained using a 2-D visco-pseudo-plastic finite-element model [13,17]. A strain-rate dependent rheology is assumed for the brittle layer to simulate the rate-dependence of frictional strength observed in laboratory studies, e.g., [64,65]. For viscous flow we assume a non-Newtonian temperature-dependent rheology [66,67]:

$$\dot{\varepsilon} = A(\sigma_1 - \sigma_3)^n \exp(-Q/RT) \tag{A.1}$$

where $\dot{\varepsilon}$ is the uniaxial strain rate, σ_1 and σ_3 are the maximum and minimum principle stresses, n is the power law exponent, Q is the molar activation energy, A is a material strength constant, T is the temperature, and R is the gas constant. Although the relationship between stress and strain rate is non-linear, we can define a linearized viscosity law, e.g., [68,69], by

$$\tau_{ij} = \sqrt{2}\eta\dot{\varepsilon}_{ij} \tag{A.2}$$

where τ_{ij} is the stress tensor, η is the effective viscosity, and $\dot{\varepsilon}_{ij}$ is the strain-rate tensor. This linearization leads to an expression for the apparent effective Newtonian viscosity

$$\eta = B\dot{\varepsilon}_{\mathrm{II}}^{(1-n)/n}\exp(Q/nRT) \tag{A.3}$$

where $\dot{\varepsilon}_{\mathrm{II}}$ is the second invariant of the stain rate tensor, and B is a material constant related to A by $B = 0.25(1.33/A)^{1/n}$ [68].

In the brittle regime, strength is assumed to be controlled by a frictional resistance law, e.g., [70,71]:

$$\tau_{\max} = C_0 - \mu\sigma_n \tag{A.4}$$

where C_0 is the cohesive strength, μ is the coefficient of friction, and σ_n is approximately equal to the lithostatic stress. The rate dependence of frictional strength is simulated by defining an apparent friction coefficient, μ', as

$$\mu' = \mu_0[1 - \gamma\log_{10}(\dot{\varepsilon}_{\mathrm{II}}/\dot{\varepsilon}_0)] \tag{A.5}$$

where μ_0 is the reference coefficient of friction, γ is the strain-rate softening coefficient, and $\dot{\varepsilon}_0$ is the reference strain-rate. This formulation not only simulates strain-rate weakening for $\dot{\varepsilon}_{\mathrm{II}} > \dot{\varepsilon}_0$, but also generates strengthening in regions where $\dot{\varepsilon}_{\mathrm{II}} < \dot{\varepsilon}_0$. Behn et al. [17] showed that $\gamma \geq 0.10$ results in efficient strain localization in models of lithospheric deformation for plausible rheological structures, and we choose $\gamma = 0.15$ for the numerical experiments presented in this study. Acknowledging that this approach neglects many of the complexities of the earthquake process, we interpret these regions of high strain-rate to be analogous to fault zones. Note that in the visco-pseudoplastic formulation implemented here, the pattern of deformation is found to be relatively insensitive to the values of μ_0. and C_0.

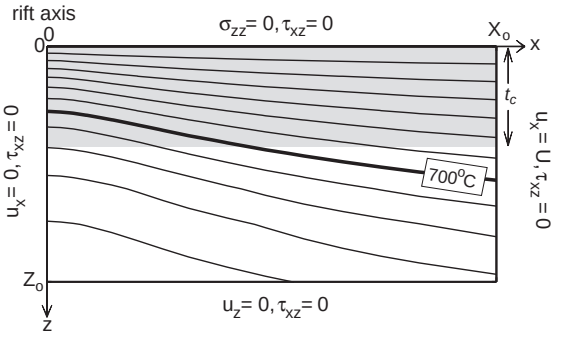

Fig. A1. Model setup for mechanical model of lithospheric stretching. The model space is symmetric about the rift axis, with dimensions X_0=300 km and Z_0=120 km. A uniform horizontal velocity U=1 km/Myr is applied to the right-hand side of the model space, and extension is continued until 1% total strain is achieved. Crustal thickness, t_c, is constant across-axis but differs for each stage of fault evolution.

Following the procedures described in [13] and [17] we calculate deformation in 2-D vertical sections of lithosphere. At each time-step the element viscosities are calculated from the temperature and evolving strain-rate fields. If the resulting maximum principle shear stress calculated from Eq. (A.2) is greater than the frictional failure criterion, τ_{max}, the effective viscosity of the element is reset to $\eta = \tau_{\max}/\sqrt{2}\dot{\varepsilon}_{\mathrm{II}}$. The initial element viscosities are calculated assuming a uniform reference strain-rate of 10^{-16} s^{-1}.

We note that the numerical experiments presented here should be treated only as a proxy for the initial pattern of faulting that develops for a given set of thermal conditions, rather than as a method to study the evolution of individual faults over geologic time. The rotation of fault blocks in highly extended terrains generates large flexural stresses, e.g., [46,47], that are not accounted for in our visco-pseudoplastic formulation. By limiting our calculations to 1% total strain, we can safely ignore these elastic stresses and eliminate numerical inaccuracies associated with the distortion of model elements. Furthermore, because we are considering only the initial pattern of faulting associated with a given set of thermal conditions we do not solve for the evolution of temperature.

The model setup and boundary conditions are illustrated in Fig. Al. Deformation is driven by applying a uniform horizontal velocity of 1 km/Myr to the right-hand side of the model space $x=X_0$, giving an initial reference strain-rate of 10^{-16} s^{-1}. For numerical efficiency, a symmetry condition is imposed on the left-hand side of model ($x=0$) by setting the horizontal velocity, u_x, and the shear stress, τ_{xz}, equal to zero. The model dimensions (X_0=300 km and Z_0=120 km) are specified to ensure that the boundaries do not influence the final solution and the finite element grid is adjusted to give maximum resolution (grid size of 1 km x 1 km) near the rift axis. The thermal gradients and crustal thickness values used for each of the stages of fault evolution, as well as material properties assumed for the crust and mantle, are given in the caption to Fig. 8.

References

[1] W.R. Buck, L.L. Lavier, A. Poliakov, How to make a rift wide, Philos. Trans. R. Soc. Lond. 357 (1999) 671–693.
[2] G.C.P. King, R.S. Stein, J.B. Rundle, The growth of geological structures by repeated earthquakes: 1. Conceptual framework, J. Geophys. Res. 93 (1988) 13307–13318.
[3] J.K. Weissel, G. Karner, Flexural uplift of rift flanks due to tectonic denudation of the lithosphere during extension, J. Geophys. Res. 94 (1989) 13919–13950.
[4] N.J. Kusznir, G. Marsden, S.S. Egan, A flexural-cantilever simple-shear/pure-shear model of continental lithosphere extension: applications to the Jeanne d'Arc Basin, Grand Banks and Viking Graben, North Sea, in: A.M. Roberts, G. Yielding, B. Freeman (Eds.), The Geometry of Normal Faults, Spec. Publ.–Geol. Soc., vol. 56, 1991, pp. 41–60.
[5] M.T. Voorde, R. Ravnås, R. Færseth, S. Cloetingh, Tectonic modelling of the Middle Jurassic synrift stratigraphy in the Oseberg–Brage area, Northern Viking Graben, Basin Res. 9 (1997) 133–150.
[6] M.T. Voorde, R. Færseth, R.H. Gabrielsen, S. Cloetingh, Repeated lithosphere extension in the northern Viking Graben: a coupled or a decoupled rheology?, in: A. Nøttvedt (Ed.), Dynamics of the Norwegian Margin, Spec. Publ.–Geol. Soc. Lond., vol. 167, 2000, pp. 59–81.
[7] P.C. England, Constraints on extension of continental lithosphere, J. Geophys. Res. 88 (1983) 1145–1152.
[8] M.T. Zuber, E.M. Parmentier, Lithospheric necking: a dynamic model for rift morphology, Earth Planet. Sci. Lett. 77 (1986) 373–383.
[9] L.J. Sonder, P.C. England, Effects of a temperature-dependent rheology on large-scale continental extension, J. Geophys. Res. 94 (1989) 7603–7619.
[10] R. Newman, N. White, The dynamics of extensional sedimentary basins: constraints from subsidence inversion, Philos. Trans. R. Soc. Lond. 357 (1999) 805–830.
[11] J. Braun, C. Beaumont, Styles of continental rifting: results from dynamic models of lithospheric extension, in: C.

Beaumont, A.J. Tankard (Eds.), Sedimentary Basins and Basin Forming Mechanisms, Can. Soc. Pet. Geol. Mem., vol. 12, 1987, pp. 241–258.
[12] G. Bassi, Relative importance of strain rate and rheology for the mode of continental extension, Geophys. J. Int. 122 (1995) 195–210.
[13] G. Neumann, M. Zuber, A continuum approach to the development of normal faults, in: J. Daemen, R. Schultz (Eds.), 35th US Symposium on Rock Mechanics, Balkema, Lake Tahoe, Nevada, 1995, pp. 191–198.
[14] J.R. Hopper, W.R. Buck, The effect of lower crustal flow on continental extension and passive margin formation, J. Geophys. Res. 101 (1996) 20175–20194.
[15] E. Burov, A. Poliakov, Erosion and rheology controls on synrift and postrift evolution: verifying old and new ideas using a fully coupled numerical model, J. Geophys. Res. 106 (2001) 16461–16481.
[16] L.L. Lavier, W.R. Buck, A.N.B. Poliakov, Factors controlling normal fault offset in an ideal brittle layer, J. Geophys. Res. 105 (2000) 23431–23441.
[17] M.D. Behn, J. Lin, M.T. Zuber, A continuum mechanics model for normal faulting using a strain-rate softening rheology: implications for thermal and rheological controls on continental and oceanic rifting, Earth Planet. Sci. Lett. 202 (2002) 202.
[18] M.D. Behn, J. Lin, M.T. Zuber, Effects of hydrothermal cooling and magma injection on mid-ocean ridge temperature structure, deformation and axial morphology, in: C.R. German, J. Lin, L.M. Parsons (Eds.), Mid-Ocean Ridges: Hydrothermal Interactions Between the Lithosphere and Oceans, American Geophysical Union Geophysical Monograph, vol. 148, 2004, pp. 151–165. doi:10.1029/148GM06.
[19] R.S. Huismans, C. Beaumont, Symmetric and asymmetric lithospheric extension: relative effects of frictional-plastic and viscous strain softening, J. Geophys. Res. 108 (B10) (2003), doi:10.1029/2002JB002026.
[20] R. Ravnås, K. Bondevik, W. Helland-Hansen, L. Lømo, A. Ryseth, R.J. Steel, Sedimentation history as an indicator of rift initiation and development: the Late Bajocian–Bathonian evolution of the Oseberg–Brage area, northern North Sea, Norsk Geol. Tiddsk. 77 (1997) 205–232.
[21] A.E. Mcleod, N.H. Dawers, J.R. Underhill, The propagation and linkage of normal faults: insights from the Strathspey–Brent–Statfjord fault array, northern North Sea, Basin Res. 12 (2000) 263–284.
[22] A.E. Mcleod, J.R. Underhill, S.J. Davies, N.H. Dawers, The influence of fault array evolution on syn-rift sedimentation patterns: controls on deposition in the Strathspey–Brent–Statfjord half-graben, northern North Sea, Bull. Am. Assoc. Pet. Geol. 86 (2002) 1061–1093.
[23] M.J. Young, R.L. Gawthorpe, S. Hardy, Growth and linkage of a segmented normal fault zone; the Late Jurassic Murchison–Stratfjord North fault, northern North Sea, J. Struct. Geol. 23 (2001) 1933–1952.
[24] P. Bellingham, N. White, A general inverse method for modeling extensional sedimentary basins, Basin Res. 12 (2000) 219–226.
[25] G. Enyon, Basin development and sedimentation in the Middle Jurassic of the northern North Sea, in: L.V. Illing, G.D. Hobson (Eds.), Petroleum Geology of the Continental Shelf of Northwest Europe, Heyden and Son, London, 1981, pp. 196–204.
[26] M.E. Badley, T. Egeberg, O. Nipen, Development of rift basins illustrated by the structural evolution of the Oseberg structure, block 30/6, offshore Norway, J. Geol. Soc. (Lond.) 141 (1984) 639–649.
[27] M.E. Badley, J.D. Price, C.R. Dahl, T. Agdestein, The structural evolution of the North Viking Graben and its bearing upon extensional modes of basin formation, J. Geol. Soc. (Lond.) 145 (1988) 455–472.
[28] K.S. Lervik, A.M. Spencer, G. Warrington, Outline of the Triassic stratigraphy and structure in the central and northern North Sea, in: J. Collinson (Ed.), Correlation in Hydrocarbon Exploration, Graham and Trotman, London, 1989, pp. 173–190.
[29] A.M. Roberts, G. Yielding, M.E. Badley, A kinematic model for the orthogonal opening of the late jurassic North Sea rift system, Denmark–mid Norway, in: D.J. Blundell, A.D. Gibbs (Eds.), Tectonic Evolution of the North Sea Rifts, Clarendon Press, Oxford, 1990, pp. 180–199.
[30] R.J. Steel, A. Ryseth, The Triassic–Early Jurassic succession in the northern North Sea: megasequence stratigraphy and intra-Triassic tectonics, in: R.F.P. Hardman, J. Brooks (Eds.), Tectonic Events Responsible for Britains Oil and Gas Reserves, Spec. Publ.–Geol. Soc., Lond., vol. 55, 1990, pp. 139–168.
[31] G. Yielding, M.E. Badley, A.M. Roberts, The structural evolution of the Brent Province, in: C. Morton, R.S. Haszeldine, M.R. Giles, S. Brown (Eds.), Geology of the Brent Group, Spec. Publ.–Geol. Soc. Lond., vol. 61, 1992, pp. 27–43.
[32] M. Tomasso, J.R. Underhill, R.A. Hodgkinson, M.J. Young. Structural styles and depositional architecture in the Triassic of the Ninian and Alwyn North fields: implications for basin development and prospectivity in the northern North Sea, Marine and Petroleum Geology, in press.
[33] R.B. Færseth, Interaction of Permo-Triassic and Jurassic extensional fault blocks during the development of the northern North Sea, J. Geol. Soc. (Lond.) 153 (1996) 931–944.
[34] R.B. Færseth, R. Ravnås, Evolution of the Oseberg fault-block in the context of the northern North Sea structural framework, Mar. Pet. Geol. 15 (1998) 467–490.
[35] T. Odinsen, P. Christiansson, R.H. Gabrielsen, J.I. Faleide, A.M. Berge, The geometries and deep structure of the northern North Sea rift system, in: A. Nøttvedt (Ed.), Dynamics of the Norwegian Margin, Spec. Publ.–Geol. Soc. Lond., vol. 167, 2000, pp. 41–57.
[36] N.H. Dawers, J.R. Underhill, The role of fault interaction and linkage in controlling syn-rift stratigraphic sequences: Late Jurassic, Statfiord East area, northern North Sea, Bull. Am. Assoc. Pet. Geol. 84 (2000) 45–64.
[37] S.J. Davies, N.H. Dawers, A.E. Mcleod, J.R. Underhill, The structural and sedimentological evolution of early synrift sucessions: the Middle Jurassic Tarbert Formation, North Sea, Basin Res. 12 (2000) 343–366.

[38] N. White, An inverse method for determining lithospheric strain rate variation on geological timescales, Earth Planet. Sci. Lett. 122 (1994) 351–371.
[39] A.M. Roberts, G. Yielding, N. Kusznir, I.M. Walker, D. Dorn-Lopez, Mesozoic extension in the North Sea: constraints from flexural backstripping, forward modelling and fault populations, in: J.R. Parker (Ed.), Petroleum Geology of Northwest Europe: Proceedings of the 4th Conference, The Geological Society, London, 1993, pp. 1123–1136.
[40] R.A. Marrett, R.W. Allmendinger, Amount of extension on "small" faults: an example from the Viking Graben, Geology 20 (1992) 47–50.
[41] H. Fossen, T. Odinsen, R.B. Færseth, R.H. Gabrielsen, Detachment and low-angle faults in the nothern North Sea rift system, in: A. Nøttvedt (Ed.), Dynamics of the Norwegian Margin, Spec. Publ.–Geol. Soc. Lond., vol. 167, 2000, pp. 105–131.
[42] D.B. Haig, The Hutton Field, Blocks 211/28, 211/27, UK North Sea, in: I.L. Abbotts (Ed.), United Kingdom Oil and Gas Fields, 25 Years Commemorative, Mem Geol. Soc. Lond., vol. 14, 1991, pp. 135–143.
[43] C.E. Gill, The role of antithetic faulting in setting up the Hudson Play, East Shetland Basin, UK Northern North Sea, AAPG Annual Convention Abstract A62.
[44] A.M. Roberts, G. Yielding, M.E. Badley, Tectonic and bathymetric controls on stratigraphic sequences within evolving half-graben, in: G.D. Williams, A. Dobb (Eds.), Tectonics and Seismic Sequence Stratigraphy, Spec. Publ.–Geol. Soc. Lond., vol. 71, 1993, pp. 87–121.
[45] R.B. Færseth, T.S. Sjøblom, R.J. Steel, T. Liljedahl, B.E. Sauar, Tectonic controls on Bathonian–Volgian synrift successions on the Visund fault block, northern North Sea, in: R.J. Steel, V.L. Felt, E.P. Johannessen, C. Mathieu (Eds.), Sequence Stratigraphy on the Northwest European Margin, no. 5 in Norwegian Petroleum Society, Special Publications, 1995, pp. 325–346.
[46] D.W. Forsyth, Finite extension and low–angle normal faulting, Geology 20 (1992) 27–30.
[47] W.R. Buck, Effects of lithospheric thickness on the formation of high- and low-angle normal faults, Geology 21 (1993) 933–936.
[48] L.L. Lavier, W.R. Buck, Half graben versus large-offset low-angle normal fault: importance of keeping cool during normal faulting, J. Geophys. Res. 107 (2002), doi:10.1029/2001JB000513.
[49] R. Hassani, J. Chéry, Anelasticity explains topography associated with basin and range normal faulting, Geology 24 (1996) 1095–1098.
[50] A.M. Roberts, N.J. Kusznir, G. Yielding, P. Styles, 2D flexural backstripping of extensional basins: the need for a sideways glance, Pet. Geosci. 4 (1998) 327–338.
[51] T. Takeshita, A. Tamaji, Acceleration of continental rifting due to thermomechanical instability, Tectonophysics (Amst.) 181 (1990) 307–320.
[52] S. Wdowinski, R.J. O'Connell, On the choice of boundary conditions in continuum models of continental deformation, Geophys. Res. Lett. 17 (1990) 2413–2416.
[53] J. Jackson, Active normal faulting and crustal extension, in: M.P. Coward, J.F. Dewey, P.L. Hancock (Eds.), Continental Extensional Tectonics, Spec. Pub.–Geol. Soc., vol. 28, 1987, pp. 3–17.
[54] C. Scholz, J. Contreras, Mechanics of continental rift architecture, Geology 26 (1998) 967–970.
[55] P.A. Cowie, A healing–reloading feedback control on the growth rate of seismogenic faults, J. Struct. Geol. 20 (1998) 1075–1087.
[56] K.M. Hardacre, P.A. Cowie, Controls on strain localisation in a two-dimensional elasto-plastic layer: Insights into size-frequency scaling of extensional fault populations, J. Geophys. Res. 108 (B11) (2003) 2529. doi:10.1029/2001JB1712.
[57] M. Ishikawa, K. Otsuki, Effects of strain gradients on asymmetry of experimental normal fault systems, J. Struct. Geol. 17 (1995) 1047–1053.
[58] M. Goldsworthy, J. Jackson, Migration, of fault activity within normal fault systems: examples from the Quaternary of mainland Greece, J. Struct. Geol. 23 (2001) 489–506.
[59] R.L. Gawthorpe, C.A.L. Jackson, M.J. Young, I.R. Sharp, A.R. Moustafa, C.W. Leppard, Normal fault growth, displacement localisation and the evolution of normal fault populations: the Hamman Faraun fault block, Suez Rift, Egypt, J. Struct. Geol. 25 (2003) 1347–1348.
[60] C.J. Ebinger, J.A. Jackson, A.N. Foster, N.J. Hayward, Extensional basin geometry and the elastic lithosphere, Philos. Trans. R. Soc. Lond. 357 (1999) 671–693.
[61] A. Gupta, C.H. Scholz, Brittle strain regime transition in the Afar depression: implications for fault growth and seafloor spreading, Geology 28 (2000) 1087–1090.
[62] T.L. Patton, A.R. Moustafa, R.A. Nelson, S.A. Abdine, Tectonic evolution and structrual setting of the Suez Rift, in: S. Landon (Ed.), Interior Rift Basins, AAPG Mem., vol. 59, 1994, pp. 9–55.
[63] P. Christiansson, J.I. Faleide, A.M. Berge, Crustal structure in the northern North Sea: an integrated geophysical study, in: A. Nøttvedt (Ed.), Dynamics of the Norwegian Margin, Spec. Publ.–Geol. Soc., Lond., vol. 167, 2000, pp. 15–40.
[64] J. Dieterich, Modeling of rock friction 1. Experimental results and constitutive equations, J. Geophys. Res. 84 (1979) 2161–2168.
[65] A. Ruina, Slip instability and state variable friction laws, J. Geophys. Res. 88 (1983) 10359–10370.
[66] S. Kirby, Rheology of the lithosphere, Rev. Geophys. Space Phys. 21 (1983) 1458–1487.
[67] D. Kohlstedt, B. Evans, S. Mackwell, Strength of the lithosphere: constraints imposed by laboratory experiments, J. Geophys. Res. 100 (1995) 17587–17602.
[68] Y. Chen, W. Morgan, A nonlinear rheology model for mid-ocean ridge axis topography, J. Geophys. Res. 95 (1990) 17583–17604.
[69] R. Boutilier, C. Keen, Geodynamic models of fault-controlled extension, Tectonics (Washington, D.C.) 13 (1994) 439–454.
[70] J.D. Byerlee, Friction of rocks, PAGEOPH 116 (1978) 615–626.
[71] C.H. Scholz, The Mechanics of Earthquakes and Faulting, Second edition, Cambridge University Press, Cambridge, 2002.

APPENDIX

Appendix 1 **Seismic reflection database**

Appendix 2 **Well database**

Appendix 3 **Fault database**

Appendix 4 **Displacement-length profiles for Visund-Gullfaks Footwall faults**

Appendix 5 **Time Maps**

Appendix 6 **Biostratigraphy for well 34/8-7**

Appendix 7 **Published papers**

Appendix 1 Seismic reflection database

The following 3D seismic reflection surveys were incorporated into the thesis:

cn01m02
dunlin
e86
e89f3d
esb2000
full
ge83
hydro_survey_1
hydrosurvey1
hydrosurvey2
lm9110
lm9229-pelical
lm95061_-
_osprey_1994
lm96083_brent
lm96083_survey
lm96105
mc3d_34_1_2_3
merge_nh9001_nh9106
mn9401
mn9601
nc95
nh9001-9
nh9101-jun92
nh9106
nh9201
nh9204_brage
nh9401
nh96_merge
ninian
nnst-84-2d
nvg96
p3_1aory
sg8420
sg8431_re
sg9201
sg9202
sg9603m
ss_survey
st8511r92
st8701
st8720-rirrui
cn
dunlin
st9101
st97m3
st98m5
st98m7
sw97106
sw97106_3
sw97115_survey
sw97191
sw98087_survey
sw98207
sw98293_survey
visund
xb90

The following 2D seismic reflection surveys were incorporated into the thesis:

esbt-89
esbt89-nnsti86
ms85
nest90
nnst-84
nnst-84-2d
nnst84
nnsti-84
nnsti-86
nnsti-88
sw85
tampen

Appendix 2 Well Database

Data from the following wells were incorporated into this thesis: Well data, including formation tops are presented in enclosure 1.

3/2-2	3/9b-10	33/5-1
3/2-3	3/9a-11	33/5-2
3/2-4	3/9a-N33	33/6-1
3/2-5	3/9a-N34	33/7-5
3/2-6	3/9a-N35	33/7-24s
3/2-7	3/9a-N38	33/7-29
3/2-8	3/9a-N39	33/9-1
3/2-9	3/9a-N40	33/9-2
3/3-1	3/10b-1	33/9-3
3/3-4A	3/10b-2	33/9-4
3/3-8	3/14-1	33/9-5
3/3-9	3/14a-2	33/9-6
3/4-1	3/14a-3	33/9-7
3/4-2	3/14a-4	33/9-8
3/4-3	3/14a-5	33/9-9
3/4-4	3/14a-6	33/9-10
3/4-5	3/14a-7	33/9-11
3/4-6	3/14a-8	33/9-12
3/4-7	3/14a-9	33/9-13s
3/4-8	3/14a-10	33/9-13
3/4a-9	3/14a-11	33/9-14
3/4a-10	3/14a-12	33/9-15
3/4a-11	3/14a-13	33/9-16
3/4a-12	3/14a-14	33/9-17
3/4a-13	3/14a-15	33/9-18
3/4a-14	3/14a-D16	33/9-18a
3/4a-15	3/14a-D22	33/9-19A
3/4a-16	3/14a-2B	33/9-a17
3/4b-17	3/15-2	33/9-a18
3/4b-18	3/15-6	33/9-a23
3/4a-18B&S1	3/18c-1	33/9-c6
3/4-M12	3/19b-2	33/9-c11
3/7-3	29/3-1	33/9-c17
3/9a-1	30/2-1	33/9-c27
3/9a-2	30/2-2	33/12-1
3/9a-3	30/2-3	33/12-2
3/9a-4	30/2-4	33/12-3
3/9a-5	30/3-1	33/12-4
3/9a-6	30/6-1	33/12-5
3/9b-7	30/8-2	33/12-6
3/9a-8	31/4-2	33/12-7
3/9a-9	31/4-4	33/12-b6

33/12-b16
33/12-b18
33/12-b21
33/12-b23
34/2-1
34/2-2
34/2-3
34/2-4
34/4-1
34/4-2
34/4-3
34/4-4
34/4-5
34/4-6
34/4-7
34/4-8
34/4-9S
34/7-1
34/7-2
34/7-3
34/7-4
34/7-5
34/7-6
34/7-7
34/7-8
34/7-9
34/7-10
34/7-11
34/7-12
34/7-13
34/7-14
34/7-15
34/7-15s
34/7-16
34/7-17
34/7-18
34/7-19
34/7-20
34/7-21
34/7-21a
34/7-21s
34/7-22
34/7-23
34/7-23a
34/7-23s
34/7-24
34/7-24s
34/7-25
34/7-25s
34/7-26
34/7-27
34/7-28
34/7-29
34/7-30
34/7-31
34/7-32
34/8-1
34/8-2
34/8-3
34/8-3A
34/8-4A
34/8-4S
34/8-5
34/8-6
34/8-7
34/8-8
34/8-9
34/8-9s
34/8-10
34/8-10s
34/8-11
34/8-12
34/8-16
34/9-3
34/9-6
34/10-1
34/10-2
34/10-3
34/10-4
34/10-5
34/10-6
34/10-7
34/10-8
34/10-9
34/10-11
34/10-12
34/10-13
34/10-14
34/10-15
34/10-16
34/10-19
34/10-20
34/10-21
34/10-23
34/10-25
34/10-26
34/10-29
34/10-32
34/10-33
34/10-34
34/10-35
34/10-36
34/10-40
34/10-41
34/10-45
34/10-46
34/11-1
34/11-2
34/11-3
34/11-4
35/4-1
35/8-1
35/9-1
35/11-1
210/24-1
210/24-a-1A
210/24-2
210/24a-3
210/24a-4
210/24a-4A
210/24a-5
210/24a-6
210/24a-8
210/24a-9
210/24a-A1
210/24a-A2
210/24a-B1
210/24a-B2
210/24a-B3
210/24a-B4
210/24a-B5
210/24a-B5Z
210/24a-B6
210/24a-B6Z
210/24b-7
210/24b-7Z
211/8-3
211/11-2
211/13a-1
211/13-2
211/13-3
211/13-6
211/13a-9Z
211/13a-13
211/14-1
211/14-2
211/14-3Z
211/14-4
211/14-5
211/14-16
211/16-3
211/16b-7
211/18-2
211/18-3
211/18-4A
211/18-14

211/18a-7
211/19-1
211/19-2
211/19-3
211/19-4
211/19-5
211/19-6
211/19a-7
211/19-a8
211/19a-10
211/23-3
211/23-4
211/23a-8
211/23-9
211/23-P3
211/23-P8Z
211/24-1
211/24-4
211/24-10Z
211/29-1
211/29-2
211/29-3
211/29-4
211/29-5
211/29-6
211/29-7
211/29-8
211/29-9
211/29-10
211/29c-15
211/29-d38
211/30-1

Appendix 3 Fault Database

The following faults were mapped on 3D and 2D seismic reflection data within the study area. Faults were named according to the order in which they were mapped. Where fault numbers are missing they were subsequently found to be contemporaneous with another mapped structure.

Name	Main Fault assciation	Syn/Anti/Main	Description
cg_2	Murchison		hangingwall fault
cg_3	Murchsion	antithetic	hangingwall fault
cg_6	Murchison	synthetic	footwall fault
cg_7	Murchison	main	
cg_8	Murchison	synthetic	footwall fault
cg_10	Murchison	synthetic	footwall fault parallel to cg_47
cg_11	Murchison	synthetic	footwall fault - small
cg_12	Murchison	main	Statfjord Nord Segment
cg_13	Murchison	synthetic	Same as cg_15
cg_14	Murchison	synthetic	footwall fault
cg_15	Murchison	synthetic	tip of cg_8 Same as cg_13
cg_16	Murchison	synthetic	footwall fault parallel to cg_7 and cg_12
cg_17	Murchison	antithetic	footwall fault
cg_19	Murchison	synthetic	footwall fault
cg_21	Murchison	synthetic	footwall fault- just behind cg_12 (SNS)
cg_22	Murchison	antithetic	footwall fault- just behind cg_12 (SNS)
cg_23	Murchison	synthetic	hangingwall fault - infront og cg_12 (SNS)
cg_25	Murchison	synthetic	footwall fault behind jog fault perpendicular to cg_26
cg_26	Murchison	synthetic	same as cg_28
cg_29	Murchison	synthetic	in footwall to Murchsion fault at northern end
cg_30	Murchison	antithetic	footwall to cg_12 (SNS)
cg_31	Murchison	antithetic	footwall to cg_12 (SNS)
cg_32	Murchison	antithetic	footwall to cg_12 (SNS)
cg_33	Murchison	synthetic	footwall to cg_12 (SNS)
cg_34	Murchison	synthetic	Define minihalf graben with cg_35 behind jog fault
cg_35	Murchison	antithetic	Define minihalf graben with cg_35 behind jog fault
cg_36	Murchison	antithetic	footwall to cg_12 (SNS) - small antithetic defines heather depocentre
cg_37	Murchison	antithetic	hangingwall fault facing cg_7
cg_38	Murchison	antithetic	Small fracture parallel to cg_36
cg_39	Statfjord	main	
cg_40	Murchison	synthetic	Defines small horst block at BCU level in W of st98m5

cg_41	Murchison	antithetic	Defines small horst block at BCU level in W of st98m5
cg_42	Visund	synthetic	Footwall Fault
cg_43	Visund	synthetic	Footwall Fault
cg_44	Statfjord	antithetic	Antithetic facing main fault
cg_45	Statfjord	synthetic	Branch from main Statfjord Fault
cg_46	Snorre	antithetic	Hangingwall fault
cg_47	Murchison	synthetic	footwall fault
cg_48	Murchison	synthetic	footwall fault
cg_49	Murchison	synthetic	footwall fault
cg_50	Murchison	synthetic	footwall fault
cg_51	Murchison	synthetic	footwall fault
cg_52	Murchison	synthetic	footwall fault - NW corner st97m3. V. small
cg_53	Murchison	synthetic	footwall fault - with cg_55 define horst in ospery
cg_54	Murchison	synthetic	footwall fault- with cg_54 defines horst in ospery
cg_55	Murchison	synthetic	
cg_vis1	Visund	Main	Main visund fault in south of area adjacent to Gullfaks
cg_vis2	Visund	synthetic	Footwall fault
cg_vis3	Visund	Main	Main visund fault in north of nh9001-9
cg_vis4	Visund	synthetic	Footwall fault: No hangingwall strat - all eroded
cg_vis5	Visund	synthetic	Footwall Fault
cg_vis6	Visund	synthetic	Footwall Fault
cg_vis8	Visund	synthetic	Footwall Fault - branch of cg_vis2
cg_vis9	Visund	synthetic	Footwall fault
cg_vis10	Visund	synthetic	Footwall fault in centre of nh9001-9 trending NE-SW
cg_vis11	Visund	antithetic	Footwall fault in cno1m02
cg_vis12	Visund	antithetic	Footwall fault in cno1m02
cg_vis13	Visund	antithetic	Footwall fault in cno1m02
cg_vis14	Visund	antithetic	Footwall fault in cno1m02
cg_vis15	Visund	synthetic	Footwall faults in immediate footwall to main Visund Fault
cg_vis16	Visund	synthetic	Footwall faults in immediate footwall to main Visund Fault
cg_vis17	Visund	synthetic	Footwall faults in immediate footwall to main Visund Fault
cg_vis18	Visund	synthetic	Footwall faults next to cg_vis6
cg_vis19	Visund	synthetic	Footwall faults next to cg_vis6
cg_vis21	Visund	synthetic	Footwal Fault
cg_vis22	Visund	synthetic	Footwall Fault
cg_vis23	Visund	synthetic	Footwall Fault
cg_vis24	Visund	synthetic	Footwall Fault
cg_vis25	Visund	synthetic	Footwall Fault
cg_vis26	Visund	synthetic	Footwall Fault
cg_vis27	Visund	antithetic	Footwall Fault
cg_vis28	Visund	synthetic	Footwall Fault
cg_vis29	Visund	synthetic	Footwall Fault

cg_vis33	Visund	synthetic	Footwall Fault
cg_vis34	Visund	synthetic	Footwall Fault
cg_vis35	Visund	synthetic	Footwall Fault
cg_vis36	Visund	synthetic	Footwall Fault
cg_vis40	Visund	antithetic	Footwall Fault
cg_vis41	Visund	synthetic	Footwall Fault
cg_vis42	Visund	synthetic	Footwall Fault - no hangingwall data
cg_vis43	Visund	synthetic	Footwall Fault - no footwall data
cg_vis44	Visund	synthetic	Footwall fault
cg_vis45	Visund	synthetic	Footwall Fault
cg_vis46	Visund	synthetic	Footwall Fault
cg_snor	Snorre	main	Main Snorre Fault
cg_mur	Murchison	main	Main Murchison Fault

Appendix 4 Displacement-length profiles for Visund-Gullfaks Footwall Faults

Displacement-length profiles for the following faults (in numerical order):

Raw data is presented in enclosure 1.

VFWF2
VFWF5
VFWF8
VFWF9
VFWF10
VFWF11
VFWF12
VFWF13
VFWF14
VFWF15
VFWF16
VFWF17
VFWF18
VFWF19
VFWF21
VFWF22
VFWF23
VFWF24
VFWF25
VFWF26
VFWF27
VFWF28
VFWF33
VFWF34
VFWF34N
VFWF35
VFWF36
VFWF40
VFWF41
VFWF46
VFWF46

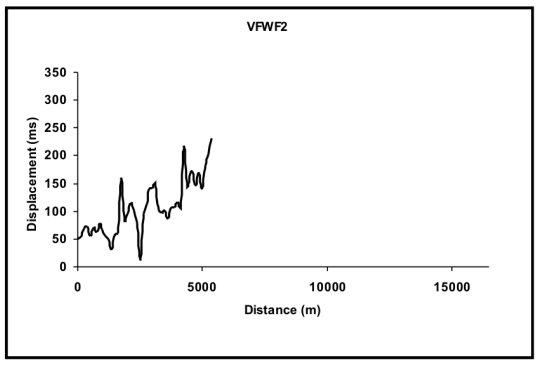
VFWF2
Displacement (ms)
350
300
250
200
150
100
50
0
0
5000
10000
15000
Distance (m)

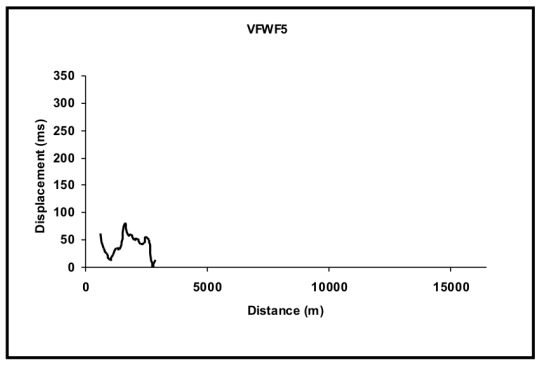
VFWF5
Displacement (ms)
350
300
250
200
150
100
50
0
0
5000
10000
15000
Distance (m)

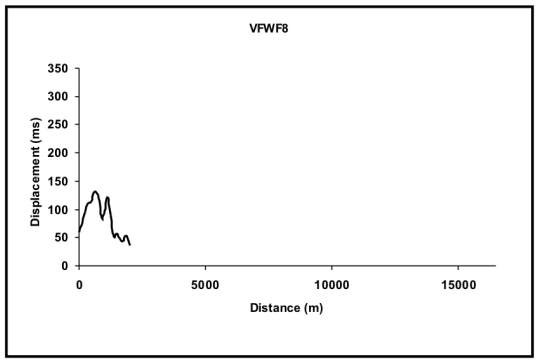
VFWF8
Displacement (ms)
350
300
250
200
150
100
50
0
0
5000
10000
15000
Distance (m)

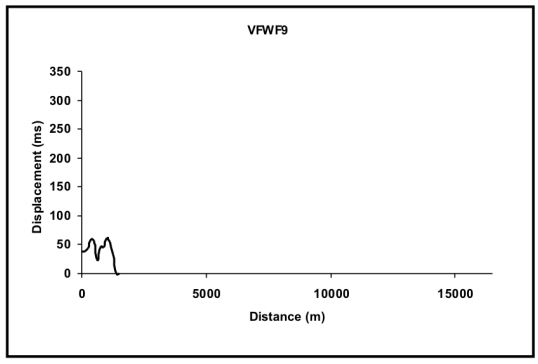
VFWF9
Displacement (ms)
350
300
250
200
150
100
50
0
0
5000
10000
15000
Distance (m)

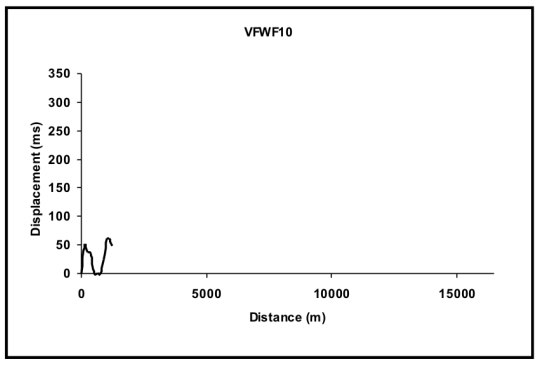
VFWF10
Displacement (ms)
350
300
250
200
150
100
50
0
0
5000
10000
15000
Distance (m)

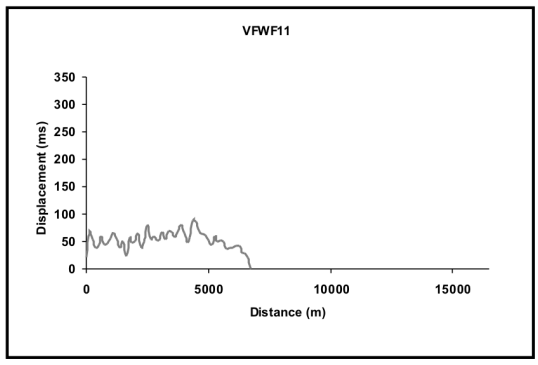
VFWF11
Displacement (ms)
350
300
250
200
150
100
50
0
0
5000
10000
15000
Distance (m)

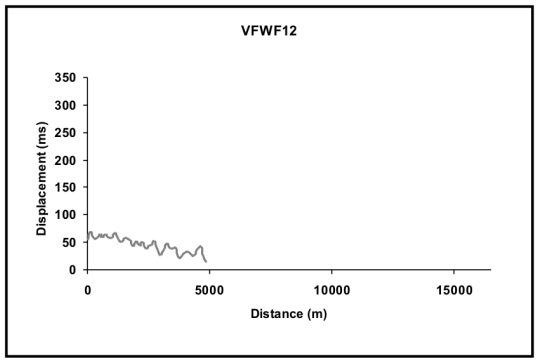
VFWF12
Displacement (ms)
350
300
250
200
150
100
50
0
0
5000
10000
15000
Distance (m)

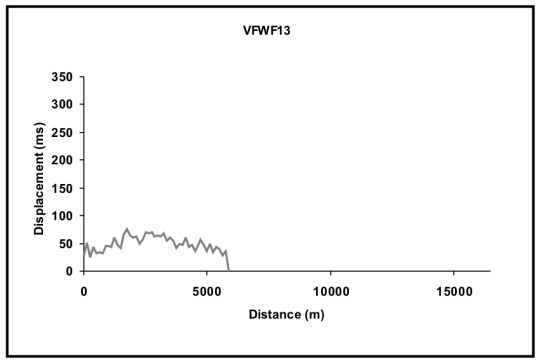
VFWF13
Displacement (ms)
350
300
250
200
150
100
50
0
0
5000
10000
15000
Distance (m)

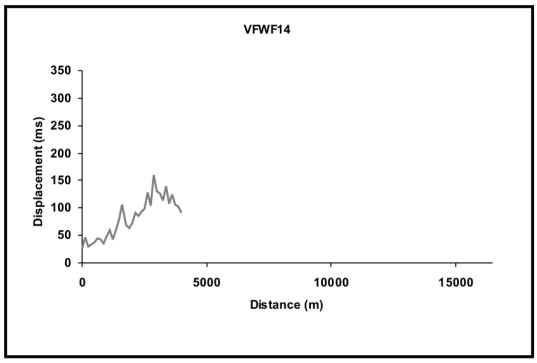
VFWF14
Displacement (ms)
350
300
250
200
150
100
50
0
0
5000
10000
15000
Distance (m)

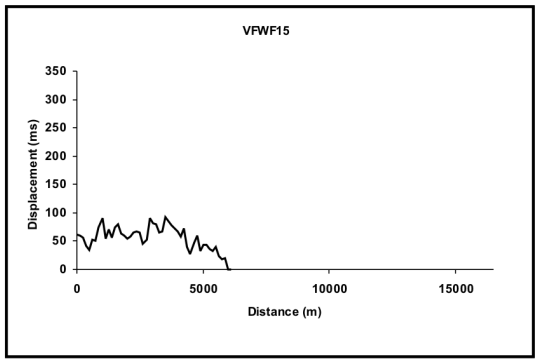
VFWF15
Displacement (ms)
350
300
250
200
150
100
50
0
0
5000
10000
15000
Distance (m)

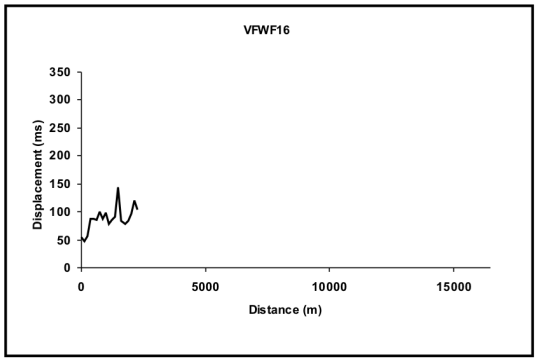
VFWF16
Displacement (ms)
350
300
250
200
150
100
50
0
0
5000
10000
15000
Distance (m)

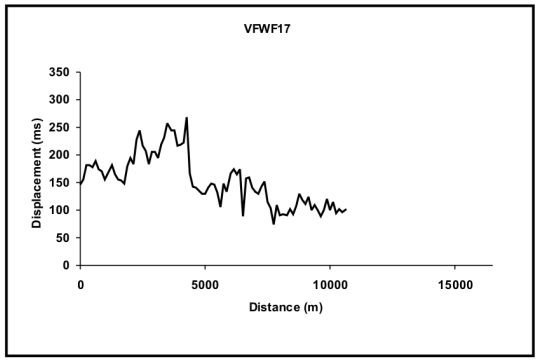
VFWF17
Displacement (ms)
350
300
250
200
150
100
50
0
0
5000
10000
15000
Distance (m)

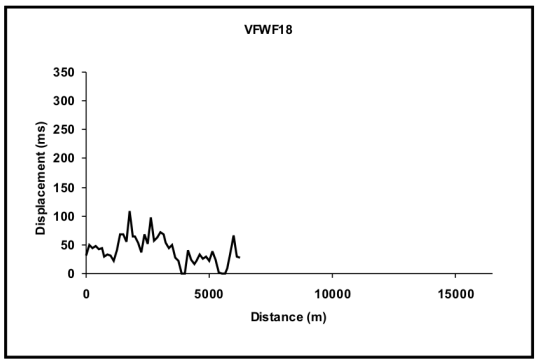
VFWF18
Displacement (ms)
350
300
250
200
150
100
50
0
0
5000
10000
15000
Distance (m)

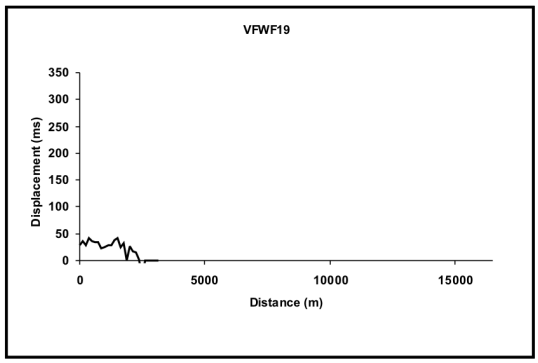
VFWF19
Displacement (ms)
350
300
250
200
150
100
50
0
0
5000
10000
15000
Distance (m)

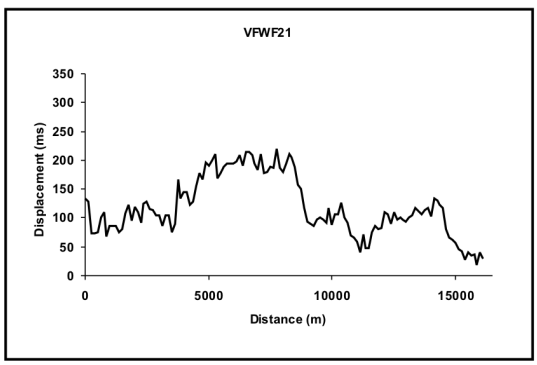
VFWF21
Displacement (ms)
350
300
250
200
150
100
50
0
0
5000
10000
15000
Distance (m)

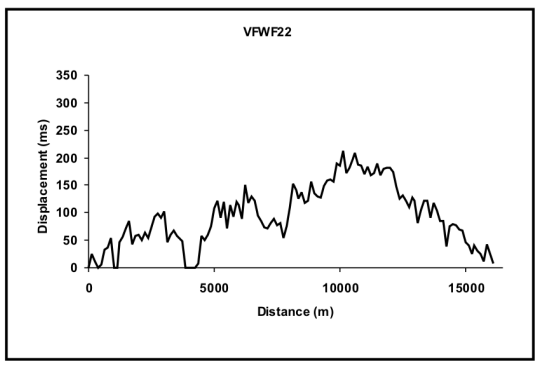
VFWF22
Displacement (ms)
350
300
250
200
150
100
50
0
0
5000
10000
15000
Distance (m)

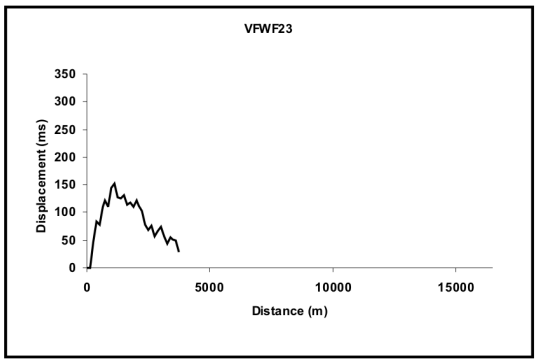
VFWF23
Displacement (ms)
350
300
250
200
150
100
50
0
0
5000
10000
15000
Distance (m)

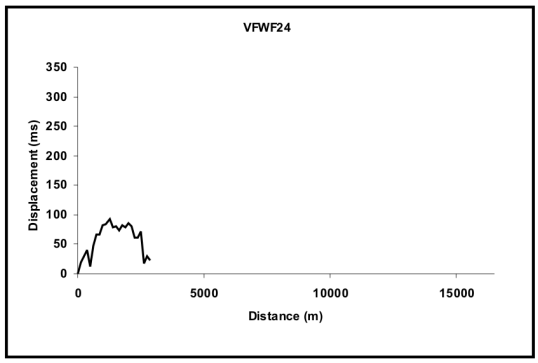
VFWF24
Displacement (ms)
350
300
250
200
150
100
50
0
0
5000
10000
15000
Distance (m)

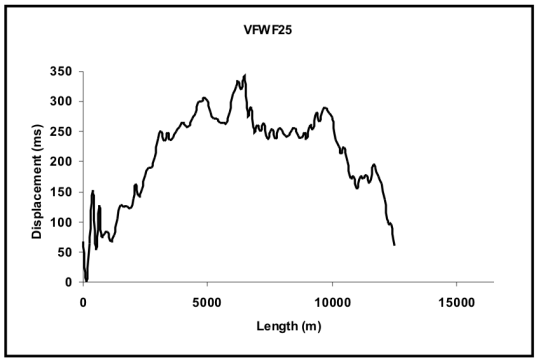
VFWF25
Displacement (ms)
350
300
250
200
150
100
50
0
0
5000
10000
15000
Length (m)

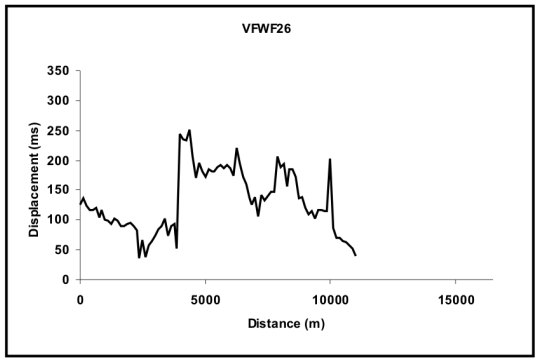
VFWF26
Displacement (ms)
350
300
250
200
150
100
50
0
0
5000
10000
15000
Distance (m)

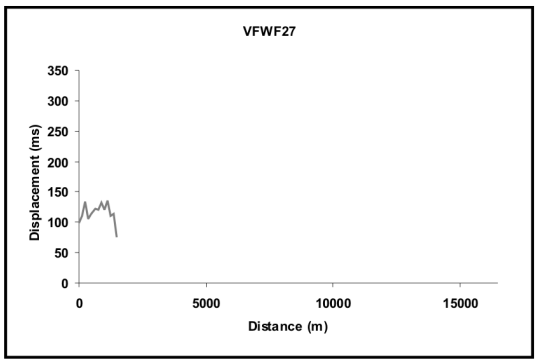
VFWF27
Displacement (ms)
350
300
250
200
150
100
50
0
0
5000
10000
15000
Distance (m)

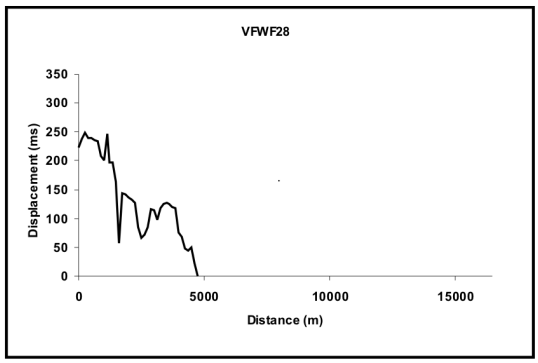
VFWF28
Displacement (ms)
350
300
250
200
150
100
50
0
0
5000
10000
15000
Distance (m)

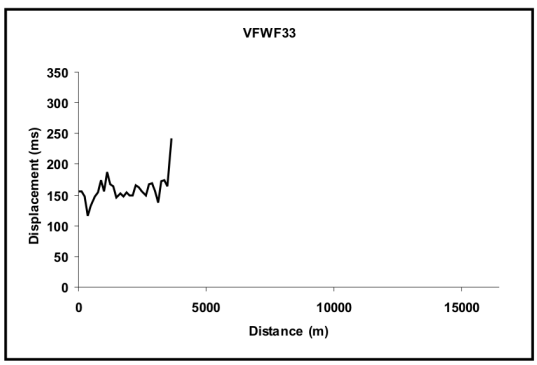
VFWF33
Displacement (ms)
350
300
250
200
150
100
50
0
0
5000
10000
15000
Distance (m)

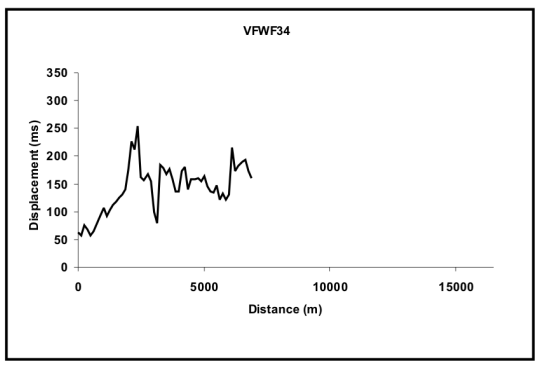
VFWF34
Displacement (ms)
350
300
250
200
150
100
50
0
0
5000
10000
15000
Distance (m)

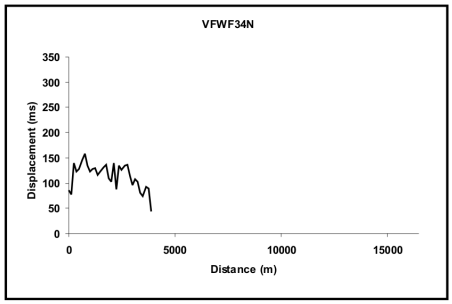
VFWF34N
Displacement (ms)
350
300
250
200
150
100
50
0
0
5000
10000
15000
Distance (m)

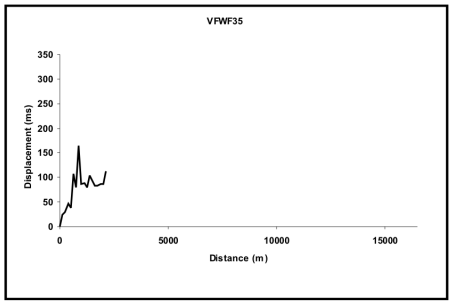
VFWF35
Displacement (ms)
350
300
250
200
150
100
50
0
0
5000
10000
15000
Distance (m)

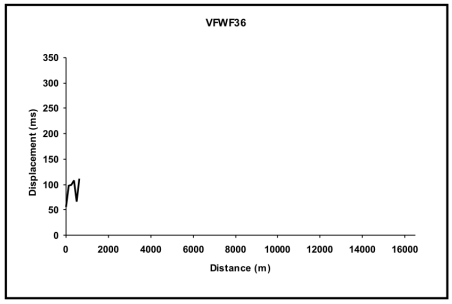
VFWF36
Displacement (ms)
350
300
250
200
150
100
50
0
0
2000
4000
6000
8000
10000
12000
14000
16000
Distance (m)

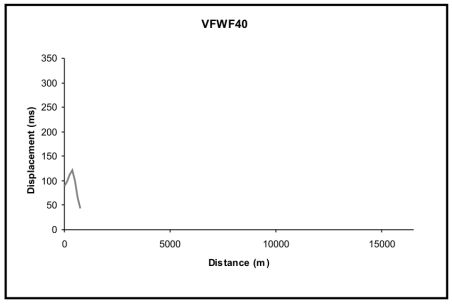
VFWF40
Displacement (ms)
350
300
250
200
150
100
50
0
0
5000
10000
15000
Distance (m)

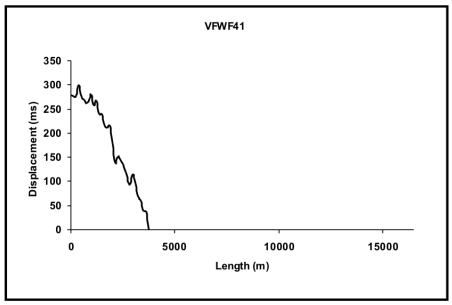
VFWF41
Displacement (ms)
350
300
250
200
150
100
50
0
0
5000
10000
15000
Length (m)

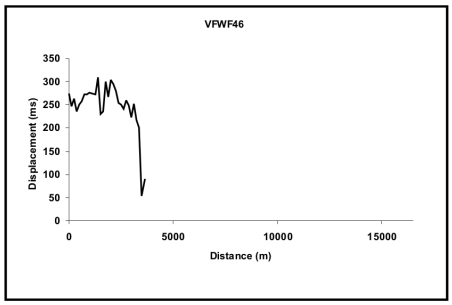
VFWF46
Displacement (ms)
350
300
250
200
150
100
50
0
0
5000
10000
15000
Distance (m)

Appendix 5 Time Maps

A5.0 Location map showing study area and main faults

A5.1 Two way time map to seabed

A5.2 Two way time map to Top Balder Formation

A5.3 Two way time map to Top Cromer Knoll Group

A5.4 Two way time map to Base Cretaceous Unconformity

A5.5 Two way time map to Intra-Kimmeridgian Horizon

A5.6 Two way time map to Top Heather Formation

A5.7 Two way time map to Top Ness Formation

A5.8 Two way time map to Top Dunlin Group

A5.9 Two way time map to Top Statfjord Formation

A5.10 Isochron map of syn-rift unit 1 (Top Brent Group to Top Heather Formation)

A5.11 Isochron map of syn-rift unit 2 (Top Heather Formation to Base Cretaceous Unconformity)

A5.12 Isochron map of syn-rift unit 2a (Top Heather Formation to Intra-Kimmeridgian Horizon)

A5.13 Isochron map of syn-rift unit 2b (Intra-Kimmeridgian Horizon to Base Cretaceous Unconformity

A5.14 Isochron map of syn-rift units 1 and 2 (Top Brent Formation to Base Cretaceous Unconformity)

A5.0 Base map showing area of interest for A5.1 to A5.14. Map shows position of main faults in black with ticks on the downthrow side.

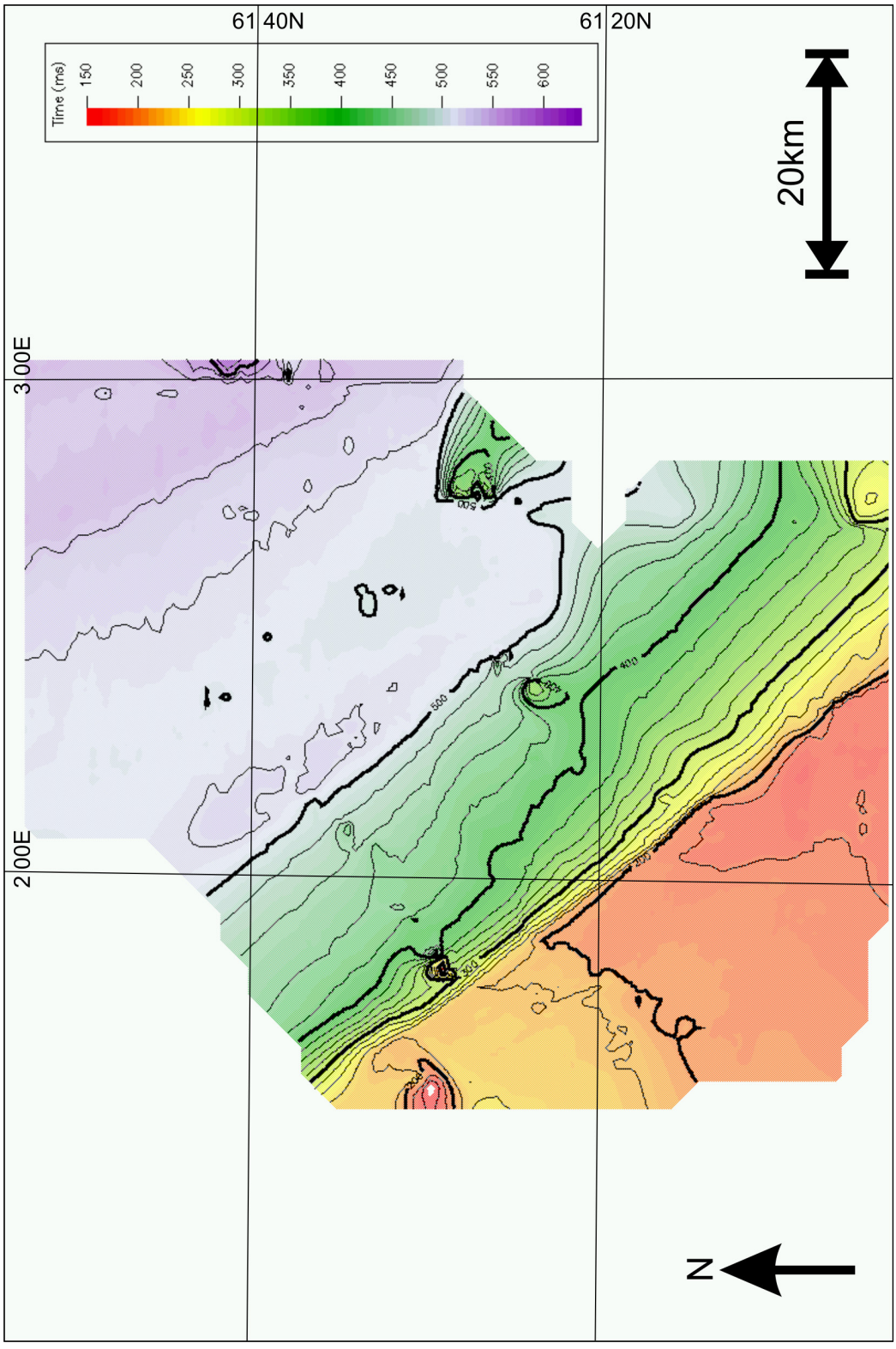

A5.1 Two way time map to seabed

A5.2 Two way time map to Top Balder Formation

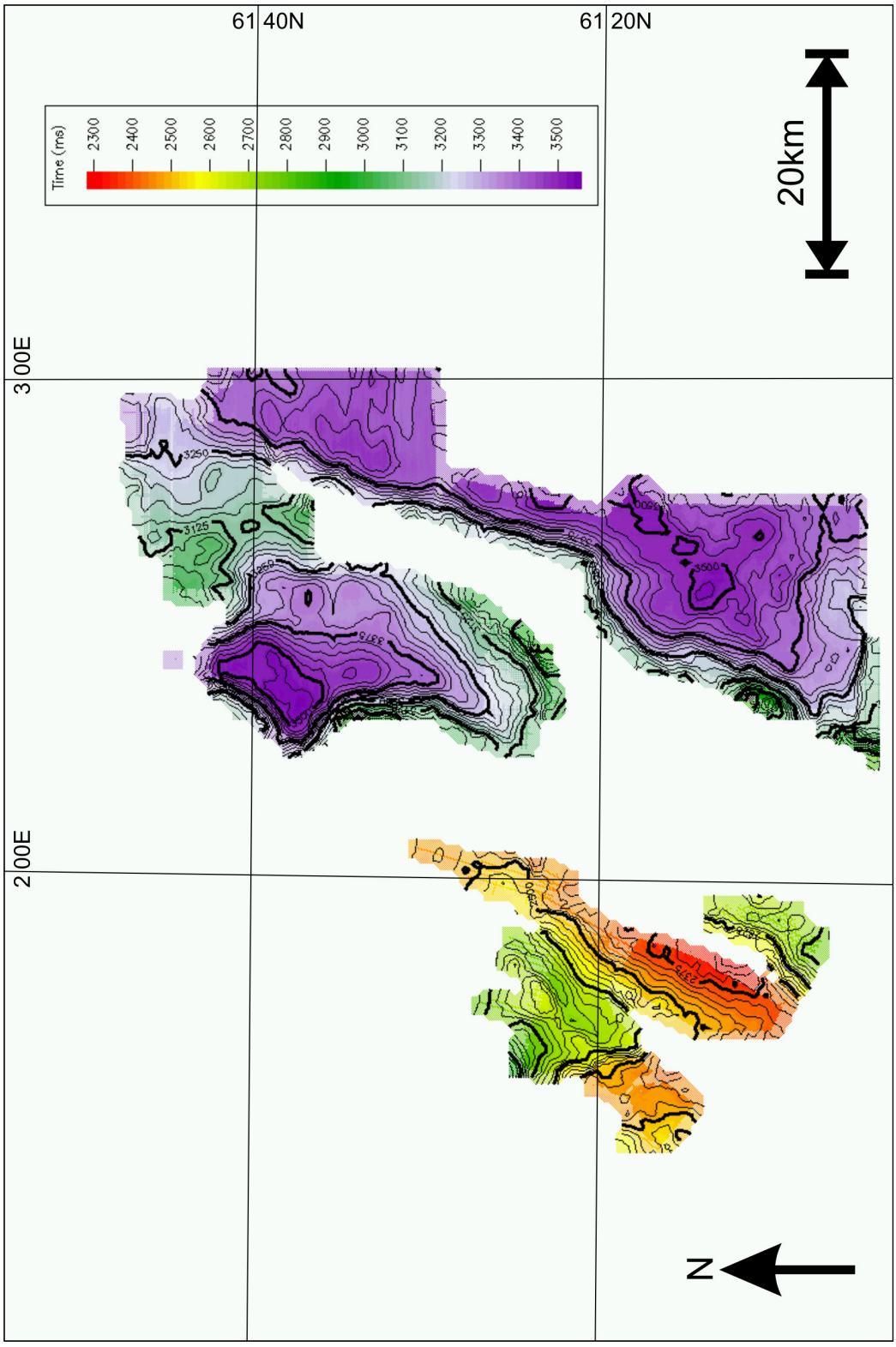

A5.3 Two way time map to Top Cromer Knoll Group

A5.4 Two way time map to Base Cretaceous Unconformity

A5.5 Two way time map to Top Kimmeridgian Horizon

A5.6 Two way time map to Top Heather Formation

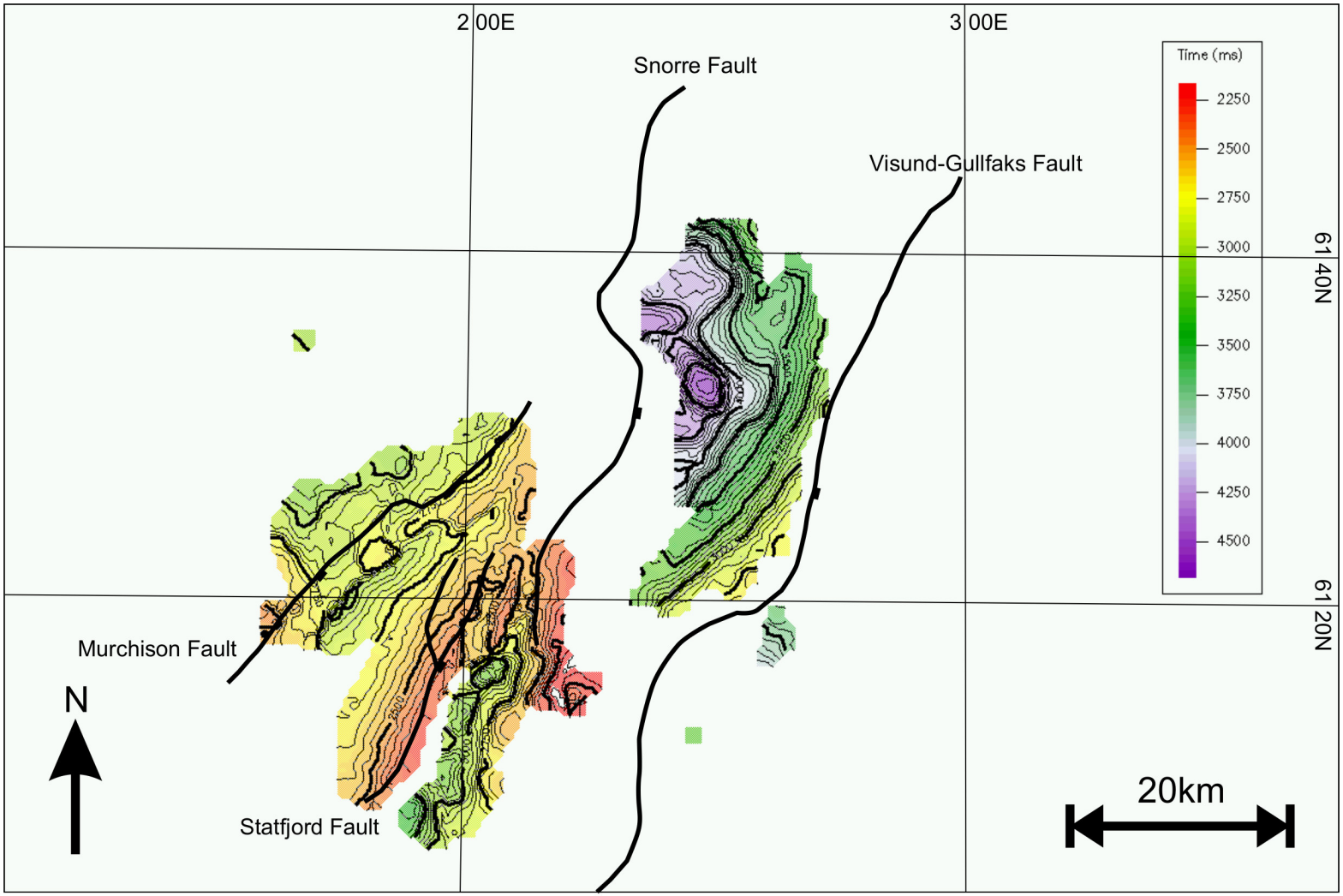

A5.7 Two way time map to Top Ness Formation/ Top pre-rift

A5.8 Two way time map to Top Dunlin Group

A5.9 Two way time map to Top Statford Formation

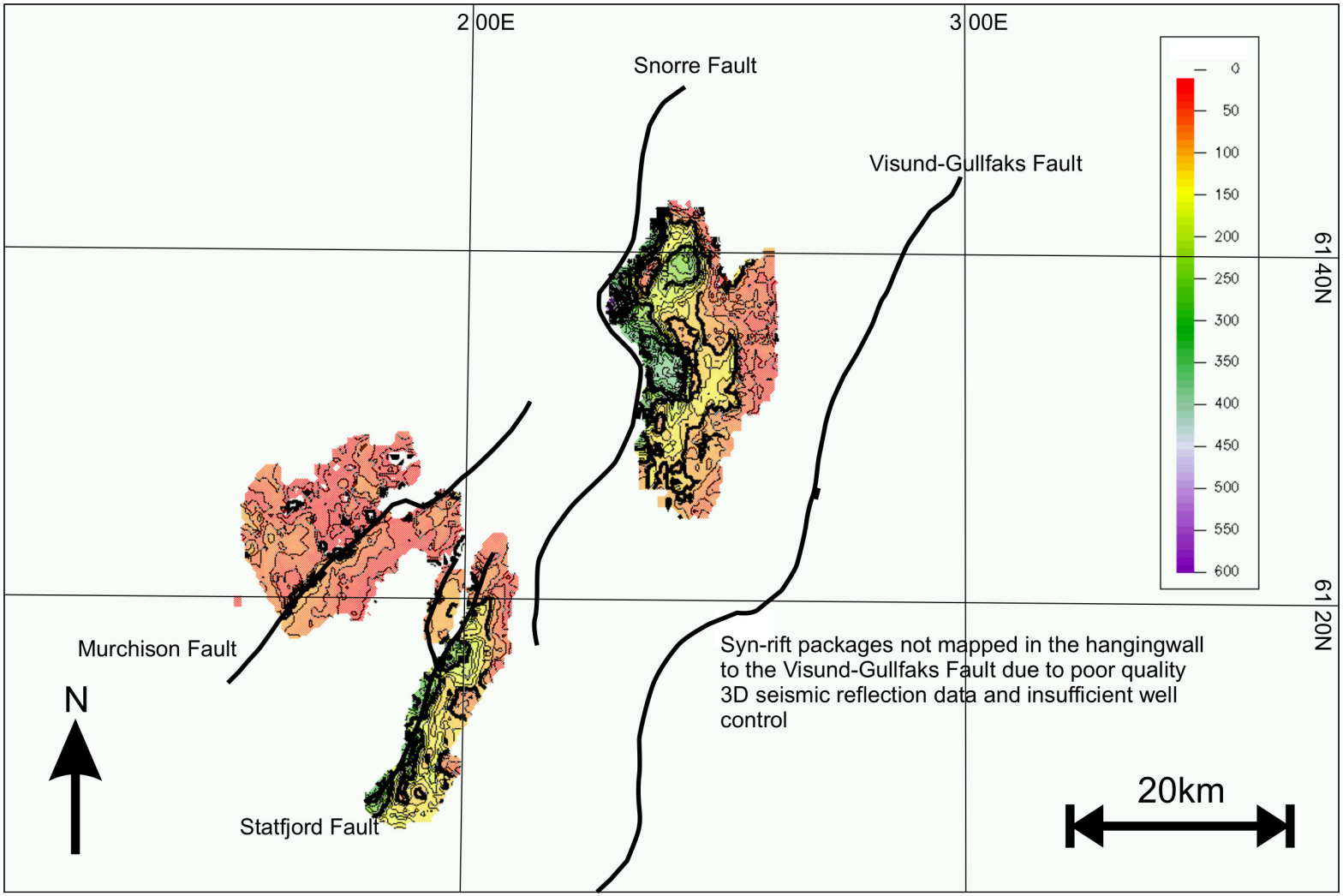

A5.10 Two way time map showing syn-rift unit 1

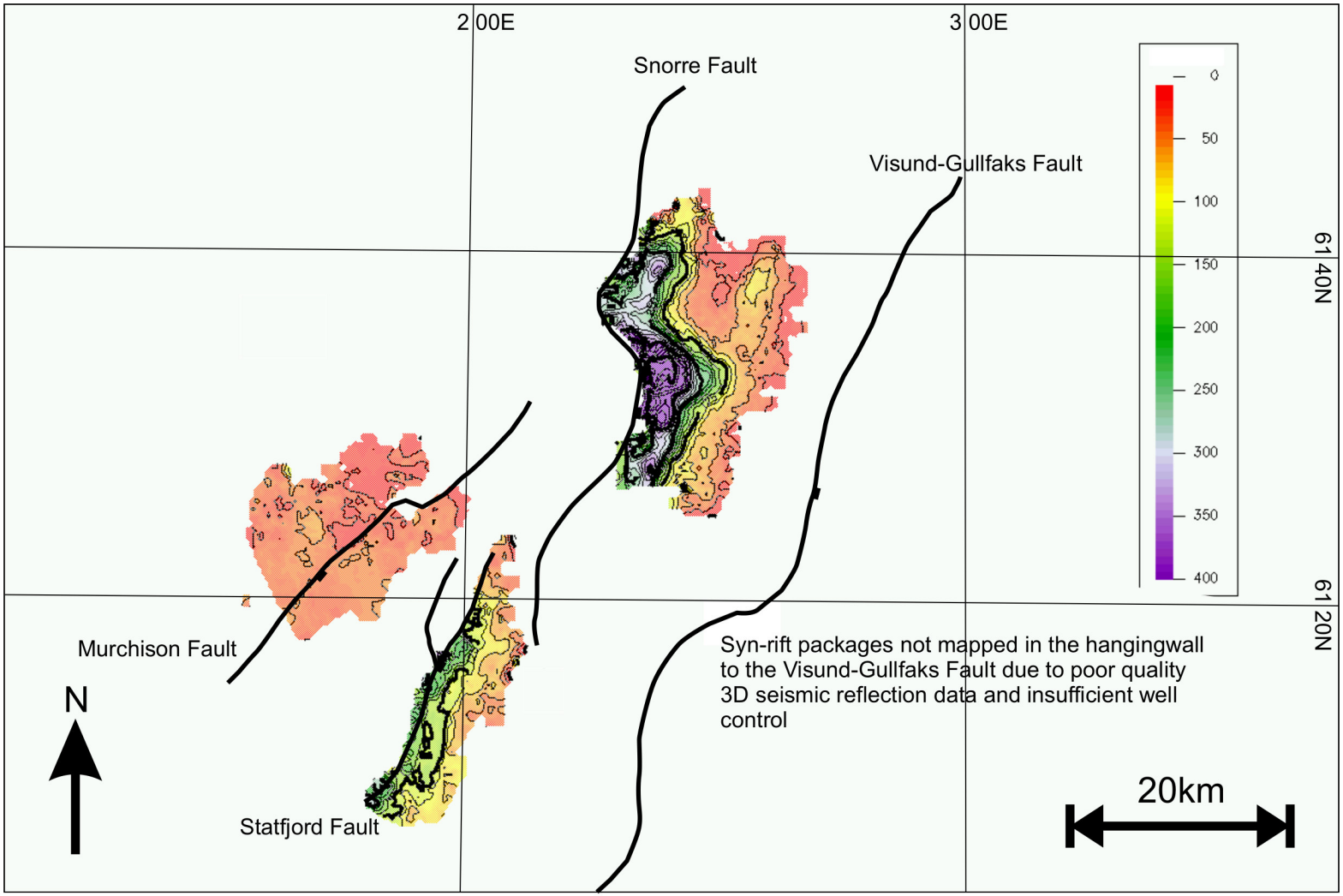

A5.11 Two way time map showing syn-rift unit 2

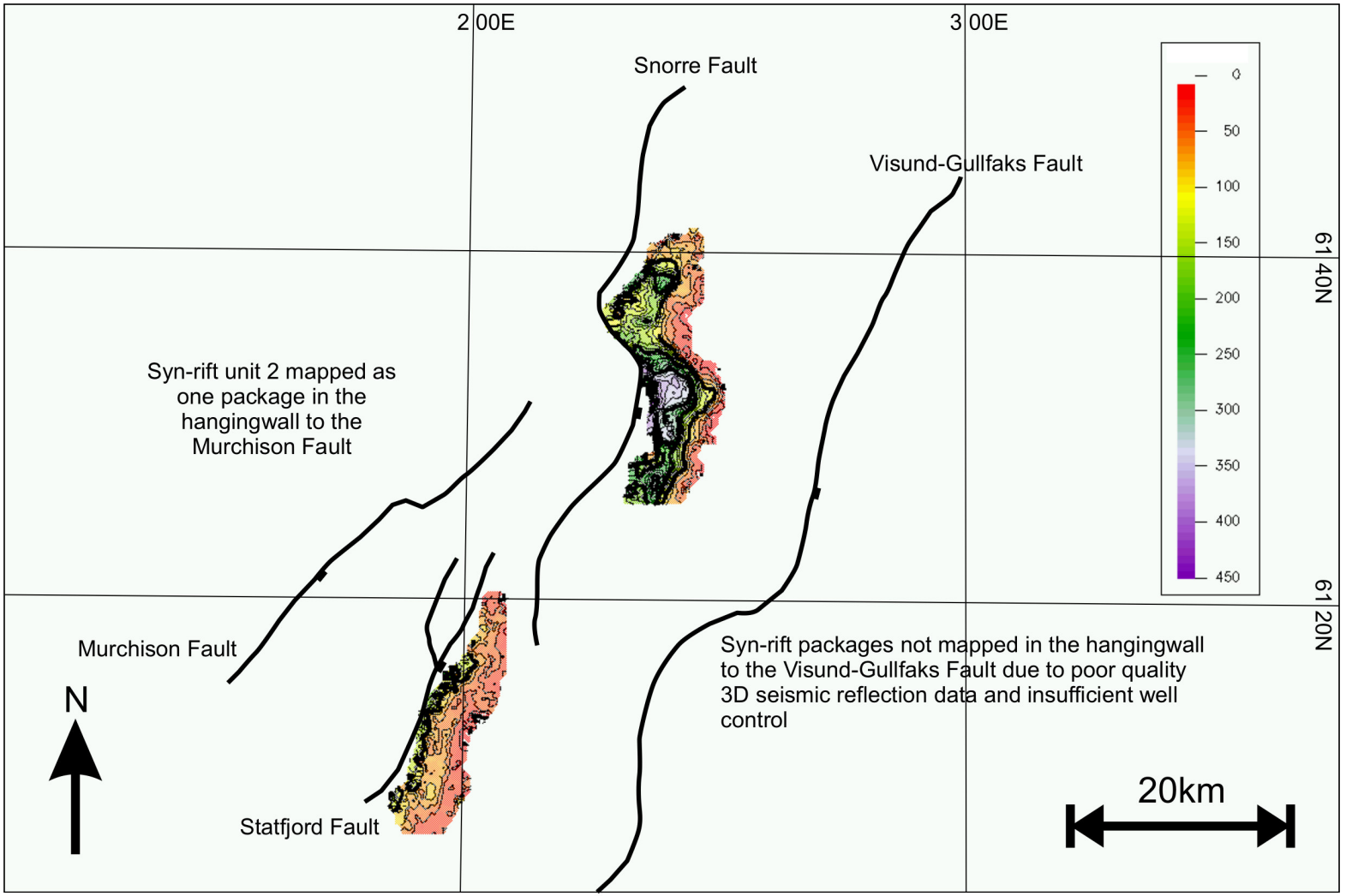

A5.12 Two way time map showing syn-rift unit 2a

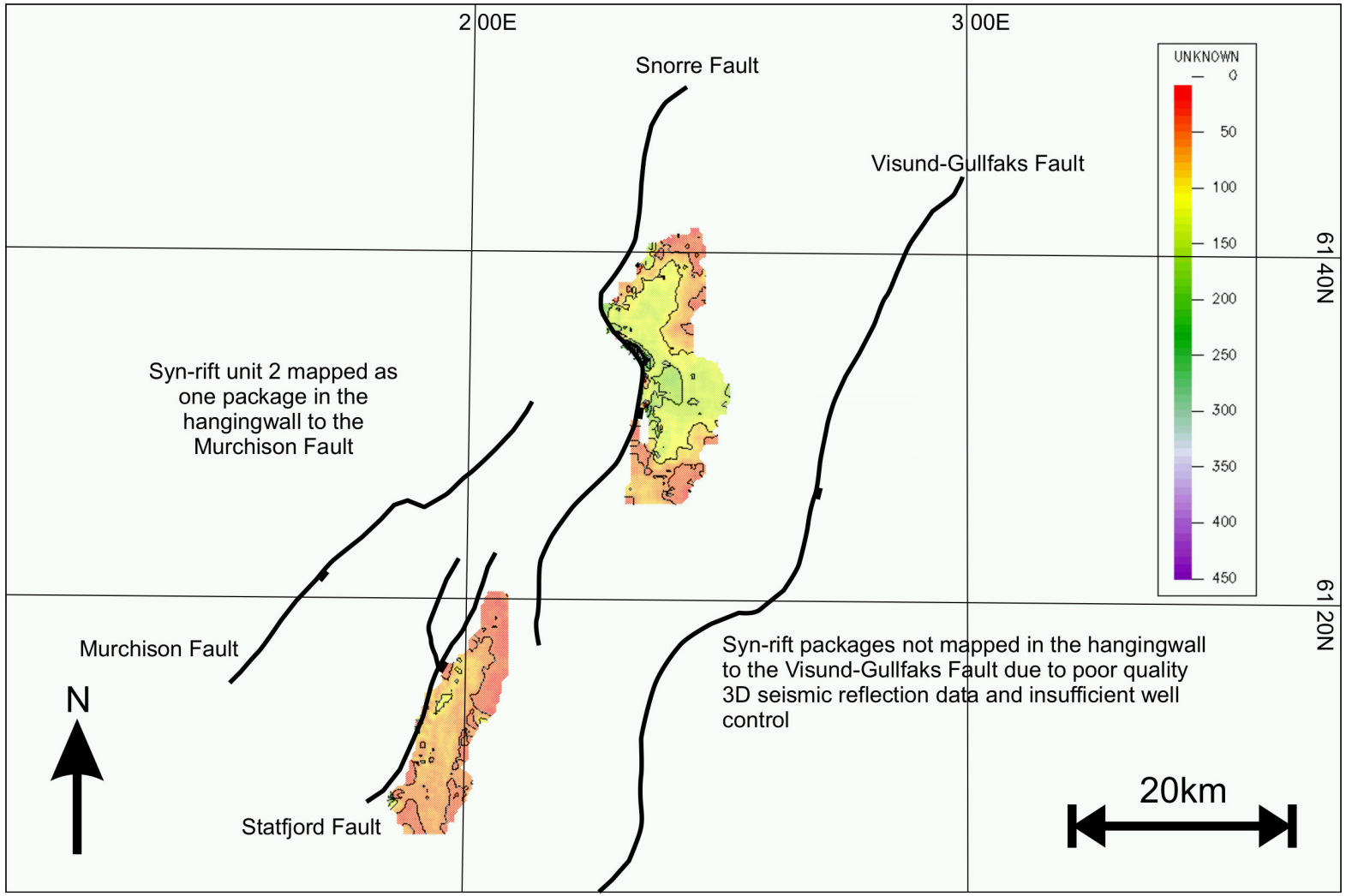

A5.13 Two way time map showing syn-rift unit 2b

A5.14 Two way time map showing syn-rift units 1 and 2

Appendix 6 Biostratigraphy Report from 34/8-7

Appendix 7 Published abstracts and papers

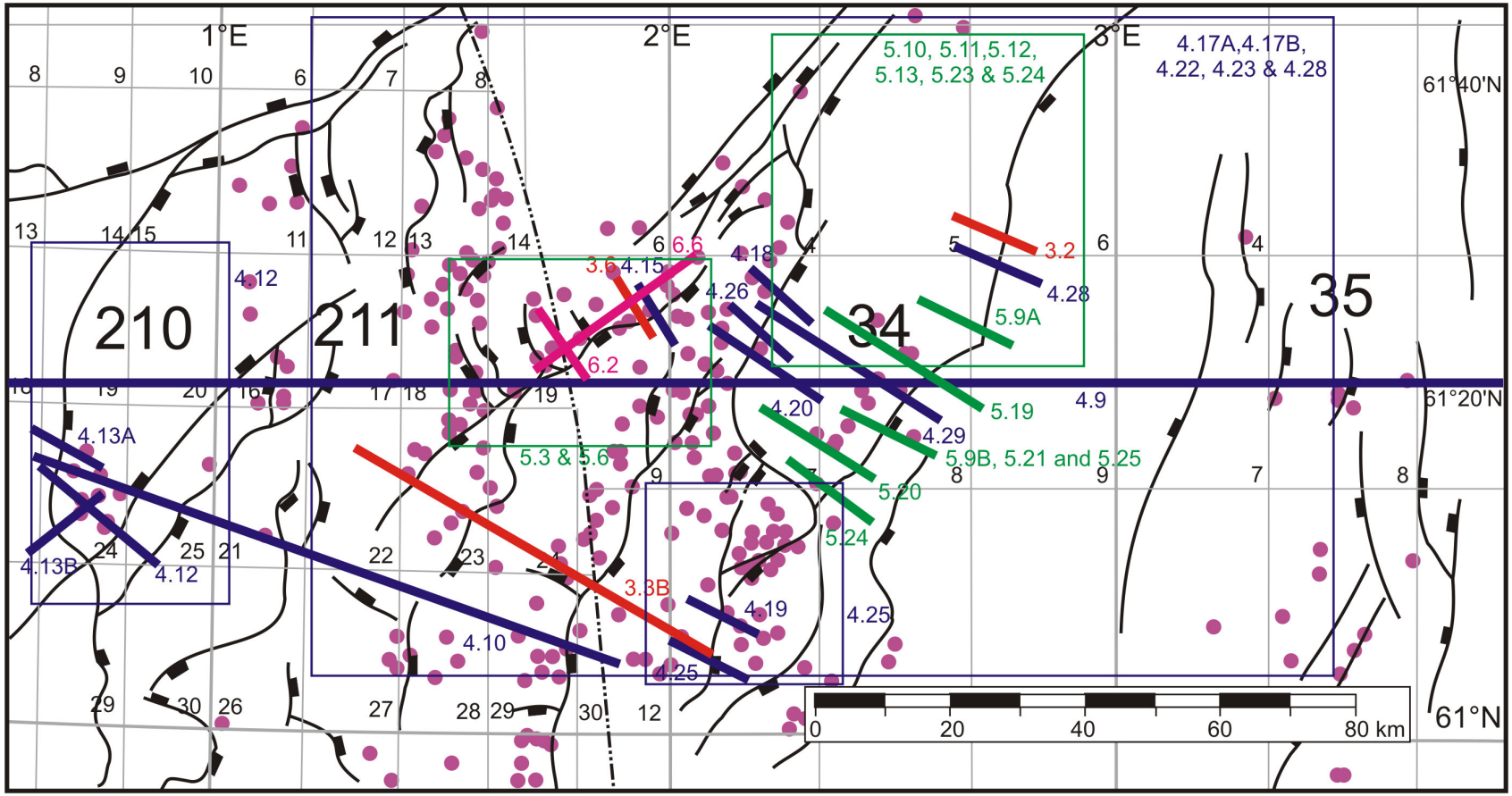

Enclosure 2
Map showing positions of seismic lines and maps presented in thesis. Red lines are presented in chapter 3, blue lines in chapter 4, green lines in chapter 5 and pink lines in chapter 6
Purple circles show positions of exploration, development and appraisal wells with logs available for incorporation into this study

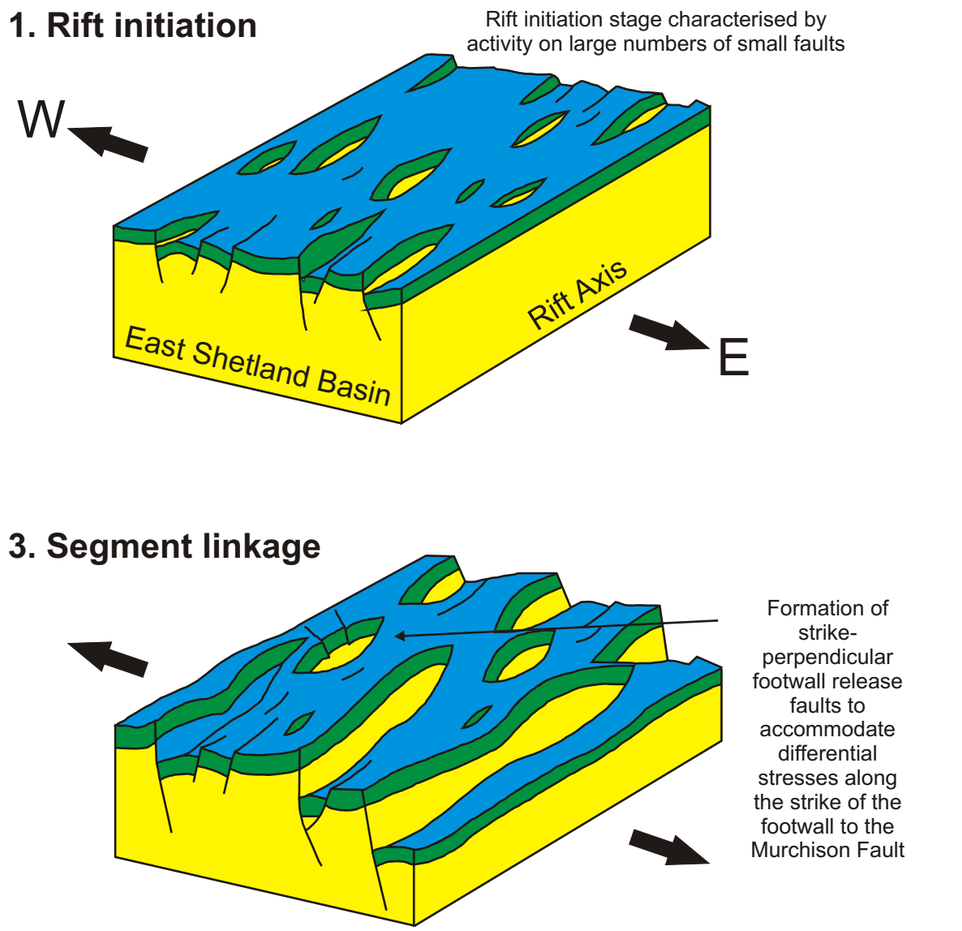

Figure 6.1
Five stage holistic model showing the development of the Mid to Late Jurassic Northern North Sea rift province.
Stage 1 is dominated by the nucleation of large numbers of small displacement faults, orientated sub-perpendicular to the extension direction in both dip directions.
Stage 2 sees the onset of along-strike segment interaction alongside continued nucleation of new faults
Stage 3 is dominated by segment linkage of optimally positioned structures to produce, long throughgoing normal faults. Coalescence of early isolated depocentres results in the formation of a single depocentre in the hangingwall to each of the throughgoing normal faults. The upward bowing of footwalls results in the formation of footwall release faults to accommodate differential stresses along the strike of the fault.
Stage 4 sees the onset of strain localisation towards the rift axis. Cessation of activity on more distal faults, such as the Murchison Fault occurs as strain is focussed onto the more proximal faults which see a gradually increasing slip rate. Footwalls may be uplifted to a sub-aerial position where they are degraded by fluvial and shallow marine processes.
Stage 5 sees the complete focussing of strain onto the rift axis. Activity is restricted to the axis-bounding fault which is active at a high slip rate.